IUTAM SYMPOSIUM

Helicity, Structures and Singularity in Fluid and Plasma Dynamics

Palazzo Franchetti, Istituto Veneto
Venice, Italy

11-15 April, 2016

BOOK OF ABSTRACTS

IUTAM

IstitutoVeneto diScienzeLettere edArti

UNIVERSITÀ DEGLI STUDI DI MILANO BICOCCA

International Scientific Committee

Professor Philip Boyland (U Florida, USA)
Professor Jens Eggers (U Bristol, UK)
Professor Marie Farge (ENS Paris, France)
Professor Yasuhide Fukumoto (Kyushu U, Japan)
Professor Tim Pedley FRS (U Cambridge, UK)
Professor Michael Proctor FRS (U Cambridge, UK)
Professor Renzo Ricca (U Milano-Bicocca, Italy – Chairman)
Professor Katepalli Sreenivasan (New York U, USA)

Local Organizing Committee

Mr. Matteo Foresti (Registration Desk Assistant)
Dott. Davide Ghilardi (Registration Desk Assistant)
Dr. Chiara Oberti (Registration Desk Assistant)
Professor Renzo Ricca (Chairman)
Professor Bernhard Schrefler (CISM & Istituto Veneto)
Ms Emilia Selvaggi (Web Assistant)
Dottor Fabio Sturaro (Web Coordinator)

In memory of
Konrad Bajer
(13 Oct, 1956 – 29 Aug, 2014)
and
Michael Monastyrsky
(3 Sept, 1945 – 24 Nov, 2015)

ACKNOWLEDGEMENTS

I would like to acknowledge the constant and continuous help with the logistics offered by Professor Bernhard Schrefler (Istituto Veneto & CISM) and Dott. Antonio Metrangolo (Istituto Veneto), Dott. Fabio Sturaro and Ms. Emilia Selvaggi, who were in charge of the website project, and my former and present students, Dr. Chiara Oberti, Dott. Davide Ghilardi and Mr. Matteo Foresti for support during the conference.

For scientific advice I am indebted to the Members of the International Scientific Committee, who have been very helpful in several occasions.

For financial support I would like to acknowledge the generous contributions received from the University of Milano-Bicocca (through a UniMiB Grant) and the Department of Mathematics and Applications (through a MatApp Grant), IUTAM (through an IUTAM Grant) and ICTP (through an ICTP Grant). These grants helped 20 young researchers and not-so-young scholars to participate and contribute with their lectures to the success of this conference, which hosted more than 100 people from 19 different nations.

Milano, April 2016

Renzo L. Ricca
Chairman of IUTAM Venice 2016

Speakers and Titles of Lectures

Speakers listed in alphabetical order

Generalizations of the Arnol'd inequality in MHD

P. M. Akhmet'ev[1], E. A. Kudryavtseva[2], A.Yu. Smirnov[3,1]

[1] *IZMIRAN, Troitsk 142190, Moscow, Russia*
[2] *Moscow State University, Moscow 119991, Russia*
[3] *National University of Science and Technology MISiS, Moscow 119049, Russia*

Summary

The Arnol'd inequality estimates the magnetic energy $U(B) = \int (B;B) dR^3$ from below by means of the magnetic helicity $\chi(B) = \int (A;B) dR^3$ [1], Theorem 1.5 p.122. We prove in [2] a modification of the Arnol'd inequality using the magnetic $U^{(4)}$, $U^{(3/2)}$—energies and the magnetic quadratic helicity $\chi^{(2)}$ introduced in [3].

References

[1] Arnold, V.I. & Khesin, B.A. (1998) *Topological Methods in Hydrodynamics*. Applied Mathematical Sciences **125**, Springer-Verlag, Berlin.

[2] P. M. Akhmet'ev, & E. A. Kudryavtseva, & A.Yu. Smirnov (2016) A generalization of the Arnol'd inequality in MHD. *Russian Conference on Magnetohydrodynamics June 22 25, 2015, Perm, Russia*, in press.

[3] P. M. Akhmet'ev (2012) Quadratic magnetic helisity and magnetic energy. Proc. Steklov Math. Inst., vol. 278, pp. 16-28.

Notes

NEW FORMULAE FOR RELATIVE MAGNETIC HELICITY AND FIELD LINE HELICITY

J.-J. Aly

AIM - Unité Mixte de Recherche CEA - CNRS - Université Paris VII, Centre d'Etudes de Saclay, 91191 Gif sur Yvette Cedex, France

Summary

We consider a magnetic field $\mathbf{B}$ occupying the domain D and having all its lines tied to the boundary S of D, and present new formulae for its relative magnetic helicity and its field line helicity (computed by imposing a specific gauge condition). These formulae make explicit the topological nature of these quantities as they express them in terms of either the magnetic mapping of $\mathbf{B}$ (associating together the two footpoints on S of any line) and its normal component on S, or (assuming $\mathbf{B}$ to have a simple topology) a couple of Euler potentials of $\mathbf{B}$. We also show that the field line helicity of a simple topology field uniquely characterizes its magnetic mapping.

1 Statement of the problems

The relative helicity of the magnetic field $\mathbf{B}$ occupying the simply connected domain D is given by

$$H = \int_D (\mathbf{A} + \mathbf{A}_\pi) \cdot (\mathbf{B} - \mathbf{B}_\pi) dv, \tag{1}$$

where $\mathbf{B}_\pi$ is the unique potential field with the same normal component as $\mathbf{B}$ on the boundary S of D ($\mathbf{B}_\pi \cdot \hat{\mathbf{n}} = \mathbf{B} \cdot \hat{\mathbf{n}} = B_n$, with $\hat{\mathbf{n}}$ the external normal to S), and $\mathbf{A}$ and $\mathbf{A}_\pi$ are arbitrary vector potentials of $\mathbf{B}$ and $\mathbf{B}_\pi$, respectively. This gauge invariant quantity, which was first introduced in [1], reduces to the usual magnetic helicity [2] when $B_n = 0$ on S.

Here we restrict our attention to fields whose magnetic lines $\mathcal{L}$ are (almost) all tied to S (a line $\mathcal{L}(\mathbf{r})$ emerging into D at a point $\mathbf{r}$ of $S^+ \subset S$ where $-B_n > 0$ and leaving D at a point of $S^- \subset S$ where $-B_n < 0$). Moreover, we assume that the subdomain $S^0 \subset S$ where $B_n = 0$ has a null area. Choosing for the vector potentials specific determinations $\mathbf{C}$ and $\mathbf{C}_\pi$ such that $\int_D \mathbf{C}_\pi \cdot \mathbf{B}_\pi dv = 0$ and $(\mathbf{C} - \mathbf{C}_\pi) \times \hat{\mathbf{n}} = 0$ on S, we thus have

$$H = \int_D \mathbf{C} \cdot \mathbf{B} dv = \int_{S^+} h(-B_n) ds, \tag{2}$$

where we have introduced the field line helicity h of $\mathbf{B}$ defined by [3]

$$h(\mathbf{r}) = \int_{\mathcal{L}(\mathbf{r})} \mathbf{C} \cdot d\mathbf{l}, \quad \mathbf{r} \in S^+. \tag{3}$$

Both the relative helicity H and the field line helicity h are ideal MHD topological invariants, i.e., their values do not change if the field $\mathbf{B}$ is subject to deformations that are constrained by the frozen-in law and keep fixed the positions of the footpoints on S [1, 3]. These quantities thus depend only on the topology of the lines of $\mathbf{B}$ and on $B_n \mid_S$, and it appears natural to address the two following questions: (i) Do H and h admit expressions in which this dependence appears explicitly? (ii) Reciprocally, does the function h characterize in a unique way the topology of the magnetic lines [4]? (This is obviously not the case for the relative helicity H).

2 Results

Our main results on these two problems are the following ones:

- Introduce the magnetic mapping $\mathbf{M}$ of $\mathbf{B}$, i.e., the mapping that associates to the footpoint $\mathbf{r}$ of $\mathcal{L}(\mathbf{r})$ on S^+ its footpoint $\mathbf{M}(\mathbf{r})$ on S^-, and assume that $\mathbf{B}$ has a simple topology (meaning that $\mathbf{M}$ is continuous). Then

$$h(\mathbf{r}) = \chi(\mathbf{r}), \quad \text{with} \quad \chi(\mathbf{r}) = \int_{\mathcal{C}(\mathbf{r}_0,\mathbf{r})} d\mathbf{l} \cdot [D\mathbf{M} \cdot \widetilde{\mathbf{C}_\pi} - \mathbf{C}_\pi], \tag{4}$$

$$H = \int_{S^+} \chi(-B_n) ds = \int_{S^+} (D\mathbf{M} \cdot \widetilde{\mathbf{C}_\pi} \times \mathbf{C}_\pi) \cdot \hat{\mathbf{n}} ds. \tag{5}$$

  Here $D\mathbf{M}$ denotes the linear application tangent to $\mathbf{M}$, $\widetilde{\mathbf{C}_\pi}(\mathbf{r}) = \mathbf{C}_\pi(\mathbf{M}(\mathbf{r}))$, and $\mathcal{C}(\mathbf{r}_0, \mathbf{r})$ is an arbitrary curve of S^+ connecting the arbitrarily chosen point $\mathbf{r}_0$ of S^0 to $\mathbf{r}$. As required, these expressions explicitly exhibit the topological invariance of h and H as neither the magnetic mapping nor B_n – and then $\mathbf{C}_\pi$ – do change when the field suffer an ideal MHD deformation keeping fixed the positions of its footpoints. For a complex topology field, D can be decomposed into cells D_k, in each of which the topology is simple and h can be expressed as in Eq. (4), but with a constant c_k added in the right-hand side. These constants are shown (at least in some cases) to stay unchanged when the field is deformed, and the expression for h – and the corresponding expression for H – still satisfy the explicit invariance condition.

- In the case where both $\mathbf{B}$ and $\mathbf{B}_\pi$ have a simple topology, we can construct couples (U, V) and (U_π, V_π) of Euler potentials such that $\mathbf{B} = \nabla U \times \nabla V$ and $\mathbf{B}_\pi = \nabla U_\pi \times \nabla V_\pi$ in D, and $U = U_\pi$ and $V = V_\pi$ on S^+. Then we have

$$H = \int_{S^-} U U_\pi (\nabla V \times \nabla V_\pi) \cdot \hat{\mathbf{n}} ds. \tag{6}$$

  Again, we have a formula that shows immediately the topological invariance of H, as U and V are well known to not suffer any change on S^- when $\mathbf{B}$ is deformed as indicated above.

- Consider two fields $\mathbf{B}_1$ and $\mathbf{B}_2$ having a simple topology and the same normal component on S, and assume that they have identical field line helicities, $h_1 = h_2$. Then they have the same magnetic mapping, $\mathbf{M}_1 = \mathbf{M}_2$, and hence the same topology. This result extends the domain of validity of a result of Yeates and Hornig [4], who restricted their attention to the case of an unidirectional field in a tube-like domain (in that situation, however, S has a lateral part S^0 of positive area on which $B_n = 0$ and we have to specify a "winding number" w on S^0 (in addition to $\mathbf{M}$) in order to characterize the topology of the lines of $\mathbf{B}$. Our argument can be completed to prove that $h_1 = h_2$ also implies $w_1 = w_2$ in such a configuration).

- All the results presented above are still valid if we substitute for $\mathbf{B}_\pi$ an arbitrary reference field $\mathbf{B}_{ref}$ having $B_{ref\,n} = B_n$ on S. In that case, however, the relative helicity is no longer an intrinsic attribute of the field $\mathbf{B}$.

References

[1] Berger, M.A. & Field, G.B. (1984) The topological properties of magnetic helicity. *J. Fluid Mech.* **147**, 133–148.

[2] Moffatt, H.K. (1969) The degree of knottedness of tangled vortex lines. *J. Fluid Mech.* **35**, 117–129.

[3] Berger, M.A. (1988) An energy formula for nonlinear force-free magnetic fields. *Astron. Astrophys.* **201**, 355–361.

[4] Yeates, A.R. & Hornig, G. (2014) A complete topological invariant for braided magnetic fields. *J. Phys.: Conf. Series* **544**, 012002.

Notes

Helicity of a small patch of quantum vorticity in superfluid helium

C.F. Barenghi[1], M. Mesgarnezhad[1] and A.W. Baggaley[1]

[1] *School of Mathematics and Statistics and Joint Quantum Centre Durham-Newcastle, Newcastle University, Newcastle upon Tyne, NE1 7RU, United Kingdom*

Summary

We numerically study the evolution of a small patch of quantised vorticity in superfluid helium, and track the helicity of the vortex configuration as a function of time.

1 Introduction

Tangled filamentary structures occur in many physical systems, from ropes to DNA. In this work we are concerned with more 'mathematical' filamentary structures consisting of field lines in fluids and plasmas, for example vortex lines and magnetic field lines. Such lines undergo reconnection events, which tend to be associated with energy losses. In the limit of no dissipation, the governing equations of motion (the Euler equation, and the magnetic induction equation in the frozen field approximation) preserve the topology of the lines. Under this approximation, helicity and magnetic helicity are conserved quantities. Recent work suggests that in the case of small dissipation helicity is partially preserved [1]. The aim of this work is to explore this partial preservation of topology in a context where vortex lines are not mathematical abstractions but have a real physical meaning: superfluids such as liquid helium (^{4}He and ^{3}He) and atomic Bose-Einstein condensates.

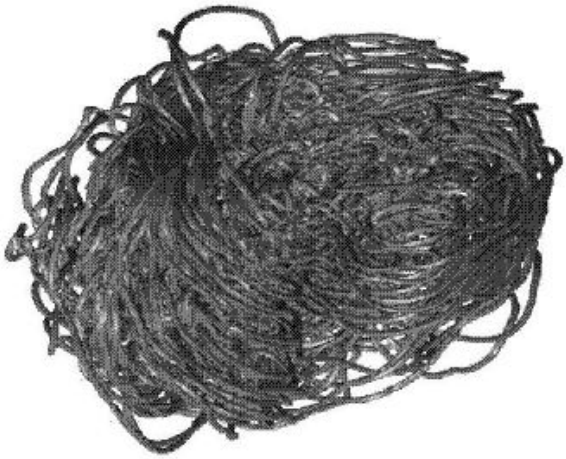

Fig. 1: Turbulent tangle of superfluid vortex lines.

2 Method

Superfluids are quantum fluids with zero viscosity and are governed by a macroscopic wavefunction $\Psi(\mathbf{x},t) = \sqrt{n(\mathbf{x},t)}e^{i\phi(\mathbf{x},t)}$ where $\mathbf{x}$ is the position, t is time, $\phi(\mathbf{x},t)$ is the phase and $n(\mathbf{x},t)$ the number density of atoms. Quantum mechanical prescriptions require that the velocity field is

$$\mathbf{v}(\mathbf{x},t) = \frac{\hbar}{m}\nabla\phi(\mathbf{x},t), \tag{1}$$

where $\hbar = h/(2\pi)$, h is Planck's constant and m the mass of one atom. Vorticity is thus either zero or takes the form of thin filaments around which the circulation is fixed:

$$\oint_C \mathbf{v} \cdot \mathbf{dr} = \kappa, \tag{2}$$

where C is an integration path around the axis of the vortex and $\kappa = h/m$ is the quantum of circulation. The vortex core is a small tubular region of radius $a_0 \approx 10^{-10}$ m (in ^{4}He), where the density goes to zero; in other words, although the velocity field around the vortex line, from Eq. (2), is $v = \kappa/(2\pi r)$ where r is the distance from the vortex axis, there are no atoms which move with infinite speed. Since in typical experiments a_0 is orders of magnitude less than the typical distance $\ell \approx 10^{-4}$ to 10^{-2} m between vortices, we model the vortex lines as space curves $\mathbf{s}(\xi, t)$ (where ξ is arc length) of infinitesimal thickness which move according to [2]:

$$\frac{d\mathbf{s}}{dt} = \mathbf{v}_{self} + \mathbf{w}, \tag{3}$$

$$\mathbf{v}_{self} = \frac{\kappa}{4\pi} \oint_{\mathcal{L}} \frac{(\mathbf{s}_1 - \mathbf{s}) \times \mathbf{s}_1}{|\mathbf{s}_1 - \mathbf{s}|^3}, \tag{4}$$

$$\mathbf{w} = \alpha \mathbf{s}' \times \mathbf{v}_{ns} - \alpha' \mathbf{s}' \times [\mathbf{s}' \times \mathbf{v}_{ns}], \qquad \mathbf{v}_{ns} = \mathbf{v}_n - \mathbf{v}_{self}, \tag{5}$$

Here $\mathbf{v}_n$ is the normal fluid and α and α' are small temperature-dependent friction coefficients arising from the interaction of vortex lines with the thermal excitations which make up the normal fluid. When numerically solving the above equations, we desingularise the Biot-Savart integral (4) using the vortex core radius a_0, and, following evidence from a more microscopic model [3], we algorithmically reconnect two vortex lines which are sufficiently close to each others. Note that in the zero temperature limit the normal fluid is negligible, α and α' vanish, and the vortices move simply as $d\mathbf{s}/dt = \mathbf{v}_{self}$.

3 Results

We start from a small number of randomly oriented vortex loop which serve as arbitrary initial condition. A localised region of normal fluid turbulence $\mathbf{v}_n$ (represented by a sum of random waves), models a local disturbance which can be be easily created in the experiments, and feeds energy into the vortex loops. The vortex loops become distorted, reconnect with each others and grow in length, until a statistical steady state is obtained - see Fig. (1) - in which the vortex length fluctuates around an average value.

During the time evolution, by numerically determining appropriate crossing numbers over given projections, we determine the linking number L_{ij} between any two loops i and j, and the (solid-angle averaged) writhing number W_i of each loop. We report the time behaviour of the helicity, defined as

$$H = \sum_{i \neq j} L_{ij} + \sum_i W_i, \tag{6}$$

and compare H to energy and length of the vortex configuration.

References

[1] Kleckner, D., Kauffman, L. H., & Irvine, T. M. How superfluid knots untie. arXiv:1507.07579 (2015).

[2] Schwarz, K. W., Three-dimensional vortex dynamics in superfluid ^{4}He: homogeneous superfluid turbulence. Phys. Rev. B **38**, 2398 (1988).

[3] Koplik, J. and Levine, H., Vortex reconnection in superfluid helium, Phys. Rev. Letters **71**, 1375 (1993).

Notes

Helicity on Compact Surfaces

Mitchell A. BERGER

Department of Mathematics, Unuiversity of Exeter, U.K.

Consider a magnetic filament or vortex tube anchored at two ends to a compact surface S. The helicity (twist plus writhe) should be conserved if the endpoints do not move, even if the filament is distorted. If the endpoints do move, then the helicity flux will arise from the spins of the two endpoints, plus an orbit term measuring how much the endpoints rotate about each other. Suppose one end is at rest, and the other moves along a path. The moving end has a natural spin (the geodesic curvature) equal to the rotation of the tangent vector to the path relative to parallel transport. The orbit term requires a vector potential. This vector potential can be determined with the help of the Gauss-Bonnet theorem. If space is foliated by a set of nested compact surfaces, then we can ask whether helicity (or relative helicity) can be considered as a sum of 'surface helicity densities'; more precisely an integral of a function on the set of surfaces. If the surfaces are parallel planes or concentric spheres, then this function can be simply described in terms of the linking of poloidal and toroidal fluxes. For less symmetric surfaces, we will generalize the poloidal-toroidal flux decomposition in a manner which allows us to maintain this idea of surface helicity density.

Notes

Helicity, topology and Kelvin waves in reconnecting quantum knots

P.C. di Leoni,[1] P.D. Mininni[1] & M.E. Brachet[2]

[1] *Departamento de Física, U. Buenos Aires & IFIBA CONICET, Argentina*
[2] *Laboratoire de Physique Statistique, ENS Paris & CNRS U Paris 6 & 7, France*

Helicity is a topological invariant that measures the linkage and knottedness of lines, tubes and ribbons. As such, it has found myriads of applications in astrophysics and solar physics, in fluid dynamics, in atmospheric sciences, and in biology. In quantum flows, where topology-changing reconnection events are a staple, helicity appears as a key quantity to study. However, the usual definition of helicity is not well posed in quantum vortices, and its computation based on counting links and crossings of vortex lines can be downright impossible to apply in complex and turbulent scenarios. We present a new definition of helicity which overcomes these problems. With it, we show that only certain reconnection events conserve helicity. In other cases helicity can change abruptly during reconnection. Furthermore, we show that these events can also excite Kelvin waves, which slowly deplete helicity as they interact nonlinearly, thus linking the theory of vortex knots with observations of quantum turbulence.

Notes

Atypical late-time singular regimes accurately diagnosed in stagnation-point-type helical solutions of 3D Euler flows

M. D. Bustamante[1], R. M. Mulungye[1], D. Lucas[2]

[1] *CASL, School of Mathematics and Statistics, University College Dublin, Belfield, Dublin 4, Ireland*

[2] *DAMTP, University of Cambridge, Cambridge CB3 0WA, UK*

Summary

We revisit numerically and analytically the finite-time blowup of an infinite-energy helical solution of 3D Euler equations [Gibbon et al. (1999)]. By employing the method of mapping to regular systems [Bustamante (2011), Mulungye et al. (2015)], we establish a curious property of this solution that was not observed previously: near singularity time T^*, a fast transient is followed by a slower late-time blowup regime that is well resolved spectrally at mid-resolutions (512^2), with a Gaussian wavenumber spectrum. The analyticity-strip width decays 'slowly' to zero at $t = T^*$, remaining above the collocation-point scale for all simulation times $t < T^* - 10^{-9000}$. Reaching such a proximity to singularity time is not possible in the original temporal variable, because of the floating-point double-precision barrier ($\approx 10^{-16}$). Due to this limitation on the *original* variables, the mapped variables now provide an improved assessment of the relevant blowup quantities, crucially with acceptable accuracy at an unprecedented closeness to singularity time: $T^* - t \approx 10^{-140}$.

1 Symmetry plane model and mapping to regular systems

We consider a class of exact solutions of the 3D Euler equations, possessing non-trivial helicity, presented by Gibbon *et al.* [1]. Writing $\mathbf{u}(x,y,z,t) = (u_x(x,y,t), u_y(x,y,t), z\,\gamma(x,y,t))$ we obtain

$$\frac{\partial \gamma}{\partial t} + \mathbf{u}_\mathrm{h}\cdot\nabla_\mathrm{h}\gamma = 2\langle\gamma^2\rangle - \gamma^2\,, \qquad \frac{\partial \omega}{\partial t} + \mathbf{u}_\mathrm{h}\cdot\nabla_\mathrm{h}\omega = \gamma\,\omega\,, \tag{1}$$

where $\mathbf{u}_\mathrm{h}(x,y,t) \equiv (u_x(x,y,t), u_y(x,y,t))$ denotes the "horizontal" component of the velocity field at the symmetry plane ($z=0$), $\nabla_\mathrm{h} = (\partial_x, \partial_y)$ denotes the horizontal gradient operator, $\omega(x,y,t) = \partial_x u_y - \partial_y u_x$, is the vorticity, γ is the stretching-rate of vorticity, which using the incompressibility condition can be defined as $\gamma(x,y,t) = -\nabla_\mathrm{h}\cdot\mathbf{u}_\mathrm{h}(x,y,t)$, and $\langle f(\cdot,t)\rangle \equiv \frac{1}{4\pi^2}\int_0^{2\pi}\int_0^{2\pi} f(x,y,t)\mathrm{d}x\mathrm{d}y$ denotes the spatial average over the periodic 2D domain.

Analytic solutions are found for supremum norms by solving along characteristics [2, 3], leading to singular behaviour controlled by a classical Beale-Kato-Majda (BKM) type of theorem: $\int_0^T \|\gamma(\cdot,t)\|_\infty \mathrm{d}t < \infty$ for bounded solutions [4]. With the initial condition $\gamma_0(x,y) = \omega_0(x,y) = \sin(x)\sin(y)$, the singularity time is $T^* = \frac{4}{\pi^2}\int_0^1 \left[K(S^2)\right]^2\, dS \approx 1.41800273492385887506 2234$, where K is the complete elliptic function of the first kind. We can identify $\|\gamma(\cdot,t)\|_\infty = -\inf\gamma(\cdot,t)$.

Bustamante [5] and later Mulungye et al. [6] presented a method to bijectively map system (1) to one that is **globally regular** in time. Such a mapping removes some of the ambiguity of numerical assessment of singular behaviour and can increase the accuracy of important quantities. The BKM theorem provides a new 'mapped' time and a rescaling to mapped variables

$$\tau(t) = \int_0^t \|\gamma(\cdot,t')\|_\infty \mathrm{d}t', \qquad \gamma_\mathrm{map}(x,y,\tau) = \frac{\gamma(x,y,t)}{\|\gamma(\cdot,t)\|_\infty}\,, \qquad \omega_\mathrm{map}(x,y,\tau) = \frac{\omega(x,y,t)}{\|\gamma(\cdot,t)\|_\infty}\,, \tag{2}$$

resulting in the mapped version of system (1), with globally regular solution in mapped time τ:

$$\frac{\partial \gamma_\mathrm{map}}{\partial \tau} + \mathbf{u}_\mathrm{map}\cdot\nabla\gamma_\mathrm{map} = 2\langle\gamma_\mathrm{map}^2\rangle - \gamma_\mathrm{map}^2 - \gamma_\mathrm{map}\left\{1 - 2\langle\gamma_\mathrm{map}^2\rangle\right\}\,, \tag{3}$$

$$\frac{\partial \omega_\mathrm{map}}{\partial \tau} + \mathbf{u}_\mathrm{map}\cdot\nabla\omega_\mathrm{map} = \gamma_\mathrm{map}\,\omega_\mathrm{map} - \omega_\mathrm{map}\left\{1 - 2\langle\gamma_\mathrm{map}^2\rangle\right\}\,. \tag{4}$$

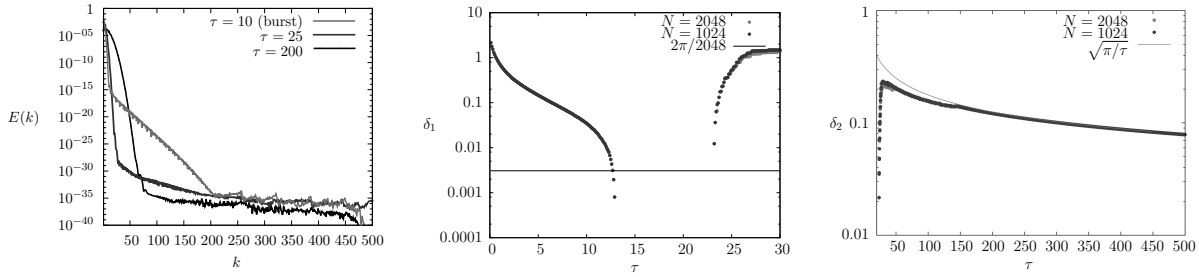

Fig. 1: γ^2-Fourier spectra snapshots (left) and time evolution of the analyticity-strip width $\delta(t(\tau))$. Centre: early-time profile from $E(k,t) \lessapprox C(t)k^{-n(t)}\mathrm{e}^{-2\delta_1(t)k}$, showing the initial burst. Right: late-time Gaussian profile from $E(k,t) \lessapprox C(t)k^{-n(t)}\mathrm{e}^{-(\delta_2(t)k)^2}$, showing the slow cascade and the rigorous estimate $\delta \approx \sqrt{\pi/\tau}$.

2 Diagnosis of singularity

We solve the evolution equations for both systems numerically using a Hou-dealiased pseudospectral method implemented on GPUs using CUDA [6], with a 4th-order Runge-Kutta time solver. Adaptive time stepping ($dt = d\tau/\|\gamma(\cdot,t)\|_\infty$) is used for the original equations and uniform steps of $d\tau$ are used in the mapped system with the resulting distribution of temporal data roughly equivalent.

The evolution of the circular-shell spectrum of stretching rate, $E(k,t) = \sum_{k-\frac{1}{2}<|\mathbf{k}|<k+\frac{1}{2}} |\hat{\gamma}(\mathbf{k},t)|^2$, shows two timescales in evidence. An initial burst can be observed, with a flux towards intermediate k which is redistributed across the modes and has the 'typical' spectrum $E(k,t) \lessapprox C(t)k^{-n(t)}\mathrm{e}^{-2\delta_1(t)k}$ [7, 3]. Provided $N > 256$ (spatial resolution) this initial phase remains well resolved and lasts only until $\tau \approx 25$ (in original variables this is $T^* - t \approx 10^{-10}$). Fig. 1 (centre) shows two resolutions ($N = 1024$ and 2048) which are essentially indistinguishable; negative values of δ_1 indicate that this ansatz ceases to be a valid analyticity measure due to the presence of a large scale Gaussian spectrum. The true late-time behaviour ($\tau > 25$) consists of a slow cascade that builds up from small k, with an 'atypical' spectrum $E(k,t) \lessapprox C(t)k^{-n(t)}\mathrm{e}^{-(\delta_2(t)k)^2}$ [3]. Fig. 1 (right) shows the slow decay of δ_2. This has been missed in previous work [7] as it only arises after the initial burst, and persists to sufficiently close to T^* to render it next to inaccessible without the mapped variables.

Errors in quantities such as stretching-rate norm $\|\gamma(\cdot,t)\|_\infty$ and singularity-time proximity $T^* - t$ (figures not shown), show that the original system's numerical solution loses accuracy beyond $\tau = 34$, corresponding to $T^* - t \approx 10^{-14}$ ('double-precision barrier'), while the mapped system's solution keeps a relative error of 10^{-7} beyond $\tau = 330$, corresponding to $T^* - t \approx 10^{-140}$. See details in [3].

Acknowledgements. We acknowledge financial support from SFI under Grant Number 12/IP/1491.

References

[1] Gibbon, J.D., Fokas, A.S. & Doering, C.R. (1999) Dynamically stretched vortices as solutions of the 3D Navier–Stokes equations. *Physica D* **132**, 497–510.

[2] Constantin, P. (2000) The Euler equations and nonlocal conservative Riccati equations. *International Mathematics Research Notices* **9**, 455–465.

[3] Mulungye, R.M., Lucas, D. & Bustamante, M.D. (2016) Atypical late-time singular regimes accurately diagnosed in stagnation-point-type solutions of 3D Euler flows. *J. Fluid Mech.* **778**, R3.

[4] Beale, J., Kato, T. & Majda, A. (1984) Remarks on the Breakdown of Smooth Solutions for the 3-D Euler Equations. *Commun. Math. Phys.* **94**, 61–66.

[5] Bustamante, M.D. (2011) 3D Euler equations and ideal MHD mapped to regular systems: Probing the finite-time blowup hypothesis. *Physica D* **240**, 1092–1099.

[6] Mulungye, R.M., Lucas, D. & Bustamante, M.D. (2015) Symmetry-plane model of 3D Euler flows and mapping to regular systems to improve blowup assessment using numerical and analytical solutions. *J. Fluid Mech.* **771**, 468–502.

[7] Ohkitani, K. & Gibbon, J.D. (2000) Numerical study of singularity formation in a class of Euler and Navier–Stokes flows. *Physics of Fluids* **12**, 3181.

Notes

Topology conserving magnetic field relaxation in plasma

S. Candelaresi[1], D. I. Pontin[1], G. Hornig[1]

[1] *School of Science & Engineering, University of Dundee, UK*

Summary

A method for computing the relaxation of magnetic fields is presented which preserves the field's topology. This method uses Lagrangian grids and mimetic differential operators, which greatly improves the accuracy, as compared to previous approaches. We use this method to study the relaxation of magnetic fields and find that, in absence of magnetic null points, they relax into a force-free state (vanishing Lorentz force) or achieve force-balance with the hydrostatic presure.

Motivated by Parker's hypothesis on the relaxation of topologically non-trivial magnetic braids [1] we develop a method to simulate the ideal (non-resistive) relaxation of magnetic fields with high accurracy. We make use of a Lagrangian grid where the grid points move with the fluid. Together with the ideal induction equation

$$\frac{\partial \mathbf{B}}{\partial t} = \nabla \times (\mathbf{u} \times \mathbf{B}), \tag{1}$$

with the magnetic field $\mathbf{B}$ and fluid velocity $\mathbf{u}$, we can compute the magnetic field at any given time just from the grid distortion $\mathbf{x}$ and initial magnetic field on the initial grid $\mathbf{X}$:

$$\mathbf{x}^*(t)\mathbf{B}(\mathbf{x}, t) = \mathbf{B}(\mathbf{X}, 0), \tag{2}$$

where $\mathbf{x}^*$ is the pull-back. Using this Lagrangian method the topology of the field is conserved at all times.

For the fluid velocity we use the magneto-frictional approach [2]

$$\mathbf{u} = \mathbf{J} \times \mathbf{B}, \tag{3}$$

where $\mathbf{J} = \nabla \times \mathbf{B}$ is the electric current density, which has been shown to be well fit for magnetic relaxation simulations, since it strictly minimizes the magnetic energy. Computing spatial derivatives on a distorted grid can be done directly by referring to the original one [2], but it is shown to be prone to numerical issues [3]. Therefore, we apply mimetic differential operators [4, 5] in order to compute the curl of the magnetic field. It is shown to greatly improve the quality of the field relaxation by several orders of magnitude, depending on the control parameter.

Acknowledgements. We acknowledge the use of the computing facilities HECToR, part of the UK National Supercomputing Service in Edinburgh. All the authors acknowledge financial support from the UKs STFC (grant number STK/K000993/1). We gratefully acknowledge the support of NVIDIA Corporation with the donation of one Tesla K40 GPU used for this research.

References

[1] Parker, E.N. (1972) Topological dissipation and the small-scale fields in turbulent gases. *Astrophys. J.* **174**, 499

[2] Craig, I.J.D. & Sneyd, A.D. (1986) A dynamic relaxation technique for determining the structure and stability of coronal magnetic fields. *Astrophys. J.* **311**, 451-459

[3] Pontin, D.I. & Hornig, G. & Wilmot-Smith A.L. & Craig, I.J.D. (2009) Lagrangian relaxation schemes for calculating force-free magnetic fields. *Astrophys. J.* **700**, 1449

[4] Hyman, J.M. & Shashkov, M. (1997) Natural discretizations for the divergence, gradient, and curl on logically rectangular grids. *Comput. Math. Appl.* **33**, 81-104

[5] Hyman, J.M. & Shashkov, M. (1999) Mimetic discretizations for Maxwell's equations. *J. Comput. Phys.* **151**, 881–909

Notes

Eroding dipoles and vorticity growth for Euler flows in $\mathbb{R}^3$

S. Childress[1], A.D. Gilbert[2], P. Valiant[3]

[1] *Courant Institute of Mathematical Sciences, New York University, New York, NY 10012, USA*
[2] *Department of Mathematics, University of Exeter, Exeter EX4 4QF, UK*
[3] *Department of Computer Science, Brown University, Providence, RI 02912, USA*

Summary

A review of analyses based upon anti-parallel vortex structures suggests that structurally stable vortex structures with eroding circulation may offer a path to the study of rapid vorticity growth in solutions of Euler's equations in $\mathbb{R}^3$. We examine here the possible formation of such a structure in axisymmetric flow without swirl, leading to maximal growth of vorticity as $t^{4/3}$. Our study suggests that the optimizing flow giving the $t^{4/3}$ growth mimics an exact solution of Euler's equations representing an eroding toroidal vortex dipole which locally conserves kinetic energy. The dipole cross-section is a perturbation of the classical Sadovskii dipole having piecewise constant vorticity, which breaks the symmetry of closed streamlines. The structure of this perturbed Sadovskii dipole is analyzed asymptotically at large times, and its predicted properties are verified numerically. The generalization of this flow to an eroding "hairpin" dipole structure in three dimensions is outlined, and proposed as an initial condition favouring a rapid stretching of vortex lines, and possibly a blow-up in finite time. It is argued that the main obstacle to such blow-up is most likely the disruptive effect of axial flow. Our analysis also suggests that conservation of kinetic energy as realized in the eroding hairpin excludes a finite time blow-up for the corresponding Navier-Stokes model.

Notes

Time-dependent helical coordinates: derivation of the fundamental system and new conservation laws

D. Dierkes[1], M. Oberlack[2]

[1],[2] *Chair of fluid dynamics, TU Darmstadt, Germany*

Summary

The current work is devided into two parts. In the first part we derived a reduced system of time-dependent helical invariant Euler and Navier-Stokes equations. By employing Lie Symmetry analysis, the spatial dependence of all independent variables is reduced by one and the remaining variables are: the cylindrical radius r and the helical variable $\xi = \frac{z}{\alpha(t)} + b\varphi$, $b = const.$ and time t. Assuming $\alpha = const.$, we retain the classical helically symmetric case discussed in [1]. Further, setting the parameters $b = 0, \alpha = 1$, we obtain the well known axisymmetric case, while $b = 1$, $1/\alpha = 0$ corresponds to a plane flow.

The reduction was done in three steps: In a first step we developed a new *helical, time-dependent* coordinate system. In the second step we expressed the Euler and Navier-Stokes equations in the new coordinate system. Therefor the dependent variables (the velocities and the pressure) and the derivatives were expressed through helical coordinates. Finally, helical invariance, i.e. $\frac{\partial}{\partial \eta} \equiv 0$ was imposed, leading to a helical invariant system of equations. This has been done both for primitive variables as well as for the vorticity formulation.

In the second part we sought new conservation laws which can be found from the helical invariant Euler and Navier-Stokes equations derived in the first part. The conservation laws were generated with the help of the GEM-tool [2] that is included into MAPLE. From this, we derived a variety of new conservation laws, mostly extensions of existing conservation laws, while certain classical conservation laws do not admit extensions in the time dependent frame.

1 Fundamental system and governing equations

To develop the new helical coordinate system, we considered the helical symmetry of the Navier-Stokes equations, which relies on the combination of two common Lie Symmetry groups: (i) generalized Galilean invariance with comprises classical Galilean group and axial translation and (ii) the rotation about the same axis. In Cylindrical coordinates the infinitesimal generators are given by

$$X_R = \frac{\partial}{\partial \varphi}, \quad X_T = \alpha(t)\frac{\partial}{\partial z} + \dot{\alpha}(t)\frac{\partial}{\partial u^z} - z\ddot{\alpha}(t)\frac{\partial}{\partial p}, \tag{1}$$

where $\alpha(t)$ is an arbitrary time-dependent function.

Considering the linear combination

$$X = \frac{1}{b}X_R - X_T \tag{2}$$

and applying the method of similarity variables, we obtain the new helical coordinates

$$\eta = b\varphi, \quad \xi = b\varphi + \frac{z}{\alpha(t)}, \quad \tilde{r} = r \tag{3}$$

in terms of Cylindrical coordinates r, φ, z.

Further, the helical velocity components and the modified pressure are given by

$$u^\xi = \left(\frac{b}{r}u^\varphi + \frac{1}{\alpha}(u^z + \dot{\alpha}b\varphi)\right) \cdot B(r,t) \tag{4}$$

$$u^\eta = \left(\frac{1}{\alpha}u^\varphi - \frac{b}{r}(u^z + \dot{\alpha}b\varphi)\right) \cdot B(r,t), \tag{5}$$

$$\tilde{u}^r = u^r, \qquad \tilde{p} = p + \frac{1}{2}\frac{\ddot{\alpha}}{\alpha} z^2, \tag{6}$$

where $B(r,t)$ is a form function and given by $B(r,t) = \frac{r\alpha(t)}{\sqrt{r^2+b^2\alpha(t)^2}}$.

A transformation of the Euler- and Navier-Stokes equations into the helical coordinate system and imposing helical invariance, i.e. $\frac{\partial}{\partial\eta} \equiv 0$, leads to a system of helically invariant equations that describe helical flows involving an arbitrary time-dependent parameter function $\alpha(t)$. Hence, we may compute helically invariant flows with a time dependent pitch. This is illustrated in figure 1.

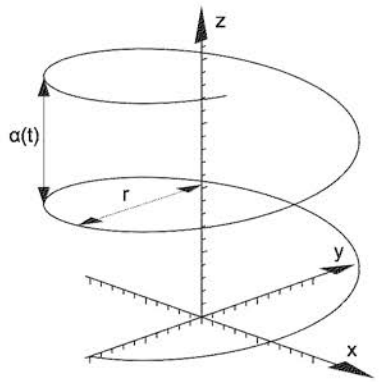

Fig. 1: An illustration of the helix ξ=const. with parameter function $\alpha(t)$ (cf. [1]).

2 New conservation laws for helical flows

In this second part we sought new local conservation laws of the form

$$\partial_t \Theta + \nabla \cdot \mathbf{\Phi} = 0, \tag{7}$$

where $\nabla \cdot \mathbf{\Phi} = \partial_i \Phi^i = \partial_1 \Phi^1 + \partial_2 \Phi^2 + \ldots + \partial_{n-1} \Phi^{n-1}$ is the spatial divergence. The quantity Θ is called density, whereas Φ^i are the spatial fluxes of the conservation law. To derive new sets of conservation laws we used the direct construction method [3]. We finally obtained multiple new local conservation laws, involving families of conservation laws, which are extensions of the classical case [1] wherein the parameter function α was assumed to be constant.

In primitive variables, one of the derived conservation laws is, e.g., an extension of the conservation of the z-projection of angular momentum:

$$\Theta = \alpha r B \left(\frac{1}{\alpha} u^\eta + \frac{b}{r} u^\xi\right) = \alpha r u^\varphi, \quad \Phi^r = \alpha r u^r u^\varphi, \quad \Phi^\xi = \alpha \left(r u^\xi u^\varphi + bBp\right) - \dot{\alpha} r \xi B u^\varphi. \tag{8}$$

We further obtained extensions of the conservation of generalized momenta and angular momenta and vorticity based conservation laws.

References

[1] Kelbin, Olga and Cheviakov, Alexei F and Oberlack, Martin (2013) New conservation laws of helically symmetric, plane and rotationally symmetric viscous and inviscid flows. In *Journal of Fluid Mechanics* 2013 **721**, pp. 340–366. Cambridge Univ Press.

[2] Cheviakov, Alexei F. (2007) GeM software package for computation of symmetries and conservation laws of differential equations. In *Computer physics communications* 2007 **176**(1), pp. 48–61. Elsevier.

[3] Bluman, George W and Cheviakov, Alexei F and Anco, Stephen C (2010) Applications of symmetry methods to partial differential equations. Springer 2010.

Notes

Models for the geodynamo

E. Dormy

DMA, Ecole Normale Supérieure & CNRS, France

Modelling the origin of the Earth magnetic field has proven to be extremely challenging. This talk will provide a review on the current state of understanding of dynamo action in rotating spherical shells. Numerical simulations will be presented, and tentatively related to theoretical expectations. In order to assess the relevance of existing numerical models to the geodynamo, it is particularly enlightening to ponder the different forces balances at work in numerical models. The over-estimated role of viscous dissipation (in the bulk of the flow or in viscous boundary layers) is shown to be particularly important in most models. An emphasis will be placed on the nature of the dynamo bifurcation. I will highlight in particular the occurrence of both the weak and the strong field dynamo branches in numerical models.

Notes

Free surface cusps and air entrainment

J. Eggers

Department of Mathematics, University of Bristol, UK

Summary

The generic pathway for entrainment of one phase into another is through singularities on the free surface between the phases. This has been well established for viscous fluids, both theoretically and experimentally. We provide evidence that similar principles are at work at low viscosity, for example for the entrainment of air into water.

Cusp singularities on the free surface of a viscous fluid have been found in Jeong and Moffatt's seminal work [1]. The tip of the cusp is regularized by the presence of surface tension, and the characteristic scale of the tip is set by a competition between viscosity and surface tension. The local scaling structure of the cusp can be understood in terms of a geometrical argument [2]. This suggests that the same structure should be observed generically, regardless of the nature of the driving flow. The same argument also puts constraints on the form of the singularity in three dimensions, which might be called the "scars" of the free surface.

In viscous flow is has been shown ([3],[4]) that cusp singularities are the locus where another phase (such as air) is entrained into the fluid. The reason is that the air which is sucked into the cusp builds up a lubrication pressure, which drives a bifurcation. A sheet of air is dragged into the fluid, which may greatly enhance the penetration of a fluid into another fluid, because the air "coates" the fluid.

These arguments suggest that air entrainment by a similar local mechanism is not possible in the case of water, because the capillary number, which sets the balance between viscous and surface tension forces, is small for realistic flow speeds. However, as shown in [5], cusp singularities may also arise as a result of inertial forces alone, at least if no surface tension is present. A similar point was made in [6], where it was argued that scars, as seen in Fig. 1, are the locus where air is entrained into the fluid [6]. Similar phenomena are observed frequently when watching a mountain stream, where places of a highly deformed free surface coincide with the presence of bubbles.

Adding surface surface tension, one finds that a inertia and surface tension cannot balance in the same way that viscous forces and surface tension balance to form a rounded cusp. Instead, entrainment of air into water must be an unsteady process, during which bubbles are entrained sequentially. Simulations using the Gerris software confirm this. We will also report on a new series of experiments with smooth jets of water impinging vertically onto a bath of water. A critical speed exists above which air is entrained. This supports the idea that entrainment at small viscosity is controlled by a local process.

Fig. 1: The free surface of a turbulent flow. On the surface a network of grooves or "scars" is visible.

References

[1] J.-T. Jeong and H. K. Moffatt. Free-surface cusps associated with a flow at low Reynolds numbers. *J. Fluid Mech.*, 241:1–22, 1992.

[2] J. Eggers and M. A. Fontelos. Cusps in interfacial problems. *Panoramas et Synthèses*, 38:69, 2013.

[3] J. Eggers. Air entrainment through free-surface cusps. *Phys. Rev. Lett.*, 86:4290, 2001.

[4] E. Lorenceau, D. Quéré, and J. Eggers. Air entrainment by a viscous jet plunging into a bath. *Phys. Rev. Lett.*, 93:254501, 2004.

[5] J. Eggers and A. F. Smith. Free streamline flows with singularities. *J. Fluid Mech. 647*, 647:187, 2010.

[6] M. Brocchini and D. H. Peregrine. The dynamics of strong turbulence at free surfaces. Part 1. Description. *J. Fluid Mech.*, 449:225–254, 2001.

Notes

Atomic superfluids: a new context for topological fluid dynamics

G. Ferrari[1], L. Galantucci[2], C. F. Barenghi[2], E. Iseni[1], T. Bienaimé[1], M. Barbiero[1], S. Serafini[1], F. Dalfovo[1], G. Lamporesi[1]

[1] *INO-CNR BEC Center and Dipartimento di Fisica, Università di Trento, Italy*
[2] *Joint Quantum Centre Durham-Newcastle and School of Mathematics and Statistics, Newcastle University, United Kingdom*

Summary

Single vortices in harmonically trapped atomic Bose-Einstein condensates (BECs) precess around the center following elliptical orbits. We experimentally image such vortices in real time and characterise their dynamics in a bounded atomic superfluid. We report evidence of vortex-vortex interaction in terms of faster dissipation and deviation of the orbits at the crossing.

Vortex interaction is an essential feature of fluids dynamics and plays a key role in superfluid helium [1], superconductors [2], neutron stars [3] and magnetohydrodynamics [4]. The interaction between vortices is crucial for understanding the formation of vortex lattices in rotating superfluids, and is the basic mechanism leading to quantum turbulence *via* vortex reconnection [5, 6]. Vortices have been extensively investigated in atomic gases [7], where a variety of techniques permits the observation of configurations consisting of one vortex up to a few hundreds vortices, interacting in a clean environment and on spatial scales ranging from the healing length (core size) ξ to few tens of ξ. The fact that atoms are confined by external fields of tunable geometry makes atomic condensates eminently suitable to explore the physics of reconnection and dissipation in inhomogeneous systems, where the presence of boundaries plays a crucial role both to the equilibrium and to the dynamical properties of vortices (see Fig. 1 (left)). Seminal experiments were performed in rotating Bose-Einstein condensates, where the effect of rotation and long-range interaction favors vortex alignment and the formation of vortex lattices and hence crossing and reconnection mechanisms are inhibited.

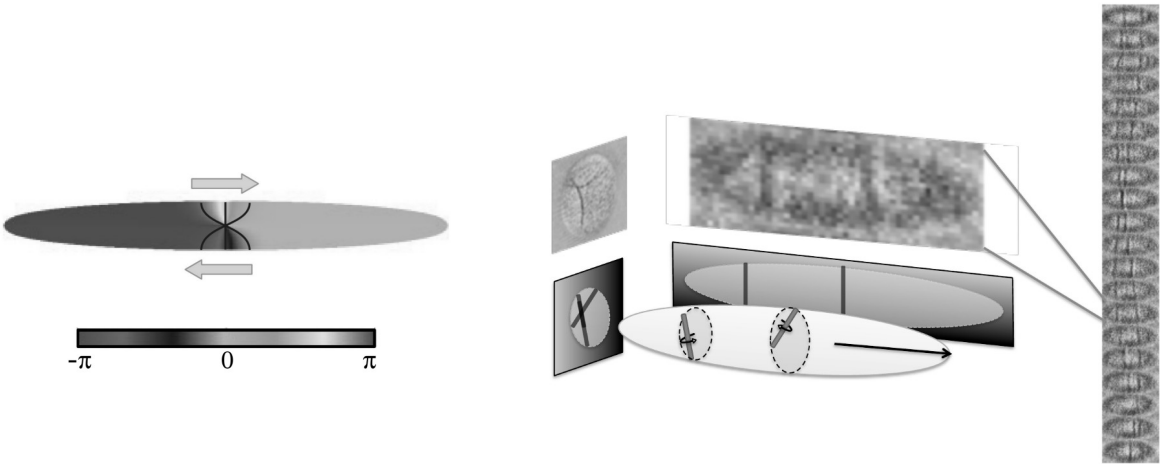

Fig. 1: (Left): phase profile of a stationary vortex in a cigar-shaped Bose-Einstein condensate shows how the boundary of the condensate deforms equiphase surfaces as compared to the usual cylindrically symmetric winding around the core in homogeneous superfluids. (Right): sketches of two vortices orbiting within an elongated, cylindrically symmetric BEC, their projection along the axial and one of the radial directions, and typical experimental images (reddish pictures). The column at the right represents a typical set of consecutive snapshots showing the evolution of a pair of vortices projected along the radial direction.

Interacting vortices have been observed in nonrotating oblate BECs, where vortex lines are short and either parallel or antiparallel, thus behaving as pointlike particles dominated by their long-range interaction in a quasi-2D background.

In our experiment we use a cigar-shaped BEC and, because of the boundary conditions imposed by the tight radial confinement, each vortex lies in a plane perpendicular to the long axis z of the trap, such to minimise its length and therefore its energy, as in the solitonic vortex configuration predicted in Refs. [8] and recently observed both in a BEC [9] and in a superfluid Fermi gas [10]. Our vortices are stochastically produced via the Kibble-Zurek mechanism [11] resulting in a random distribution both of the alignment and of the orbits; vortex dynamics is studied using a quasi-real time imaging (see Fig. 1 (right)) [12]. This experimental set-up represents an ideal testbed for the study of 3D vortex-vortex interactions. The capability of monitoring the position of vortices in real-time [12] allows us to characterise reconnection dynamics, and opens the possibility of studying the role of helicity in quantum vortex systems.

References

[1] Russell J. Donnelly. *Quantized Vortices in Helium II.* Cambridge University Press, 1991.

[2] M. Tinkham. *Introduction to superconductivity.* Dover Publications, 1996.

[3] G. Baym and C. Pethick. Neutron stars. *Ann. Rev. Nucl. Sci.*, 25:27–77, 1975.

[4] C. C. Lalescu, Yi-K. Shi, G. L. Eyink, T. D. Drivas, E. T. Vishniac, and A. Lazarian. Inertial-range reconnection in magnetohydrodynamic turbulence and in the solar wind. *Phys. Rev. Lett.*, 115:025001, 2015.

[5] Matthew S. Paoletti and Daniel P. Lathrop. Quantum turbulence. *Ann. Rev. Cond. Matter Phys.*, 2(1):213–234, 2011.

[6] S. Zuccher, M. Caliari, A.W. Baggaley, and C.F. Barenghi. Quantum vortex reconnections. *Phys. of Fluids*, 24:125108, 2012.

[7] A.L. Fetter. Rotating trapped Bose-Einstein condensates. *Rev. Mod. Phys.*, 81:647, 2009.

[8] J. Brand and W. P. Reinhardt. Solitonic vortices and the fundamental modes of the snake instability: Possibility of observation in the gaseous Bose-Einstein condensate. *Phys. Rev. A*, 65:043612, 2002.

[9] S. Donadello, S. Serafini, M. Tylutki, L. P. Pitaevskii, F. Dalfovo, G. Lamporesi, and G. Ferrari. Observation of solitonic vortices in Bose-Einstein condensates. *Phys. Rev. Lett.*, 113:065302, 2014.

[10] M. J. H. Ku, W. Ji, B. Mukherjee, E. Guardado-Sanchez, L. W. Cheuk, T. Yefsah, and M. W. Zwierlein. Motion of a solitonic vortex in the BEC-BCS crossover. *Phys. Rev. Lett.*, 113:065301, 2014.

[11] G. Lamporesi, S. Donadello, S. Serafini, F. Dalfovo, and G. Ferrari. Spontaneous creation of Kibble-Zurek solitons in a bose-einstein condensate. *Nat. Phys.*, 9(10):656–660, 2013.

[12] S. Serafini, M. Barbiero, M. Debortoli, S. Donadello, F. Larcher, F. Dalfovo, G. Lamporesi, and G. Ferrari. Dynamics and interaction of vortex lines in an elongated Bose-Einstein Condensate. *Phys. Rev. Lett.*, 115:170402, 2015.

Notes

Are all the topological invariants of vortcity representable as cross-helicities?

Y. Fukumoto

Institute of Mathematics for Industry, Kyushu University, Japan

Summary

Integrals of an arbitrary function of the vorticity, two-dimensional topological invariants of an ideal barotropic fluid, take different guise from the helicity. Noether's theorem associated with the particle relabeling symmetry group for the Euler-Poincaré equations, leads us to a unified view that all the topological invariants of a barotropic fluid are variants of the cross-helicity. We show that the similar holds for the baroclinic fluid flows, the MHD and the relativistic fluid motion. It is likely that the topological invariants associated with the vorticity are necessarily representable in the form of the cross-helicities.

1 Introduction: Ideal Barotropic Flows

The helicity $\mathcal{H}[\boldsymbol{\omega}] = \int_{\mathcal{D}} \boldsymbol{u}\cdot\boldsymbol{\omega}\mathrm{d}\mathcal{V}$, with the velocity $\boldsymbol{u}(\boldsymbol{x},t)$ and the vorticity field $\boldsymbol{\omega} = \nabla\times\boldsymbol{u}$, is a distinguishing integral invariant of three-dimensional Euler flows of an ideal barotropic fluid. This invariant is tied with the invariance of linkage and knottedness of vortex filaments [1, 2]. For two-dimensional ideal barotropic flows on the xy-plane, the vorticity vector has the only the z-component $\boldsymbol{\omega} = \omega\boldsymbol{e}_z$ with $\boldsymbol{e}_z$ being the unit vector along the z-axis. Denoting the density field by ρ, there is a family of integral invariants, called the generalized enstrophy $Q[\omega,\rho] = \int \omega f\,(\omega/\rho)\,\mathrm{d}A$, where f is an arbitrary function of ω/ρ. In the Hamiltonian mechanics, Q is a Casimir invariant.

By topological invariants we mean integrals that are invariant with respect to arbitrary diffeomorphisms of the domain $\mathcal{D}$ onto itself. The diffeomorphism is generated by the velocity field $\boldsymbol{u}(\boldsymbol{x},t)$. For an ideal fluid, the generator $\boldsymbol{u}(\boldsymbol{x},t)$ is ruled by the Euler equations. The original definitions $\mathcal{H}$ and Q mask their genuine topological structure. For given $\boldsymbol{\omega}(\boldsymbol{x},t)$, there exists a vector potential $\boldsymbol{v}(\boldsymbol{x},t)$ satisfying $\boldsymbol{\omega} = \nabla\times\boldsymbol{v}$. If we forget the relation $\boldsymbol{\omega} = \nabla\times\boldsymbol{u}$ and take the uncurl of the vorticity equations, we obtain a generalized form of the Euler equations

$$\frac{\partial v_i}{\partial t} + (\boldsymbol{u}\cdot\nabla)\,v_i + v_j\frac{\partial u_j}{\partial x_i} = \frac{\partial \pi}{\partial x_i}, \tag{1}$$

where $\pi(\boldsymbol{x},t)$ is an arbitrary scalar field, and summation is taken for repeated index j. We call (1) the *Euler-Poincaré* equations [3]. When specialized to $\boldsymbol{v} = \boldsymbol{u}$, (1) reduces to the Euler equations. Noether's theorem dictates that behind every conservation lies a varitional symmetry. A topological invariant is characterized by the particle relabeling symmetry. By effecting this for (1), we obtain the cross-helicity as the Noether charge, regardless of spatial dimension,

$$\mathcal{H}_{\mathrm{C}}[\boldsymbol{\omega},\boldsymbol{F}] = \int_{\mathcal{D}} \boldsymbol{v}\cdot\boldsymbol{F}\,\mathrm{d}V; \quad \frac{D}{Dt}\left(\frac{\boldsymbol{F}}{\rho}\right) = \left(\frac{\boldsymbol{F}}{\rho}\cdot\nabla\right)\boldsymbol{u}, \quad \nabla\cdot\boldsymbol{F} = 0. \tag{2}$$

It is easy to show that $\boldsymbol{F} = \nabla\times f\boldsymbol{e}_z$ satisfies the second of (2). Upon substitution, the left of (2) reproduces Q in 2D [4], except for the surface term arising from partial integration.

The cross-helicity (2) unifies $\mathcal{H}$ and Q In the following sections, we inquire into the stratified flows, endowed with the baroclinic effect, and the ideal magnetohydrosynamics (MHD).

2 Stratified Flows

For motion of a stratified flow, the baroclinic effect no longer respects the property of the vorticity of being frozen into the flow. As a consequence, the vortex-line topology is no longer preserved.

We are requested to develop a means for identifying topological invariants. We appeal to Noether's theorem for the Euler-Poncaré equations extended to include the baroclinic effect. The end product of the associated conservation law is again the cross-helicity (2), though a constraint is enforced on the second equation of (2) so as to be compatible with the baraoclinic effect.

For three-dimensional non-isentropic ideal gas flows, Ertel's potential vorticity is convected without change of its magnitude, in addition to the specific entropy s,

$$q = \frac{1}{\rho}(\nabla \times \boldsymbol{u}) \cdot \nabla s; \quad \frac{Dq}{Dt} = 0. \tag{3}$$

The Casimir invariant is $C = \int \rho F(s, q) \mathrm{d}V$, for an arbitrary function F.

In the same way as before, we can prove that (2) is derived from the cross-helicity with the solenoidal vector field being subjected to the constraint $(\boldsymbol{F} \cdot \nabla)s = 0$. It is shown that the Casimir invariant C can be gained, with an appropriate choice of $\boldsymbol{F}$, from the cross-helicity of the form (2).

3 Magnetohydrodynamics (MHD)

For an ideal magnetohydrodynamics, the Lorentz force destroys the property of the vorticity being frozen into the fluid. Hameiri [6] showed that the most general conservation quantity takes the form of the cross helicity involving the solenoidal vector field $\boldsymbol{C}$ compatible with the magnetic field $\boldsymbol{B}$,

$$\mathcal{H}_{\mathrm{c}}[\boldsymbol{u}, \boldsymbol{C}] = \int_{\mathcal{D}} \boldsymbol{u} \cdot \boldsymbol{C} \mathrm{d}V, \quad \frac{\partial \boldsymbol{C}}{\partial t} = \nabla \times (\boldsymbol{u} \times \boldsymbol{C}), \quad \nabla \times \left(\boldsymbol{B} \times \frac{\boldsymbol{C}}{\rho} \right) = \boldsymbol{0}. \tag{4}$$

Noether's theorem in the variational framework for the Euler-Poncaré equations extended to include the Lorentz force brings in the cross helicity $\mathcal{H}_{\mathrm{c}}[\boldsymbol{v}, \boldsymbol{C}]$, with $\boldsymbol{u}$ replaced by the general one $\boldsymbol{v}$, for the Noether charge associated with the particle relabeling symmetry.

4 Conclusion

For relativistic motion of a charge fluid, the helicity can be defined as a three-dimensional integral with respect to the proper time [7]. The relativistic helicity is obtainable in the form of the cross-helicity by Noether's theorem [8]. With a collection of these examples, we are led to a belief that all the topological invariants including the vorticity are representable as the cross-helicities.

References

[1] Moffatt, H.K. (1969) The degree of knottedness of tangled vortex lines. *J. Fluid Mech.*1969 **35**, 117–129.

[2] Moffatt, H.K. & Ricca, R.L. (1992) Helicity and the Călugăreanu invariant. *Proc. R. Soc. Lond. A* 1992 **439**, 411–429.

[3] Holm, D.D., Marsden, J.E. & Ratiu, T.S. (1998) The Euler-Poincaré equations and semidirect products with applications to continuum theories, *Adv. Math.* 1998 **137**, 1–81.

[4] Fukumoto, Y. (2008) A unified view of topological invariants of fluid flows. *Topologica* 2008 **1**, 003.

[5] Fukumoto, Y. & Sakuma, H. (2013) A unified view of topological invariants of barotropic and baroclinic fluids and their application to formal stability analysis of three-dimensional ideal gas flow. *Procedia IUTAM* 2013 **7**, 213-222.

[6] Hameiri, E. (1998) Variational principles for equilibrium states with plasma flow, Phys Plasmas 1998 **5**, 3270-3281.

[7] Yoshida, Z. Kawazura, Y. & Yokoyama, T. (2014) Relativistic helicity and link in Minkowski space-time *J. Math. Phys.* 2014 **55**, 043101.

[8] Kawazura, Y., Yoshida, Z. & Fukumoto, Y. (2014) Relabeling symmetry in relativistic fluids and plasmas. *J. Phys. A: Math. Theor.* 2014 **47**, 465501.

Notes

Quantum vortex dynamics and reconnections in trapped Bose-Einstein Condensates

L. Galantucci[1], C. F. Barenghi[1], S. Serafini[2], F. Dalfovo[2], G. Lamporesi[2], G. Ferrari[2]

[1] *Joint Quantum Centre Durham-Newcastle and School of Mathematics and Statistics, Newcastle University, United Kingdom*

[2] *INO-CNR BEC Center and Dipartimento di Fisica, Università di Trento, Italy*

Summary

Numerical investigations of the trajectory of two vortices in three-dimensional elongated trapped Bose Einstein Condensates (BECs) are performed in the zero temperature limit. In particular, we observe unperturbed precession of the vortices around the centre of the condensate, bouncing dynamics and double reconnection events. A central role is played by features peculiar to trapped BECs namely density gradients and the influence of images. The numerical results are compared to very recent experimental observations of vortex reconnections.

Vortex dynamics and reconnections play a fundamental role in quantum turbulent flows which can be loosely defined as the most general dynamical motion of tangles of thin quantized vortex lines in quantum fluids [1]. In particular, quantum vortex reconnections are, to a large extent, responsible for energy and helicity transfers between different scales [2, 3], and the change of topology induced by reconnecting events plays a central role in the balance of the total helicity of the flow [3, 4]. This last topic, i.e., whether helicity is conserved in superfluid systems exhibiting reconnection events, is of great interest due to the fact that although dissipative processes are absent in superfluids in the zero temperature limit as in ideal (Euler) fluids, reconnection events may take place, changing, hence, the topology of the flow. Additional motivation arises from the growing interest in the topology of plasmas, liquid crystals, optical and biological structures. Several recent numerical studies have examined quantum vortex reconnections in homogeneous superfluids [3, 5, 6], as, due to their discrete nature, quantum vortices are easier identified and tracked than classical vortices. Experimentally, direct visualization of the dynamics of vortex lines in an elongated BEC has been recently investigated [7] (see Fig. 1 (left)), suggesting the possibility of *double reconnections*.

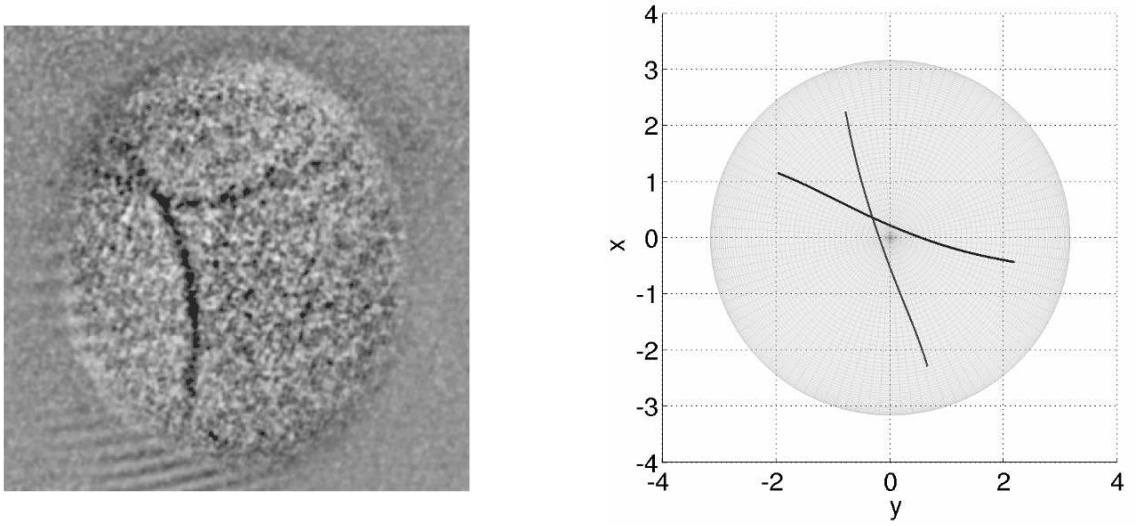

Fig. 1: (left): Experimental observation in a trapped BEC of two vortices produced via the Kibble–Zurek mechanism [8, 7]; (right): snapshot of the results achieved via the numerical simulations performed in the present study.

In this work we numerically solve the non–homogeneous Gross–Pitaevskii Equation for the condensate wavefunction inside an anisotropic harmonic trapping potential. The core of the vortices is tracked employing an algorithm based on the pseudo vorticity field [9] which allows to finely resolve the reconnection dynamics (Fig. 1 (right) shows, for instance, an instantaneous snapshot of the condensate where two vortices have been trailed). We observe different two–vortex interaction regimes depending on the orientation and curvature of the two vortices, their orbits and their initial distance: unperturbed precession around the centre of the condensate; *bounce dynamics*, where the vortices get closer before moving apart without reconnecting; double reconnection events. We reckon that the key ingredients driving the two–vortex dynamics are the anti–parallel preferred alignment of the two vortices due to energy conservation contraints, the impact of density gradients and the role of the images of the vortices with respect to the condensate's boundaries. The last two factors listed are peculiar to non–homogeneous trapped BECs, determining hence different reconnection dynamics with respect to homogeneous BECs [10].

References

[1] C. F. Barenghi, L. Skrbek, and K. P. Sreenivasan. Introduction to quantum turbulence. *Proc. Natl. Acad. Sci. USA*, 111(1):4647–4652, 2014.

[2] C. F. Barenghi, R. J. Donnelly, and Vinen W. F. *Quantized vortex dynamics and superfluid turbulence*. Springer Science & Business Media, 2001.

[3] M. W. Scheeler, D. Kleckner, D. Proment, G. L. Kindlmann, and W. T. M. Irvine. Helicity conservation by flow across scales in reconnecting vortex links and knots. *Proceedings of the National Academy of Sciences*, 111:15350, 2014.

[4] C. E. Laing, R. L. Ricca, and L. S. De Witt. Conservation of writhe helicity under anti-parallel reconnection. *Scientific reports*, 5, 2015.

[5] D. Kleckner, L. H. Kauffman, and W. T. M. Irvine. How superfluid vortex knots untie. *arXiv preprint arXiv:1507.07579*, 2015.

[6] S. Zuccher and R. L Ricca. Helicity conservation under quantum reconnection of vortex rings. *Physical Review E*, 92(6):061001, 2015.

[7] S. Serafini, M. Barbiero, M. Debortoli, S. Donadello, F. Larcher, F. Dalfovo, G. Lamporesi, and G. Ferrari. Dynamics and interaction of vortex lines in an elongated bose-einstein condensate. *Physical Review letters*, 115(17):170402, 2015.

[8] G. Lamporesi, S. Donadello, S. Serafini, F. Dalfovo, and G. Ferrari. Spontaneous creation of kibble-zurek solitons in a bose-einstein condensate. *Nature Physics*, 9(10):656–660, 2013.

[9] C. Rorai, J. Skipper, R. M. Kerr, and K. R. Sreenivasan. Approach and separation of quantum vortices with balanced cores. *arXiv preprint arXiv:1410.1259*, 2014.

[10] S. Zuccher, M. Caliari, A. W. Baggaley, and C. F. Barenghi. Quantum vortex reconnections. *Phys. Fluids*, 24:125108, 2012.

Notes

The life and science of Konrad Bajer

A.D. Gilbert

Mathematics Research Institute, University of Exeter, UK

In August 2014, Dr. Konrad Bajer sadly passed away, leaving behind many friends, students and colleagues who were inspired by his scientific contributions, his ability and enthusiasm for organising all manner of conferences, his teaching, and his irrepressible zest for life. This short talk will aim to outline his life and his scientific legacy.

Notes

Geometric generalised Lagrangian mean theories

Andrew D. Gilbert[1], Jacques Vanneste[2]

[1] *Mathematics and Computer Science, University of Exeter, U.K.*
[2] *School of Mathematics, University of Edinburgh, U.K.*

Summary

In many applications an ensemble of fluid flows consists of waves riding on a mean flow. Averaging over waves then yields terms in the equation for the mean flow which parameterise the effect of the waves. Theory based on Lagrangian averaging — so called *Generalised Lagrangian Mean* theory — that is tracking the location of fluid parcels, goes back to the works of Soward in 1972 and Andrews & McIntyre in 1978 for *GLM*, and more recently Soward & Roberts 2010 who introduced another averaging method called *glm*. Our goal here is to give a unified approach to these theories using tools from differential geometry and working in the general setting of a flow on a manifold M. As well as the GLM and glm, we introduce Lagrangian means based on geodesics in SDiff(M) as a geometrically sound definition in a general setting. We discuss the advantages and disadvantages of these theories.

Notes

Exact solutions describing MHD vortex flows

S.V. Golovin[1,2]

[1] *Lavrentyev Institute of Hydrodynamics, Novosibirsk, Russia*
[2] *Novosibirsk State University, Novosibirsk, Russia*

Summary

We present two types of exact solutions of MHD equations describing vortex flows of electrically conducting fluid. In the first type of solutions the total pressure is constant. The fluid is ideal with infinite magnetic and kinematic Reynolds numbers. The solutions possess a significant functional arbitrariness and describe jet flows with non-trivial shape of magnetic tubes. The second type of solutions determines a stationary cylindrical vortex inside a resting cylinder with a conductor of an electrical current on the axis. The fluid is viscous with a finite electrical conductivity. The vortex fluid flow concentrates the magnetic field near the axis of the cylinder.

Vortex flows of electrically conducting fluid are widely presented in natural and technical processes. Localized vortex structures in liquid core of the Earth driven by the convection are thought to be responsible for the generation of the Earth's magnetic field [1]. Experimental and numerical modelling of such dynamo processes also extensively use various vortex-type flows [2]. Theoretical analysis of MHD equations based on the geometrical interpretation of the equations and on invariants such as the helicity [3] produces general theorems concerning the behaviour of the electrically conducting fluid. Most of these theories lack examples of exact solutions of MHD equations that describe 3D structures in case of non-collinear velocity and magnetic fields. In our work we present two types of exact solutions to MHD equations describing vortex flows for ideal and viscous electrically conducting fluid.

1 Solutions with constant total pressure

We observe a system of nonlinear ideal MHD equations (zero kinematic and magnetic viscosities). In the general case of non-collinear velocity and magnetic vector fields we introduce a special curvilinear coordinate system where streamlines and magnetic lines of the flow plays a role of coordinate curves [4]. This reduces MHD equations to a certain simpler form. Any solution of the obtained system allows explicit description of the geometry of the flow due to the direct representation of magnetic lines and particles trajectories. For this system of equations we observe a class of solutions with constant total pressure. It is possible to give a complete classification of such solutions in case of stationary flows [5]. In particular, we show that magnetic surfaces of the stationary MHD flows with constant total pressure are translational surfaces, i.e. are swept out by translating one curve rigidly along another curve.

In the non-stationary case the complete classification of solutions with constant total pressure is not yet given due to the technical difficulty of the problem. However, particular examples demonstrate that class of such solutions is very reach and contain topologically non-trivial flows. In particular, we obtained explicit solutions describing fluid flows with toroidal and knotted magnetic tubes (see Figure 1a,b) [6], or non-stationary solutions describing jet flows within fixed cylindrical magnetic tubes (see Figure 1c,d) [7].

2 Stationary cylindrical vortex

For the case of finite magnetic and kinematic viscosities we construct an exact solution of MHD equations describing a flow in a stationary semi-infinite cylinder with a conductor of electrical current

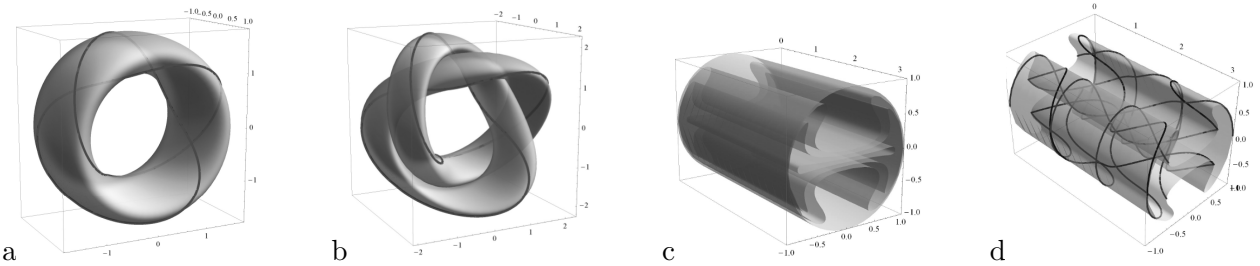

Fig. 1: Examples of magnetic surfaces on exact solutions. The curves on the surfaces are magnetic lines and particle trajectories.

along the cylinder axis. Kinematics of the flow coincide with the one in absence of the magnetic field [8]. Magnetic field has only radial and axial components in the cylindrical coordinates. Action of the Lorenz force is compensated by the additional fluid pressure [9].

In case of non-zero kinematic viscosity of fluid, the flow is directed from the periphery to the axis of the cylinder under the pressure gradient; at that the flow changes the direction as it reaches the bottom of the cylinder and turns around the cylinder axis. The fluid flow concentrates the magnetic lines near the axis so that the magnetic field exponentially decreases towards the periphery. In case of zero kinematic viscosity and finite magnetic viscosity, the solution describes more complicated flow patterns, where the flow is stratified in cylindrical layers with a vortex flow in each layer. The magnetic field is concentrated near the attracting cylinders within the flow.

The obtained classes of exact solutions can be usefusl for theoretical analysis of vortex flows of electrically conducting fluid as well as for testing numerical algorithms.

Acknowledgements. The work is partially supported by RSF (grant 15-11-20013).

References

[1] Moffatt H. K. (1992) Helicity in laminar and turbulent flow. *Ann. Rev. Fluid Mech.* 24 281–312.

[2] Stefani F., Gailitis A., Gerbeth G. (2008) Magnetohydrodynamic experiments on cosmic magnetic fields. *ZAMM.* 88(12) 930–954.

[3] Arnold, V.I. & Khesin, B.A. (1998) *Topological Methods in Hydrodynamics.* Applied Mathematical Sciences **125**, Springer-Verlag, Berlin.

[4] Golovin S. V. (2010) Analytical description of stationary ideal MHD flows with constant total pressure. *Phys. Lett. A.* 374 901-905.

[5] Golovin S. V., Krutikov M. K. (2012) Complete classification of stationary flows with constant total pressure of ideal incompressible infinitely conducting fluid. *J. Phys. A: Math. Theor.* 45 235501 (24pp)

[6] Golovin S. V. (2011) Natural curvilinear coordinates for ideal MHD equations. Non-stationary flows with constant total pressure. *Phys. Lett. A* 375 283-290.

[7] Golovin, S. V., Dudnik, M. N. (2014) Unsteady flows with a constant total pressure, described by the equations of ideal magnetohydrodynamics. *J. Appl. Mech. Tech. Phys.* 55(2) 234–246.

[8] Aristov, S. N. (2001) A stationary cylindrical vortex in a viscous fluid. *Dokl. Phys.* 46(4) 251–253.

[9] Baikin, A. N., Golovin, S. V. (2013). Stationary cylindrical vortex in a viscous electrically conducting fluid. *J. Appl. Mech. Tech. Phys.* 54(4) 541–551.

Notes

Instabilities in viscosity and density stratified flow

Rama Govindarajan[1], Sharath Jose[1], Kirti Chandra Sahu[2]

[1] *TIFR Centre for Interdisciplinary Sciences, Tata Institute of Fundamental Research, Hyderabad, India*

[2] *Department of Chemical Engineering, Indian Institute of Technology, Hyderabad, India*

Summary

Viscosity stratification can create new instabilities in a shear flow, or act to stabilise it. This talk will examine mechanisms of such instabilities, and situations where they can occur. It will also contrast these with instabilities in density-stratified flows, and examine the combination of the two. The aim of this talk is to invite future research on viscosity stratification in the context of the Sun or Earth's interior.

1 Viscosity stratification

Viscosity variations occur in any flow where temperature or concentration is a function of space and time. Viscosity can also be a function of pressure at very high pressure, or a function of shear and its history (non-Newtonian behaviour). Such variations can affect the flow in a profound manner, especially in its stability behaviour, as first shown by Yih [1]. In the Sun, the Earth's core and mantle [2], blood and sugar syrup, viscosity stratifications occur, sometimes viscosity varies by several orders of magnitude.

At high Reynolds numbers, viscous terms appear as a singular perturbation in the linear stability operator of shear flows. Even a small stratification in viscosity, caused for example by variations in composition, temperature or due to the non-Newtonian nature of the fluid, can therefore have a large effect on the stability. This can result in new modes of instability or in large stabilisation. One mechanism for a new instability is when a viscosity-stratified layer overlaps with the critical layer of the dominant disturbance eigenmode.

The talk will first summarise work on instabilities in viscosity stratified flow (mainly from [3] and references therein). This will be followed by an examination of density stratification and how the two kinds of stratification work together. Linear instability, transient growth and behaviour in the regime of nonlinear dynamics will be discussed.

2 Conclusions

A broad indication (with many exceptions) is that flow becomes more unstable as the Reynolds number increases (this is to be expected), as the viscosity in the higher shear region increases, and as the ratio of diffusivities (the Schmidt or Prandtl number) increases.

Acknowledgements. Financial support from the conference organisers is gratefully acknowledged.

References

[1] Yih, C.S. (1967) Instability due to viscosity stratification. *J Fluid Mech.* 1967 **27**:337-352.

[2] Rudolph, M.L., Leki?, V., & Lithgow-Bertellon, C. (2015) Viscosity jump in Earths mid-mantle. *Science* 2015 **350.6266**: 1349-1352.

[3] Govindarajan, R. & Sahu, K.C. (2014) Instabilities in viscosity stratified flow *Ann. Rev. Fluid Mech.* 2014 **46**: 331-353.

Notes

Role of vortex reconnection in creation of strong vortices

Y. Hattori[1]

[1] *Institute of Fluid Science, Tohoku University, Japan*

Summary

It is shown by direct numerical simulation that selective decay of inviscid invariants leads to concentration of vorticity in a destabilized vortex. In addition to our previous results it is observed in time evolution of the two-dimensional flattened Taylor-Green vortices disturbed by an unstable eigenmode and a vortex pair disturbed by a localized wave packet. Reconnection and the subsequent annihilation of pair of thin vortex tubes are responsible for the selective decay as the loss of circulation is much larger than that of angular momentum.

1 Introduction

Creation of concentrated vortices like tornadoes and tropical cyclones in rotating fluids is of much interest in atmospheric flows since they sometimes cause severe natural disasters. As pointed out by Scorer [1] purely hydrodynamic mechanism by which weak vorticity scattered in a wide region concentrates to form a strong vortex is believed to be important at least for tropical cyclones. However, there have been no satisfactory theory that explains it and predicts under what conditions it works.

Recently we showed that selective decay of inviscid invariants leads to concentration of vorticity in a destabilized vortex [2]. Here by selective decay we mean that circulation of the mean flow decays much faster than the angular momentum or energy. In this study localized disturbances of small amplitude were super-imposed onto the two-dimensional flattened Taylor-Green vortices to trigger the elliptic instability. Direct numerical simulation showed that circulation decays much faster than angular momentum and energy in the later stage of nonlinear evolution of the disturbance; simultaneously a sharp peak is formed in the vorticity distribution of the mean flow. The key mechanism of the selective decay turned out to be *reconnection* and the subsequent annihilation of pairs of thin vortices at the cell boundaries.

In this paper, we show that the mechanism found in [2] works in general by investigating two problems: Evolutions of (i) the two-dimensional flattened Taylor-Green vortices disturbed by an unstable eigenmode; and (ii) a vortex pair disturbed by a localized wave packet.

2 Creation of strong vortices and role of vortex reconnection

Here we show that not only localized disturbance but also unstable eigenmode can trigger selective decay and thereby concentration of vorticity in the Taylor-Green vortices provided that the wavelength is short. The unstable eigenmodes are obtained by numerical stability analysis of the linearized Navier-Stokes equations. Then the three-dimensional (nonlinear) Navier-Stokes equations are solved by Fourier spectral method. The Reynolds number based on the circulation is $Re_\Gamma = 1.31 \times 10^5$. The wavenumber of the unstable eigenmode is $k_z = 8.95$.

Figure 1 shows that sharp peak of vorticity is observed in the averaged mean flow at $t = 170$ and 260. In the iso-surface of the magnitude of vorticity at $t = 240$ pairs of thin vortex tubes appear near the cell boundaries as in [2]. The loss of circulation of mean flow is much larger than that of angular momentum when these pairs reconnect and eventually annihilate as explained for a 2D vortex in a circular domain: if we express circulation and angular momentum in terms of vorticity $\Gamma = \int \omega dA$, $A = \int (1/2)(r_0^2 - r^2)\omega dA$, the weight function for circulation is constant while that of angular momentum vanishes at the cell boundary; thus the cancellation of vorticity at the cell boundary does not change the angular momentum very much.

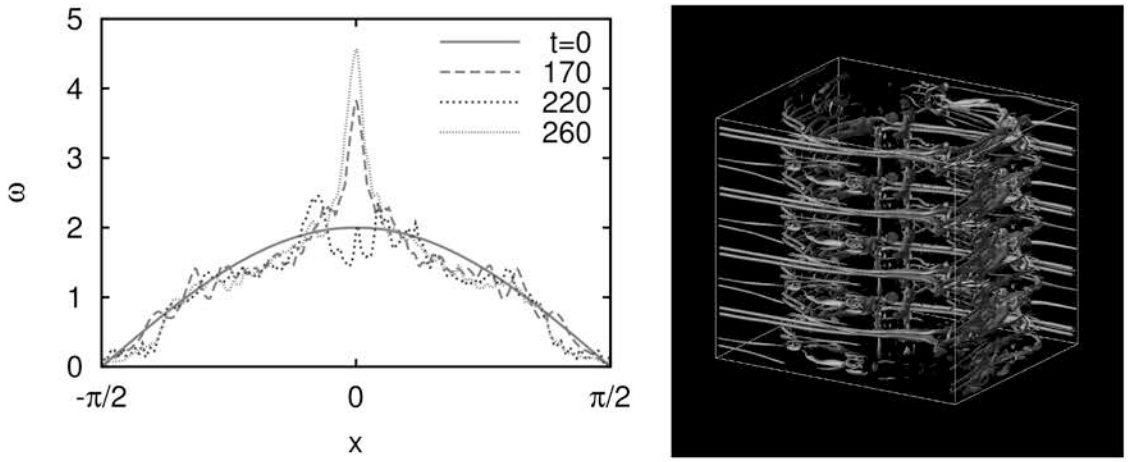

Fig. 1: (Left) Vorticity distribution showing concentration of vorticity. (Right) Iso-surface of magnitude of vorticity before concentration of vorticity.

3 Concentration of vorticity in a vortex pair

Next, we show that selective decay and concentration of vorticity occur in a vortex pair disturbed by a localized wave packet. The size of the unit region is $2\pi \times 2\pi \times \pi/4$, the shortest z-direction being parallel to the undisturbed vorticity.

Figure 2 shows that selective decay is observed for $25 \leq t \leq 30$; circulation decreases faster than angular momentum and energy. At $t = 26$ strong vorticity is observed near the center of the vortices; the maximum vorticity is about 2.5 times the initial maximum. The detailed mechanism of selective decay in this case will be reported in the talk.

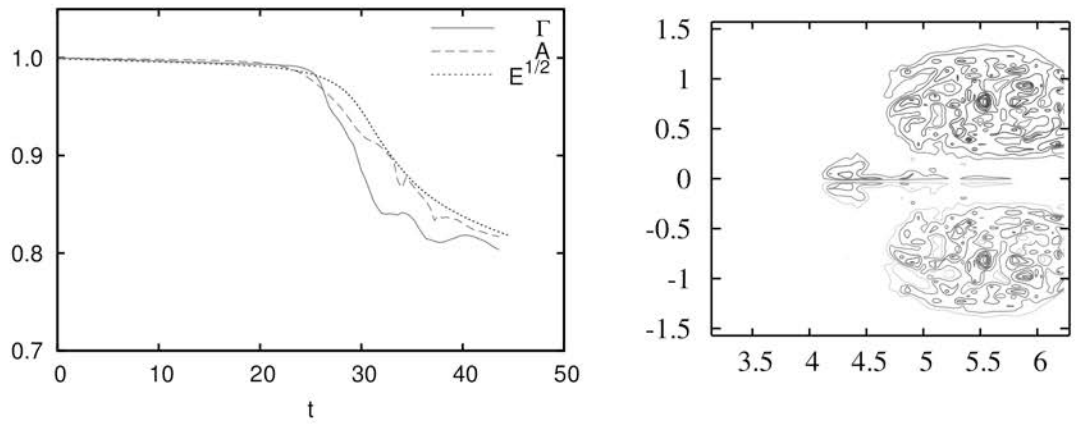

Fig. 2: (Left) Time evolution of inviscid invariants showing selective decay. (Right) Contours of averaged vorticity at $t = 26$.

References

[1] Scorer, R. S. (1966) Origin of cyclones. *Science J.* 1966 **2**, 46–52,

[2] Hattori, Y. (2016) Concentration of Vorticity in a Destabilized Vortex due to Selective Decay. submitted.

Notes

The intrinsic twist of superfluid vortices: Can a line be twisted?

N. Hietala, R. Hänninen

Department of Applied Physics, Aalto University, Finland

Summary

Since superfluid vortices are line defects, the idea of intrinsic structure sounds bizarre. Vortex filament model simulations show that the intrinsic twist is required for the helicity conservation. The intrinsic twist may be defined as the winding of the quantum mechanical phase. The level surfaces of the phase are Seifert surfaces. In Seifert framing the helicity is always zero. This makes the conservation of helicity trivial for superfluids.

1 Introduction

Close to absolute zero, superfluids resemble ideal fluids perhaps better than any other system. Vorticity is possible only in form of line-like topological defects. Since superfluid vortices are line objects, it is hard to think them to have any intrinsic structure. Recently, it has been suggested that the quantum mechanical phase endows superfluid vortices with intrinsic structure [1, 2, 3]. One can use the direction of the zero phase to define a spanwise vector giving the intrinsic twist. Here, we explore the consequences of this definition.

If the vorticity is confined to tube-like structures, the helicity, $H = \int \mathbf{v} \cdot \boldsymbol{\omega} \, \mathrm{d}V$, is the sum of the (Gauss) linking numbers and self-linking numbers [4]. The self-linking number is given by the sum of the writhe (W) and the twist (T) of the vortex. Twisting is possible in two ways: the Frenet–Serret frame may turn along the vortex (T_{tors}, torsion) or the direction of the intrinsic structure may change in relation to the Frenet–Serret frame (T_{twist}, intrinsic twist).

Thus the helicity may be given as:

$$H = \sum_{i \neq j} \Gamma_i \Gamma_j Lk_{ij} + \sum_i \Gamma_i^2 (W + T_{\mathrm{tors}} + T_{\mathrm{twist}}). \tag{1}$$

Linking number and self-linking number are topological invariants, but the components of the self-linking number are not. Writhing of the vortex may be converted to twisting and vice versa. Also, the self-linking number is an invariant, but its value depends on a chosen frame, i.e. how we determine the spanwise vector.

2 Superfluid vortices

The superfluid component of helium-4 superfluid is described with a complex scalar order parameter $\psi = \psi_0 e^{i\phi(\mathbf{r})}$. The quantum mechanical phase is the velocity potential of the fluid motion, and the velocity is given as $\mathbf{v}_s(\mathbf{r}) = \nabla\phi(\mathbf{r})$. Potential motion is always irrotational. Vorticity is possibly only in form of quantized line-like topological defects all having the same circulation.

In reality, superfluid vortices have a small but finite core size. However, the density of the superfluid component goes to zero in the core. Vortices can be thought as empty cavities, and hence lacking any intrinsic structure. Yet it is possible to define a direction of intrinsic structure using the phase.

Taking a vector on the level surface $\phi = 0$ and requiring it to be perpendicular to the tangent of the vortex line, we can define the spanwise vector and endow the vortex with a ribbon structure. This definition is equivalent to the Seifert framing. It can be shown that the level surfaces of the phase are Seifert surfaces of the vortex knot (or unknot). This means that the helicity is zero [5].

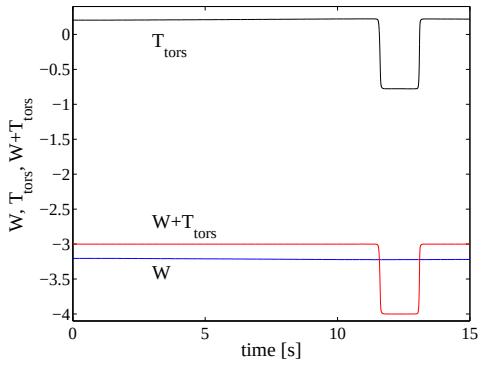

Fig. 1: Evolution of writhe and torsion in the vortex filament model simulation of a trefoil knot at zero temperature. During the dynamics, an inflection point appears and the torsion jumps. This jump must be compensated by a change in the intrinsic twist.

One way to add helicity to the fluid is to have intrinsic twisting. Let us consider a perfectly circular vortex loop. We cannot twist the phase since it would have singularity in the center of the ring. The phase must be defined everywhere, except exactly on the vortex lines.

The phase is twisted when another vortex threads the ring. For two vortex rings in a form of the Hopf link, the phases wound in both vortices. If we now calculate the helicity, we have contributions both from the linking number and the intrinsic twists giving zero total helicity. If the two rings reconnect, we end up with a single ring with zero helicity, so the helicity conservation is trivial.

In the vortex filament model, one has the freedom to choose the tangential velocity of the vortex points. By exploiting this freedom, one may add axial velocity which answers for the conservation of the helicity just like the intrinsic twist would do.

3 Conclusions

The phase is the most natural way to endow the superfluid vortices with an intrinsic structure. As a result, superfluids have zero helicity. The alternative is to say that vortices have no intrinsic structure and there is no twist. This would mean that the helicity is not an invariant of superfluids, since the writhe may change during the dynamics. The change in the writhe must be compensated by change in the twist, if we want that the helicity is conserved. It is not even enough to include just the torsion part of the total twist, since inflection points may occur in the dynamics (see Figure 1). Internal twist is needed to compensate the jump in torsion at the inflection points.

Another possibility is to say that since superfluid vortices have a finite core size, it is possible for the vorticity to have some intrinsic twisting just like in classical vortex tubes. However, thinking about the superfluid vortices really as an approximation of the ideal single vorticity lines fits well with the idea of quantization of the circulation. Thus we can only conclude that superfluids significantly differ from classical fluids.

Acknowledgements. We wish to thank H. Salman, J. Karimäki and S. Autti for useful discussions.

References

[1] Baggaley, A. W. (2014) Helicity transfer during quantized vortex reconnection. *arXiv*:1403.81821v1.

[2] Klecner, D., Kauffman, L. H. & Irvine, W. T. M. (2015) How superfluid vortex knots untie. *arXiv*:1507.07579.

[3] Zuccher, S. & Ricca, R. L. (2015) Helicity conservation under quantum reconnection of vortex rings. *Phys. Rev. E* 2015 **92**, 061001.

[4] Moffatt, H. K. & Ricca, R. L. (1992) Helicity and the Călugăreanu Invariant. *Proc. R. Soc. A* 1992 **439**, 411–429.

[5] Akhmet'ev, P. & Ruzmaikin, A. (1992) Borromeanism and Bordism. In *Topological aspects of the dynamics of fluids and plasmas* (ed. H.K. Moffatt et al.), pp. 249–264. Dordrecht, Kluwe.

Notes

Variational formalism for linear growth rates of collisionless tearing modes

M. Hirota

Institute of Fluid Science, Tohoku University, Japan

Summary

Growth rates of linear tearing instabilities in collisionless plasmas are investigated by formulating a variational principle in the form of Rayleigh quotient. In contrast to the conventional asymptotic matching, this method is basically applicable to static (no $E \times B$ and diamagnetic drifts) and non-dissipative (purely collisionless) plasmas, but it can elucidate the general roles of the microscopic effects such as electron inertia and finite gyroradius, without specifying the equilibrium geometry or assuming the separations among the microscopic scales. The variational form is also useful from numerical point of view, in that the maximum growth rate can be calculated efficiently by using an iteration algorithm.

1 Outline

Magnetic reconnection in collisionless plasma is one of the phenomena that are being most actively researched in plasma physics. Since the magnetic reconnections in astrophysical and magnetically-confined plasmas are often too fast to be explained by the resistive diffusion process, other non-dissipative effects (such as electron inertia, Hall current, finite gyroradius and so on) should be taken into account for the purpose of extending the classical MHD framework. Although these effects are usually effective only in the neighborhood of the reconnection point, one has to choose a plausible model from a variety of two-fluid, gyrofluid, gyrokinetic equations, depending on how generally and how accurately one wants to incorporate the microscopic "nonideal MHD" effects. The fundamental problem is to understand the multiscale physics that causes fast magnetic reconnection, which remains challenging both theoretically and computationally.

The tearing instability is regarded as the trigger of magnetic reconnection. In both collisional and collisionless cases, the linear growth rate of the tearing mode is well investigated by using asymptotic matching expansion, in which the nonideal MHD effects are considered only inside the thin reconnection layer whereas the exterior region is solved by assuming the ideal MHD solution. This method is powerful, but it is generally difficult to see what is happening in the microscopic scales since the inner solution is solved in the Fourier space for a technical reason.

In this work, we attempt to formulate linear growth rates of tearing modes in collisionless plasmas as a variational problem (or a *Rayleigh quotient*). For ideal MHD instabilities, this variational formalism is widely known as the energy principle. In the same spirit, we show that the collisionless tearing instability can also admits the variational formalism by assuming the absence of *dissipation* (or collision) and *flow* including the $E \times B$ and diamagnetic drifts. When this variational formulation is available, the eigenvalue problem is actually self-adjoint and the maximum growth rate can be evaluated efficiently by using an iteration algorithm for maximizing Rayleigh quotient. As is demonstrated below, the variational method is applicable not only to slab configuration (so-called Harris sheet) but also to any smooth equilibrium.

2 Variational formulation in a gyrofluid model

We assume the existence of a guide magnetic field $B_0 = \text{const.}$ in the z direction and plasma is magnetized to it. When ion and electron temperatures are sufficiently low but the ion gyroradius ρ_i and the ion-sound gyroradius ρ_S are not negligible, the two-dimensional dynamics of plasma is

governed by a gyrofluid model [1, 2] for electrostatic potential $\phi(x,y,t)$ and the z component of vector potential $\psi(x,y,t)$ (see also [3, 4] for a detailed exposition);

$$\frac{\partial n_e}{\partial t} + [\phi, n_e] + [\nabla^2\psi, \psi] = 0, \tag{1}$$

$$\frac{\partial \psi_e}{\partial t} + [\phi, \psi_e] - \rho_S^2[n_e, \psi] = 0, \tag{2}$$

$$n_e - n_{i0} = \frac{\nabla^2}{1-\rho_i^2\nabla^2}\phi, \qquad \psi_e = \psi - d_e^2\nabla^2\psi, \tag{3}$$

where a constant n_{i0} is the ion density, and d_e is the electron skin depth manifesting the effect of electron inertia. The neglect of all microscopic scales, $\rho_i = \rho_S = d_e = 0$, corresponds to the ideal MHD model.

Without the flow $\phi \equiv 0$, the only equilibrium condition is $[\nabla^2\psi, \psi] = 0$, and it is solved by $\nabla^2\psi = f(\psi)$ with $f : \mathbb{R} \mapsto \mathbb{R}$ being an arbitrary function. For smooth ψ such that $|d_e^2\nabla^2\psi| \ll |\psi|$, however, we may use an approximation $\psi \simeq \psi_e$ to leading order. By denoting the linear perturbations by $\tilde{\phi}, \tilde{\psi}, \tilde{\psi}_e$ and $\tilde{n}_e$, the linearized equations can be written in terms of a variable $\lambda(x,y,t)$ that is defined by $\tilde{\psi}_e = -[\lambda, \psi_e]$. Then, the maximum growth rate γ is finally represented by a variational principle,

$$\gamma^2 = -\min_\lambda \frac{\delta W}{\delta I} := -\min_\lambda \frac{\int \left([\lambda, \psi_e]\frac{-\nabla^2}{1-d_e^2\nabla^2}[\lambda, \psi_e] + [\lambda, \psi_e][\lambda, \nabla^2\psi] \right) dxdy}{\int \left(\lambda \frac{-\nabla^2}{1-(\rho_i^2+\rho_S^2)\nabla^2}\lambda \right) dxdy}. \tag{4}$$

Note that the denominator is positive definite ($\delta I > 0$) and hence instability $\gamma^2 > 0$ occurs if and only if there is a λ that makes δW negative. The first integrand in δW is also positive definite, which represents the stabilizing effect of the magnetic field-line's tension. It is clear that the role of the electron inertia is to weaken this stabilizing effect in a short wavelength scale $\lesssim d_e$. The collisionless tearing instability is understood as an instability $\delta W < 0$ that is enabled by $d_e \neq 0$ in spite of $\delta W|_{d_e=0} > 0$ in the ideal MHD limit $d_e = 0$. For the case of $\rho_S = \rho_i = 0$, we have already proven $\delta W < 0$ in a slab configuration by substituting a test function into λ, and estimated the growth rate which agrees with the asymptotic matching result [5]. Since ρ_i and ρ_S appear only in δI and an inequality $\delta I|_{\rho_i=\rho_S=0} > \delta I$ holds, we can generally conclude that these gyroradii do not change the stability boundary but always enhance the growth rate.

More analytical and numerical results on the above and another two-fluid model will be given in the presentation.

Acknowledgements. This work was supported by JSPS KAKENHI Grant Number 25800308 and by JSPS Strategic Young Researcher Overseas Visits Program for Accelerating Brain Circulation # 55053270.

References

[1] Schep, T., Pegoraro, F. and Kuvshinov, B. (1994) Generalized two-fluid theory of nonlinear magnetic structures. *Phys. Plasmas* **1**, 2843–2852.

[2] Grasso, D. *et al.* (2000) Ion Larmor Radius Effects in Collisionless Reconnection. *Plasma Phys. Rep.* **26**, 512–518.

[3] Waelbroeck, F. L. and Tassi, E. (2012) A compressible Hamiltonian electromagnetic gyrofluid model. *Commun. Nonlinear Sci. Numer. Simul.* **17**, 2171–2178.

[4] Comisso, L. *et al.* (2013) Gyro-induced acceleration of magnetic reconnection. *Phys. Plasmas* **20**, 092118.

[5] Hirota, M. *el al.* (2013) Nonlinear variational method for predicting fast collisionless magnetic reconnection. *Nucl. Fusion* **53**, 063024.

Notes

Relaxation of Braided Magnetic Fields

G. Hornig[1], A.R. Yeates[2], D.I. Pontin[1], A.J.B. Russell[1], S. Candelaresi[1]

[1] *School of Science and Engineering, University of Dundee, UK*
[2] *Department of Mathematical Sciences, Durham University, UK*

Summary

Magnetic fields in the solar atmosphere can become braided due to the turbulent motion of the plasma on the Sun's surface. Once a critical level of braiding has been reached instabilities trigger a relaxation process that can be turbulent in nature and typically involves a cascade of magnetic reconnection processes. The relaxation is constrained by invariants, which survive the turbulent reconnection processes. Until recently is was believed that the total magnetic helicity is the only invariant which has this property. We present results of numerical simulations on the relaxation of braided magnetic fields in plasmas of high magnetic Reynolds number, which show that certain properties of the helicity distribution are preserved as well. A generalised flux function (or field line helicity) can be defined for magnetic braids, which helps to understand qualitatively and quantitatively the relaxation process and can be used to predict possible relaxed states.

Eugene Parker suggested already in the 1970s [1] that coronal loops should undergo a braiding process due to the turbulent motion of their foot points rooted in the photosphere. He argued further that no force-free equilibria can exist for these braided fields and hence singular current sheets have to form, which then lead to magnetic reconnection. While there is still an ongoing debate whether the end state of an ideal relaxation of a braided field contains singular or just thin current sheets [2], many authors have shown that the process can indeed trigger magnetic reconnection. More recent numerical simulations revealed that it requires surprisingly little non-trivial braiding to trigger the onset of a turbulent cascade of reconnection processes [3], and that the higher the magnetic Reynolds number the more more efficient is the relaxation [4]. These results have led us to the question whether the end state of these turbulent relaxation processes can be predicted, similar to the way in which the Taylor hypothesis [5] predicts that the final state of a turbulent relaxation in a toroidal domain is a linear force-free field with the same total helicity and toroidal flux as the initial state. We found that the end states after the turbulent relaxation are typically not linear force-free states[4] (see also [6]), neither under line-tied nor under periodic boundary conditions. Although the relaxation process does preserve the total helicity, the redistribution of helicity density seems to also preserve the helicity spectrum, that is in particular the annihilation of helicity between regions of positive and negative helicity density is suppressed [8]. We use a generalised flux function or field line helicity [7], which can be defined for magnetic braids, to show that the final states can be predicted in some cases using the assumption that the magnetic flux corresponding to the level sets of the field line helicity are also preserved.

Acknowledgements. The authors acknowledge financial support from the UK's STFC (grant numbers ST/K000993 and ST/K001043/1).

References

[1] Parker, E. N. (1972), Topological dissipation and the small-scale fields in turbulent gases, *A*strophys. J., **174**, 499.

[2] Pontin, D. I. and Hornig, G. (2015), The structure of current layers and degree of field-line braiding in coronal loops, *Astrophys. J.*, **805**, 47.

[3] Wilmot-Smith, A. L., Pontin, D. I., and Hornig, G. (2010), Dynamics of braided coronal loops - I. Onset of magnetic reconnection, *Astron. Astrophys.*, **516**, A5.

[4] Pontin, D. I., Wilmot-Smith, A. L., Hornig, G., and Galsgaard, K. (2011), Dynamics of braided coronal loops. II. Cascade to multiple small-scale reconnection events. *Astron. Astrophys.*, **525**, A57.

[5] Taylor, J. B. (1974), Relaxation of Toroidal Plasma and Generation of Reverse Magnetic Fields, *Physical Review Letters*, **33**,1139.

[6] Moffatt, H. K. (2015), Magnetic relaxation and the Taylor conjecture, *Journal of Plasma Physics*, **81**(06), 905810608.

[7] Yeates, A. R. and Hornig, G. (2013), Unique topological characterization of braided magnetic fields, *Physics of Plasmas*, 20(1):012102.

[8] Yeates, A. R., Russell, A. J. B., and Hornig, G. (2015), Physical role of topological constraints in localized magnetic relaxation, *Proc. R. Soc. A.*, **471**, 20150012.

Notes

The role of helicity in dynamos driven by rapidly rotating convection

D. W. Hughes[1]

[1] *Department of Applied Mathematics, University of Leeds, UK*

Summary

Recent work has shown how large-scale vortices may form in rapidly rotating (and hence helical), plane layer convection. Here we consider the nature of the dynamo that may result from such vortices, and explain how this new dynamo mechanism fits in with classical mean-field dynamos and small-scale (fast) dynamos that have previously been found in this convective system.

1 Helicity and large-scale magnetic field generation

Understanding the generation of large-scale magnetic fields remains one of the most important problems in astrophysical fluid dynamics. Mean field electrodynamics (see, for example, [1, 2]) is a beautiful theory that describes the evolution of large-scale (mean) magnetic fields in terms of transport tensors, the most important being the so-called α tensor, whose properties depend on the statistics of the small-scale turbulence. The most striking result of mean field dynamo theory is that mean field generation can occur through the α-effect only if the flow lacks reflexional symmetry. The simplest measure of lack of reflexional symmetry is the flow helicity; helical flows therefore underpin all large-scale dynamos. However, the picture is not entirely straightforward. Whereas non-zero helicity is a necessary condition for large-scale field generation (at least through an α-effect), helical flows of themselves are not guaranteed to act as large-scale dynamos. The situation at high magnetic Reynolds number Rm, the case of astrophysical relevance, is particularly complicated.

Here I shall consider the particular example of dynamos driven by rotating, plane layer convection — possibly the simplest non-trivial dynamo configuration — in order to illustrate the various types of dynamo that can occur in flows with helicity.

2 Plane layer rotating convection

Dynamos driven by rotating, plane layer Boussinesq convection were first considered in the pioneering studies of [3, 4], and have subsequently received considerable attention through both analytical and numerical investigations.

Close to the onset of convection, the local value of Rm, based on the narrow convective cell size, is small. The fluctuating and mean magnetic fields are then simply related (so-called 'first order smoothing') and mean field theory can be readily applied; furthermore, there is a direct link between the helicity of the flow and the mean magnetic field generated. For more vigorous, although still strongly helical, convection, two other factors come into play. One is that the mean e.m.f. may be much smaller than local values of the e.m.f. [5]; this may be thought of as a lack of correlation between cyclonic eddies in Parker's classical picture. The other is that small-scale dynamo action may become dominant [6], thereby swamping any mean field mechanism.

Recent work has revealed that rotating convection may support yet another type of dynamo mechanism. Computational studies [7, 8] have shown that large-scale vortices (LSVs) may form as the result of a mean-field *hydrodynamic* instability (see figure 1). Here we look at the nature of the dynamo action that can result from these LSVs, showing how the magnetic field may be either large-scale (i.e. on the scale of the LSVs) or small-scale (on the scale of the convective eddies), depending on the magnetic Prandtl number [9]. Thus there are three very different types

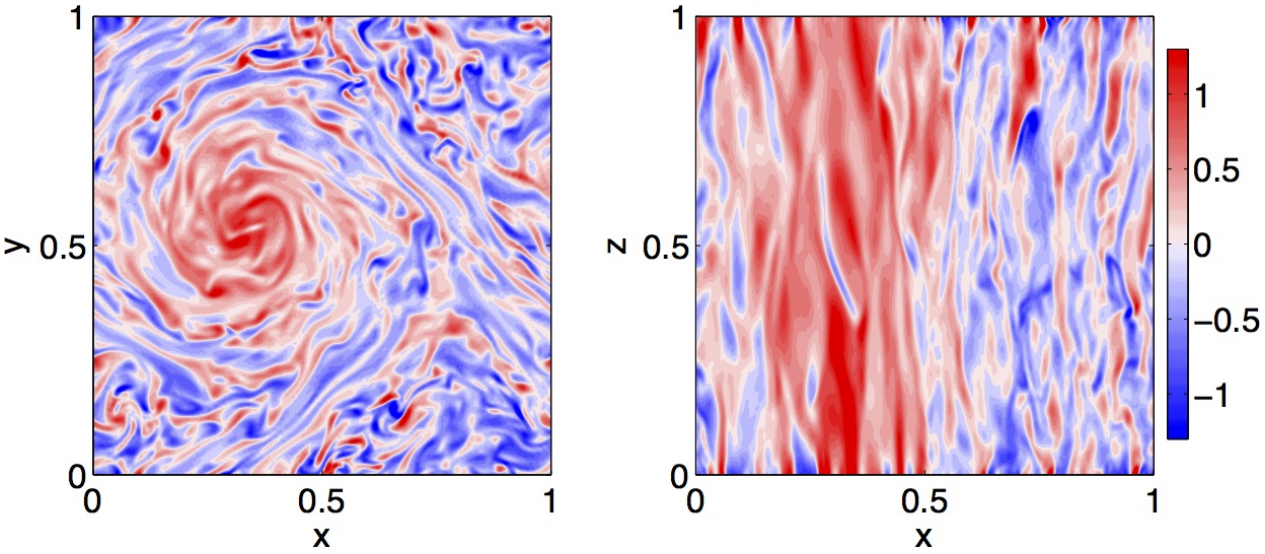

Fig. 1: Top and side views of the vertical vorticity: Ekman number $= 5 \times 10^{-6}$, Rayleigh number $= 8 \times 10^{8}$, Prandtl number $= 1$.

of dynamo mechanism possible in this system. We shall discuss where these lie in the parameter space defined by the Rayleigh number, the Ekman number and the magnetic Prandtl number, and where each of these might be of significance in planetary and stellar dynamos.

References

[1] Moffatt, H.K. (1978) *Magnetic Field Generation in Electrically Conducting Fluids*, Cambridge University Press.

[2] Krause, F. & Rädler, K.-H. (1980) *Mean-field Magnetohydrodynamics and Dynamo Theory.* Oxford: Pergamon.

[3] Childress, S. & Soward, A.M. (1972) Convection driven hydromagnetic dynamo. *Phys. Rev. Lett.* **29**, 837–839.

[4] Soward, A.M. (1974) A convection driven dynamo I. The weak field case. *Phil. Trans. R. Soc. Lond. A* **275**, 611–651.

[5] Hughes, D.W. & Cattaneo, F. (2008) The alpha-effect in rotating convection: size matters. *J. Fluid Mech.* **594**, 445-461.

[6] Cattaneo, F. & Hughes, D.W. (2006) Dynamo action in a rotating convective layer. *J. Fluid Mech.* **553**, 401-418.

[7] Guervilly, C., Hughes, D.W. & Jones, C.A. (2014) Large-scale vortices in rapidly rotating Rayleigh-Bénard convection. *J. Fluid Mech.* **758**, 407-435.

[8] Favier, B., Silvers, L.J. & Proctor, M.R.E. (2014) Inverse cascade and symmetry breaking in rapidly-rotating Rayleigh-Bénard convection. *Phys. Fluids* **26**, 096605.

[9] Guervilly, C., Hughes, D.W. & Jones, C.A. (2015) Generation of magnetic fields by large-scale vortices in rotating convection. *Phys. Rev. E* **91**, 041001.

Notes

Reconstruction of magnetic flux tubes and magnetic field lines from observational and simulated data

E. Illarionov[1], D. Sokoloff[2], M. K. Georgoulis[3]

[1] *Department of Mechanics and Mathematics, Moscow State University, Russia*
[2] *Department of Physics, Moscow State University, Russia*
[3] *Academy of Athens, Greece*

Summary

We consider different methods of tracing of magnetic flux tubes from observational solar data and simulated examples and discuss to what extent the obtained structures are applicable for calculation of some topological invariants.

1 Magnetic flux tubes in solar data

Topology of magnetic flux tubes plays an important role in MHD processes. A set of invariants, developed in [1], acts as a natural limiter for enhancing and relaxation of magnetic field. Remarkably, these invariants remain an intuitive topological meaning in terms of individual flux tubes, which can be also extended on infinite number of tubes after an appropriate adaptation [2]. From a theoretical point of view, presentation of magnetic field as a set of flux tubes allows to introduce topological invariants that describe higher helicity moments and advanced parameters of knottedness. On the other hand, practical implementation of these concepts require detailed information about magnetic field. Typically we are very limited in observation of magnetic fields of astrophysical objects and can operate only with its small parts. Complex extrapolation methods give us information in 3D volume, but we are basically unable to come out the bounding box. However, finite resolution of data and discretization of signal are the main problems for applying theoretical formulas. We consider different approaches to the problem of tracing of magnetic flux tubes in observational and simulated data and discuss which of them are the most suitable for MHD problems.

2 Algorithmic ways of flux tubes tracing

Classical approaches to the flux tubes tracing usually reconstruct individual magnetic field lines and consider them as thin flux tubes. However, it does not provide a flux balance at the footpoints of flux tubes. A natural idea is to set a number of field lines proportional to the strength of magnetic field, but it trace a central line of the tube rather than its 3D shape. We introduce a method, that considers flux tubes as clusters composed from individual magnetic field lines. The procedure of clustering of many field lines can be adjusted in a such way that provides both minimal flux disbalance and lateral diameter of tubes. The method also gives an optimal number of clusters. We demonstrate that the algorithm works reasonably well in both observational and simulated data and enables topological characterisation of individual flux tubes and its mutual knottedness.
Acknowledgements. The research presented is supported by RFBR project 15-02-01407.

References

[1] Moffatt, H.K. (1969) The degree of knottedness of tangled vortex lines. *J. Fluid Mech.* 1969 **35**, 117–129.

[2] Arnold, V.I. & Khesin, B.A. (1998) *Topological Methods in Hydrodynamics.* Applied Mathematical Sciences **125**, Springer-Verlag, Berlin.

Notes

The life of vortex knots and links and the conservation of helicity across scales

Martin Scheeler[1], Dustin Kleckner[1], Hridesh Kedia[1], Stephane Perrard[1], William T.M. Irvine[1]

[1] *James Franck Institute and Department of Physics University of Chicago*

Summary

Hydrodynamic helicity - a measure of the knottiness of vortex lines - is a conserved quantity in idealized fluids and thus offers the potential for fundamental insights into fluid flow. In real fluids, progress has been hindered by lack of accessible experimental and model systems. I will describe how to make vortex knots and links in water (in experiment), in the wave function of a superfluid (on a computer) and what happens thereafter. In particular, I will talk about how in helicity conservation, linking, coiling and twisting interplay across scales and types of flow. Finally, I will describe some progress towards exploring the effects of helicity on turbulent flows.

1 Hydrodynamic helicity

In addition to energy, momentum, and angular momentum, idealized (Euler) fluids have an additional conserved quantity, the hydrodynamic helicity $\mathcal{H}$:

$$\mathcal{H} = \int \mathbf{u} \cdot \omega \, \mathrm{d}V \tag{1}$$

where $\mathbf{u}$ and ω are respectively the velocity and vorticity of the flow. A natural interpretation of the hydrodynamic helicity is as a measure of the the linking and knotting of the vortex lines composing a flow. For an Euler fluid, the conservation of helicity follows from the Helmholtz laws of vortex motion, which forbid vortex lines from crossing and preserve the flux of vorticity, making it impossible for linked or knotted vortices to untie.

Conservation laws are of fundamental importance in understanding flows so the question of whether this topological conservation law extends to real, dissipative flows is of clear and considerable interest. Furthermore, since the dynamics of helicity are intrinsically geometric and topological in nature, lessons learned in fluids may well extend to the physics of tangling in other types of flow (e.g. plasmas) as well as other physical systems such as liquid crystals.

The robustness of helicity conservation in real fluids is unclear because dissipation allows the topology of field lines to change when nearby vortex tubes to "reconnect", apparently creating or destroying the topological linking of vortices. Analogous reconnection events have also been experimentally observed in superfluids and coronal loops of plasma on the surface of the sun and in general reconnection events exhibit divergent, nonlinear dynamics that makes it difficult to resolve helicity dynamics theoretically.

2 Generation of vortex knots

Thanks to a recent advance in experimental vortex production [1] it is now possible to generate vortices with controlled shape and topology, such as the one shown in Figure 1 (Left). The technique is based on the acceleration of 3D printed hydrofoils in an otherwise stationary fluid. Upon acceleration, a "starting vortex" whose shape traces the trailing edge of the hydrofoil is shed and subsequently evolves under its own influence. In our experiments, we use this technique to produce vortex knots and links in water having a total length of approximately $1m$, a typical width of 150 mm and circulation $\Gamma = 20,000 mm^2/s$; the Reynolds number is of order $Re \sim 2 \times 10^4$.

This enables us to *measure* the evolution of helicity in a viscous fluid and probe how well it is conserved as well as what mechanisms exist for its conservation, for example through reconnections.

3 Evolution of helicity

We find that in both cases, the vortices distort towards a series of localized reconnections that appear to change their coarse topology. To quantitatively measure the evolution of the helicity we consider the three

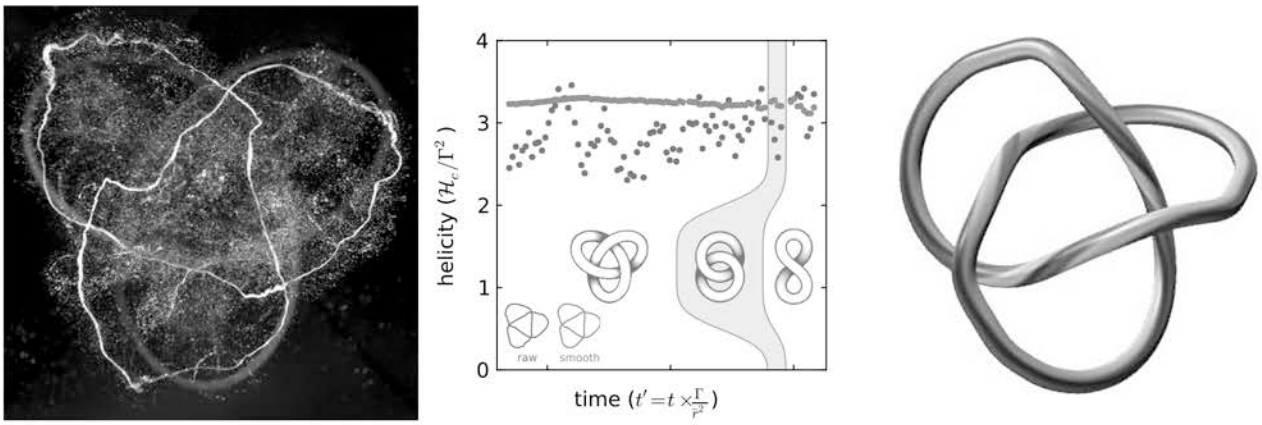

Fig. 1: (Left: A vortex knot in water. Middle: The evolution of link and writhe in a reconnecting vortex trefoil knot. Right: a vortex knot in the Gross Pitaevskii model of a superfluid.

geometrically distinct contributions to helicity for thin vortex tubes: Linking, coiling and twist. These three geometrically distinct but topologically equivalent contributions arise in the case of finite thickness vortex tubes, by subdividing the tube into N infinitesimal filaments each with strength $\Gamma = \Gamma_0/N$, and computing their linking in the limit $N \to \infty$:

$$\mathcal{H} = \sum_{i \neq j} \Gamma_i \Gamma_j \; \mathcal{L}_{ij} + \sum_i \Gamma_i^2 \; (Wr_i + Tw_i)\,, \tag{2}$$

where L_{ij} is the linking number between tubes i and j, Wr_i is the writhe of the tube center-line, and Tw_i is the total twist of each tube.

Remarkably, we find that immediately following the reconnections, the loss of linking between vortex tubes is completely balanced by the presence of writhe in the reconnected tube centerlines (Figure 1, center). This occurs through a geometric mechanism that converts link to writhe. By further decomposing the writhe on different scales using a 'helistogram' we track the flow of helicity across scales [2].

The mechanism we find for helicity conservation through reconnections is entirely geometric, suggesting it may be present in other fluid-like systems as well. To test this possibility, we simulate the evolution of vortex knots in a superfluid with the Gross-Pitaevskii equation (GPE). Although superfluids are inviscid, they are not ideal Euler fluids: vortex reconnections are possible and vortex cores do not have unconstrained structure. By simulating vortices with hundreds of distinct topologies we find that both aspect of topological vortex evolution outlined so far are general: all vortex knots untie efficiently and as they reconnect conserve the helicity of their centerline [3].

Measuring the total helicity however, requires additional information about how the vortex lines are locally twisted inside the vortex core. To bridge this gap, we have developed a novel technique for experimentally measuring twist helicity. Using this method, we are able to measure the production and eventual decay of twist for a variety of vortex evolutions. Remarkably, we observe twist dynamics capable of conserving total helicity even in the presence of rapidly changing writhe. Injecting helicity in a turbulent flow (in experiment) enables us to explore the role helicity has to play in complex flows.

References

[1] Kleckner D., Irvine W.T.M.: Creation and dynamics of knotted vortices in fluids. Nature Physics **9** 253-258, 2013.

[2] Scheeler M., Kleckner D., Proment D., Kindlmann G., Irvine W.T.M: Helicity conservation by flow across scales in reconnecting vortex links and knots. Proceedings of the National Academy of Sciences **111** 15356-15361, 2014.

[3] Kleckner D., Kauffman H., Irvine W.T.M.: How superfluid vortex knots untie. Nature Physics, in press.

Notes

What trefoil reconnection says about Navier-Stokes regularity

R.M. Kerr

Department of Mathematics, University of Warwick, United Kingdom

Summary

Scheeler et al. [1] have recently demonstrated that one can experimentally investigate helicity by imprinting high Reynolds number helical vortex knots into a fluid by yanking 3D-printed aerofoils covered with hydrogen bubbles out of a water tank. Some surprising claims were made based upon the evolution of the resulting vortex filaments. This contribution will address those claims by simulating the evolution and self-reconnection of a similarly perturbed trefoil vortex knot over a range of Reynolds numbers and core diameters. The surprisingly long time it takes for reconnection to begin is confirmed. However, the simulations suggest that the significance of the trefoil it is not just in the initial preservation of helicity, but in how it is dissipated in a finite time once reconnection begins. This result implies that the trefoil's vortex dynamics is controlled primarily by the helicity, and not the energy, enstrophy or peak vorticity.

One of the fundamental, unanswered questions about turbulence is why every physical turbulent flow dissipates finite energy in a finite time. Which seems to be inconsistent with the best current mathematics, which indicates that no Navier-Stokes solution from any smooth initial condition can dissipate finite energy in a finite time as the viscosity goes to zero.

This presentation will use the unique properties of a trefoil vortex to address this paradox by taking a step back and asking what defines the evolution of the vortices in incompressible fluids. Is it the energy and enstrophy/dissipation? Or the topology and helicity of the configuration? And if it is the helicity, what is the limit as the diameter of the filament goes to zero?

The trefoil vortex knots that these simulations [2] and the earlier experiments have generated seem particularly well-suited for addressing these questions for the following reasons.

- First, the helicity of these simulations is roughly 1/4 the upper bound given by a single perfectly helical Fourier mode. The most helical I have seen.
- Second, to fully address the Navier-Stokes regularity problem one must have initial conditions whose major Sobolev and Lebesgue norms are finite in Whole (infinite) Space. Other initial conditions such as initially anti-parallel and orthogonal vortices do not have this property.
- Third, if one decreases the filament's diameter a while holding its circulation Γ fixed, its kinetic energy and enstrophy grow without bound, while the configuration's helicity $\mathcal{H} = \Gamma^2 \mathcal{L}$ remains constant. Γ is the circulation and the self-linking number is $\mathcal{L} = \mathcal{W} + \mathcal{T}$ (writhe+twist).

* These contrasting trends make it easy to see whether the timescales are governed by the circulation and helicity, or the energy, enstrophy and the maximum vorticity.

Two figures are given. Fig. 1 illustrates the contortions of the trefoil just as reconnection begins using a vorticity isosurface, three closed vortex loops and two particular points. One where reconnection is beginning and the other the maximum of vorticity. The closed trajectories allow one to make qualitative comparisons with the bubble trajectories in the experiments [1] and relate the topological changes to some recent theoretical work [3]. Which is that the topological changes up to this time are independent of the viscosity of the calculations and the thickness of the filament, there has been very little reconnection and the helicity has not changed. All consistent with the surprisingly long period of helicity preservation in the experiments.

Note that in a classical fluid, reconnection is not instantaneous, so one of the curves (green) follows its original trajectory, while the red and blue curves represent a portion that has reconnected. At this early time, following predictions [3], the red and blue together preserve the total linking number of the trefoil. By determining the writhe, twist and the self-linking directly, primarily using

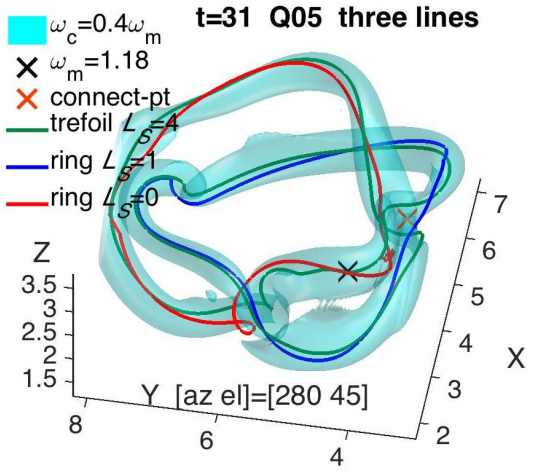

Fig. 1: A single vorticity isosurface plus three closed vortex lines at $t = 31$. The green line follows a remaining trefoil trajectories seeded near ω_m, indicated by **X**. Its $\mathcal{L}_S = 4$, split into $\mathcal{W} + \mathcal{T} = 2.85 + 1.15 = 4$ The **orange cross** is the "reconnection point", the point between the closest approach of the trefoil's two loops and where, due to an extra twist, the loops are locally anti-parallel. The **Red** $\mathcal{L}_S = 0$ and **blue** $\mathcal{L}_S = 1$ lines originate on either side of the reconnection point and are linked, which gives a total linking of $\mathcal{L}_t = 2\mathcal{L}_{rb} + \mathcal{L}_{Sb} + \mathcal{L}_{Sr} = 2 + 1 + 0 = 3$, the linking of the original trefoil.

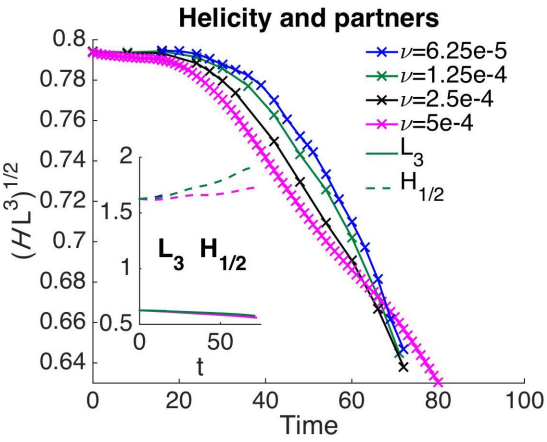

Fig. 2: Time evolution of the normalised helicity $(\mathcal{H}L)^{1/2}$ for 5 cases. Four with radius $a = 0.25$ for the viscosities listed, and one with radius $a = 0.175$ and $\nu = 0.0005$ that lies on the $\nu = 0.00025$ case shown. By $t \approx 72$ all cases have roughly the same decrease in helicity. The inset shows normalised L_3 and $H^{(1/2)} = \|u\|_{\dot{H}^{1/2}}$ for two of the calculations. L_3, $H^{(1/2)}$ and $\mathcal{H}$ are all normalised to have the units of circulation. $H^{(1/2)}$ must bound both L_3 and $|\mathcal{H}|$ from above and increases slowly, as required by its upper bound of $\sqrt{2EZ}$. None of which prevents the strong decrease in $\mathcal{H}$.

different forms of the Gauss-linking integral [2], it can be confirmed that the self-induced velocity along the filaments has three parts: The self-Biot-Savart term whose integral is the writhe, the traditional bi-normal self-induction, plus the torsion whose integral is the twist.

Fig. 2 illustrates how the helicity and related norms evolve in the period after reconnection begins for the five simulations [2] described in the caption. All dissipate approximately 1/3 of their helicity by $t = 65$. Over this period there is minimal energy loss, which decreases as the viscosity $\nu \to 0$. All three norms have been normalised to have the same units.

If $L_3 = \|u\|_{L^3} < \infty$ then Navier-Stokes is regular. Here L_3 is controlled as it decays just a bit more slowly than L_2 (2×energy). $|\mathcal{H}| \leq H^{(1/2)}$ is an upper bound for helicity magnitude. Together these tell us why the energy spectrum [2] goes as k^{-4}. It is necessary for helicity dissipation.
How $a = 0.175$, $\nu = 0.0005$ lays on the $a = 0.25$, $\nu = 0.00025$ case suggests that as $a \to 0$:

A. It is the helicity, not the energy, that controls the dynamics.

B. The time between when reconnection begins and ends goes to zero.

C. If seems possible that there can be finite helicity dissipation in a finite time.

* None of this violates any mathematics related to fixed smooth initial conditions.

What these calculations don't tell us is the conditions necessary for there to be finite energy dissipation in a finite time.

References

[1] Scheeler, M. W., Kleckner, D., Proment, D., Kindlmann, G. L., & Irvine, W.T.M. (2014) *Helicity conservation by flow across scales in reconnecting vortex links and knots.* Proc. Nat. Acac. Sci. **111**, 1535015355.

[2] Kerr, R.M. (2015) *Simulated Navier-Stokes trefoil reconnection.* arXiv:1410.1259v1.

[3] Laing, C.E., Ricca, R.L. & Sumners, D.W.L (2015) *Conservation of writhe helicity under anti-parallel reconnection.* Sci. Rep. **5**, 9224.

Notes

Chiral magnetic effect and the evolution of magnetic helicity in relativistic fluids

D. Kharzeev[1,2]

[1] *Department of Physics and Astronomy, Stony Brook University, Stony Brook, New York 11794-3800, USA*
[2] *Department of Physics and RIKEN-BNL Research Center, Brookhaven National Laboratory, Upton, New York 11973-5000, USA*

Summary

For systems with charged chiral fermions, the imbalance of chirality in the presence of magnetic field generates an electric current - this is the Chiral Magnetic Effect (CME). I will describe the recent discovery of CME in experiments with Dirac semimetals, and an evidence for the effect in relativistic heavy ion collisions at RHIC and LHC. The CME stems from the chiral anomaly, and is thus linked to the topology of the gauge field – in particular, it provides a mechanism for the dynamical real-time evolution of magnetic helicity. I will present the recent finding that the chiral anomaly induces the inverse cascade of magnetic helicity towards the large distances, and that at late times this cascade becomes self-similar, with universal exponents. We also find that in terms of gauge field topology the inverse cascade represents the transition from linked electric and magnetic fields (Hopfions) to the knotted configuration of magnetic field (Chandrasekhar-Kendall states). The magnetic reconnections are accompanied by the pulses of the CME current directed along the magnetic field lines.

The anomaly-induced transport of charge in systems with chiral fermions has attracted a significant interest recently. This interest stems from the possibility to study a new kind of a macroscopic quantum dynamics. While the macroscopic manifestations of quantum mechanics are well known (for example, superfluids, superconductors and Bose-Einstein condensates), so far they have been mostly limited to systems with broken symmetries characterized by a local order parameter, e.g. the density of Cooper pairs in superconductors. The effects induced by quantum anomalies in systems with chiral fermions are of different nature.

Let us consider as an example the Chiral Magnetic Effect (CME) in systems with charged chiral fermions – the generation of electric current in an external magnetic field induced by the chirality imbalance [1], see [2] for a review and references. The experimental observation of CME in a Dirac semimetal $ZrTe_5$ has been reported recently [3]. In this case, no symmetry has to be broken, and the system is in its normal state. However the chirality imbalance is linked by the Atiyah-Singer theorem to the non-trivial global topology of the gauge field. Since the global topology of the gauge field cannot be determined by a local measurement, there is no corresponding local order parameter, and we deal with "topological order".

This has very interesting implications for the real-time dynamics of a system composed by charged chiral fermions and a dynamical electromagnetic field. Indeed, let us initialize the system by creating a lump of chirality imbalance localized within a magnetic flux that forms a closed loop. Magnetic field will induce the CME current flowing along the lines of magnetic field $\mathbf{B}$ (note that this effect is absent in Maxwell electromagnetism). Because the vector CME current acts as a source for the magnetic field, the current flowing along $\mathbf{B}$ will twist the magnetic flux and induce a non-zero expectation value for the *magnetic helicity* known since Gauss's work in XIX century and introduced in magnetohydrodynamics by Woltjer [4] and Moffatt [5], see also [6]:

$$h_m \equiv \int d^3x \; \mathbf{A} \cdot \mathbf{B} \, . \tag{1}$$

Magnetic helicity is a topological invariant (Chern-Simons three-form) characterizing the global topology of the gauge field. It is mathematically related to the knot invariant, and measures the

chirality of the knot formed by the lines of magnetic field. Because of this, the generation of magnetic helicity will create the chiral knot out of the closed loop of magnetic flux – so the topology of magnetic flux will change. In a recent paper [7] we have quantified this statement, and studied how the topology of magnetic flux changes in real time. We have found that as a consequence of chiral anomaly and the CME, the magnetic field evolves to the self-linked Chandrasekhar - Kendall states. During the evolution, the size of the knot of magnetic flux increases. Moreover, at late times this evolution becomes self-similar, and is characterized by universal exponents.

References

[1] K. Fukushima, D. E. Kharzeev and H. J. Warringa, Phys. Rev. D **78**, 074033 (2008) [arXiv:0808.3382 [hep-ph]].

[2] D. E. Kharzeev, Prog. Part. Nucl. Phys. **75**, 133 (2014) doi:10.1016/j.ppnp.2014.01.002 [arXiv:1312.3348 [hep-ph]].

[3] Q. Li, D. E. Kharzeev, C. Zhang *et al.*, Nature Physics (2016), *in press*; arXiv:1412.6543 [cond-mat.str-el].

[4] L. Woltjer, Proc. Nat. Acad. Sci. **44**, no. 6, 489 (1958).

[5] H. K. Moffatt, J. Fluid Mech. **35**, 117 (1969).

[6] V. I. Arnold and B. A. Khesin, "Topological methods in hydrodynamics", Springer, Berlin, 1998.

[7] Y. Hirono, D. Kharzeev and Y. Yin, Phys. Rev. D **92**, no. 12, 125031 (2015) doi:10.1103/PhysRevD.92.125031 [arXiv:1509.07790 [hep-th]].

Notes

Helicity dynamics in the flow driven by a precessing sphere

S. Kida

Doshisha University, Tatara-Miyakodani 1-3, Kyotanabe-shi, Japan

Summary

A non-trivial periodic motion was found numerically on the verge of stability boundary of steady flow in a precessing sphere. The structure and dynamics of this flow are investigated with particular attention to the helicity dynamics.

1 Flow in a precessing sphere

We consider the motion of an incompressible viscous fluid in a precessing sphere with constant spin angular velocity Ω_s and constant precession angular velocity Ω_p. The two axes are assumed to be orthogonal. The flow state in this system is characterized by two non-dimensional parameters, the Reynolds number $Re = a^2\Omega_s/\nu$ and the Poincaré number $Po = \Omega_p/\Omega_s$, where a is the sphere radius and ν is the kinematic viscosity of fluid.

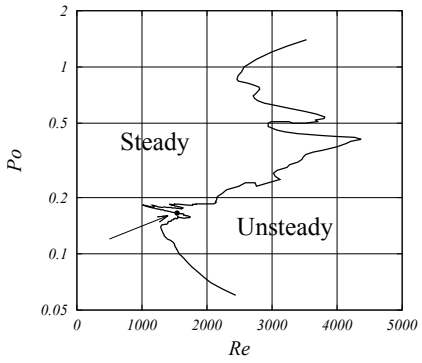

Fig. 1: Stability boundary of the steady flow.

Since this system is not simple enough to find the analytical solution of the steady flow except for a few limiting cases (such as $\max(Re, RePo) \ll 1$, $\min(Po, RePo) \gg 1$, $Po^2 \ll 1/Re \ll 1$), we must rely on the numerical method to study it. In order to clarify the stability characteristics of the steady flow over the entire range of the control parameters the present author have examined the stability boundary of the steady flow by direct numerical simulation. This work is not completed yet, but for the sake of explanation of the present paper we show the incomplete results in Fig. 1, in which the stability boundary numerically obtained so far is drawn with a solid line.

This figure tells us that starting from an arbitrary initial condition the flow tends to approach a steady flow on the left side of the stability boundary, whereas the unsteady state lasts for ever on the right side. It may be expected that the flow does weakly fluctuate, i.e. sinusoidally, in the vicinity of the most part of the stability boundary. There is, however, a part of the stability boundary across which the flow state changes drastically, as described below.

2 Non-trivial periodic motion

At $(Po, Re) = (0.1652, 1540)$ (indicated by a point in front of an arrow in Fig. 1) we found a wildly changing periodic motion (see Figs. 2 and 3). whereas the flow tends to be steady at the close vicinity $(Po, Re) = (0.1651, 1540)$ (see Figs. 4).

The temporal evolutions of the volume integrals of the kinetic energy of fluid motion $\int_V \frac{1}{2}|\boldsymbol{u}|^2 \mathrm{d}V$, the enstrophy $\int_V |\boldsymbol{\omega}|^2 \mathrm{d}V$, and the helicity $\int_V \boldsymbol{u} \cdot \boldsymbol{\omega} \mathrm{d}V$ for the former case are drawn in Figs. 2. Observe that the thick curve of the helicity, which is shifted to the left by 210 time unit and made upside down, is overlapped with the original thin curve. Therefore the time span plotted is one period though the energy and enstrophy repeat twice. The state trajectory projected in the energy

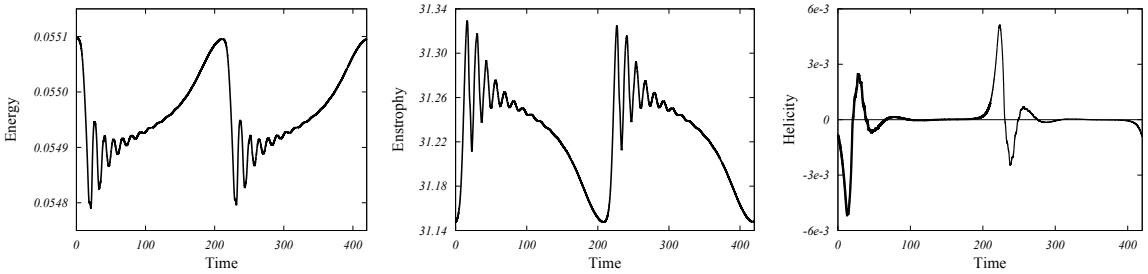

Fig. 2: Temporal evolution of energy (left), enstrophy (center) and helicity (right) over one period (≈ 420). $(Po, Re) = (0.1652, 1540)$.

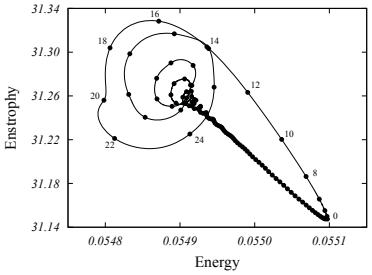

Fig. 3: State trajectory in energy-enstrophy plane. $(Po, Re) = (0.1652, 1540)$.

and enstrophy plane is plotted over a half period in Fig. 3. The numbers attached to the curve indicate the time. There are two particular states: one is around the center of circular trajectory and the other is around the right-bottom tip. The flow state moves from the former to the latter slowly, but comes back quickly. It is interesting to see that the helicity changes the sign every turn of the trajectory on the energy-enstrophy plane.

Next, we change only one of the control parameters, Po, slightly from 0.1652 to 0.1651 and start the numerical simulation from the state at time 19 (see Fig. 3). The results are shown in Figs. 4. It is rather surprising that as seen in left and central figures the

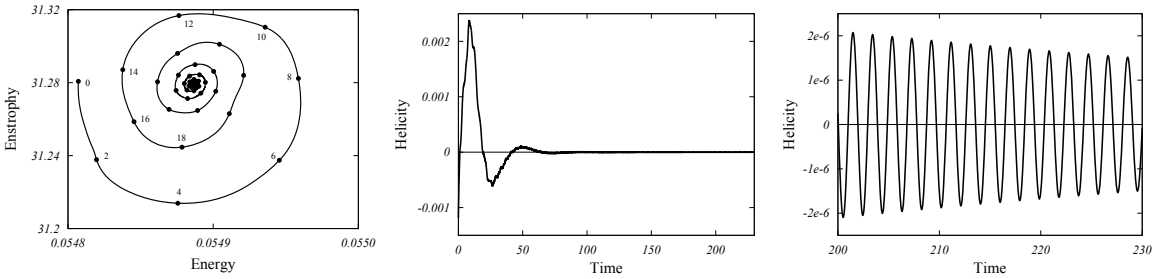

Fig. 4: State trajectory in the energy-enstrophy plane (left), and the temporal evolution of helicity over the whole period computed (center) and for the last 30 time unit. $(Po, Re) = (0.1651, 1540)$.

flow approaches quickly to the steady state despite of quite small change (only 0.06%) of Po. Another interesting fact is that very short oscillation pariod (≈ 1.9 time unit) appears in the helicity variation (see the right of Fig. 4, whereas those of energy and enstrophy are about 13.3 time unit (see the left of Fig. 4).

3 Visulization analysis

The non-trivial periodic flow we have just seen has many mysterious features: a drastic change in the flow state is caused by a small change of control parameter, what is the mechanism of the flip-flop of the helicity sign, etc. The author is currently working with it by the use of 3D visualization of the flow as well as by quantifying various field quantities.

Acknowledgements. This work was partially supported by Grant-in-Aid for Scientific Research (24540416, 15K25219) from the Japan Society for the Promotion of Science. The numerical calculations were carried out on SR16000 at YITP in Kyoto University.

Notes

Reconnection of skewed vortex and magnetic flux tubes

Y. Kimura[1] and H. K. Moffatt[2]

[1] *Graduate School of Mathematics, Nagoya University, Japan*
[2] *Department of Applied Mathematics and Theoretical Physics, University of Cambridge, UK*

Summary

Based on experimental and numerical evidence that nearly anti-parallel vortices have often been observed in the early stage of vortex reconnection, a linearized model is developed in which two Burgers-type vortices are driven together by an axisymmetric straining velocity field. With this linearized model which neglects the nonlinear vortex-vortex interaction, it is demonstrated that the initial helicity with the skewed geometry is eliminated during the reconnection process. The model can be extended to the reconnection of magnetic flux tubes under the action of a straining field by adding the effect of Lorentz forces to the driving velocity.

As an initial stage of vortex reconnection, nearly anti-parallel segments of vorticity have often been observed experimentally and numerically [1],[2]. Inspired by the recent experiment by Kleckner and Irvine on the dynamics of a trefoil knot vortex [3], we have developed a linearized model in which two Burgers-type vortices are driven together by an axisymmetric straining velocity field [4].

When these Burgers vortices are exactly anti-parallel, they annihilate leaving a decaying dipole moment as the leading order vorticity. If the straining velocity field is prescribed as $\mathbf{U} = (-\alpha x, -\alpha y, 2\alpha z)$, the decay rate of the dipole is given by the rate of strain α even as the kinematic viscosity tends to be zero. These analytic results of the linearized model are compared with the numerical results by Buntine & Pullin [5].

Now at $t = 0$, we place symmetrically one Burgers-type vortex $\boldsymbol{\omega}_1(\mathbf{x}, t)$(circulation Γ) with straight centerline L_0 on the plane $y = y_0$ titled at an angle β_0 to the z-axis and a second vortex $\boldsymbol{\omega}_2(\mathbf{x}, t)$(circulation $-\Gamma$) with centerline on the plane $y = -y_0$ tilted at an angle $-\beta_0$ to the z-axis. If these vortices are under the same straining action, we can write down the development of them as

$$\boldsymbol{\omega}_1(\mathbf{x}, t) = \frac{\Gamma}{\pi\sigma(t)^2} \exp\left[-\frac{\mathbf{r}_p^2(\mathbf{x}, t)}{\sigma(t)^2}\right] \mathbf{e}(t), \qquad (1)$$

$$\boldsymbol{\omega}_2(\mathbf{x}, t) = -\frac{\Gamma}{\pi\sigma(t)^2} \exp\left[-\frac{\mathbf{r'}_p^2(\mathbf{x}, t)}{\sigma(t)^2}\right] \mathbf{e}'(t), \qquad (2)$$

where
$\mathbf{r}_p^2(\mathbf{x}, t) = (x\cos\beta(t) - z\sin\beta(t))^2 + (y - y_0 e^{-\alpha t})^2$,
$\mathbf{r'}_p^2(\mathbf{x}, t) = (x\cos\beta(t) + z\sin\beta(t))^2 + (y + y_0 e^{-\alpha t})^2$,
with $\beta(t) = \tan^{-1}(e^{-3\alpha t}\tan\beta_0)$, $1/\sigma(t)^2 = \frac{\alpha}{4\nu}(3\cos^2\beta(t) - 1)$ (ν: kinematic viscosity)
and $\mathbf{e}(t) = (\sin\beta(t), 0, \cos\beta(t))$ and $\mathbf{e}'(t) = (-\sin\beta(t), 0, \cos\beta(t))$.

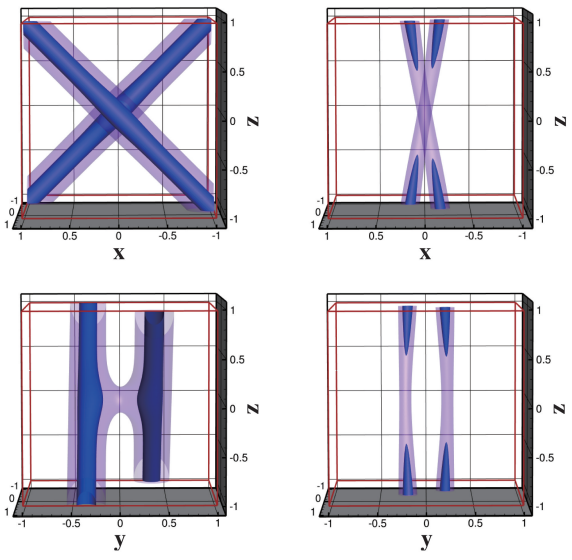

Fig. 1: Contour plots of $|\boldsymbol{\omega}_1(\mathbf{x}, t) + \boldsymbol{\omega}_2(\mathbf{x}, t)|$ at $\tau \equiv e^{-\alpha t} = 0$ and $= 0.63$. Two levels of contours are depicted, one at the 95% of the maximum (darker) and the other at 85% [4].

Figure 1 shows two views of contour plots of $|\boldsymbol{\omega}_1(\mathbf{x}, t) + \boldsymbol{\omega}_2(\mathbf{x}, t)|$ at $\tau \equiv e^{-\alpha t} = 0$ and at $\tau = 0.63$. The initial separation $y_0/\delta = 1.356$ is chosen where $\delta = \sqrt{2\nu/\alpha}$ is the radial scale of the Burgers vortex, and the initial angle $\beta_0 = \pi/4$ is set. The initial two orthogonally offset vortices approach the anti-parallel configuration, and by the time $\tau = 0.63$, reconnection is well observed in particular for the center parts with strong vorticity.

Helicity is a topological invariant for Euler flows, and it is a crucial problem whether the helicity of the vorticity distribution changes during the viscous reconnection process discussed above. By recalling the velocity field of the Burgers vortex,

$$\mathbf{u}(\mathbf{x}) = \frac{\Gamma}{2\pi r^2}(1 - \mathrm{e}^{-r^2/\delta^2})(-y, x, 0), \tag{3}$$

we can explicitly calculate the helicity for the skewed Burgers-type vortices as

$$\mathscr{H}(\tau) = \int_V \mathbf{u}\cdot\boldsymbol{\omega}\, dV \;\; = \frac{s^{1/2}\Gamma^2}{\pi^{1/2}} \int_0^\infty \mathrm{erf}\hat{y}\, (e^{-s(\hat{y}-\hat{y}_0 e^{-\tau})^2} - e^{-s(\hat{y}+\hat{y}_0 e^{-\tau})^2})\, d\hat{y}. \tag{4}$$

where $s(\tau) = (3\cos^2\beta(\tau) - 1)/2$ and $\hat{y} = y/\delta$.

In Fig. 2, the integral (4) is evaluated for the initial skewness angle $\beta_0 = \pi/4$ and for six values of the initial dimensionless separation $\hat{y}_0 = y_0/\delta$. For $\hat{y}_0 \gg 1$, $\mathscr{H}/\Gamma^2$ remains nearly equal to 1 while the vortices are well separated. As $\hat{y}_0\mathrm{e}^{-\tau}$ decreases to $O(1)$ and smaller, $\mathscr{H}/\Gamma^2$ decays exponentially to zero in time of order α^{-1}. Therefore with the present linearized model, we can conclude that the initial helicity is destroyed during the viscous reconnection process. We should recall, however, that the present model neglects the vortex-vortex interaction. The effect of this nonlinear interaction on the helicity development is still an open problem, and to address this, a perturbation procedure taking the first-order of the interaction term might be necessary. Also calculation of Lagrangian particle trajectories around the vortices might provide a useful information for straightening out the problem.

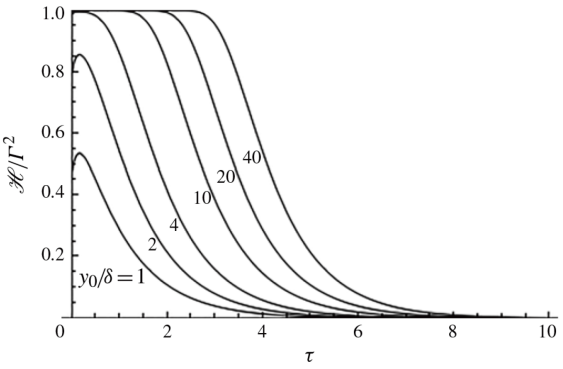

Fig. 2: Helicity development (4). [4].

If we notice the analogy between vorticity and magnetic field, the present model for vortex reconnection applies directly to the reconnection of weak magnetic flux tubes under the action of strain field. The model can also be extended to more general magnetic reconnection problems by taking the effect of Lorentz forces, $J \times B \sim (\nabla \times B) \times B$, into the driving velocity field.

Acknowledgements. YK acknowledges the support of Grant-in-Aid for Scientific Research(A) (No. 24247014).

References

[1] Kida, S & Takaoka, M. (1994) Vortex reconnection. *Ann. Rev. Fluid Mech.* **26**, 169–189.

[2] Laing, C.E., Ricca, R.L. & Sumners, De W. L. (2015) Conservation of writhe helicity under anti-parallel reconnection. *Scientific Reports* **5**: 9224. doi: 10.1038/srep09224.

[3] Kleckner, D. & Irvine, W.T.M. (2013) Creation and dynamics of knotted vortices. *Nature Physics* **9**, 253258. doi: 10.1038/nphys2560.

[4] Kimura, Y & Moffatt, H.K. (2014) Reconnection of skewed vortices. *J. Fluid Mech.* **751**, 329–345.

[5] Buntine, J.D. & Pullin, D.I. (1989) Merger and cancellation of strained vortices. *J. Fluid Mech.* **205**, 263–295.

Notes

Finding topological defects in turbulent superfluid flows.

A. Villois[1], D. Proment[1], H. Salman[1] and G. Krstulovic[2]

[1] *School of Mathematics, University of East Anglia, Norwich Research Park, Norwich, UK*
[2] *Laboratoire J.L. Lagrange, UMR7293, Université de la Côte d'Azur, CNRS, Nice. France.*

Summary

We study superfluid dynamics by numerical integration of the Gross-Pitaevskii equation. We develop a vortex tracking algorithm that allows for finding with high accuracy the topological defects of an arbitrary configuration. The algorithm is first used to study vortex reconnections in different settings. Then it is used to track and study some topological and statistical properties of a turbulent tangle generated by the evolution of large-scale initial condition.

Superfluids are usually described by the Gross-Pitaevskii equation that in its dimensionless form reads

$$i\frac{\partial\psi}{\partial t} + \nabla^2\psi - |\psi|^2\psi = 0\,, \tag{1}$$

where $\psi(\mathbf{x},t)$ is a complex wave-function describing the superfluid *order parameter*. The Gross-Pitaevskii equation, also known as the defocusing nonlinear Schrödinger equation, has been largely used to study vortex dynamics and quantum turbulence. By introducing the Madelung transformation $\psi = \sqrt{\rho}\exp(i\phi)$, the equation (1) can be mapped into a set of equations for the density field $\rho(\mathbf{x},t)$ and the velocity field $\mathbf{v}(\mathbf{x},t) = 2\nabla\phi(\mathbf{x},t)$ of a compressible, inviscid, irrotational and barotropic fluid. Although the vorticity $\omega = \nabla\times\mathbf{v}$ is formally zero, at points where the density vanishes, the phase ϕ is not defined and vortices may arise as topological line defects. They mutually influence themselves and, correspondingly, the fluid dynamics. These topological defects, called quantum vortices, have a quantised circulation and correspond to zeros of the wave function. Several questions regarding the superfluid vortex dynamics modelled using the Gross-Pitaevskii equation remain nowadays open. For instance, it is not clear how the energy of vortex configurations initially stored at large scales spreads over scales and eventually decay into phonons (sound radiation).

The Gross-Pitaevskii equation is a rich model that naturally contains reconnections and sound (phonon) emission. However, it does not provide explicit information of vortices and such information must be extracted by some tracking algorithm. Using a specifically-designed algorithm to detect topological defects in the complex wave-function $\psi(\mathbf{x},t)$ [1], we are able to track with high accuracy the vortex line positions all along the dynamics of any initial vortex line configuration. The algorithm can be use for instance to track all vortices in a turbulent tangle as displayed in figure 1.

This algorithm allows us to measure the time evolution of useful physical quantities like the total vortex line length, and curvature and torsion distributions, which may give useful insights to understand how energy is transferred trough the system scales. We first use the algorithm to study vortex reconnections in different geometries. Then we use the algorithm in a turbulent tangle generated by numerical integration of the Gross-Pitaevskii equation with the so-called Taylor-Green initial condition. From it we are able to infer some information about the spectrum of Kelvin waves, that are helicoidal excitations of vortex lines which are believed to be responsible of the energy cascade in the weakly nonlinear limit.

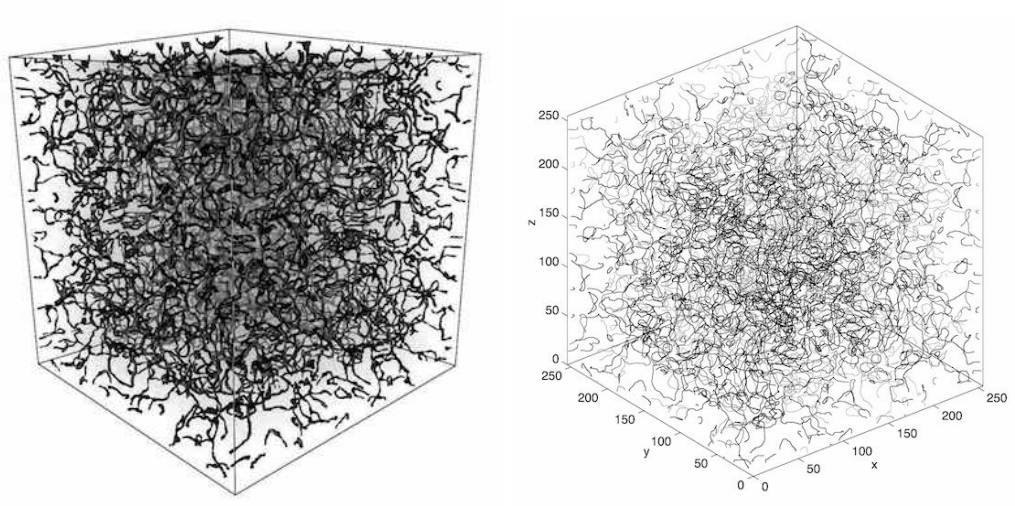

Fig. 1: *Left*: 3D visualisation of the density field. Vortices are represented in blak by an isosurface of the low density regions. *Right*: Corresponding tracking of the vortex tangle. Different tones of gray corresponds to different tracked lines. The turbulent tangle is generated by numerical integration of the Gross-Pitaevskii equation with the so-called Taylor-Green initial condition.

References

[1] A. Villois, H. Salman, D. Proment, and G. Krstulovic. *An accurate and efficient tracking algorithm to detect topological defects in the Gross-Pitaevskii model.* in preparation.

Notes

Collision of point vortices

P. Henryk Kudela[1]

[1] *Mechanical-Engineering Faculty, Wrocaw University of Technology, Poland*

Summary

The system of a finite number $n > 3$ of point vortices under suitable conditions can converged (collapse) to the point with finite time. It was described how to find the initial positions of vortices that collapsed. An explicit solution for collapsing trajectory was derived. The numerical evidence was presented that initial position of collapsing vortices organized their self in vortex sheets. Examples of the collapsing configurations with different number of vortices were presented.

1 INTRODUCTION

The collapse of the vortices belongs to one of the most interesting problems related to the dynamics of vortices. We will show that collapse vortices is possible for any number of the vortices, $n \geq 3$. The presence of the one or two strong vortices in the set of collapsing vortices lead to rising of the filaments created by point vortices. It can be interpret as vortex sheets [6].

2 EQUATIONS OF MOTION AND THEIR INVARIANTS

The equations of motion of the system of n-point vortices on the plane with distinct positions $\mathbf{z} = (z_1, z_2, \ldots, z_n) \in \mathbb{C}^n$, $z_k = x_k + iy_k$, and circulations $\Gamma_1, \Gamma_2, \ldots, \Gamma_n$, each $\Gamma_j \in \mathbb{R} \setminus 0$ are

$$\frac{dz_k(t)}{dt} = \mathbf{v}_k(\mathbf{z}(t)) = \frac{i}{2\pi} \sum_{l=1, l\neq k}^{n} \Gamma_l \, \frac{z_k - z_l}{|z_k - z_l|^2} \tag{1}$$

It is well known that the systems (1) posses several invariants [1, 5, **?**]

$$\begin{aligned} M_x = \sum_k^n \Gamma_k x_k, \quad M_y = \sum_k^n \Gamma_k y_k, \quad S = \sum_k^n \Gamma_k (x_k^2 + y_k^2), \\ V = \frac{1}{2\pi} \sum_{k>j} \Gamma_k \Gamma_j, \quad H = -\frac{1}{4\pi} {\sum_{k,j}}' \Gamma_k \Gamma_j \ln r_{kj} \end{aligned} \tag{2}$$

3 SELF-SIMILAR MOTIONS AND COLLAPSE

Assuming the similarity motion of system of vortices $\frac{\mathrm{d}z_k}{\mathrm{d}t} = v_k = \lambda(t) z_k, \qquad k = 1, 2, \ldots, n$, one can check (see [5]) that $\mathbf{v}_1 z_k = \mathbf{v}_k z_1 \quad (k = 1, .., n-3)$. Collapsing trajectory are disrobed by the formula

$$z_k(t) = \sqrt{2\lambda_r(0)t + 1} e^{\left(i \frac{\lambda_i(0)}{2\lambda_r(0)} \ln(2\lambda_r(0)t+1) \right)} z_k(0) \tag{3}$$

The critical (collision) time $t \to T_c$ is $T_c = -\frac{1}{2\lambda_r(0)}$. The Hamiltonian H in(2) during the motion will be conserve, when the invariant V in (2) is equal zero, $V = 0$. Now one should find the $z_k(0)$. Without loosing the generality we assumed that $M_x = 0$ and $M_y = 0$.The collapsing positions of vortices can be determined by common zeros of the functions $V = 0$, $M_x = 0$, $M_y = 0$, $S = 0$ and $2(n-3)$, $f_j = \mathbf{v}_1 z_{j+2} - \mathbf{v}_{j+2} z_1, j = 2, \ldots, n-2$. To complete the systems to $2n$ equations, it was assumed that one of the vortex in the system e.g z_n has the fixed position, and it was included to the system of equation the identity $\sum_j \Gamma_j z_j^* \mathbf{v}_j = 0$ [3, 4]. The nonlinear algebraic system of equation was solved by the Newton method [3, 4].

4 NUMERICAL RESULTS

In Figures 1 A), B), C) were presented the cases with different number of stronger vortices in set of the collapsing 72 vortices. In Figure 1 A) intensities were $\Gamma_{1\ to\ 71} = 1$ and only one vortex had dominat value $\Gamma_{72} = -35$($T_c = 5.86232$, $H = 49.036$). In Figure 1 B) intensities were $\Gamma_{1\ to\ 70} = -1$ and two vortices had dominat value $\Gamma_{71,72} \approx 20.1502$,($T_c = 32.72233$, $H = 21.961502$) and in Figure 1 C) intensities were the same as in Figure 1 B) but now $H = 14.8442$ and collision time was very long $T_c \cong 63511.8$. Figure 1 B) there were two strong vortices $\Gamma_{71,72} \approx 20.1502$,and $\Gamma_{1\ to\ 70} = -1$. Collision time was $T_c = 32.72233$ and $H = 21.961502$. In Figure 1 C) there were also two strong vortices $\Gamma_{71,72} \approx 20.1502$, $\Gamma_{1\ to\ 70} = -1$, and $H = 14.8442$ but collision time was very long $T_c \cong 63511.8$. One can noticed (see Figure 1 C)) that vortices created the circle that took part in collapsing. Changing the Hamiltonian value in some intervals ($[H_{nim}, H_{max}]$) one can find the continuous collapsing curves where vortices lie. That curves originate (H_{nim}) and terminate H_{max} for points that are very closed to relative equilibrium ($T_c = \infty$).

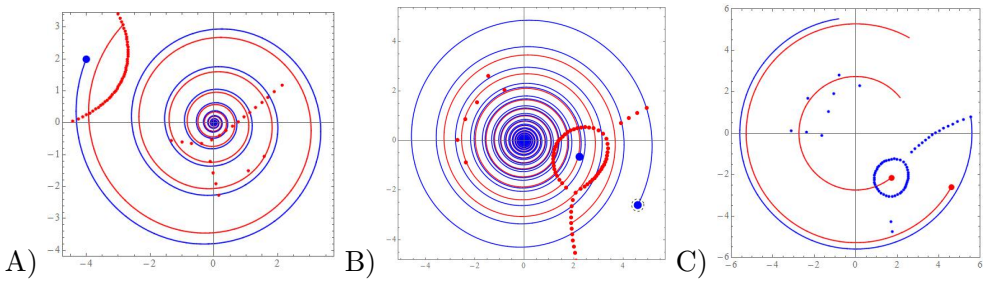

Fig. 1: Examples of collapsing systems of 72 vortices; In order to keep the readability of the graph it was shown only a few trajectories. Thick points mark the stronger vortices. The blue color related to negative intensity, the red color to the positive one.

5 CONCLUSIONS

From examples it is clear that the presence a few stronger vortices in the set of vortices for which we are looking the collapsing positions of vortices caused that the vortices accumulated in the pieces of curves that can be interpret as vortex sheets. In the atmospheric physics, it seems that collapsing vortices have relevance to the meteorological phenomenon of a polar cyclone [4]. Spirals and filaments of vorticity are characteristic feature of two-dimensional turbulent flows [2].

References

[1] Aref H.: Motion of three vortices. Phys. Fluids 22:393-400, 1979.

[2] Kevlahan N.K-R , Farge M.: Vorticity fiaments in two-dimensional turbulence: reation, stability and effect.J. Fluid Mech 346:49-76, 1997

[3] Kudela H.: Collapse of n–point vortices in self-similar motion. Fluid Dyn. Res. 46: 1-16, 2014

[4] Kudela H.: Self-Similar collapse of n point vorticies. J. Nonlinear Sci. 24: 913-933, 2014

[5] O'Neil K. A.: Stationary configurations of points vortices. Trnas. Amer. Math. Society 302: 383-425, 1987

[6] O'Neil K. A.: Relative equilibria of vortex sheets. Physica D 238:379-383, 2009

Notes

Tracking dissipative structures from PIV measurements: a new criterion to detect singularities in experimental flows

D. Kuzzay[1], E.W. Saw[1], D. Faranda[2], A. Guittonneau[3], F. J. W. A. Martins[4], J.-M. Foucaut[4], F. Daviaud[1], C. Wiertel-Gasquet[1], V. Padilla[1], B. Dubrulle[1]

[1] *DSM/IRAMIS/SPEC/SPHYNX, CNRS UMR 3680, CEA, Universit Paris-Saclay, F-91191 Gif-sur-Yvette, France*

[2] *DSM/LSCE, CNRS UMR 8212, CEA, Universit Paris-Saclay, F-91191 Gif-sur-Yvette, France*

[3] *ENS Lyon, 46 Alle d'Italie, F-69007 Lyon, France*

[4] *Laboratoire de Mcanique de Lille, France*

A well known experimental fact is that the energy dissipation rate of turbulent flows remains constant in the limit of vanishing viscosity [1], a phenomenon referred to as the dissipation anomaly . In the late 40's, Onsager [2] suggested to connect this observation to the appearance of singularities in solutions to the Navier-Stokes equations, the existence of which was postulated by Leray in 1934 [3]. Since then, mathematicians have failed to prove rigorously such a conjecture [4]. From a physicist point of view, most attempted detection of singularities have been done via numerical simulations. They are, however, strongly limited by the resolution and the computing time. Part of these limitations are relaxed when performing experiments with turbulent flows. Indeed, in a well-designed experiment, one can reach fairly easily large Reynolds numbers and monitor the velocity field for time long enough (minutes to hours) to accumulate enough statistics for reliable data analysis. In the past, exploration about the dissipative anomaly and potential singularities of Navier-Stokes equations has been limited by the data instrumentation, since only global (torque), or local measurements in space (hot wire) or in time (photography) were available. With the advent of modern Particle Image Velocimetry, measurements of the velocity fields over the decimetric to millimetric size range are now available, at frequencies from 1Hz to 1kHz, providing data comparable with outputs of large eddy simulations. In this presentation, we discuss the Duchon-Robert energy balance equation [5] to infer a singularity criterion based on energy dissipation through scales. From this criterion, we derive a PIV-based method to detect potential singularities in experimental flows.

References

[1] Taylor, G.I. Statistical theory of turbulence. *Proc. R. Soc. A* **151,** (1935) 421-444.

[2] Onsager, L. Statistical hydrodynamics. *Nuovo Cimento* **6,** (Suppl.) (1949) 279287.

[3] Leray, J. Essai sur le mouvement d'un liquide visqueux emplissant l'espace. *Acta Math.* **63,** (1934) 193248.

[4] Fefferman, C. L. Existence and smoothness of the Navier-Stokes equation. The millenium prize problems, Clay Math. Inst., Cambridge, MA, 2006, pp. 57-67.

[5] Duchon, J., Robert, R. Inertial energy dissipation for weak solutions of incompressible Euler and Navier-Stokes equations. *Nonlinearity* **13,** (2000) 249255.

Notes

Curvature instability in vortex rings and helical vortices

F. J. Blanco-Rodríguez, S. Le Dizès

IRPHE, Aix Marseille University, CNRS, Centrale Marseille, France

Summary

We provide theoretical predictions for the growth rate of the curvature instability in a curved Batchelor vortex as a function of the axial velocity parameter, the local curvature and the Reynolds number. The results are validated by direct numerical results of the linearized equations. They are then applied to rings and helices and compared to recent experimental observations.

Most vortices observed in nature are curved. The local curvature of the vortex affects the displacement of the vortex structure but it also modifies its internal structure by generating dipolar corrections. Callegari & Ting [1] showed that these corrections can be calculated for any vortex model using asymptotic techniques when the vortex core size is small compared to the curvature radius. These corrections are responsible for the so-called curvature instability [2]. This short-wavelength instability develops in the core of curved vortices. It results from the resonant coupling of two Kelvin modes of the underlying straight vortex with the dipolar correction associated with curvature. This instability is similar to the elliptical instability for which the coupling occurs through quadripolar corrections (i.e. strain field) [3].

The curvature instability has been analyzed by Hattori & Fukumoto [2, 4] for a Rankine vortex (uniform vorticity in the vortex core). Such a vortex model is convenient as it allows a complete analytic treatment. However, it possesses properties which are not shared by smoother vortex profiles such as the Lamb-Oseen vortex (Gaussian vorticity). For the Rankine vortex, the Kelvin mode frequencies cover the entire range $((-2+m)\Omega_{\max}, (2+m)\Omega_{\max})$ for each azimuthal wavenumber m ($\Omega_{\max}$ being the maximum angular velocity of the Rankine vortex). This property is not satisfied by the Lamb-Oseen vortex which possesses a gap in its spectrum of Kelvin Modes. In particular, no regular Kelvin mode of azimuthal wavenumber $m > 0$ exists in the frequency range $(0, m\Omega_{\max})$: These modes would exhibit a singularity at the critical point r_c where the mode frequency ω satisfies $\omega = m\Omega(r_c)$. The main effect of this singularity is to damp the modes, with a damping rate which becomes important when the critical point gets close to the vortex core [5].

The curvature instability requires the existence of two Kelvin modes of azimuthal wavenumbers m and $m + 1$ with the same frequency and axial wavenumber. For the Lamb-Oseen vortex, we show that this condition of resonance necessarily involves a singular Kelvin mode. The instability can therefore be present only if the growth associated with the resonant coupling can overcome the critical layer damping of the Kelvin mode. This is a strong constraint which selects very few possible resonant configurations. Only Kelvin modes of azimuthal wavenumbers $m = 0$ and $m = 1$ with a high radial complexity are found to be possible. However, the complexity of these modes makes them more sensible to viscous effects. We show that they are stable for the moderate Reynolds numbers considered in most vortex ring experiments, which could explain why they have never been observed.

When a Gaussian axial flow is present in the vortex core, the Lamb-Oseen vortex becomes the so-called Batchelor vortex. Such a model is usually used to describe tip vortices as generated by wings or rotor blades. In the present work, we have analyzed the effect of the amplitude of the axial flow (defined as $W_0 = 2\pi a^2 W_{\max}/\Gamma$ where $W_{\max}$ is the maximum axial velocity, Γ the vortex circulation, a the vortex core radius) on the curvature instability in the regime where the Batchelor vortex is not affected by the swirling jet instability [6], that is for $W_0 < 0.6$. We show that the curvature instability is possible in the presence of axial flow. We obtain that it still involves Kelvin modes of azimuthal wavenumbers $m = 0$ and $m = 1$ but their radial complexity becomes simpler as W_0 increases. When $W_0 = 0.5$, the most unstable mode resembles the elliptic instability

mode developing in vortices without axial flow but its wavelength is almost twice larger. It could correspond to the short-wavelength instability mode recently observed in experiments by Leweke et al [7] in the helical vortex created by a single-blade rotor (see Fig. 1). The experimental visualization

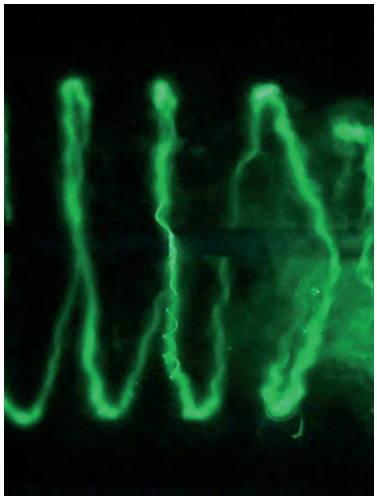

(a)

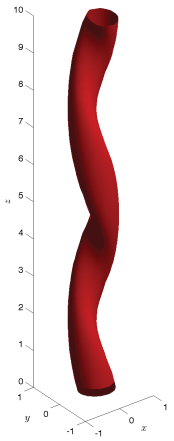

(b)

Fig. 1: (a) Visualisation of the short-wavelength instability developing in the core of a helical vortex (From T. Leweke, private communication). (b) Most unstable mode of the curvature instability for the experimental parameters of (a). Here is plotted an axial vorticity contour of the vortex deformed by the most unstable mode.

indeed shows a single strand structure with a wavelength $\lambda \approx 6a$ close to the theoretical prediction ($\lambda = 5.7a$).

The theoretical results are also validated by performing direct numerical simulations of the equations linearized around the base flow formed by the Batchelor vortex plus its dipolar correction. Both the structure and the growth rate of the perturbations obtained for large time from white noise initial conditions are compared to the theory, and a good agreement is demonstrated.

Acknowledgements. Financial support from the french Agence Nationale de la Recherche (ANR Helix project ANR-12-BS09-0023-01; LABEX MEC Project ANR-11-LABX-0092) is kindly acknowledged.

References

[1] Callegari, A. J. & Ting, L. (1978) Motion of a curved vortex filament with decaying vortical core and axial velocity. *SIAM Journal of Applied Mathematics* **35**, 148–175.

[2] Fukumoto, Y. & Hattori, Y. (2005) Curvature instability of a vortex ring. *J. Fluid Mech.* **526**, 77–115.

[3] Moore, D. W. & Saffman, P. G. (1975) The instability of a straight vortex filament in a strain field. *Proc. R. Soc. Lond. A.* **346**, 413–425.

[4] Hattori, Y. & Fukumoto, Y. (2014) Modal stability analysis of a helical vortex tube with axial flow. *J. Fluid Mech.* **738**, 222–249.

[5] Fabre, D., Sipp, D., & Jacquin, L. (2006) The Kelvin waves and the singular modes of the Lamb-Oseen vortex. *J. Fluid Mech.* **551**, 235–274.

[6] Ash, R. L. & Khorrami, M. R. (1995) Vortex stability. In *Fluid Vortices* (ed. S. I. Green), chapter VIII, pp. 317–372. Kluwer Academic Publishers.

[7] Leweke, T. Quaranta, H. U., Bolnot, H., Blanco-Rodriguez, F. J. & Le Dizs, S. (2014) Long- and short-wave instabilities in helical vortices. *J. Phys.: Conf. Ser.* **524** 012154.

Notes

Cascade of vortex knots detected by HOMFLYPT polynomial

Xin Liu[1] and Renzo L. Ricca[2]

[1] *BDIC & Institute of Theoretical Physics, Beijing University of Technology, P.R. China*
[2] *Department of Mathematics & Applications, University of Milano-Bicocca, Italy*

Summary

When unlinked, unknotted vortex loops are formed helicity may fail to detect topological complexity accurately. Here we prove that by using the recently derived HOMFLYPT polynomial for fluid knots (Liu & Ricca, 2015) each stage of a cascade process, that follows a complexity-reducing path given by a sequence of $T(2, 2n+1)$ torus knots and $T(2, 2n)$ torus links produced by consecutive reconnections, can be detected by a unique, monotonically decreasing sequence of HOMFLYPT numerical values. This opens the doors to useful applications in the study of the decay process of classical and quantum vortex tangles.

1 HOMFLYPT polynomial for vortex knots

Classical and quantum vortex tangles tend to interact and reconnect by undergoing a similar cascade process, that seems to consistently reduce topological complexity and structural scale by stepwise unlinking till final production and dissipation of small-scale loops [1]-[2]. Kinetic helicity is an appropriate measure of topological complexity, but it is known to suffer from some serious limitations. To overcome these difficulties Liu & Ricca have derived various knot polynomials (Kauffman bracket, Alexander–Conway, Jones and HOMFLYPT) for fluid knots as new invariants of ideal fluid mechanics. By applying knot theoretical techniques to vortex flows the HOMFLYPT polynomial $P = P_K$ has been recently derived from the kinetic helicity H of vortex knots [3].

Theorem (Liu & Ricca, 2015). *Let K denote a physical knot. If the helicity of K is $H = H(K)$, then*

$$e^{H(K)} = e^{\oint_K \mathbf{u}\cdot \mathrm{d}\mathbf{l}} \,, \tag{1}$$

appropriately re-scaled, satisfies (with a plausible statistical hypothesis) the skein relations of the HOMFLYPT polynomial $P = P_K$.

Remark 1. If K is a vortex knot, then $\mathbf{u}$ is the self-induced velocity associated with vorticity aligned along the knot centerline of elementary line element $\mathrm{d}\mathbf{l}$. To make sense of $e^{H(K)}$, $H(K)$ must be normalized with respect to some reference value of the vortex circulation Γ.

Remark 2. The derivation of the result above relies on a statistical hypothesis, that assumes equally probable state decomposition of the crossing sites in the minimal knot diagram. This is equivalent to the ergodic assumption that all possible (virtual) reconfiguration states of the given knot or link are equally admissible.

2 Cascade of vortex knots by stepwise unlinking detected by HOMFLYPT

Reconnections characterize the evolution and interaction of vortex filaments in both classical and quantum fluids and determine a change of topology of the system. While details of the process depend on specific local mechanisms that may differ from classical to quantum case, certain qualitative features — such as the preservation of the original strand orientation after reconnection — are generic and common to both systems. According to recent observations based on laboratory experiments and direct numerical simulations of decaying Bose-Einstein condensates [1]-[2], vortex knots

and links seem to undergo a generic cascade process through an alternate sequence of $T(2, 2n+1)$ torus knots and $T(2, 2n)$ torus links, as n (integer) decreases to 0. After every reconnection the knot/link gradually unties by removing a single crossing at a time, by reducing consistently topological complexity and scale. Remarkably, the sequence of topological transitions seems to follow an identical topological decay pattern, to some extent irrespective of the physical context considered, even consistent with recombinant DNA plasmid reactions [4].

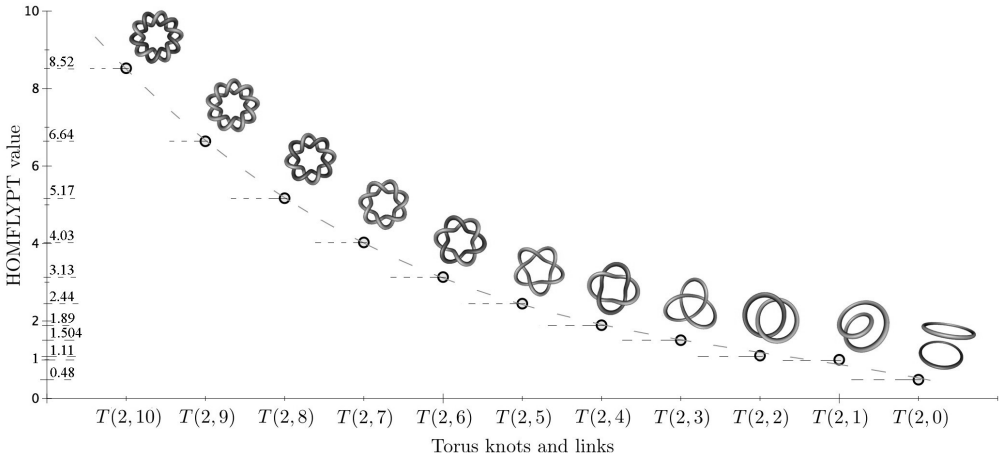

Figure 1: Cascade of torus knots and links detected by a monotonically decreasing sequence of HOMFLYPT numerical values.

Here we show that HOMFLYPT polynomial not only detects topological differences between knots and links (as standard knot polynomials typically do), but it can be used to *quantify* topological differences between the various stages of the cascade process by a unique, monotonically decreasing sequence of numerical values (see Figure 1). This result, anticipated by the recursive application of the HOMFLYPT skein relations on minimal knot diagrams, is proven analytically here by direct application of the skein relations [5]. Direct comparison of the decreasing sequence of numerical values of topological complexity with kinetic energy data of corresponding vortex knots [6] shows remarkable, similar features.

References

[1] Kleckner, D. & Irvine, W.T.M. (2013) Creation and dynamics of knotted vortices. *Nature Physics* **9**, 253–258.

[2] Zuccher, S. & Ricca, R.L. (2016) Cascade process of linked quantum vortex loops. Abstract submitted to this IUTAM Symposium.

[3] Liu, X. & Ricca, R. L. (2015) On the derivation of the HOMFLYPT polynomial invariant for fluid knots. *J. Fluid Mech.* **773**, 34–48.

[4] Shimokawa, K., Isihara, K., Grainge, I., Sherratt, D. J. & Vazquez, M. (2013) FtsK-dependent XerCD-dif recombination unlinks replication catenanes in a stepwise manner. *PNAS USA* **110**, 20906–20911.

[5] Liu, X. & Ricca, R.L. (2016) Knots cascade detected by a monotonically decreasing sequence of values. *Sci. Rep.* **6**, 24118.

[6] Maggioni, F., Alamri, S.Z., Barenghi, C.F. & Ricca, R.L. (2010) Velocity, energy, and helicity of vortex knots and unknots. *Phys. Rev. E* **82**, 26309–26317.

Notes

Groundstate magnetic energy vs bending energy of knots and links

Francesca Maggioni[1] and Renzo L. Ricca[2]

[1] *Department of Management, Economics & Quantitative Methods, University of Bergamo, Italy*
[2] *Department of Mathematics & Applications, University of Milano-Bicocca, Italy*

Summary

The groundstate magnetic energy spectra of the first 250 prime knots and 130 prime links are compared with the corresponding spectra obtained by computing the bending energy from data given by the `RIDGERUNNER` tightening algorithm (Ashton *et al.*, 2011). We find a remarkable similarity of power laws that demonstrate that even at fundamental energy level curvature information provides a good estimate for magnetic energy contents of complex structures.

1 Groundstate magnetic energy vs bending energy

The groundstate magnetic energy spectra of the first 250 prime knots and 130 prime links were determined by using earlier analytical results [2] and ropelength data given by the `RIDGERUNNER` tightening algorithm [1]. By normalizing magnetic energy with respect to the tight torus configuration we obtained an extremely simple formula for the non-dimensional magnetic energy $\tilde{m}(K)$ of a knot/link type K in terms of its ropelength λ_K [3], that is

$$\tilde{m}(K) = \left(\frac{\lambda_K}{2\pi}\right)^{4/3} . \tag{1}$$

The corresponding energy spectra are shown in Figure 1, where we see that the best-fit curves follow an almost identical logarithmic law. By assuming that the number of knot types grows exponentially with the topological crossing number $c_{\min}$, this common behaviour can be justified by relating ropelength and crossing number according to

$$\lambda(\#_K) \propto c_{\min}^{3/4} , \tag{2}$$

and more precisely

$$\langle \lambda(\#_K) \rangle_{c_{\min}} \geq 2\pi^{1/4} c_{\min}^{3/4} , \tag{3}$$

where angular brackets denote average over each $c_{\min}$-family.

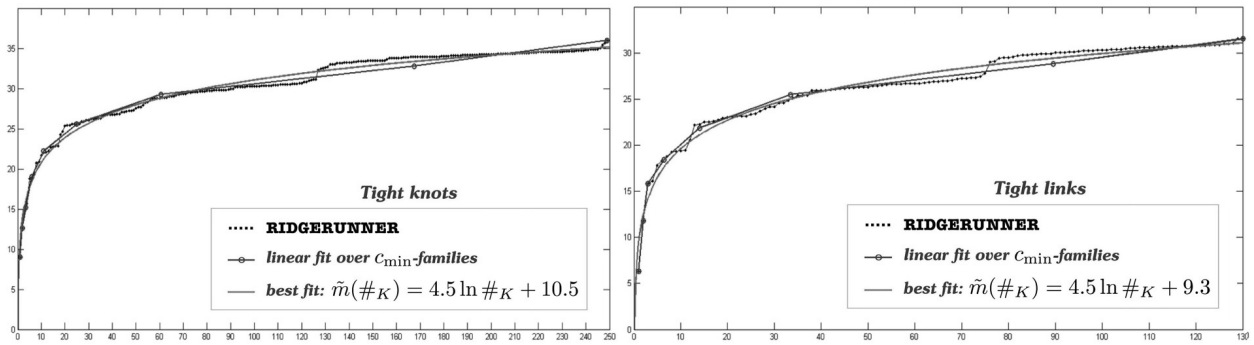

Figure 1: Magnetic energy spectra $\tilde{m} = \tilde{m}(\#_K)$ of the first (a) 250 prime knots and (b) 130 prime links, plotted against the position $\#_K$ of the knot/link listed according to increasing value of ropelength $\lambda_K = \lambda(\#_K)$ (from Ricca & Maggioni, 2013).

2 Comparative analysis between energy spectra of knots and links

Here we compare the groundstate magnetic energy spectra with the spectra obtained by considering the non-dimensional bending energy given by the standard curvature energy divided by that of a tight torus, i.e.

$$\tilde{e}(K) = \frac{\int_K [c(s)]^2 \mathrm{d}s}{2^{4/3}\pi^{5/3}} \ . \tag{4}$$

As suggested by a preliminary analysis [4] both spectra show a remarkable similarity, demonstrating that even at groundstate energy level curvature information provides good estimate for minimum magnetic energy contents. Since curvature is a geometric quantity that can be more easily estimated by direct inspection, this comparative study shows that morphological information can be used to estimate magnetic energy in contexts where direct measurements are more difficult or more expensive to obtain.

References

[1] T. Ashton, J. Cantarella, M. Piatek & E. Rawdon (2011) Knot tightening by constrained gradient descent. *Experim. Math.* **20**, 57–90.

[2] Maggioni, F. & Ricca, R.L. (2009) On the groundstate energy of tight knots. *Proc. R. Soc. A* **465**, 2761–2783.

[3] Ricca, R.L. & Maggioni, F. (2014) On the groundstate energy spectrum of magnetic knots and links. *J. Phys. A: Math. & Theor.* **47**, 205501–9.

[4] Ricca, R.L. (2013) New energy and helicity lower bounds for knotted and braided magnetic fields. *Geophys. Astrophys. Fluid Dyn.* **107**, 385–402.

Notes

Methods of topological data analysis to compare MHD simulations with observations

I. Makarenko, A. Shukurov, P. Bushby, A. Fletcher, R. Henderson

School of Mathematics and Statistics, Newcastle University, United Kingdom

Summary

We show how to apply methods of topological data analysis to compare and quantify the random fields appearing in MHD simulations and observations. We use the Betti numbers, persistence diagrams, and persistence barcodes to achieve the goal.

Due to recent advances in radio telescope instrumentation a number of wide-field high resolution surveys, especially radio emission from hydrogen atoms, are now becoming available. The data are rich enough to distinguish between different physical effects. We also have constantly improving MHD models that simulate the multiphase interstellar medium. The density and velocity distributions in observations, as well as the results of numerical simulations, appear as random fields with anisotropies and complex topology widely believed to be related to turbulence and outflows from the Galactic disk.

What tools can we use to compare and quantify the complicated topology of the random fields appearing in our observations and simulations? How to explore the degree of similarity of images dominated by random structures? How to confirm or disprove the adequacy of MHD models based on comparison with observations? In this talk we use some methods of topological data analysis to answer these questions.

Over the last decade topological approaches to the analysis of random fields have become more popular ([1]-[3]). The topological invariants called the Betti numbers, the Euler characteristic, which can be written as an alternating sum of the Betti numbers, persistence diagrams, and persistence barcodes for the random fields − all these new and rapidly developing techniques are being applied ([4]-[5]).

This talk includes a brief introduction to the basic concepts of topological data analysis illustrated by simple examples in 1 and 2 dimensions. The most promising and popular topological data analysis techniques for analysing images will be demonstrated using slices from MHD simulations of the interstellar medium. I will also use TDA to compare maps of the interstellar hydrogen distribution in different regions of the Galaxy. Using persistence diagrams and persistence barcodes I try to estimate how realistic the MHD model of the interstellar medium is.

Acknowledgements. This work is supported by the Leverhulme Trust Grant "Observations and models of turbulent flows: a topological approach" (2015-2019), RPG-2014-427.

References

[1] Adler, R. & Taylor, J.E. (2011) Topological Complexity of Smooth Random Functions: École d'Été de Probabilités de Saint-Flour XXXIX-2009. *Lecture Notes in Mathematics*. Springer Berlin Heidelberg. 122 p.

[2] Ghrist, R. (2014) Elementary Applied Topology. CreateSpace. 276 p.

[3] Edelsbrunner, H., Letcher D., & Zomorodian A. (2002) Topological persistence and simplification. *Discrete and Computational Geometry.* 2002 **4**, 511–533.

[4] Sousbie, T. (2011) The persistent cosmic web and its filamentary structure I. Theory and implementation. *MNRAS.* 2011 **414** (1), 350–383.

[5] Kramar M., Levanger R., Tithof J., Suri B., Xu M., Paul M., Schatz M. & Mischaikow, K. (2015) Analysis of Kolmogorov Flow and Rayleigh-Bénard Convection using Persistent Homology. ArXiv preprint, arXiv:1505.06168, 2015.

Notes

Entanglement Transitions in Confined Fluid Flows

K. C. Millett[1], E. Panagiotou[2]

[1] *Department of Mathematics, University of California, Santa Barbara, USA*
[2] *Department of Mathematics, University of California, Santa Barbara, USA*

Summary

Employing a course grained Periodic Boundary Condition (PBC) simulation, we consider the entanglement of fluid flow trajectories, vortex lines, confined to a tube with square cross section when subjected to flow alignment constraints. We study these as a function of the complexity of the system, the scale of the cross section, and the strength of the alignment constraint. To do so, we employ Panagioutous periodic linking number and periodic self-linking number, notions related to the helicity of the system, as well as the associated periodic linking matrix and the eigenvalues that are determined by this matrix. These provide physical measures of the structure and, thereby, insights into the resulting character of the entanglement in these models. As a consequence, we are able to determine the topological transitions associated to changes in the structural complexity of the system, the cross section scale, and the alignment constraint.

1 Introduction

In 1877, Gauss defined the linking number associated to two closed oriented smooth curves, $\mathbf{L_1}$ and $\mathbf{L_2}$, in space [3]:

$$lk(\mathbf{L_1}, \mathbf{L_2}) = \frac{1}{4\pi} \int_{\mathbf{L_1} \times \mathbf{L_2}} \frac{(\gamma_1(t) - \gamma_2(s)) \cdot dA}{\|\gamma_1(t) - \gamma_2(s)\|} \quad (1)$$

For a system of two line vortices , $\mathbf{L_1}$ and $\mathbf{L_2}$, of strengths $\kappa_\mathbf{1}$ and $\kappa_\mathbf{2}$, satisfying certain conditions, in 1969 Moffat defined the helicity in an appropriate spatial region, V, related to the linking number [1, 2]:

$$H = \int_V \vec{u} \cdot \vec{\omega} \; dV = 2 \; lk(\mathbf{L_1}, \mathbf{L_2}) \; \kappa_1 \; \kappa_2 \quad (2)$$

establishing a relationship between the helicity and properties of a discrete course-grained simulation that can be employed in simulations such as the Periodic Boundary Condition (PBC) models we employ here, [4, 5].

Our PBC models are generated by a cell, with square cross-section, containing polygonal arcs with identical normal intersection on the two opposing faces or interior endpoints. This structure generates the infinite *periodic system* whose polygonal arcs are required, in the present case, to be finite. The *periodic linking number* between distinct arcs is definded to be the sum of the linking numbers of the first with all the translates (in the periodic system) of the second [5], Analogously, one may define the *periodic self-linking number* of an arc. These determine the *periodic linking matrix* consisting of entries determined by these periodic linking numbers and the resulting eigenvectors (since this is a real symmetric matrix) that expresses topological properties of the system. The constraints are realized by using unit length polygon edges, varying the edge length of the square cross-section to realize the confinement, and the degree of alignment of the directed edges with the positive axis of the system to control the character of the flow, evolving between *chaotic* and *strongly aligned*.

2 Structural Transitions

As the number and length of the vortex lines change, the degree of confinement measured by the dimension of the square cross-section, and the directional strength of the flow as measured by the strength of alignment to the axis, we report the evolution of the densitiy of the flow (measured by the squared radius of gyration of the vortex lines) and the evolution of the topoplogical entanglement (measured by the eigenvalues of the periodic linking matrix). This evolution reports the entanglement transitions in these course grained simulations of confined fluid flows.

References

[1] Moffatt, H.K. (1969) The degree of knottedness of tangled vortex lines. *J. Fluid Mech.* 1969 **35**, 117–129.

[2] Ricca, R.L. (2009) Structural complexity and dynamical systems. In *Lectures on Topological Fluid Mechanics* (ed. R.L. Ricca), pp. 169–188. Springer-CIME Lecture Notes in Mathematics **1973**. Springer-Verlag.

[3] Gauss, K.F. 1877 Zur Mathematischen Theorie der Electrodynamischen Wirkungen *Werke vol 5* 1877, 605 Konigl. Ges. Wiss. Gottingen.

[4] Panagiotou, E., Millett, K. & Lambropoulou, S. 2012 Quantifying entanglement for collections of chains in models with periodic boundary conditions. *Procedia IUTAM: Topological Fluid Dynamics II*2012 **7**, 251 – 260.

[5] Panagiotou, E. 2015 The linking number in systems with Periodic Boundary Consitions. *J. Comp. Physics*2015 **300**,533–573 .

Notes

Mean MEF in current sheets

K. A. Mizerski[1], H. K. Moffatt[2]

[1] *Department of Magnetism, Institute of Geophysics, Polish Academy of Sciences, Warsaw, Poland*
[2] *Department of Applied Mathematics and Theoretical Physics, University of Cambridge, Cambridge, UK*

Summary

We present the study of the spatial structure of the so-called tearing modes in current sheets and the mean electromotive force induced by finite resistivity instability. The dependence of the mean EMF on the magnetic helicity of the large-scale field is obtained.

1 Formulation of the problem

The aim is to calculate the mean electromotive force, $\boldsymbol{\mathcal{E}}$, generated by finite resistivity instabilities of a sheet pinch, studied by [1], but in the limit of constant resistivity and negligible gravity. In such case the formulation of the problem must be somewhat different than in the famous aforementioned paper [1], since without gravity and with uniform resistivity the basic unperturbed state, which by assumption possesses a current sheet, requires the presence of strong gas pressure balancing the Lorentz force. Therefore we formulate the problem as follows. The unperturbed state, denoted by subscript 0 satisfies the following equations

$$\mathbf{u}_0 = 0, \quad \nabla p_0 = \frac{1}{\mu_0} \left(\nabla \times \mathbf{B}_0\right) \times \mathbf{B}_0, \quad \frac{\partial \mathbf{B}_0}{\partial t} = \eta \nabla^2 \mathbf{B}_0, \tag{1}$$

and $\mathbf{B}_0$, by assumption, possesses a current sheet and has the form

$$\mathbf{B}_0 = B_{0x}(y)\hat{\mathbf{e}}_x + B_{0z}\hat{\mathbf{e}}_z, \tag{2}$$

where $B_{0z} = \text{const}$. Because the growth rates of the tearing modes are very large, the time of growth of the instability is very short in comparison with the magnetic diffusion timescale, δ^2/η, where δ denotes the thickness of the current sheet and hence the basic state can be considered quasi-stationary in the stability analysis. We, therefore, neglect the time dependence of the unperturbed magnetic field distribution $\mathbf{B}_0$ in the following. Furthermore, with the form (2) of the basic field the Lorentz force is potential and the Navier-Stokes equation in (1) is simply an equation for the basic pressure distribution.

2 Results

Introducing perturbations, $\mathbf{B} = \mathbf{B}_0 + \mathbf{b}(y)\exp[i(k_x x + k_z z) + \sigma t]$ and $\mathbf{u}(y)\exp[i(k_x x + k_z z) + \sigma t]$, we arrive at th followinge non-dimensional, linearised equations for perturbation fields

$$b_y'' = \left(\kappa^2 + \sigma\right) b_y - \mathrm{i}\kappa\beta u_y, \tag{3}$$

$$u_y'' = \kappa^2 \left(1 + \frac{H^2}{\sigma}\beta^2\right) u_y + \mathrm{i}H^2 \left(\beta - \frac{1}{\sigma}\beta''\right) b_y, \tag{4}$$

where $\kappa = k\delta$, $H = B_0\delta/\eta\sqrt{\mu_0\rho_0}$ and

$$\beta(y) = \frac{k_x B_{0x}(y) + k_z B_{0z}}{k B_0}. \tag{5}$$

Considering most unstable cases with $\beta(y) = (\kappa_x/\kappa)\tanh(y)$ it is possible to find asymptotic solutions of the above equations (3)-(4) in the limit $H \gg 1$. This, then, allows to calculate the mean electromotive force, which in the additionl limit of thin current sheet, $\kappa \ll 1$ possesses a dominant y-component of the form

$$\mathcal{E}_y \sim \frac{\mathbf{J}_0 \cdot \mathbf{B}_0}{1 + \mathrm{const}\mathbf{J}_0 \cdot \mathbf{B}_0}. \tag{6}$$

Acknowledgements. This work was supported within statutory activities no. 3841/E-41/S/2015 and by the grant no. IP2014 031373 of the Ministry of Science and Higher Education of Poland.

References

[1] Furth, H.P., Killeen, J. & Rosenbluth, M.N. (1963) Finite-Resistivity Instabilities of a Sheet Pinch. *Phys. Fluids* 1963 **6**, 459–484.

Notes

Magnetic Relaxation and the Taylor Conjecture

H.K.Moffatt[1]

[1] *Department of Applied Mathematics and Theoretical Physics, University of Cambridge, Wilberforce Road, Cambridge CB3 0WA, UK*

Summary

Helicity plays a dual role in astrophysical MHD: on the one hand, mean helicity in a turbulent velocity field is known to be extremely conducive to dynamo action, the large-scale magnetic field that is generated usually then exhibiting magnetic helicity of the opposite sign. On the other hand, if we start with a helical magnetic field in a perfectly conducting fluid at rest, assumed perfectly conducting, and allow the field to relax to a minimum energy state, then the invariance of magnetic helicity (Woltjer 1958) acts as a powerful constraint, leading to the formation of tangential discontinuities, i.e. current sheets, where dissipative plasma heating tends to be concentrated. This happens both in the incompressible (volume-preserving) limit (Moffatt 1985), and in the very low-density limit when magnetic pressure dominates over fluid pressure. It is these properties of helicity that makes it of such fundamental interest, as recognised by the theme of this IUTAM Symposium.

This lecture will be devoted to a generalisation of a simple one-dimensional Cartesian model of magnetic relaxation in a pressureless low-resistivity plasma, as introduced by Bajer & Moffatt (2013) and subsequently developed in a manner that incorporates evolution of helicity density (Moffatt 2015). In this situation, a velocity field is driven solely by the gradient of magnetic pressure, and is dissipated by viscosity. Relaxation occurs in two phases: a rapid initial phase in which the magnetic energy drops sharply and the magnetic pressure becomes approximately uniform; the helicity density is redistributed during this phase but remains non-uniform. The total helicity remains constant , but a Taylor state of uniform helicity (Taylor 1974,1986) is not established. The second phase is one of slow diffusion, in which the velocity is weak, though still driven by persistent weak non-uniformity of magnetic pressure; during this phase, magnetic energy and helicity decay slowly at the same rate through the combined effects of persistent pressure equalisation and finite resistivity. The density field, initially uniform, develops rapidly during the initial phase, and continues to evolve, developing sharp maxima, throughout the diffusive stage. In this lecture, this model will be extended to a cylindrical geometry with both axial and toroidal magnetic field components, for which a radial velocity field is driven by a combination of hoop stress and magnetic pressure. Results concerning the evolution of helicity and density fields in this still idealised situation will be presented.

References

[1] Bajer, K. & Moffatt, H. K. (2013) Magnetic relaxation, current sheets, and structure formation in an extremely tenuous fluid medium. *Astrophys. J.* **779**, 169-182.

[2] Moffatt, H. K. (1985) Magnetostatic equilibria and analogous Euler flows of arbitrarily complex topology. 1. Fundamentals. *J. Fluid Mech.* **159**, 359-378.

[3] Moffatt, H.K.(2015) Magnetic relaxation and the Taylor conjecture. *J. Plasma Phys.* **81**, 905810608.

[4] Taylor, J. B. (1974) Relaxation of toroidal plasma and generation of reverse magnetic fields, *Phys. Rev. Lett.* **33**, 1139-1141.

[5] Taylor, J. B. (1986) Relaxation and magnetic reconnection in plasmas, *Rev. Mod. Phys.* **58**, 741-763.

[6] Woltjer, L. (1958) A theorem on force-free magnetic fields. *Proc. Nat. Acad. Sci.* **44**, 489-491.

Notes

Cyclonic vortices inside a precessing cylinder flow : instability and change of topology

W. Mouhali[1], T.Lehner[2], J.Sommeria[3], C.Elagoz[3]

[1] *Licorne, ECE Paris School of Engineering, France*
[2] *Luth, CNRS, Observatoire de Paris-Meudon, France*
[3] *Legi, CNRS, Université de Grenoble, France*

Summary

We report results from the observation of cyclones in our experiment involving water in a precessing cylinder: it creates a radical change of topology and induces a strong change in the differential rotation profile. We propose a mechanism explaining their generation from the mode coupling of two inertial waves with azimuthal wavenumber $m = 0$ and $m = 1$ (mode forced by the precession) in the inviscid regime. This nonlinear coupling creates a differential rotation regime which has been observed in the same experiment at small enough Poincar number ε (ratio of the precession to the rotation angular speed). We apply a generalized criteria with axial flow from Billant & Gallaire. Then, we show that when the parameter ε is increased from low values one mode becomes the most instable which can induce further the observed cyclones. Radial jets coming from the lateral boundary layers have been also observed which can drive additional instabilities in the boundary shear layer.

1 Description of experimental results

Our study is motivated by the fluid dynamo context, since it has been proposed that precession could be a good candidate for driving dynamo action in a conducting fluid. The system consists of a right cylinder filled with water and put into rotation at the angular velocity Ω_0 around its symmetry axis (defining the z direction). It is mounted on an horizontal platform rotating at the angular velocity Ω_P (in the x direction). The cylinder spin axis is tilted relative to the rotation axis of the platform with a fixed angle of $\pi/2$. Each rotation can be independently varied. All measurements were obtained by usual PIV techniques. We have observed in the laminar phase of our flow three well identified regimes according to the values of the forcing parameter [1]: laminar steady flow, instability at a critical value $\varepsilon = \varepsilon_{th}$ and then a regime dominated by cyclones at higher ε. For very small ε ranging up to about 10^{-3} to 10^{-2}, the flow appears as a quasi-steady solution in the precessing frame and vorticity distributions remains smooth: the flow behaves closely to the stationary linearized solution(dominance of the forced by precession $m = 1$ inertial mode (m is azimutal wavenumber).
Keeping here a fixed aspect ratio of the cylinder, when ε exceeds a critical value ε_{th} here of about 0.025, the flow changes radically and a new regime sets in (Fig.1). In a cross section of the flow normal to the rotation axis, a few vortices become visible, rotating in the same direction as the one of the container [1]. We can notice the global increase of the differential rotation as a function of ε. Furthermore, one can notice inflectional points (not shown here, see [2]) on the axial vorticity ω_z of the mean flow.

We also observed radial jets coming from the lateral boundary layers. They can drive additional instabilities in the boundary shear layer (Fig.2).

2 Theoretical analysis for the instability mechanism

From weakly nonlinear coupling between a base flow (v_{bf}) and two inertial waves, we can calculate the differential rotation profile. Using the explicit expressions for the Kelvin inertial modes radial

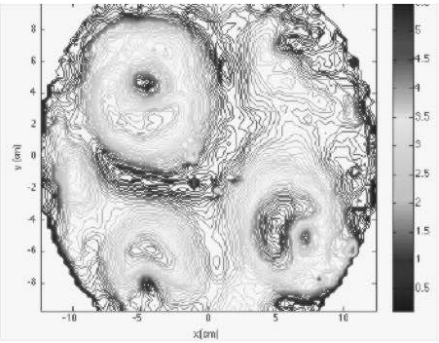

Fig. 1: Change of topology : apparition of cyclonic vortices from instability (magnitude of the 2D velocity field). [1]

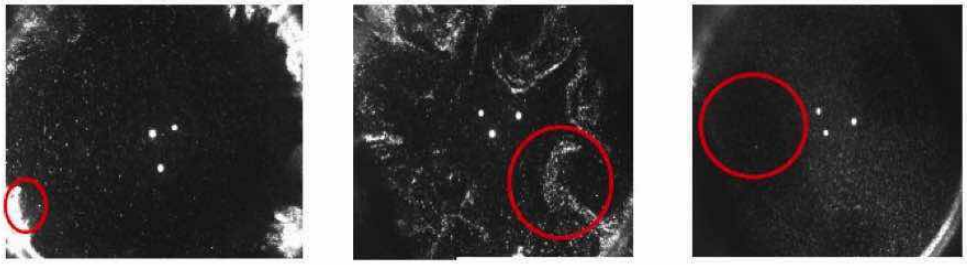

Fig. 2: Instability from boundary layer. [1]

profiles, we get the azimuthal velocity correction $v_{bf}^{(2)}$(and $\Omega(r)^{(2)}$) at 2nd order perturbation as [2]

$$\frac{\mathrm{v}_{bf}^{(2)}(r)}{a_{10}} = \frac{(J_1(\lambda r)J_1'(\lambda r))}{(\mu c_1\,(4-c_0^2))} + \frac{J_0'(\lambda r)((c_1+2)J_0(\mu r)+(c_1-2)J_2(\mu r)}{(2\lambda c_0\,(4-c_1^2))} \tag{1}$$

with $J_m = \frac{dJ_m}{dr}$, $c_0 = \frac{\pm\omega}{\Omega_0}$, $c_0 = c_1 + m$, $a_{10} = \frac{k_z}{k_0}$, $k_0 = \frac{\Omega_0}{V_0} = 1/R$. Here, J_i stands for Bessel function ; ω the pulsation of Kelwin waves ; m the azimutal wavenumber ; k_z the axial wavenumber.

For the numerical coefficients (coupling point coefficient), we have : $a_{10} = 0.878$; $c_0 = -0.451$; $\lambda = 3.83$; $\mu = 3.05$.[2]

From this differential profile, we apply a generalized Rayleigh criterion for system with axial flow [3]. We derive new growth rates for the unstable mode and we can predict a threshold for the observed instability. This is in good agreement with the experimental results.

References

[1] Mouhali, W., Lehner, T., Lorat, J., Vitry, R.(2012) *Evidence for a cyclonic regime in a precessing cylindrical container.*. Experiments in fluids, **53(6)**, 1693-1700

[2] Lehner, T., Mouhali, W., Leorat, J., Mahalov, A. (2010) Mode coupling analysis and differential rotation in a flow driven by a precessing cylindrical container. *Geophysical and Astrophysical Fluid Dynamics* 2010 **104(4)**, 369-401.

[3] Billant, P., & Gallaire, F. (2013) A unified criterion for the centrifugal instabilities of vortices and swirling jets. *Journal of Fluid Mechanics* 734, 5-35.

Notes

Relationships between eigen-vortical-axis line and vorticity line

K. Nakayama[1], H. Hasegawa[2]

[1] *Department of Mechanical Engineering, Aichi Institute of Technology, Aichi, Japan*
[2] *Division of Mechanical Engineering, Graduate School of Engineering, Aichi Institute of Technology, Aichi, Japan*

Summary

Eigen-vortical-axis line has been proposed (Nakayama et al. (2015) *AIP Proc.*) as a vortical axis derived from the invariant local flow topology, and shown that it follows a vortical core region whereas the vorticity line may deviate from it. The present study shows that their difference is derived from the vorticity components parallel to the swirl plane and that these components incline both lines to the swirl plane and may deviate the vorticity line.

1 Eigen-vortical-axis line and its feature

In the velocity field, the local flow around a point can be expressed by the velocity gradient tensor $\nabla \boldsymbol{v}$, thus the local flow topology is specified by the eigenvalues and eigenvectors of $\nabla \boldsymbol{v}$ [1]. If $\nabla \boldsymbol{v}$ has a pair of complex conjugate eigenvalues $\varepsilon_R \pm i\psi$ ($\psi > 0$) and a real one ε_a, and their respective eigenvectors $\boldsymbol{\xi}_{pl} \pm i\boldsymbol{\eta}_{pl}$ and $\boldsymbol{\zeta}$, then the flow trajectory can be represented as $\boldsymbol{x} = 2e^{\varepsilon_R t}\{\boldsymbol{\xi}_{pl}\cos(\psi t) - \boldsymbol{\eta}_{pl}\sin(\psi t)\} + e^{\varepsilon_a t}\boldsymbol{\zeta}$, where the local flow swirls in the swirl plane $\mathcal{P}$ defined by $\boldsymbol{\xi}_{pl}$ and $\boldsymbol{\eta}_{pl}$, with converging or diverging according to ε_R, and proceeds (or approaches) along a vortical axis $\boldsymbol{\zeta}$. Then $\boldsymbol{\zeta} = [\zeta_i]$ ($i = 1, 2, 3$) represents the local axis direction of the vortical flow, and eigen-vortical-axis line is defined as an axis line in which an axis point $\boldsymbol{\alpha} = [\alpha_i]$ ($i = 1, 2, 3$) is derived from the following equation [2]:

$$\frac{d\alpha_1}{\zeta_1} = \frac{d\alpha_2}{\zeta_2} = \frac{d\alpha_3}{\zeta_3}. \tag{1}$$

$\nabla \boldsymbol{v}$ ($= [\partial v_i/\partial x_j] = [a_{ij}]$ ($i, j = 1, 2, 3$)) in an orthonormal coordinate system x_i with unit bases $\boldsymbol{e}_i$ where $\boldsymbol{e}_1$ and $\boldsymbol{e}_2$ are parallel to $\boldsymbol{\xi}_{pl}$ and $\boldsymbol{\eta}_{pl}$, respectively, can be expressed as:

$$\nabla \boldsymbol{v} = \begin{bmatrix} \varepsilon_R & c\psi & a_{13} \\ -\psi/c & \varepsilon_R & a_{23} \\ 0 & 0 & \varepsilon_a \end{bmatrix}, \tag{2}$$

where $c = |\boldsymbol{\xi}_{pl}|/|\boldsymbol{\eta}_{pl}|$ given by the eigenequations of $\nabla \boldsymbol{v}$. c specifies the vortical flow symmetry in $\mathcal{P}$ [3]. a_{13} and a_{23} are associated with the vorticity component $\boldsymbol{\omega} = [\omega_i]$ ($i = 1, 2, 3$), i.e., $\omega_1 = -a_{23} = (\boldsymbol{\omega}, \boldsymbol{e}_1)$ and $\omega_2 = a_{13} = (\boldsymbol{\omega}, \boldsymbol{e}_2)$. Note that $\omega_3 = (c + 1/c)\varphi$, and ω_3 is equal to the eigen helicity density [4] that is the vorticity component normal to $\mathcal{P}$ [3]. $\boldsymbol{\zeta}$ is expressed as $\boldsymbol{\zeta} \parallel (-c\psi\omega_1 - \varepsilon\omega_2, \varepsilon\omega_1 - \psi\omega_2/c, \varepsilon^2 + \psi^2)$ where $\varepsilon = \varepsilon_R - \varepsilon_a$. $\boldsymbol{\zeta}$ is not orthogonal to $\mathcal{P}$ in general, and the angle θ between $\boldsymbol{\zeta}$ and $\boldsymbol{e}_3$ (normal vector of $\mathcal{P}$) is influenced by ω_1 and ω_2. If $\omega_1 = \omega_2 = 0$, then $\boldsymbol{\zeta} \perp \mathcal{P}$ and $\boldsymbol{\zeta} \parallel \boldsymbol{\omega}$.

2 Numerical Analysis

The eigen-vortical-axis and vorticity lines in the vortical region are analyzed in isotropic homogeneous decaying turbulence in Direct Numerical Simulation by the pseudo-spectral method with the phase shifting method and the wavenumber $|k| < 121$ [2, 5]. Figure 1 shows the vortical regions (in subregion of the analytical domain) specified by the swirlity φ [3] that represents the swirling intensity in terms of the geometrical mean and is equal to ψ in the vortical region. φ is nondimensionalized by its root mean square value at the corresponding time, and Taylor Reynolds number

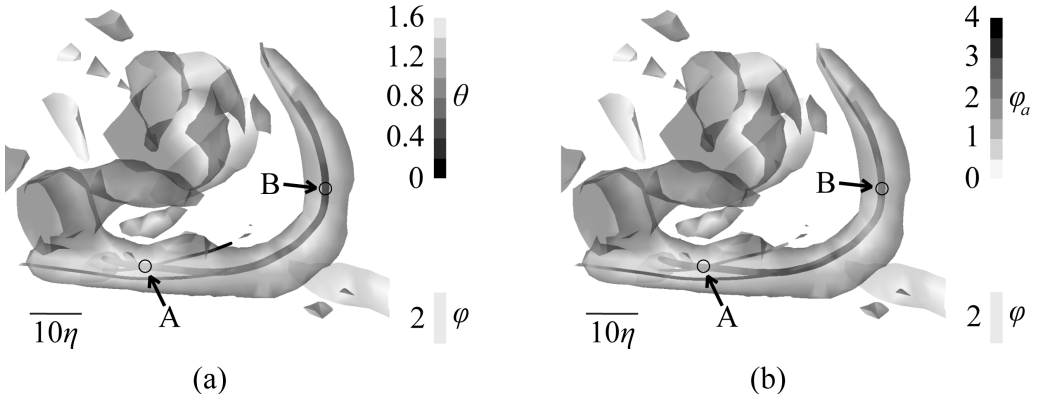

Fig. 1: Vortical regions represented by contours of $\varphi = 2$, and an eigen-vortical-axis line (bold line) and two vorticity lines (narrow lines) in $37\eta \times 37\eta \times 37\eta$ domain (η: Kolmogorov length; $\eta = 0.012$). The arrows indicate the initial points of tracing the lines. The colors of the lines show (a) θ and (b) φ in axes (denoted as θ_a and φ_a, respectively).

$\mathrm{Re}_\lambda = 35$. An eigen-vortical-axis line and two vorticity lines are also shown in Fig. 1 that are traced with the initial points in the vortical region indicated by the two arrows (A and B). The eigen-vortical-axis lines traced from two initial points have the same orbit, and follow the vortical region with strong φ, where the vorticity and eigen helicity density have the similar features. On the other hand, one vorticity line traced from the initial point A with a large θ as shown in Fig. 1 (a) deviates from the vortical core region (contour) and has weaker φ. However, another vorticity line traced from the point B with a small θ follows the vortical region. ω_1 and ω_2 incline both $\boldsymbol{\zeta}$ and $\boldsymbol{\omega}$ to $\mathcal{P}$, and they may effect deviation from the vortical region. But a vorticity line that passes a point in the vortical core region with a small θ, i.e., with small ω_1 and ω_2 values, seems to follow the vortical core region.

3 Conclusion

The eigen-vortical-axis line is influenced by the vorticity components parallel to the swirl plane, and they derive the difference between the axis and vorticity line. They incline the both lines to the swirl plane, and may deviate the vorticity line from the vortical core region.

Acknowledgements. This study was supported by the 31st grant from The Nitto Foundation.

References

[1] Chong, M. S., Perry, A. E., & Cantwell, B. J. (1990) A general classification of three-dimensional flow fields. *Phys. Fluids* **A2**(5), 765–777.

[2] Nakayama, K. & Hasegawa, H. (2015) A numerical method of tracing a vortical axis along local topological axis line. *AIP Proc.* (ICNAAM2015) (in press).

[3] Nakayama, K. (2014) Physical properties corresponding to vortical flow geometry. *Fluid Dyn. Res.* **46**, 055502.

[4] Zhang, S. & Choudhury, D. (2006) Eigen helicity density: a new vortex identification scheme and its application in accelerated inhomogeneous flows. *Phys. Fluids* **18**, 058104.

[5] S. Kida, S. & Miura, H. (1998) Identification and analysis of vortical structures. *E. J. Mech. B/Fluids* **17**(4), 471–488.

Notes

Non-linear Schrödinger equation, helicity and strings with applications to proteins

A.J. Niemi

Department of Physics and Astronomy, Uppsala University, Sweden

Summary

We argue that the Landau free energy of a three dimensional string-like object coincides with the Hamiltonian of non-linear Schrödinger equation (NLSE), with an additional helicity contribution. The solitons of the NLSE have a geometric correspondence with loop-like structures that interpolate between helical structures. As an application we show that proteins in their native state can be modelled in terms of multi-soliton solutions of the NLSE, with atomic level precision. Background material for the presentation can be found at Les Houches 2014 lectures

`http://arxiv.org/pdf/1412.8321.pdf`

Notes

Magnetic energy and helicity of torus knots and unknots

Chiara Oberti and Renzo L. Ricca

Department of Mathematics and Applications, University of Milano-Bicocca, Italy

Summary

In this paper we present new results on magnetic energy and helicity of steady magnetic fields in the shape of torus knots and unknots in ideal MHD. Bounds on energy and new estimates of energy and helicity in terms of geometric properties are given. In particular we demonstrate that in the case of toroidal knots/unknots information on the writhing number provides a very good approximation for magnetic helicity. These results are particularly useful for energy and helicity estimates of braided magnetic fields in the solar corona and in fusion physics.

1 Magnetic torus knots and unknots in ideal conditions

Magnetic torus knots and unknots are given by steady magnetic fields in the shape of a torus knot/unknot. Torus knots $\mathcal{T}_{p,q}$ are closed, space curves wrapped uniformly around the surface of a mathematical torus p times along the longitudinal (toroidal) direction and q times along the meridian (poloidal) direction. Knots are given by $p > 1$ and $q > 1$ wraps, with p and q co-prime integers, while unknots are obtained by taking $p = 1$ or $q = 1$. By using standard parametrization in terms of the torus aspect ratio λ and winding number $w = q/p$ we can study magnetic knots by simply identifying the magnetic field $\mathbf{B}$ with the knot type, assuming an infinitesimally thin cross-section and constant flux. Since for every $\mathcal{T}_{p,q}$ there is a critical aspect ratio for which the knot has q points of inflexion [2] and since inflexional configurations are highly unstable [1], we prescribe the conditions for inflexion-free configurations.

2 Energy and helicity estimates by geometric information

Under the above assumptions magnetic energy becomes simply proportional to the knot length, growing with the number of coils and aspect ratio [2]. Lower and upper bounds on magnetic energy are prescribed in terms of geometry and topological complexity of the knot type. By reducing the Biot-Savart integral to a line integral we can compute magnetic helicity by its integral definition and compare the results with those obtained by using information on total writhe Wr and normalized total torsion T. We show that computation of these geometric quantities provides a very good estimate of the exact value obtained by the integral definition of helicity [3].

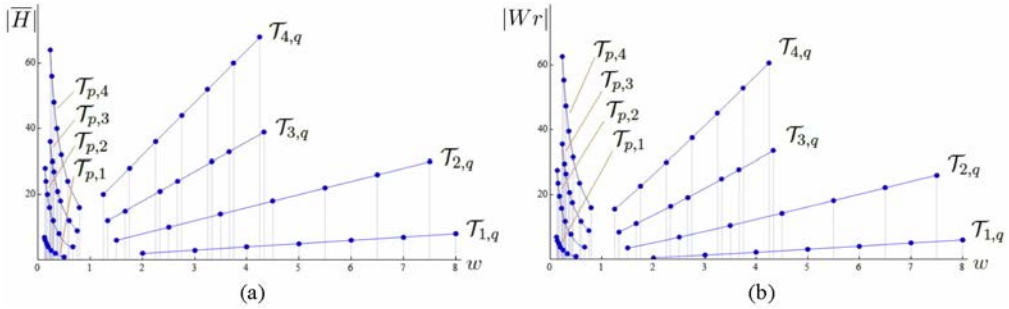

Figure 1: (a) Non-dimensional helicity $|\overline{H}|$ and (b) writhing number $|Wr|$ plotted against the winding number w for torus knots $\mathcal{T}_{p,1}$, $\mathcal{T}_{1,q}$, $p, q \in \{2, 3, 4, 5, 6, 7, 8\}$; $\mathcal{T}_{p,2}$, $\mathcal{T}_{2,q}$, $p, q \in \{3, 5, 7, 9, 11, 13, 15\}$; $\mathcal{T}_{p,3}$, $\mathcal{T}_{3,q}$, $p, q \in \{4, 5, 7, 8, 10, 11, 13\}$; $\mathcal{T}_{p,4}$, $\mathcal{T}_{4,q}$, $p, q \in \{5, 7, 9, 11, 13, 15, 17\}$ and $\lambda = 0.5$. Interpolation is for visualization purposes only.

Moreover, since contributions from T are one order of magnitude smaller than those due to Wr, we demonstrate that total writhe provides a very good approximation for (non-dimensional) magnetic helicity (see Figure 1 above). For toroidal knots/unknots the mean relative error $\Delta_{Wr} = (|\overline{H}| - |Wr|)/|\overline{H}|$ is generally well below 9%. Since torus knots are particularly simple types of closed braids, these results provide useful information for energy and helicity estimates of braided magnetic fields in solar coronal structures and fusion physics [4].

References

[1] Ricca, R.L. (2005) Inflexional disequilibrium of magnetic flux tubes. *Fluid Dyn. Res.* **36**, 319–332.

[2] Oberti, C. & Ricca, R.L. (2016) On torus knots and unknots. *J. Knot Theory & Its Ramif.* **25**, 1–18.

[3] Oberti, C. & Ricca, R.L. (2016) On magnetic knots and unknots. In *New Directions in Geometric and Applied Knot Theory* (edited by A. Schikorra, S. Blatt & P. Reiter), in preparation. Series on OA Measure Theory, De Gruyter, Basel.

[4] Ricca, R.L. (2013) New energy and helicity lower bounds for knotted and braided magnetic fields. *Geophys. Astrophys. Fluid Dyn.* **107**, 385–402.

Notes

A TOY FOR TURBULENCE

P. Orlandi[1], S.Pirozzoli[1], M.Bernardini[1] & G.F. Carnevale[2]

[1] *DIMA, Università di Roma "La Sapienza", Italia*
[2] *Scripps Institution of Oceanography, University of California San Diego, USA*

Summary

The present research is aimed at understanding the subtle (and not yet fully understood) relationship between the complex nonlinear dynamics of fluid turbulence and Kolmogorov power-law scaling in wavenumber space. Time evolution is often overlooked in DNS of turbulent flows, hence investigation of a suitably simple Minimal Flow Unit (MFU) can help to understand the passage from a vortical-dominated stage to a turbulent stage having all the ingredients of turbulent flows. In particular, we aim at clarifying the physical phenomena associated with the formation of a finite-time singularity (FTS) in the Euler equations and of Kolmogorov's $k^{-5/3}$ scaling in the Navier-Stokes equations. For that purpose, high-resolution simulations of the Euler and Navier-Stokes equations are carried out and analyzed by means of state-of-the-art eduction techniques to isolate the contribution of tube-like and sheet-like structures. Equipping the MFU with passive scalars (relevant in turbulent combustion) further helps understanding why passive scalar spectra have a different behavior than the velocity field spectra close to the FTS, but they also attain a $k^{-5/3}$ power spectrum at subsequent times, in the presence of finite viscosity. By adding a passive vector (relevant in MHD flows), dynamical differences with respect to the vorticity field can also be established.

The MFU has been also used to investigate the possibility to destroy the coherence of wake vortices generate by airplanes during landing or take-off. Simulations of Lamb dipoles interacting with walls with solid obstacles of different shape or with walls with an array of small jets demonstrate that it is possible to reduce the energy content of the wake vortices. The practical results is to increase the airport capacity.

Notes

Eye formation in rotating convection

L. Oruba[1], P.A. Davidson[2] and E. Dormy[3]

[1] *Department of Physics, Ecole Normale Supérieure (Paris), France*
[2] *Department of Engineering, University of Cambridge, United Kingdom*
[3] *Department of Physics, Ecole Normale Supérieure (Paris), France*

Summary

Rotating Rayleigh-Bénard convection has been extensively studied in the case on a container with an aspect ratio close to unity. Here we stress news effects associated with rotating thermal convection in elongated domains. Perhaps, surprisingly, we find that in such domains, an eye develops near the axis of the convective cell, in the form of a reversed vortex, reminiscent of Moffatt vortices. Although our system is very idealised compared with atmospheric convection, we highlight connections between the mechanism at work in our model and the formation of eye in tropical cyclones.

Notes

Magnetic helicity conservation in a solar active event

E. Pariat[1], G. Valori[2], P. Démoulin[1], K. Dalmasse[3]

[1] *LESIA, Observatoire de Paris, PSL Research University, CNRS, Sorbonne Universités, UPMC, Univ. Paris Diderot, Sorbonne Paris Cité, France*
[2] *UCL-Mullard Space Science Laboratory, UK*
[3] *CISL/HAO, National Center for Atmospheric Research, CO, USA*

Summary

Magnetic helicity has the remarkable property of being a conserved quantity of ideal magnetohydrodynamics (MHD). Therefore, it could be used as an effective tracer of the magnetic field evolution of magnetized plasmas. Magnetic helicity is thus at the center of an increasing attention in order to understand solar active events such as flares and eruptions.

Theoretical estimations indicate that magnetic helicity is also essentially conserved with non-ideal MHD processes, e.g. magnetic reconnection. This conjecture has however been barely tested, either experimentally or numerically. Thanks to recent advances in magnetic helicity estimation methods, it is now possible to te st numerically its dissipation level in general three-dimensional datasets.

In Pariat et al. 15, we recently introduced a method to estimate the dissipation of magnetic helicity independently of the type of non-ideal MHD processes occurring. Usung a state-of-the-art 3D MHD numerical simulation of a solar-like eruptive event (based on Pariat et al. 09,cf. Figure 1, left pannel), we compare its estimation in a finite volume with its time-integrated flux through the boundaries, hence testing the conservation and dissipation of helicity.

We provide an upper bound of the real dissipation of magnetic helicity (cf. Figure 1, right pannel): It is quasi-null during the quasi-ideal MHD phase. Even when magnetic reconnection is acting the relative dissipation of magnetic helicity is also very small ($< 2.2\%$), in particular compared to the relative dissipation of magnetic energy (> 30 times larger).

Our study paves the way for more extended and diverse tests of the magnetic helicity conservation properties. Our study confirms the central role that helicity can play in the study of MHD plasmas. For instance, the conservation of helicity can be used to track the evolution of solar magnetic fields, from its formation in the solar interior until their detection as magnetic cloud in the interplanetary space.

References

[1] Pariat, E.; Valori, G.; Démoulin, P. & Dalmasse, K. (2015); *Testing magnetic helicity conservation in a solar-like active event*; Astronomy Astrophysics, Volume 580, id.A128 .

[2] Pariat, E.; Antiochos, S. K.; DeVore & C. R. K. (2009); *A Model for Solar Polar Jets*; The Astrophysical Journal, Volume 691, pp. 61-74.

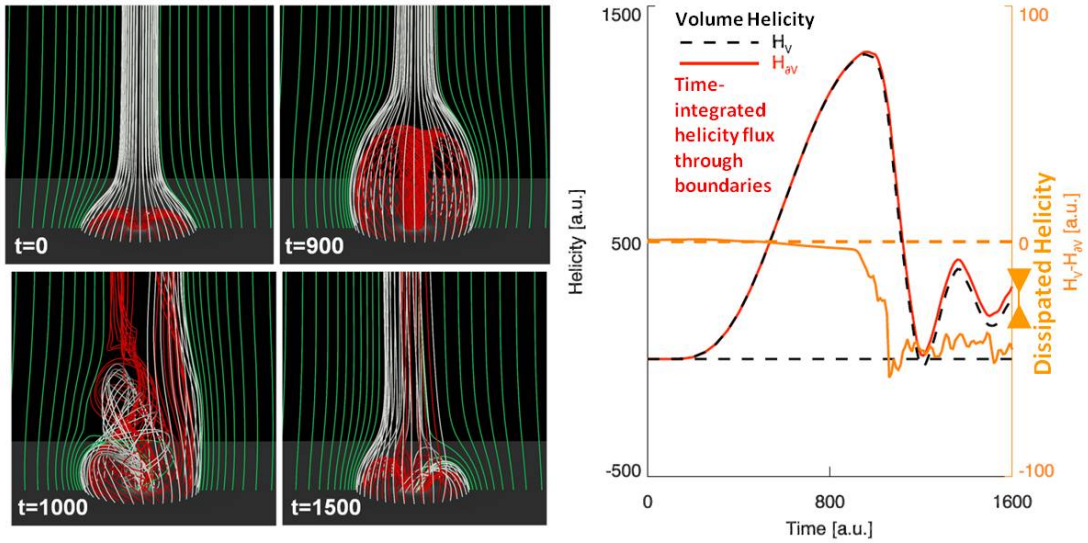

Fig. 1: Helicity conservation in a numerical simulation of a solar eruptive event (adapted from Pariat et al. 15). Right: snapshots of the magnetic field lines configuration during the generation of an helical solar jet. Left: comparison of the helicity in the domain and its flux through the boundaries: helicity conservation is smaller than 2%.

Notes

Submanifold helicities

Jason Cantarella[1], Jason Parsley[2]

[1] *Department of Mathematics, University of Georgia, USA*
[2] *Department of Mathematics and Statistics, Wake Forest University, USA*

Summary

The helicity of a vector field is a measure of the average linking of pairs of integral curves of the field. The authors have previously translated this to the helicity of a differential form, dual to the vector field. This allows helicity to be viewed as a cohomology class on an appropriate manifold, the configuration space $C_2[\Omega]$; here Ω has the same dimension as the ambient space $\mathbb{R}^n$. We now consider the case where Ω has a lower dimension than the ambient space, and define *submanifold helicity* in this case. This submission represents an introduction to our work. We are able to show that the ambient space must have dimension $4i+3$, and that some submanifold helicities exhibit diffeomorphism invariance, while some do not.

1 Helicity via Cohomology Classes

The helicity of a magnetic field was first defined by Woltjer [5] in 1958 and named by Moffatt [3] in 1969. The helicity of a divergence-free vector field is invariant under volume-preserving diffeomorphisms which are homotopic to the identity. In our paper [1], we define helicity for closed differential forms and easily obtain this diffeomorphism invariance by viewing helicity as a cohomology class on the configuration space $C_2[\Omega]$. Here, $C_2(\Omega)$ is the configuration space of ordered pairs of points in the subdomain $\Omega^n \subset \mathbb{R}^n$, while $C_2[\Omega]$ is its Fulton-Macpherson compactification. See also [2, 4] for details on using configuration spaces to approach problems of knot and vector field invariance.

2 Submanifold Helicities

In our paper [1], we have only considered the case where Ω is a top-dimensional subdomain of $\mathbb{R}^{2k+1}$. We turn our attention now to the case where Ω has smaller dimension than the ambient space. We say α is a *Dirichlet (differential) form* on Ω if α vanishes on the boundary of Ω.

Definition 1. The *submanifold helicity* $\mathrm{H}_{n,m}$ is defined for closed Dirichlet $(k+1)$-forms on an n-dimensional submanifold Ω of $\mathbb{R}^m$ by

$$\mathrm{H}_{n,m}(\alpha) = \int_{C_2[\Omega]} \alpha_x \wedge \alpha_y \wedge g^* \operatorname{dvol}_{S^{m-1}} . \tag{1}$$

In order for the integrand $\Phi_m = \alpha_x \wedge \alpha_y \wedge g^* \operatorname{dvol}_{S^{m-1}}$ to be a $2n$-form, we require that $2k+2+m-1 = 2n$, i.e., that $k = n - (m+1)/2$. We will also refer to $\mathrm{H}_{n,m}$ as (n,m)-*helicity*.

Observe that the ambient space must have odd dimension m; we may consider submanifold dimensions $(m-1)/2 \leq n \leq m$. Below we show that all submanifold helicities are identically zero when $m = 4i+1$ and thus the only interesting results occur when m is of the form $4i+3$.

Example 2. Here are a few examples of submanifold helicities.

1. Submanifold helicities generalize the standard definition of helicity. Indeed, the $(3,3)$-helicity $\mathrm{H}_{3,3}$ represents standard helicity.
2. In [1], we extended the definition of helicity to $(k+1)$-forms defined on top-dimensional subdomains of $\mathbb{R}^{2k+1}$; this appears as $\mathrm{H}_{2k+1,2k+1}$.

3. The $(1,3)$-helicity $\mathrm{H}_{1,3}$ of 0-forms on a curve in $\mathbb{R}^3$ turns out to be precisely the writhing number of the curve, so we know that submanifold helicities are not always invariant under diffeomorphisms (since writhe is not).
4. The $(2,3)$-helicity $\mathrm{H}_{2,3}$ measures the linking of a 1-form on a surface in $\mathbb{R}^3$.
5. We do not know whether $\mathrm{H}_{5,7}$, which measures the linking of a 2-form on a 5-dimensional surface in $\mathbb{R}^7$, is an invariant.

Question. Two questions arise immediately. (1) Which submanifold helicities $\mathrm{H}_{n,m}$ are invariant under diffeomorphisms? (2) When is $\mathrm{H}_{n,m}$ nontrivial?

As for helicity, we know that submanifold helicity will be an invariant if the closed form $\alpha_x \wedge \alpha_y \wedge g^* \operatorname{dvol}_{S^{m-1}}$ is Dirichlet, i.e., if it vanishes on the boundary of $C_2[\Omega]$. Following arguments from [1], we only have to worry about the face (12) of this boundary, which is diffeomorphic to $\Omega \times S^{m-1}$. On this face, $\alpha_x \wedge \alpha_y$ pulls back to $\alpha \wedge \alpha$. Our previous argument depended on the observation that this was a $(2k+2)$-form $\alpha \wedge \alpha$ on the $n = (2k+1)$-manifold Ω. In general, $2k+2$ may not be greater than n, so we cannot depend on this argument. However, we note that if $k+1$ is odd, then $\alpha \wedge \alpha$ vanishes on Ω by antisymmetry, providing a partial answer to the first question above.

Proposition 3. *If $k+1 = n-(m-1)/2$ is odd, then $\mathrm{H}_{n,m}$ is invariant.*

What about the second question? For a contractible domain $\Omega = D^n$, the configuration space $C_2[\Omega]$ has the topology of $D^n \times D^n - \{\mathrm{pt}\} = D^{n+1} \times S^{n-1}$. In this case, only the cohomology groups $H^*(C_2[\Omega], \partial C_2[\Omega])$ where $* = 0, n+1, 2n$ are nontrivial. So for $H_{n,m}$ to be nontrivial in this case, we must have $2k+2 = n+1$, which only occurs for $\mathrm{H}_{2k+1,2k+1}$. But if Ω has nontrivial homology, then $C_2[\Omega]$ has more homology and (n,m)-helicity might be nontrivial. For example, we conjecture that if Ω has 1-dimensional homology, then the invariant $\mathrm{H}_{2,3}$ is nontrivial on Ω.

When $m = 4i+1$, the generalization of helicity must be identically zero, as we proved in [1]. The corresponding result holds for (n,m)-helicities.

Proposition 4. *If the ambient space has dimension $4i+1$, then $\mathrm{H}_{n,m}$ is identically zero for any $(k+1)$-form α.*

Proof. We consider the automorphism a of $C_2(\Omega)$ that interchanges x and y; it extends naturally to $C_2[\Omega]$. It changes the orientation of $C_2[\Omega]$ by a factor of $(-1)^{n^2} = (-1)^n$.

Next, we take the pullback $a^*\Phi_m = \alpha_y \wedge \alpha_x \wedge a^* g^* \operatorname{dvol}_{S^{m-1}}$. The map a induces an antipodal map on S^{m-1}; since m is odd, such a map has degree -1. Hence, $a^* g^* \operatorname{dvol}_{S^{m-1}} = -g^* \operatorname{dvol}_{S^{m-1}}$. Also, $\alpha_y \wedge \alpha_x = (-1)^{(k+1)^2} \alpha_x \wedge \alpha_y$. Combining these results, $a^*\Phi = (-1)^k \Phi$. We then compute

$$\int_{C_2[\Omega]} a^*\Phi = \int_{a(C_2[\Omega])} \Phi \qquad \Rightarrow \qquad (-1)^k \,\mathrm{H}_{n,m}(\alpha) = (-1)^n \,\mathrm{H}_{n,m}(\alpha) \tag{2}$$

For $m = 4i+1$, then k and n have the opposite parity, which implies that $\mathrm{H}_{n,m}(\alpha) = -\,\mathrm{H}_{n,m}(\alpha)$, i.e., that helicity is zero, and proves our proposition. For $m = 4i+3$, the conclusion is a tautology: $\mathrm{H}_{n,m}(\alpha) = \mathrm{H}_{n,m}(\alpha)$. □

References

[1] Jason Cantarella and Jason Parsley. A new cohomological formula for helicity in $\mathbb{R}^{2k+1}$ reveals the effect of a diffeomorphism on helicity. *J. Geom. Phys.*, 60(9):1127–1155, 2010.

[2] Dennis DeTurck, Herman Gluck, Rafal Komendarczyk, Paul Melvin, Clayton Shonkwiler, and David Shea Vela-Vick. Generalized Gauss maps and integrals for three-component links: toward higher helicities for magnetic fields and fluid flows. *J. Math. Phys.*, 54(1):013515, 48, 2013.

[3] H. K. Moffatt. The degree of knottedness of tangled vortex lines. *J. Fluid Mech.*, 106:117–129, 1969.

[4] Ismar Volić. A survey of Bott-Taubes integration. *J. Knot Theory Ramifications*, 16(1):1–42, 2007.

[5] L. Woltjer. A theorem on force-free magnetic fields. *Proc. Nat. Acad. Sci. U.S.A.*, 44:489–491, 1958.

Notes

Magnetic Connection Hypersurfaces in Relativistic Magnetohydrodynamics

F. Pegoraro

Physics Department, University of Pisa, Italy

Summary

In the single fluid, nonrelativistic, ideal-Magnetohydrodynamic (MHD) plasma description magnetic field lines play a fundamental role by defining dynamically preserved "magnetic connections" between plasma elements. Here we show how the concept of magnetic connection needs to be generalized in the case of a relativistic MHD description where we require covariance under arbitrary Lorentz transformations. This is performed by defining 2-D *magnetic connection hypersurfaces* in the 4-D Minkowski space. This generalization accounts for the loss of simultaneity between spatially separated events in different frames and is expected to provide a powerful insight into the 4-D geometry of electromagnetic fields when $\vec{E} \cdot \vec{B} = 0$.

1 Physical motivation

The dynamics of large scale relativistic plasma configurations plays an important role in our understanding of high energy astrophysical phenomena such as, just to mention a recently discovered one, the flaring of the Crab nebula. Even without including general relativistic effects, as would be the case e.g., in the neighbourhood of a black hole, the phenomena we need to describe involve velocities close to the speed of light and internal energies that can be larger than the electron rest mass energy. With this in mind, several concepts that have been introduced for nonrelativistic plasmas needs to be extended to relativistic regimes. In such a generalization space and time properties are necessarily combined since the basic invariance properties of the matter equations are now given in terms of the Lorentz group of transformation between different reference frames. This is particularly important since, in the presence of very large velocity differences between different parts of the plasma configuration, there may not be a clear way to define on physics grounds a preferred reference frame. In addition, the observer reference frame may move with a relativistic velocity with respect to the plasma under observation and thus observe as simultaneous events that are not simultaneous in the plasma frame.

A number of basic phenomena of nonrelativistic MHD, such as e.g., magnetic reconnection, have been reconsidered in relativistic plasma regimes both in the laboratory and in astrophysics. In particular in the astrophysical context relativistic magnetic reconnection has been considered mostly as a mechanism of energy conversion, usually choosing a preferred frame of reference possibly thought of as an "average comoving frame" i.e. as a frame in which the plasma region under consideration is globally at rest. As mentioned above, such an approach may not be fully unambiguous in situations where very large velocity relativistic variations can be present between different plasma regions, in particular since magnetic fields and electric fields are transformed one into the other when seen in a Lorentz boosted reference frame. Thus an important point in the relativistic extension of the MHD plasma description is to provide a frame independent definition of magnetic reconnection.

Although a clearcut definition of magnetic reconnection is not simple to formulate even for a non relativistic plasma, its common definition is not simply limited to the fact that magnetic energy is converted to kinetic and/or internal plasma energy, but refers to the local violation of the magnetic topology and in particular to the local breaking of the structure of magnetic connections. Magnetic connections are defined by the fundamental property of ideal MHD (see Ref.[1]) that if two plasma elements, moving with plasma in a smooth flow, are connected at time t by a magnetic field line then at any following time there exists a magnetic field line that connects them. Thus in order to define

magnetic reconnection in a covariant way we must first obtain a covariant definition of magnetic connections. Again, such a definition is not *a priori* obvious because of two already mentioned related reasons: the distinction between electric and magnetic fields and the very concept of field lines are frame dependent. This point was explicitly addressed in Ref.[2] where it was shown that the covariant formulation of magnetic connections can be restored by means of a *time resetting* projection along the trajectories of the plasma elements. This projection is consistent with the ideal Ohm's law and compensates for the loss of simultaneity in different reference frames between spatially separated events.

2 Mathematical developments

Here we address this same issue and show that the time resetting along the trajectories of the fluid elements introduced in Ref.[2] is essentially equivalent to a redefinition of the geometrical object that we use in order to define magnetic connections. We argue that, while in 3-D (coordinate) space magnetic connections are defined by 1-D curves (field lines), in the 4-D Minkowski space they are defined by 2-D hypersurfaces that are generated by a suitably defined magnetic (space-like) 4-vector field (see Refs.[3, 4]) and by the velocity (time-like) 4-vector field of the plasma.
We show that if the electromagnetic (e.m) field tensor satisfies an ideal Ohm's law, it exhibits special geometrical properties that are simply the consequence of the homogeneous Maxwell's equations and that make it possible to define such 2-D hypersurfaces so that, if in a given frame two plasma elements in 4-D Minkowski space lie on the same 2-D hypersurface, they do so in any other reference frame. We call these 2-D hypersurfaces *Covariant Magnetic Connection Hypersurfaces*. The standard magnetic connections in 3-D space can then be recovered in any chosen reference frame by taking sections of these surfaces at a fixed (in that frame) time. We stress that these 2-D hypersurfaces bear no relation to the 3-D magnetic surfaces of nonrelativistic MHD that, if generalized to 4-D Minkowski space, would involve 3-D "volumes".

We stress that the violation of the ideal Ohm's law leads to a violation of the geometrical properties of the e.m. field tensor that make it possible to define the connection hypersurfaces. Thus in this 4-D framework magnetic reconnection, caused by a local violation of the ideal Ohm's law, can be interpreted in a frame independent way as a local "pierching and merging" of connection hypersufaces that lose their identity only locally, in exactly the same way as magnetic field lines do in the standard 3-D space setting.
We note that, even remaining within the validity of the ideal Ohm's law i.e., without allowing for magnetic reconnection to occur, important questions will need to be investigated: in particular how to generalize the topological properties, such as e.g. field line braiding, that have been investigated within a fixed frame 3-D description to the properties of connection hypersurfaces in 4-D Minkowski space.

References

[1] Newcomb W.A. (1958), Motion of Magnetic Lines of Force, *Ann. Phys.*, **3**, 347.

[2] Pegoraro F. (2012), Covariant form of the ideal magnetohydrodynamic "connection theorem" in a relativistic plasma, *EPL*, **99**, 35001.

[3] Lichnerowicz A. (1967), in *Relativistic Hydrodynamics and Magnetohydrodynamics*, (New York: Benjamin).

[4] Anile M. (1989), in *Relativistic fluids and magneto-fluids*, Cambridge Monographs on Mathematical Physics, Cambridge.

Notes

Helicity is the only integral invariant of volume-preserving transformations

D. Peralta-Salas

Instituto de Ciencias Matemáticas, Consejo Superior de Investigaciones Cientficas, 28049 Madrid, Spain

Helicity is a remarkable conserved quantity that is fundamental to all the natural phenomena described by a vector field whose evolution is given by volume-preserving transformations. This is the case of the vorticity of an inviscid fluid flow or of the magnetic field of a conducting plasma. The topological nature of the helicity was unveiled by Moffatt, but its relevance goes well beyond that of being a new conservation law. Indeed, the helicity defines an integral invariant under any kind of volume-preserving diffeomorphisms. A well-known open problem is whether any integral invariants exist other than the helicity. We answer this question by showing that, under some mild technical assumptions, the helicity is the only integral invariant. Specifically, given a functional $\mathcal{I}$ defined on exact divergence-free vector fields of class C^1 on a compact 3-manifold that is associated with a well-behaved integral kernel, we prove [1] that $\mathcal{I}$ is invariant under arbitrary volume-preserving diffeomorphisms if and only if it is a function of the helicity.

References

[1] Enciso, A., Peralta-Salas, D. & Torres de Lizaur, F. (2016) Helicity is the only integral invariant of volume-preserving transformations. *Proc. Natl. Acad. Sci. USA* **113** 2035–2040.

Notes

Existence of force-free magnetic fields, and formation of electric current singularities

D. I. Pontin[1], G. Hornig[1], S. Candelaresi[1], I. J. D. Craig[2]

[1] *School of Science & Engineering, University of Dundee, UK*
[2] *Department of Mathematics, University of Waikato, New Zealand*

Summary

We discuss the existence of smooth equilibria – or as an alternative, the formation of current singularities – in plasmas with low dissipation. We examine in particular magnetic braids, and note that when these braids are 'line-tied' at perfectly conducting planes, smooth equilibria in general exist, though exhibit thin current layers with length scales determined by the field line mapping. In a periodic domain, exact equilibria typically do not exist, while approximate equilibria exhibit thin current layers. We also discuss the case of magnetic null points, at which current singularities develop in response to rather generic perturbations to an initial equilibrium.

1 Background and outline of contribution

The magnetic field is an important driver of plasma dynamics in a wide range of environments. Many phenomena of interest involve explosive release of stored magnetic energy, though our understanding of the mechanisms by which this energy release occurs is in its infancy. Magnetic fields in laboratory and astrophysical environments typically have complex three-dimensional structure, and are often inherently disordered, being characterised by field lines that are tangled with one another in non-trivial ways. This complexity may be measured in various ways, using for example the topological entropy or field line helicity.

Magnetic braids (magnetic flux tubes within which the field lines have some non-trivial winding or linkage) have been used for some time to model coronal loops in the Sun's atmosphere, or *corona*. This was initially a response to Parker's proposed nanoflare heating mechanism [2, 3]. Therein, the corona may be heated to the observed multi-million degree temperatures as a result of turbulent convective motions in the outer layers of the solar interior that tangle or braid the field lines in the corona about one another. A crucial ingredient of this mechanism is the hypothesis that for sufficiently braided magnetic fields no smooth force-free equilibrium exists, but rather the field develops current singularities. Here we present work that challenges this hypothesis by demonstrating the existence of smooth equilibria for a class of magnetic braids [6]. This result holds for the case in which the field is line tied at perfectly conducting plates, as is the case in the solar atmosphere (where the part of the conducting plates in played by the solar surface (or *photosphere*). However, we show that thin current layers must be present in the equilibria, and that these current layers become increasingly thin as the field becomes more tangled. Thus, one may still release energy from the magnetic field by braiding the field sufficiently that these current layers approach the diffusive length-scale. By contrast to the above, when one considers a periodic domain as is relevant for many laboratory devices, smooth equilibria can be shown not to exist, while a field close to equilibrium must contain thin current layers [4].

We subsequently contrast the case of magnetic braids with magnetic fields that contain null points (points in space at which is magnetic field strength falls to exactly zero). In this case, it is shown that a rather generic perturbation of the field leads to an unbounded growth of the electric current, corresponding to a current singularity in the perfectly-conducting limit [1, 5].

Acknowledgements. Financial support from the UK's STFC (grant number ST/K000993) is gratefully acknowledged.

References

[1] Klapper, I., Rado, A., and Tabor, M. (1996). A lagrangian study of dynamics and singularity formation at magnetic null points in ideal three-dimensional magnetohydrodynamics. *Phys. Plasmas*, 3(11):4281–4283.

[2] Parker, E. N. (1972). Topological dissipation and the small-scale fields in turbulent gases. *Astrophys. J.*, 174:499.

[3] Parker, E. N. (1988). Nanoflares and the solar x-ray corona. *Astrophys. J.*, 330:474–479.

[4] Pontin, D. I. Candelaresi, S. and Russell, A. J. B. and Hornig, G. (2016). Braided magnetic fields: equilibria, relaxation and heating. Submitted to *Plasma Phys. Contr. Fusion.*

[5] Pontin, D. I. and Craig, I. J. D. (2005). Current singularities at finitely compressible three-dimensional magnetic null points. *Phys. Plasmas*, 12:072112.

[6] Pontin, D. I. and Hornig, G. (2015). The structure of current layers and degree of field-line braiding in coronal loops. *Astrophys. J.*, 805:47.

Notes

A definative definition of the open field magnetic helicity

Chris Prior[1], Anthony Yeates[1]

[1] *Mathematical sciences, Durham University, United Kingdom*

Summary

The magnetic helicity is invariant under ideal flows which vanish at the domain boundary. However, the quantity is not gauge invariant where there are open field lines. Berger and Field first proposed a meaningful definition of this quantity [1] which was gauge invariant but depended on comparison to a fictitious reference field. Since then there has been a significant number of authors proposed alternative definitions of the open helicity, but none have been shown to be unambiguously preferable. We present published work [2] showing all these definitions can be interpreted in terms of the average pair-wise net winding of the fields curves (an open analogue of the linking number) and that all but one one possible definition (choice of gauge) have some non-physical contribution. New results presented will show this definition can be used to uniquely classify braided magnetic fields and hence accurately characterise magnetic re-connection.

Magnetic helicity $H(\mathbf{B}) = \int_V \mathbf{A}\cdot\mathbf{B}\,\mathrm{d}^3x$, with $\mathbf{B} = \nabla\times\mathbf{A}$, has long been recognized as an important dynamical invariant in ideal magnetohydrodynamics. The integral $H(\mathbf{B})$is independent of the particular gauge chosen for $\mathbf{A}$, provided that V is simply connected and magnetically closed ($B_n = 0$ on the boundary ∂V) [3].

Physically, $H(\mathbf{B})$ may be interpreted as the flux-weighted average, over all pairs of magnetic field lines $\mathrm{d}\mathbf{x}/\mathrm{d}s = \mathbf{B}(\mathbf{x})$, $\mathrm{d}\mathbf{y}/\mathrm{d}s = \mathbf{B}(\mathbf{y})$, of the Gauss linking integral

$$L(\mathbf{x},\mathbf{y}) = \frac{1}{4\pi}\oint_{\mathbf{x}(s)}\oint_{\mathbf{y}(s)} \frac{d\mathbf{x}}{ds}\cdot\frac{d\mathbf{y}}{ds}\times\frac{\mathbf{r}}{|\mathbf{r}|^3}\,\mathrm{d}s\,\mathrm{d}s'. \tag{1}$$

Gauge invariance of H relies on the condition $B_n|_{\partial V} = 0$ often violated in solar physics. Berger and Field[1] showed how gauge invariance may be restored by measuring the helicity with respect to a reference magnetic field $\mathbf{B}'$ sharing the same distribution of B_n on ∂V. This relative helicity is then an ideal invariant under motions that vanish on ∂V. It has since been widely applied to the open magnetic fields arising in solar physics, but still requires the choice of an arbitrary reference field. Other authors have proposed alternative definitions of the magnetic helicity which certain desirable properties (see a discussion and references in [2]). None of the proposed open helicity definitions had previously been shown to be unambiguously preferable.

In [2] we showed each of these quantities (including the relative helicity) can be interpreted in terms of an open analogue of the linking number, the *net winding* $\mathcal{L}(\mathbf{x},\mathbf{y})$ of an angle Θ made by the two curves in a plane of fixed Cartesian z coordinate,

$$\mathcal{L}(\mathbf{x},\mathbf{y}) = \int_0^h \frac{\mathrm{d}\Theta}{\mathrm{d}z}\,\mathrm{d}z = \frac{1}{2\pi}\Big(\Theta(\mathbf{x}(h),\mathbf{y}(h)) - \Theta(\mathbf{x}(0),\mathbf{y}(0))\Big) + N, \tag{2}$$

with N a signed number of integer windings (see Figure 1(a)). This quantity is clearly invariant to all motions which vanish at the end planes. In general the curves will turn back on themselves and in order to maintain invariance $\mathcal{L}(\mathbf{x},\mathbf{y})$ the curve must be split into sections by its turning points and the winding of each individual section must be measured [4] (see Figure 1(b) and (c)).

Crucially it was demonstrated in [2] that all possible definitions of the magnetic helicity, save one particular choice of gauge, measure the rotation of Θ with respect to a moving basis, so that untwisted curves can be measured as entangled when they are not (see Figure 2). This additional rotation is defined entirely by a gauge transformation form the preferred gauge/reference field and hence has no physical interpretation.

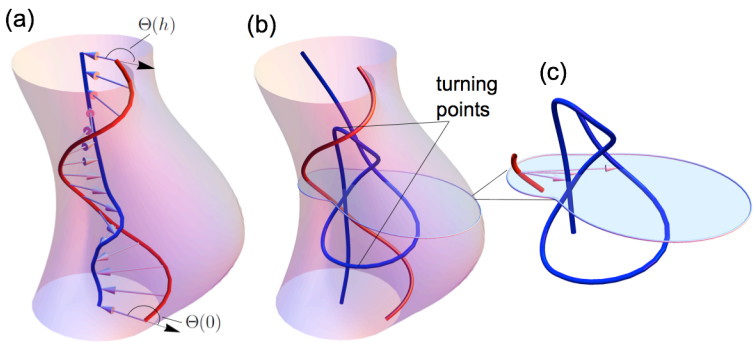

Fig. 1: Geometrical interpretation of the winding number.

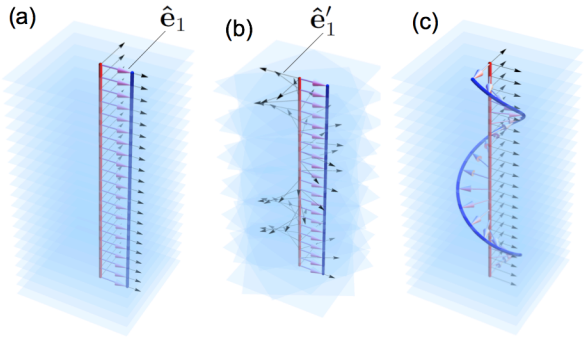

Fig. 2: How a straight field can appear twisted when measured with respect to a rotating frame. (c) the curves in (c) are wound equivalently to the straight curves of (a) as seen form a rotating basis (b)

We shall present these results in more detail and further show the quantity $\mathcal{L}(\mathbf{x}, \mathbf{y})$ can be used provide a complete topological invariant for braided magnetic fields. This allows us to accurately measure reconnection in braided fields In addition, if time permits we shall present some recent work applying this topological framework to experimental data of two reconnection magnetic flux ropes obtained form the UCLA basic plasma facility.

References

[1] Berger, M.A. and Field, G.B., 1984. The topological properties of magnetic helicity. Journal of Fluid Mechanics, 147, pp.133-148.

[2] Prior, C. and Yeates, A.R., 2014. On the Helicity of Open Magnetic Fields. The Astrophysical Journal, 787(2), p.100.

[3] Moffatt, H.K., 1969. The degree of knottedness of tangled vortex lines. Journal of Fluid Mechanics, 35(01), pp.117-129.

[4] Berger, M.A. and Prior, C., 2006. The writhe of open and closed curves. Journal of Physics A: Mathematical and General, 39(26), p.8321.

Notes

Nonlinear behaviour of the Yousef shear dynamo

M.R.E. Proctor[1], R.J. Teed[1]

[1] *DAMTP, University of Cambridge, UK*

Summary

We present preliminary results from a nonlinear simulation of the shear dynamo investigated in the linear regime by Yousef *et al.*, which show that large scale flows typically come to dominate the dynamics.

Turbulent motions of plasma within the Sun are believed to be responsible for the generation and sustainment of its magnetic field via dynamo action. It is well understood how small scale magnetic fields can be induced by the small scale turbulence. A less understood phenomenon, however, is the ability of the field to display larger structure on the scale of the Sun itself. Mean field dynamo theory which utilises non-zero net helicity via the α-effect has long been used to explain the generation of the large scale fields, although there is recent evidence suggesting that the theory suffers from considerable inaccuracies in the solar regime where turbulence is generated by convection [11]. However, if the α-effect is not a plausible model, then how else is large-scale structure to be obtained?

Starting with the work of Yousef *et al.*([1]), several authors [2, 3, 4] have demonstrated an apparently different mechanism. They investigated forced *non-helical* motion in a long domain in the presence of a uniform shear. They found that magnetic fields with long-range order (and extended lifetimes) can be induced, though the large-scale structures move irregularly and are hard to identify with cyclic behaviour common to the solar field. Their work implemented non-helical forcing in order to eliminate the α-effect as an amplification mechanism as well as a large aspect ratio to allow for large scale structure to develop whilst conserving computational resolution. A number of theoretical mechanisms have been suggested to explain the ability of shear to generate large-scale fields: an enhanced α via greater correlation of small-scale motions by the shear [5]; an interaction with the fluctuating α-effect [6, 7, 8]; or an enhancement of the shear-current effect [9, 10]. The enhancement of dynamo action due to shear without an α-effect has also been observed in models incorporating convection [12, 13]. Recently, [14] showed that it was possible to produce large-scale field with periodic behaviour using a shear dynamo mechanism although this was not a fully 3D simulation.

Our work, reported in [15], is an extension of the original 'shear dynamo' calculation. The work of [1, 2] was performed for the kinematic case only so we have investigated the natural extension of the model by including the Lorentz forces due to the magnetic field. This allows us to determine how the velocity and magnetic fields equilibrate and whether the large scale structures persist into the nonlinear regime. Our preliminary findings are that when the dynamo generated field becomes large enough to influence the flow, there is indeed a period of time when similar large scale structures continue to exist, with equilibrated amplitudes. However at later times - the interval apparently depending on the strength of the imposed shear and on the magnetic Prandtl number- large flows develop in the direction of the original shear, and the large scale structures are destroyed (see the Figure). I will discuss the force balances giving rise to this phenomenon, and will hope to present further calculations for more general shear flow profiles to see if the simple uniform shear treated here gives typical results.

Acknowledgements. This research is supported by the UK STFC.

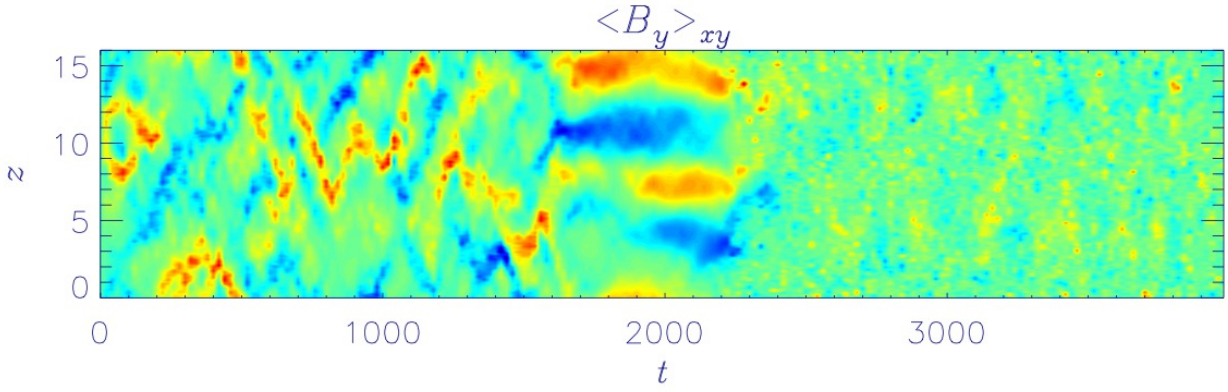

Fig. 1: Plot of the average magnetic field in the direction of the shear, averaged over the x and y directions, as a function of z (the coordinate in the direction of the longest box length) and time, for a moderate shear (from [15]). The left hand portion shows the linear behaviour, the centre portion the nonlinear equilibration with large scale structures, and the right hand portion the regime with large induced shear and no large scale structure.

References

[1] Yousef T., Heinemann T., Schekochihin A., Kleeorin N., Rogachevskii I., Iskakov A., Cowley S., McWilliams J. (2008a) *Phys. Rev. Lett.* 2008 **100**, 184501.

[2] Yousef T., Heinemann T., Rincon F., Schekochihin A., Kleeorin N., Rogachevskii I., Cowley S., McWilliams J. (2008b) *Astr. Nachr.* 2008 **329**, 737.

[3] Heinemann T., McWilliams J., Schekochihin A. (2011) *Phys. Rev. Lett.* 2011 **107**, 255004.

[4] McWilliams J. C. (2012) *J. Fluid Mech.* 2012 **699**, 414. *Phys. Rev. Lett.* 2008 **100**, 184501.

[5] Courvoisier A., Hughes D. W., Tobias S. M. (2009) *J. Fluid Mech.* 2009 **627**, 403.

[6] Proctor M. R. E. (2007) *Mon. Not. R. Astron. Soc. Letters* 2007 **382**, L39.

[7] Richardson K., Proctor M., (2012) *Mon. Not. R. Astron. Soc. Letters* 2007 **422**, L53.

[8] Sridhar S., Singh N. K. (2014) *Mon. Not. R. Astron. Soc. Letters* 2014 **445**, 3770.

[9] Rogachevskii I., Kleeorin N. (2003) *Phys. Rev. E* 2003 **68**, 036301.

[10] Brandenburg A., Rädler K.-H., Rheinhardt M., Käpylä P. (2008) *Astrophys. J.* 2008 **676**, 740.

[11] Hughes D. W., Cattaneo F. (2008) *J. Fluid Mech.* 2008 **594**, 445.

[12] Hughes D. W., Proctor M. R. E. (2009) *Phys. Rev. Lett.* 2009 **102**, 044501.

[13] Hughes D. W., Proctor M. R. E. (2013) *J. Fluid Mech.* 2013 **717**, 395.

[14] Tobias S., Cattaneo F. (2013) *Nature* 2013 **497** 463.

[15] Teed R. J., Proctor M. R. E. (2016) *Mon. Not. R. Astron. Soc.* 2016 to be submitted, March 2016.

Notes

Helicity-Enhanced Extreme Vortex States and the Hydrodynamic Blow-Up Problem

B. Protas

Department of Mathematics & Statistics, McMaster University, Hamilton, ON, L8S 4K1, Canada

Summary

We present a variational framework for analyzing the effect of helicity on the structure and properties of extreme vortex states in viscous incompressible flows. These states arise as the flows exhibiting the largest growth of enstrophy allowed by the system dynamics under some imposed constraints and are therefore intimately related to the question of the possible singularity formation in the 3D Navier-Stokes and Euler systems, know as the "blow-up problem". A key element of the approach is a multiobjective formulation of the underlying optimization problem. In the presentation we will review details of this formulation and survey some of the properties of the helicity-enhanced extreme vortex states.

1 Introduction

The *extreme vortex states* are defined as the flows saturating certain fundamental mathematical estimates, such as the bounds on the maximum enstrophy growth in 3D [1], in the presence of suitable constraints on the flow field. Similar problems are also relevant in the context of the 1D Burgers and 2D Navier-Stokes systems. While these systems are known *not* to lead to singularity formation in finite time, the question of the accuracy of their worst-case estimates is still important, as these bounds are obtained using analogous methods as in the 3D case. By framing these questions in terms of variational PDE optimization problems, which are solved computationally using discrete gradient flows, we are able to provide new insights concerning the "sharpness" of these estimates, understood as the existence of actual vector fields which realize these bounds [2, 3, 4, 5]. In offering a systematic approach to finding flow solutions which may saturate known estimates, this paradigm thus provides a bridge between rigorous mathematical analysis and scientific computation.

2 Estimates of Enstrophy Growth

As regards flows in 3D unbounded or periodic domains $\Omega \subseteq \mathbb{R}^3$, the Navier-Stokes system is known to admit classical solutions $\mathbf{u}(t,\mathbf{x})$ which are *globally* well-posed as long as the enstrophy $\mathcal{E}(\mathbf{u}(t)) := \int_\Omega |\boldsymbol{\nabla}\times\mathbf{u}(t,\mathbf{x})|^2\,d\Omega$ remains bounded. At the same time, the best upper bound on the instantaneous rate of growth of enstrophy is

$$\frac{d\mathcal{E}}{dt} \leq C\,\mathcal{E}^3 \tag{1}$$

with some $C>0$. By solving variational problems of the type

$$\widetilde{\mathbf{u}}_{\mathcal{E}_0} = \underset{\mathbf{u}\in H^1(\Omega)}{\arg\max}\ \mathcal{R}(\mathbf{u}) \quad \text{subject to:} \quad \mathcal{E}(\mathbf{u}) = \mathcal{E}_0, \tag{2}$$

where $\mathcal{R}(\mathbf{u}) := d\mathcal{E}(\mathbf{u})/dt = -\nu\int_\Omega |\boldsymbol{\Delta}\mathbf{u}|^2\,d\mathbf{x} + \int_\Omega \mathbf{u}\cdot\boldsymbol{\nabla}\mathbf{u}\cdot\boldsymbol{\Delta}\mathbf{u}\,d\mathbf{x}$, for a range of different values of $\mathcal{E}_0$. Lu & Doering [1] found a family of divergence-free vector fields $\widetilde{\mathbf{u}}_{\mathcal{E}_0}$ saturating the upper bound in (1), thereby demonstrating that this instantaneous estimate is sharp. However, as shown in [5], these extreme vortex states are characterized by a very simple structure involving two colliding, nearly axisymmetric vortex rings (Fig. 1a). In fact, these optimal vector fields have the structure of generalized Beltrami flows with vanishing helicity $\mathcal{H}(\widetilde{\mathbf{u}}_{\mathcal{E}_0}) = 0$, where $\mathcal{H}(\mathbf{u}) := \int_\Omega \mathbf{u}\cdot(\boldsymbol{\nabla}\times\mathbf{u})\,d\Omega$. As a result, the initially large rate of growth of enstrophy saturating (1) is not sustained yielding only a modest increase of enstrophy in finite time. Maintaining a rapid rate of growth $d\mathcal{E}(\mathbf{u})/dt$, sufficient for the enstrophy $\mathcal{E}(t)$ to become unbounded in finite time, is a necessary precursor of blow-up in the 3D Navier-Stokes system [1].

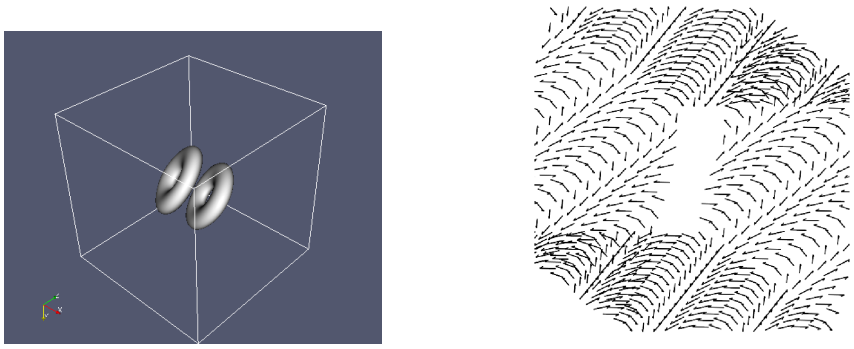

(a) (b)

Fig. 1: (a) Extreme vortex state $\widetilde{\mathbf{u}}_{\mathcal{E}_0}$ with $\mathcal{E}_0 = 20$ [5] (corresponding to solutions of (2), or (3) with $\alpha = 1$). (b) Eigenfunction of the *curl* operator maximizing helicity $\mathcal{H}(\mathbf{u})$ for given enstrophy $\mathcal{E}_0$ (corresponding to solutions of (3) with $\alpha = 0$).

3 Extreme Vortex States with Finite Helicity

To produce a larger sustained growth of enstrophy, it is therefore necessary to construct optimal vortex states with nontrivial structure which can be achieved by ensuring that they possess nonzero helicity $\mathcal{H}(\mathbf{u})$. It is known that the growth of enstrophy at a rate somewhat slower than given in (1), namely $d\mathcal{E}(t)/dt \sim CE^{\beta}$ for some $\beta > 2$, is still sufficient to produce blow-up in finite time. Thus, to push the limit of the maximum enstrophy growth, it is necessary to construct extreme vortex states $\widetilde{\mathbf{u}}^{\alpha}_{\mathcal{E}_0,\mathcal{H}}$ characterized by a suboptimal instantaneous rate of growth of enstrophy (i.e., with $2 < \beta < 3$), but at the same time having a nontrivial topological structure reflected in nonzero helicity $\mathcal{H}(\widetilde{\mathbf{u}}^{\alpha}_{\mathcal{E}_0,\mathcal{H}}) \neq 0$. The latter property will ensure that a rapid rate of growth of enstrophy can be sustained over longer time windows. Such states can be constructed based on a variational formulation relying on multiobjective optimization which generalizes (2). Given parameter $\alpha \in [0, 1]$, the new objective function blending helicity and the instantaneous rate of enstrophy growth can be defined as $\mathcal{Q}_{\alpha}(\mathbf{u}) := \alpha\mathcal{R}(\mathbf{u}) + (1-\alpha)\mathcal{H}(\mathbf{u})$, so that the corresponding optimization problem becomes

$$\widetilde{\mathbf{u}}^{\alpha}_{\mathcal{E}_0,\mathcal{H}} = \underset{\mathbf{u}\in H^1(\Omega)}{\arg\max}\ \mathcal{Q}_{\alpha}(\mathbf{u}) \quad \text{subject to:} \quad \mathcal{E}(\mathbf{u}) = \mathcal{E}_0. \tag{3}$$

Thus obtained extreme vortex states $\widetilde{\mathbf{u}}^{\alpha}_{\mathcal{E}_0,\mathcal{H}}$ will constitute a one-parameter family of solutions known as the "Pareto front". They connect two limiting solutions, namely, the original extreme vortex states $\widetilde{\mathbf{u}}_{\mathcal{E}_0}$ maximizing $d\mathcal{E}(t)/dt$, cf. (1), are recovered when $\alpha = 1$, whereas for $\alpha = 0$ we obtain fields which for given enstrophy $\mathcal{E}(\mathbf{u})$ possess the largest possible helicity $\mathcal{H}(\mathbf{u})$. It can be demonstrated that these fields, illustrated in Fig. 1b, are given in terms of the eigenfunctions of the *curl* operator associated with the smallest nonzero eigenvalue.

References

[1] Lu, L. and Doering, C. R. (2008) Limits on Enstrophy Growth for Solutions of the Three-dimensional Navier-Stokes Equations *Indiana University Mathematics Journal* **57**, 2693–2727.

[2] Ayala, D. and Protas, B. (2011) On Maximum Enstrophy Growth in a Hydrodynamic System, *Physica D* **240**, 1553–1563.

[3] Ayala, D. and Protas, B. (2014) Maximum Palinstrophy Growth in 2D Incompressible Flows, *Journal of Fluid Mechanics* **742** 340–367.

[4] Ayala, D. and Protas, B. (2014) Vortices, Maximum Growth and the Problem of Finite-Time Singularity Formation, *Fluid Dynamics Research*, (Special Issue for IUTAM Symposium on Vortex Dynamics), **46** 031404.

[5] Ayala, D. and Protas, B. (2015) Extreme Vortex States and the Growth of Enstrophy in 3D Incompressible Flows, (in preparation).

Notes

Singularities in viscous flows

V.V. Pukhnachev[1,2], E.N. Zhuravleva[1,2]

[1] *Lavrentyev Institute of Hydrodynamics, Siberian Branch, Russian Academy of Sciences, Russia*
[2] *Novosibirsk State University, Russia*

Summary

Available steady solutions of Navier–Stokes equations with singularities are reviewed, and new examples of such solutions are given. Examples of unsteady solutions are also given, which demonstrate the change in the flow region topology or the structure of streamlines with time. The problem of deformation of a strip bounded by a solid wall and a parallel free boundary is studied. Conditions of solution failure within a finite time are found.

This work consists of two parts. The first one is a review of steady solutions of Navier–Stokes equations for an incompressible fluid with singularities [1]. They include the classical solutions obtained by Jeffery, Hamel, Slezkin, Landau, Goldshtik, and also the solutions obtained by the authors of the present text in [2] and [3], which describe plane and axisymmetric flows with a free surface. We also consider the asymptotic character of singularities of the source, sink, or point vortex type. In particular, we consider the problem of plane motion of a viscous fluid in an arbitrary bounded domain with a solid boundary. This motion is induced by rotation of a solid disk of small radius α with an angular velocity ω inside the domain. It is proved that the solution of the point vortex problem can be approximated in a suitable metrics by the solution of the rotating disk problem as $\alpha \to 0$ and $\omega \to \infty$, so that $\alpha^2\omega \to |\Gamma|$ [4].

The problem of a rotating ring is a seldom example of the problem where the time evolution of the flow topology can be traced [5], [6]. In this solution, the free boundaries are circumferences, and the solution of two-dimensional Navier–Stokes equations is independent of the polar angle. The problem has two integrals of motion: S (ring area) and M (moment of momentum). Let us denote $\beta = \left(\rho\sigma S^{5/2}\right)^{-1} L^2$, where ρ is the fluid density and σ is the surface tension coefficient. Let us assume that $\beta < \beta^* \approx 0.831$. Then the rotating ring transforms to a circle within a finite time; moreover, this process is irreversible. [5].

Let us give an example of the flow where the structure of streamlines changes instantaneously [7]. Let the fluid fill the sector $0 < \varphi < \alpha$ with solid boundaries, and let the stream function of the plane flow at the time $t = 0$ be constant on each ray $\varphi = const$. The resultant motion is self-similar and serves as a two-dimensional extension of the classical Jeffery–Hamel solution. If the flow rate of the fluid through the origin is equal to zero and the angle α is sufficiently small, then the information about the initial velocity distribution is entrained to infinity as $t \to \infty$, and a sequence of vortices originates from the origin. These vortices become decelerated with time, and their shape approaches the famous Moffatt vortices [8].

To conclude, we consider a plane problem where one velocity component is a linear function of the x coordinate and the other velocity component and the pressure are independent of x. The proposed solution is interpreted as unsteady motion in a strip bounded by the solid wall $y = 0$ and the free boundary $y = a(t)$. The problem has a self-similar solution where $y/\sqrt{t} = const$ [9]. The numerical analysis of the problem shows that there may exist two stable regimes in addition to the unstable self-similar regime, depending on the initial data [10]. In one of them, $a \to const$ as $t \to \infty$, and the motion stabilizes to the quiescent state. In the other regime, $a \to \infty$ as $t \to t^* < \infty$. The asymptotic behavior of the collapsing solution is described by the relation $a(t - t^*) \to const$ typical for solutions of Euler equations with a straight free boundary [11], [12].

References

[1] Pukhnachev V.V. (2014) Singular solutions of Navier–Stokes equations. In *Proc. of St.Petersburg Math. Soc., Volume XV. Advances in Math. Analysis of Partial Diff. Equations. Dedicated to the memory of O.A. Ladyzhenskaya* (eds. D. Apushkinskaya and A.I. Nazarov), Series 2, **232**, 193–218. American Mathematical Society **2014** Providence, Rhode Island.

[2] Andreev V.K., Kaptsov O.V., Pukhnachov V.V. & Rodionov A.A. (1998) *Applications of group-theoretical methods in hydrodynamics.* **xii+396**, Kluwer Academic Publishers, Dordrecht/Boston/London.

[3] Zhuravleva E.N. & Pukhnachev V.V (2014) Numerical study of bifurcations in spiral fluid flow with free boundary. *Chislennye metody mekhaniki sploshnoi sredy* 2014 **7(1)**, 82–90.

[4] Pukhnachev V.V. (2014) Point vortex in a viscous incompressible fluid. *Journal of Applied Mechanics and Technical Physics* 2014 **55(2)**, 345–351. (Translated from Prikladnaya Mekhanika i Tekhnicheskaya Fizika, Vol. 55, No. 2, pp. 180–187, March–April, 2014.)

[5] Lavrenteva, O.M. (1980) Asymptotical regimes in the rotating viscous ring motion. *Dinamika neodnorodnoy zhidkosti* 1980 **44**, 15–35.

[6] Pukhnachev, V.V. (2002) Quasistationary approximation in the rotating ring problem. *Siberian Mathematical Journal* 2002 **43(3)**, 525–548. (Translated from Sibirskii Matematicheskii Zhurnal, Vol. 43, No. 3, pp. 652–677, May–June, 2002.)

[7] Shapeev, A.V. (2004) Unsteady self-similar flow of a viscous incompressible fluid in a plane divergent channel. *Fluid Dynamics* 2004 **39(1)**, 36–41. (Translated from Izvestiya Rossiiskoi Academii Nauk, Mekhanika Zhidkosti i Gaza, No. 1, 2004, pp. 41–46.)

[8] Moffatt, H.K. (1964) Viscous and resistive eddies near a sharp corner *J. Fluid Mech.* 1964 **18**, 1–18.

[9] Pukhnachev, V.V. (1999) On a problem of viscous strip deformation with a free boundary. *C.R. Acad.Sci.Paris* 1999 **328(1)** 357–362.

[10] Zhuravleva, E.N. (2016) Numerical study Navier-Stokes equations for motion with free boundary. *Journal of Applied Mechanics and Technical Physics* 2016 **2**.(Translated from Prikladnaya Mekhanika i Tekhnicheskaya Fizika, No. 2, 2016, in press)

[11] Ovsiannikov, L.V. (1967) General equations and examples. In *Problem on time-dependent liquid motion with free boundary.* 5–75. Nauka **1967** Novosibirsk (in Russian).

[12] Longuet-Higgins, M.S. (1972) A class of exact, time-dependent, free-surface flows. *J. Fluid Mech.* 1972 **55(3)**, 529–543.

Notes

The elastic trefoil is the twice covered circle

H. Gerlach[1], Ph. Reiter[2], H. von der Mosel[3]

[1] *LCVMM, EPF Lausanne, Switzerland*
[2] *Faculty of Mathematics, University of Duisburg–Essen, Germany*
[3] *Institute for Mathematics, RWTH Aachen University, Germany*

Summary

In order to investigate the elastic behavior of knotted loops of springy wire, we minimize the classic bending energy regularized by ropelength, i.e., the quotient of length over thickness, in order to penalize self-intersection. Our main objective is to characterize the limit configurations of energy minimizers as the regularization parameter tends to zero, which will be referred to as *elastic knots*.

For every odd $b > 1$ and the respective class of $(2, b)$-torus knots (containing the trefoil) we obtain a complete picture showing that the respective elastic $(2, b)$-torus knot is the twice covered circle.

Fig. 1: Springy knots: figure-eight knot, mathematician's loop, and Chinese button knot. Wire models manufactured by WHY KNOTS, Aptos; photographs by B. Bollwerk, Aachen.

Knotted loops made of elastic wire spring into some (not necessarily unique) stable configurations when released, such as the beautiful toy models shown in Figure 1. The aim of this project is to characterize the corresponding shapes.

Neglecting any additional torsional effects and also excluding external forces and friction that might be present these toy models, we follow Bernoulli's approach to consider the *bending energy*

$$E_{\mathrm{bend}}(\gamma) := \int_\gamma \kappa^2 \mathrm{d}s \tag{1}$$

as the only intrinsic elastic energy. Here the wire is represented by a sufficiently smooth *unit loop*, i.e., a closed curve $\gamma : \mathbf{R}/\mathbf{Z} \to \mathbf{R}^3$ of unit length, parametrized by arclength. Its local curvature is denoted by $\kappa = |\gamma''|$.

To respect a given knot class when minimizing the bending energy we have to preclude self-crossings. As proposed in [1], we could add any self-repulsive *knot energy* for that matter, imposing infinite energy barriers between different knot classes. But a solid (albeit thin) wire motivates a steric constraint in form of a fixed (small) thickness of all curves in competition. This and the geometric rigidity it imposes on the curves lead us to adding a small amount of *ropelength* $\mathcal{R}$ to form the *total energy*

$$E_\vartheta := E_{\mathrm{bend}} + \vartheta\mathcal{R}, \qquad \vartheta > 0, \tag{2}$$

to be minimized within a prescribed (tame) knot class $\mathcal{K}$, that is, on the class $\mathcal{C}(\mathcal{K})$ of all unit loops representing $\mathcal{K}$. The thickness $\triangle[\cdot]$ may be expressed as

$$\triangle[\gamma] := \inf_{\substack{u,v,w\in\mathbf{R}/\mathbf{Z}\\ u\neq v\neq w\neq u}} R(\gamma(u), \gamma(v), \gamma(w)), \tag{3}$$

where $R(x, y, z)$ denotes the unique (possibly degenerate) circle passing through $x, y, z \in \mathbf{R}^3$.

Fig. 2: Minimizers of E_ϑ, $\vartheta = 0.1$ (left) and $\vartheta = 0.001$ (right), for the trefoil knot class. The figures have been produced by simulated annealing.

It can be shown that in every given (tame) knot class $\mathcal{K}$ and for every $\vartheta > 0$ there is indeed a unit loop $\gamma_\vartheta \in \mathcal{C}(\mathcal{K})$ minimizing the total energy E_ϑ within $\mathcal{K}$, see [3, Thm. 2.1].

To understand the behaviour of very thin springy knots we investigate the limit $\vartheta \searrow 0$, see [1]. To this end, we consider arbitrary sequences $(\gamma_\vartheta)_{\vartheta>0}$ of minimizers in a fixed knot class $\mathcal{K}$ and look at their possible limit curves γ_0 as $\vartheta \searrow 0$, calling any such limit curve an *elastic knot for* $\mathcal{K}$. For any tame knot class, there is at least one elastic knot. Unless $\mathcal{K}$ is the unknot, none of these elastic knots is embedded.

In [3] we rigorously prove that, for any non-trivial knot class attaining the smallest possible lower bound $(4\pi)^2$ on the bending energy, the *only* possible shape of an elastic knot is that of the twice-covered circle. Moreover, we show that the former condition holds *exactly* for the class of $(2, b)$-torus knots for any odd integer b with $|b| \geq 3$.

This result confirms our numerical and mechanical experiments (see Figure 2 and Figure 3 on the left), as well as the heuristics and simulations of Gallotti and Pierre-Louis [2].

Twisting the wire in the experiments before closing it at the hinge (without releasing the twist) leads to completely different stable configurations; see Figure 3 on the right. In that case a more general Lagrangian taking into account also these effects would need to be considered, and the question of classifying *twisted* elastic knots is wide open.

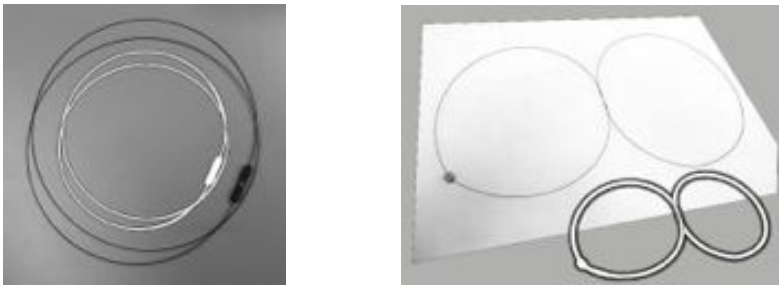

Fig. 3: Mechanical experiments. Left: The springy trefoil knot is close to the twice-covered circle. Right: Adding a 2π-twist leads to a stable flat trefoil configuration close to a planar figure-eight. Wire models by courtesy of J. H. Maddocks, Lausanne.

Acknowledgements. This project is supported by the German Research Foundation (DFG).

References

[1] H. von der Mosel. Minimizing the elastic energy of knots. *Asymptot. Anal.*, 18(1-2):49–65, 1998.

[2] R. Gallotti and O. Pierre-Louis. Stiff knots. *Phys. Rev. E (3)*, 75(3):031801, 14, 2007.

[3] H. Gerlach, Ph. Reiter, and H. von der Mosel. The elastic trefoil is the twice covered circle. *ArXiv e-prints*, 2015. `http://arxiv.org/abs/1510.06171`

Notes

Helical vortices: linear and nonlinear dynamics

M.Rossi[1], C.Selçuk[2],I. Delbende[2]

[1] *CNRS, UPMC, d'Alembert, 75232 Paris Cedex 05, France*
[2] *UPMC,LIMSI-CNRS, Campus Universitaire,rue John von Neuman, 91405 Orsay Cedex, France*

Summary

We present results on the dynamics of helical vortices. In particular we analyse equilibrium states and their linear and nonlinear stability.

The near wake behind helicopter rotors, wind turbines and more generally behind rotating devices are dominated by helical vortices. Investigating their stability properties is a necessary step to predict their dynamics. The base flows considered here are helically symmetric : fields are invariant through combined axial translation of distance Δz and rotation of angle $\theta = \Delta z/L$ around the z-axis, where $2\pi L$ denotes the helix pitch. In order to simulate the evolution of such flows, we use a Navier-Stokes code based on a formulation in which the helical symmetry is enforced into the equations [1]. Basic states are obtained which consist of multiple diffusing helical vortices, for various values of the helical pitch.

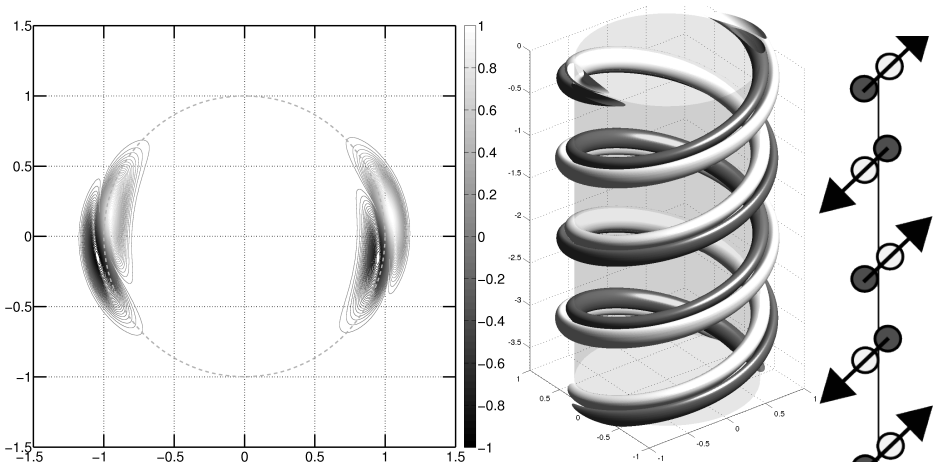

Fig. 1: Linear stability analysis: (a) Structure of the most unstable mode. The base flow corresponds to two helical vortices with pitch $2\pi L = 0.3$ and core size $a_b = 0.09$. The mode is represented by the helical vorticity component of the perturbation field in the horizontal (x, y)-plane by colored contours. (b) Mode in a 3-D representation. The arrows indicate the perturbation action on the base flow. The displacement induced by the mode has two components: one along the radial direction and one along the z direction. On the radial direction, one vortex goes inwards while the other goes outwards. (c) Schematic representation: the structure is analogous to the pairing instability mode for an infinite row of point vortices.

Instabilities in such vortex systems have mainly been studied theoretically [2]–[3] in an inviscid framework for small core size vortices. The aim of the present study is to generalize these works to the viscous framework for arbitrary core sizes and vorticity profiles. We first perform a linear temporal stability analysis of such base flows, using an Arnoldi procedure. Two different codes are used : (i) a linearised version of the nonlinear helical code, (ii) another code which computes the dynamics of *arbitrary perturbations* in the vicinity of a helically symmetric base flow. These codes allows investigating different instability modes : (i) modes having the same helical symmetry as the base flow generalizing the Okulov modes ; (ii) modes with arbitrary wavenumber k along

z generalizing the Widnall modes. In the first case, instabilities are found to be dominated by displacement modes of the type presented in figure 1 for the case of two vortices. In the second case, modes are compared to those observed in recent experimental work [4].

The nonlinear dynamics of a basic flow perturbed with a linear mode of type (i) with an initial weak amplitude is computed. The displacement mode is shown to be responsible for leap-frog dynamics and vortex merging with characteristics depending on the various parameters.

Acknowledgements. Financial support from ANR HELIX project ANR-12-BS09-0023-01 is kindly acknowledged.

References

[1] I. Delbende, M. Rossi, O. Daube (2012), DNS of flows with helical symmetry, *Theor. Comput. Fluid Dynam.* **26**(1) 141–160.

[2] S. E. Widnall (1972) The stability of a helical vortex filament. *J. Fluid Mech.* **54**, 641–663.

[3] V. L. Okulov and J. N. Sørensen (2007) Stability of helical tip vortices in a rotor far wake *J. Fluid Mech.* **576**, 1–25.

[4] H.Quaranta, H.Bolnot & Th.Leweke (2015) Long-wave instability of a helical vortex *J. Fluid Mech.* **780**, 687–716.

Notes

Field line helicity and magnetic reconnection

A. J. B. Russell[1], A. Yeates[2], G. Hornig[1], A. L. Wilmot-Smith[3]

[1] *Mathematics, University of Dundee, U.K.*
[2] *Mathematics, Durham University, U.K.*
[3] *Mathematics, University of St Andrews, U.K.*

Summary

It is often useful to know not only the global helicity of a magnetic field, but also how the total is composed and how that changes over time. The tool that best achieves this is *field line helicity*, which assigns a helicity value to every field line and can therefore distinguish between different magnetic fields with the same total helicity. Here, I will discuss the properties of field line helicity, demonstrate its practical application to magnetic fields, and (the main result) show how an evolution equation can be derived for it. Finally, the evolution of field line helicity is characterised for two important cases: ideal evolution and localised reconnection in a complex magnetic field. The latter has interesting implications for Taylor relaxation.

1 Introduction

Magnetic helicity is a valuable tool that quantifies the overall linking of magnetic field lines and can be extended to open domains either by using relative helicity or by suitable restriction of the gauge. This global measure of the topology is complemented by a local measure that we refer to as the *field line helicity* [1, 2].

2 Definition and example

For field lines that close, or that enter and exit the domain, the field line helicity at $\mathbf{x}$ is defined as

$$\mathcal{A}(\mathbf{x}) \quad = \quad \int_{F(\mathbf{x})} \mathbf{A} \cdot \mathrm{d}\mathbf{l} \tag{1}$$

where $\mathbf{A}$ is the vector potential, $\mathrm{d}\mathbf{l}$ is the line element parallel to $\mathbf{B} = \nabla \times \mathbf{A}$, and the integral is over the field line through the point of interest. The total helicity of any flux tube can be obtained from $\mathcal{A}$ by evaluating the flux integral over any cross-section, C, of the tube, since

$$H \quad = \quad \int_V \mathbf{A} \cdot \mathbf{B} \, \mathrm{d}^3x = \int_C \mathcal{A}\mathbf{B} \cdot \mathbf{n} \, \mathrm{d}^2x, \tag{2}$$

where $\mathbf{n}$ is the unit normal to the cross-section; this property justifies the name *field line helicity*.

$\mathcal{A}$ is valuable because it is an ideal invariant (unlike $\mathbf{A} \cdot \mathbf{B}$) and it retains more topological information than the total helicity. Figure 1 demonstrates the second point – the braided magnetic field shown has zero total helicity but $\mathcal{A}$ captures its considerable topological complexity.

3 Evolution

For any Ohm's law, a *generalised field line velocity*, $\mathbf{w}$, exists such that

$$\frac{\partial \mathbf{B}}{\partial t} \quad = \quad \nabla \times (\mathbf{w} \times \mathbf{B}) \tag{3}$$

i.e. $\mathbf{B}$ evolves as though frozen in to the flow of $\mathbf{w}$ (here, we exclude null points, spines and fan surfaces). In the absence of parallel electric field, $\mathbf{w}$ reduces to the plasma velocity; when

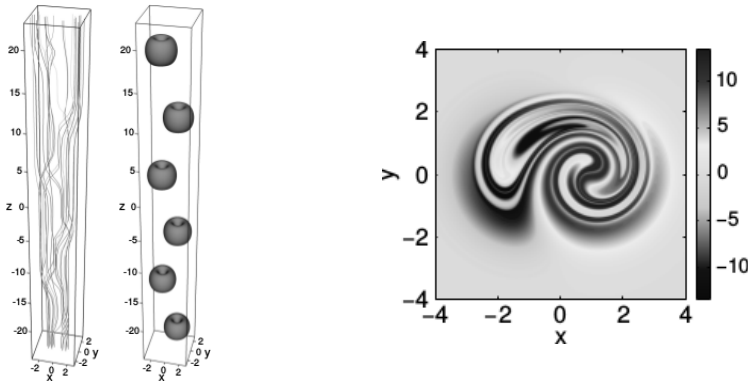

Fig. 1: (Left) Visualisation of the E^3 magnetic braid [3]: the two boxes show (leftmost) a selection of the field lines and (adjacent) the six flux rings that are superimposed on a uniform vertical field to create the braid. (Right) Field line helicity on the base of the domain.

reconnection occurs, $\mathbf{w}$ also captures the apparent slipping of field lines with respect to the plasma. One can then show [4] that for a suitable restriction of the gauge,

$$\frac{\partial \mathcal{A}}{\partial t} \;=\; -\mathbf{w}\cdot\nabla\mathcal{A} + \mathbf{w}\cdot\mathbf{A}\big|_{\text{exit}} - \mathbf{w}\cdot\mathbf{A}\big|_{\text{entry}} - \Delta\psi, \tag{4}$$

where $\Delta\psi$ is the voltage drop along the field line and the $\mathbf{w}\cdot\mathbf{A}\big|_{\text{entry}}$ and $\mathbf{w}\cdot\mathbf{A}\big|_{\text{exit}}$ terms are evaluated where the field line meets the boundary (these terms are dropped for closed field lines).

For ideal evolutions, $\Delta\psi = 0$. If the plasma is static at the boundaries then the $\mathbf{w}\cdot\mathbf{A}$ terms also vanish and Eq. (4) reduces to an advection equation. Hence, $\mathcal{A}$ is an ideal invariant. If motions are permitted on the boundaries, then these displacements change the winding of magnetic field lines and this topology change is captured in the evolution of $\mathcal{A}$ due to the "work-like" $\mathbf{w}\cdot\mathbf{A}$ terms.

In general, when reconnection occurs the full form of Eq. (4) applies. However, a powerful simplification is obtained in fields that have significant topological entropy, e.g. as is typical for turbulent reconnection. Then, the terms on the RHS have a useful ordering: the advection term dominates; followed by the $\mathbf{w}\cdot\mathbf{A}$ terms, which have a well-ordered structure of oppositely signed pairs; and the voltage drop term makes the least contribution. Thus, to leading order reconnection rearranges field line helicity, with the next order effect being small pairwise exchanges.

An interesting implication is that while turbulent reconnection approximately conserves total helicity, it cannot arbitrarily change how the helicity is composed, contrary to the assumption underlying standard Taylor relaxation. We therefore suggest that more accurate estimates of the relaxation end-state and the energy released may be obtained by using this more rigorous constraint.

Acknowledgements. This work was supported by STFC through consortium grants ST/K000993/1 and ST/K001043 to the University of Dundee and Durham University.

References

[1] Berger, M.A. (1988) An energy formula for nonlinear force-free magnetic fields. *Astron. Astrophys.* **201**, 355.

[2] Yeates, A.R. & Hornig, G. (2013) Unique topological characterization of braided magnetic fields *Phys. Plasmas* **20**, 012102.

[3] Wilmot-Smith, A.L., Hornig, G. & Pontin, D.I. (2009) Magnetic braiding and parallel electric fields. *Astrophys. J.* **696**, 1339.

[4] Russell, A.J.B., Yeates, A.R., Hornig, G. & Wilmot-Smith, A.L. (2015) Evolution of field line helicity during magnetic reconnection. *Phys. Plasmas* **22**, 032106

Notes

Topology of flows and finite-time singularity: On the kernel of helicity and spirality

Taliya Sahihi

Department of Physics, Iran University of Science and Technology, Iran

Summary

The aim of this note is to draw a connection between topology and geometry of fluid flows and finite time singularity in vanishing helicity fluids. Our inquiry leads to characterizing the vortex flows according to their knottedness and integrability of the velocity field. Since the helicity is zero, we will use polynomial invariants on vortex lines to distinguish different systems in our examples. The hope to use more mathematical results inspired us to redefine helicity and spirality in more general forms as operators acting on differential forms on odd dimensional smooth manifolds. The fluid dynamical assumptions and previous results will be transformed in the terms of differential forms. In the next step, we will use a new cohomological structure to redefine the operators on topological manifolds.

1 Introduction

The zero helicity for ideal flows neither characterizes the vortex structure nor bounds the enstrophy (i.e., energy of the vorticity field). This situation recently investigated by more powerful tools, from constructing higher-helicity via Massey product and Milnor μ invariant toward using the polynomial knot invariants [1]–[3]. At first we focus on this kind of flows and try to find the relation between possibility of happening the finite-time singularity and existence a gauge transformation on the impulse function $\gamma = u - \nabla\phi$, where u is the velocity of fluid and ϕ is the Bernoulli's function. Sprirality, that is a Lagrangian invariant is defined in the Russo notion as follows

$$Sp = \frac{\gamma \cdot \omega}{\rho}, \tag{1}$$

where ω is vorticity and ρ is fluid density [4]. The above quantity is only depend on the initial condition and therefore remains constant on the fluid trajectory for a fluid particle. The Integral of $\gamma \cdot \omega$ on a domain of fluid D (with $\omega \cdot n = 0$ on ∂D) is the helicity. Obviously any gauge transformation as $\gamma \to \gamma - \nabla\varphi_0$ such that φ_0 be a time independent function of initial position, changes the spirality but holds the vorticity and helicity of the fluid. The main question of this note is finding the topological and geometrical conditions of the initial fluid flows that guarantee the existence of a gauge transformation to bring the spirality to zero [5]. It seems, having this kind of gauge increase the possibility of occuring the singularity for vorticity field on the finite number of points on the trajectory of the fluid particles, in finite intervals of time. Although the complete answer to this question is not available now, we have two separate necessary and sufficient conditions for the existence of this gauge. The necessary condition corresponds to the knottedness of the vortex lines such that the total flux passing through any embedded Seifert surface of a non singular vortex lines should be zero. We will show this behavior with a few examples of vortex tubes tabulated by Alexander and Jones polynomials. The sufficient condition tell us if the velocity field (harmonic part of velocity in high genus boundary surface) satisfies the Frobenius integrability condition (i.e., have a collection of locally normal surfaces) the gauge is principally exist.

The hope to use some mathematical achievements in the literature, inspired us to generalize the helicity and spirality to operators acting on a quotient class of differential forms on three dimensional smooth manifolds and reconstruct the necessary and the sufficient conditions in the new format [6]. In this condition, if $j_M : \partial M \hookrightarrow M$ be the inclusion map, $j_M^*(d\alpha) = 0$ (or $\iota_{\frac{\partial}{\partial\xi}}(*d\alpha) = 0$ for

any $\frac{\partial}{\partial\xi}$ normal to the boundary ∂M) describe the tangent to the boundary property of the vector field related to the form $d\alpha$. Now if we defined the subset $\Omega^p_T(M)$ of $\Omega^p(M)$ as the exact forms $d\omega$ with tangent property, the spirality operator Sp on $2p+1$ manifold M defined as the map from $\Omega^p_T(M)/Im(d)$ to $\Omega^{2p+1}(M)/\Omega^{2p+1}_T(M)$, sending the class of p-forms $[\alpha]_{\Omega^p_T(M)/Im(d)}$ to the class of top degree forms $[\alpha\wedge d\alpha]_{\Omega^{2p+1}(M)/\Omega^{2p+1}_T(M)}$ and helicity defined as $\int_M Sp([\alpha])$. Again the transformation $\alpha\to\alpha+d\beta$ for a given p-form β holds the helicity.

A smooth map $f: N\to M$ pullbacks the above structures from M to N. Therefore, for $g:=f|_{\partial N}:\partial N\to\partial M$ we have the commutative relation $f\circ j_N=j_M\circ g$. Here the problem of existing the gauge in the special case of vanishing helicity giving rise to the difference between the kernels of helicity and spirality.

In the next step, the previous objects translated in the language of a special class of singular cochains on topological manifolds and the standard cup product $\smile$ modified to a new form $\smile$ to be compatible with the wedge product $\wedge$ of forms in smooth condition ([6], [7]). The spirality becomes as follows

$$Sp(\alpha)=\alpha\smile\delta\alpha, \tag{2}$$

where δ is the boundary operator. By applying the above helicity on the fundamental class, we reach to the helicity of singular cochains. The obtained cohomology in the above argument can make a platform for new topological version of more invariants e.g., triple-product, Chern-Simons action and also the Calabi invariant that is the even dimensional sibling of helicity. The compatibility of each singular quantity with the original smooth version, will be checked by using the isomorphism between de Rham cohomology and singular cohomology [8].

Acknowledgements. Financial support from IUTAM, the Department of Mathematics and Applications of the University of Milano-Bicocca, and ICTP is kindly acknowledged.

References

[1] R. Komendarczyk, The third order helicity of magnetic fields via link maps. *Commun. Math. Phys.* **292** 431-456 (2009).

[2] X. Liu, R. L. Ricca, Tackling Fluid Structures Complexity by the Jones Polynomial, *Procedia IUTAM*, **7** pp 175?182 (2013).

[3] X. Liu, R. L. Ricca, On the derivation of HOMFLYPT polynomial invariant for fluid knots, *J. Fluid Mech.*, **773** pp 4-48 (2015).

[4] G. Russo, P. Smereka, Impulse formulation of the Euler equations: general properties and numerical meth- ods, *J. Fluid Mech.* **391** pp 189-209 (1999).

[5] H. Eshraghi, Y. Abedini, A special class in vanishing helicity ideal flows, *J. Math. Phys.* **46** pp 043102 (2005).

[6] T. Sahihi, H. Eshraghi, Helicity kernel and odd dimensional Manifolds, (preprint, 2016).

[7] T. Sahihi, H. Eshraghi, Alternative singular cohomology, (preprint, 2015).

[8] F. W. Warner, *Foundations of Differentiable Manifolds and Lie Groups*, (Springer-Verlag, New York, 1983).

Notes

Role of the helicity in the energy transfer in three-dimensional turbulence

Ganapati Sahoo[1], Luca Biferale[1]

[1] *Department of Physics and INFN, University of Rome Tor Vergata, Italy*

Summary

We investigated the effects of the helicity in the dynamics of the energy transfer in turbulent flows using a modified version of the Navier-Stokes equations (NSE) with explicit breaking of the mirror symmetry. With an external parameter that controls the imbalance between the number of positive and negative helical Fourier modes we aim to disentangle the role of helicity in the direction of the turbulent energy transfer. In an earlier study with helical projection, an inverse cascade of energy was observed in the three-dimensional NSE when helicity was maintained sign-definite [1]. In this study we measure the degree to which the parity symmetry controls the direction of the cascade. We introduce a mechanism in which the parity is broken stochastically but in a time frozen manner with helical constraints. We keep triadic interactions in Fourier space involving modes with definite sign of helicity and decimate the triads of other modes with opposite sign of helicity with a fixed probability. We observed a singular behaviour of the direction of the energy cascade measuring a positive forward flux as soon as only a few modes with different helical polarities take part in the dynamics.

Direct numerical simulations (DNS) of three-dimensional NSE for incompressible flows and experiments in the three-dimensional homogeneous and isotropic turbulence show cascade of energy from the forced scales to the dissipative scales. The direction of the energy transfer is however believed to be determined by the invariants of the system. In two-dimensions the two positive-definite invariants, energy and enstrophy, effect in transfer of energy to the large scales. For the three-dimensional NSE two inviscid invariants are the energy $E = \int d^3r\ \vec{u}\cdot\vec{u}$ and the helicity $H = \int d^3r\ \vec{u}\cdot\vec{\omega}$, where $\vec{u}$ is the velocity and $\vec{\omega} = \nabla\times\vec{u}$ is the vorticity. The energy is positive and definite whereas the helicity could be either positive or negative. Helicity is known to play a key role in hydrodynamical and magnetohydrodynamical systems [2]. In hydrodynamics both energy and helicity cascade forward from large scales to small scales [3]. However, There are evidences of inverse energy transfer to the large scales under special conditions. A turbulent flow confined in thick fluid layers due to formation of large scale vortex suppresses vertical motions and supports large scale energy transfer [4]. In a rotational turbulent flow with helical force a direct cascade of helicity and direct and inverse cascade of energy is observed [5]. Dynamics of the inverse energy transfer is studied in a subset of all interactions in the NSE as in Ref. [1]. Positive definiteness of helicity leads to inverse energy transfer. In this work we show that when relative weight between the positive and negative helical modes present in the system is changed a critical behaviour of the energy transfer is observed [6]. We, using a method to separate positive and negative helical modes to understand the dynamics of the energy cascade, show a transition of forward to inverse energy transfer.

Each Fourier mode of velocity $\boldsymbol{u}(\boldsymbol{k},t)$ has two degrees of freedom as it satisfies the incompressibility condition $\boldsymbol{k}\cdot\boldsymbol{u}(\boldsymbol{k},t) = 0$. If we chose these degrees of freedom to be the projections on orthonormal helical waves with definite sign of helicity [7] we could write $\boldsymbol{u}(\boldsymbol{k},t) = \boldsymbol{u}^{+}(\boldsymbol{k},t) + \boldsymbol{u}^{-}(\boldsymbol{k},t)$. Using the complex eigenvectors of the curl operator $i\boldsymbol{k}\times\boldsymbol{h}^{\pm}(\boldsymbol{k}) = \pm k\boldsymbol{h}^{\pm}(\boldsymbol{k})$ we could define a projection operator $\mathcal{P}^{\pm}(\boldsymbol{k}) \equiv \frac{\boldsymbol{h}^{\pm}(\boldsymbol{k})\otimes\boldsymbol{h}^{\pm}(\boldsymbol{k})^{*}}{\boldsymbol{h}^{\pm}(\boldsymbol{k})^{*}\cdot\boldsymbol{h}^{\pm}(\boldsymbol{k})}$ such that $\boldsymbol{u}^{\pm}(\boldsymbol{k},t) = \mathcal{P}^{\pm}(\boldsymbol{k})\boldsymbol{u}(\boldsymbol{k},t)$. The NSE could be then independently written for each modes as

$$\partial_t\boldsymbol{u}^{\pm}(\boldsymbol{k},t) = \mathcal{P}^{\pm}(\boldsymbol{k})\boldsymbol{N}_{u^{\pm}}(\boldsymbol{k},t) + \nu k^2\boldsymbol{u}^{\pm}(\boldsymbol{k},t) + \boldsymbol{f}^{\pm}(\boldsymbol{k},t) \tag{1}$$

where ν is the kinematic viscosity and $\boldsymbol{f}$ is the external forcing and the nonlinear term containing all triadic interactions is $\boldsymbol{N}_{u^{\pm}}(\boldsymbol{k},t) = \mathcal{F}T(\boldsymbol{u}^{\pm}\cdot\boldsymbol{\nabla}\boldsymbol{u}^{\pm} - \boldsymbol{\nabla}p)$.

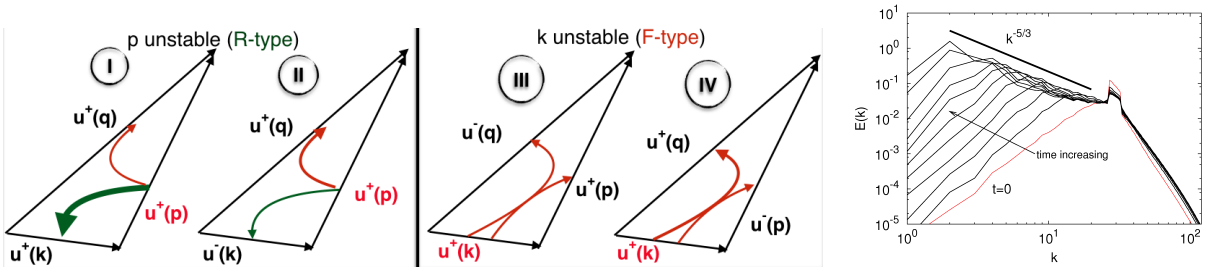

Fig. 1: (a) All possible triadic interactions in Navier-Stokes equations based on the helicity content of the involving Fourier modes. The triads with only $\boldsymbol{u}^+$ (Class-I) lead to reversal of energy cascade (left). (b) Energy spectra $E(k) = \sum_{\boldsymbol{k}\ni|\boldsymbol{k}|=k} |\mathbf{u}(\boldsymbol{k})|^2$ in the inverse cascade regime shows $k^{-5/3}$ slope [1] (right).

There are four classes of nonlinear triadic interactions with definite helicity signs under helical decomposition of NS equations shown in Fig.1a. Energy and helicity are conserved for each triads. Restricting dynamics to subsets of these triads affects the direction of the energy transfer [7, 8]. Full decimation of triads involving either $\boldsymbol{u}^+$ or $\boldsymbol{u}^-$ shows inverse cascade of energy [1, 9] as shown in Fig.1b. To understand the transition of the forward energy transfer to the inverse energy transfer we decimated a fraction α of modes with helicity of one sign instead of all of them. We numerically found a *critical value* of α at which forward cascade of energy stops when force is applied at the large scales and alternatively, inverse cascade of energy stops if forced at small scales. We define the projection operator using the parameter α,

$$\mathcal{P}^+_\alpha(\boldsymbol{k})\boldsymbol{u}(\boldsymbol{k},t) = \boldsymbol{u}^+(\boldsymbol{k},t) + \theta_\alpha(\boldsymbol{k})\boldsymbol{u}^-(\boldsymbol{k},t) \tag{2}$$

where $\theta_\alpha(\boldsymbol{k})$ is 0 or 1 with probability α and $1-\alpha$, respectively. When $\alpha = 0$ we obtain the results for standard NSE and when $\alpha = 1$ we recover results for fully helical-decimated NSE. We performed DNSs of Eq.(1) using a pseudo-spectral method on a periodic cubic domain of size $L = 2\pi$ with resolutions up to 1024^3 collocation points.

We observe that as we increase α, the contribution of triads leading to inverse energy cascade grows. Only when α is very close to 1 inverse energy cascade takes over the forward cascade; critical value of α is found to be $\simeq 1$ our simulations. We also measure the relative changes in the intermittency in the forward cascade regime at changing α.

We acknowledge support from European Research Council under the ERC AdG No. 339032.

References

[1] L. Biferale, S. Musacchio, and F. Toschi, *Phys. Rev. Lett.* **108**, 164501 (2012); *J. Fluid Mech.* **730**, 309 (2013).

[2] H. K. Moffatt, *J. Fluid Mech.* **35**, 117 (1969); H. K. Moffatt and A. Tsinober, *Annu. Rev. Fluid Mech.* **24**, 281 (1992).

[3] Q. Chen, S. Chen, and G. Eyink, *Phys. Fluids* **15**, 361-374 (2003).

[4] H. Xia, D. Byrne, G. Falkovich, and M. G. Shats, *Nat Phys* **7**, 321-324 (2011).

[5] P. D. Mininni, A. Alexakis, and A. Pouquet, *Phys. Fluids* **21**, 015108 (2009).

[6] G. Sahoo, F. Bonaccorso, and L. Biferale, *Phys. Rev. E* **92**, 051002(R) (2015).

[7] F. Waleffe, *Phys. Fluids A* **4**, 350-363 (1992).

[8] G. Sahoo and L. Biferale *Euro. Phys. J. E* **38** (10), 114 (2015).

[9] L. Biferale and E.S. Titi, *Journ. Stat. Phys.* **151**, 1089 (2013).

Notes

Helicity Conservation and Twisted Seifert Surfaces for Superfluid Vortices

H. Salman[1]

[1] *School of Mathematics, University of East Anglia, Norwich Research Park, Norwich, UK*

Summary

In recent years, there has been increasing interest in properties of superfluid vortices as these provide an excellent paradigm of an ideal inviscid fluid. Vorticity in such fluids is well described by vortex filaments in which the rotation is concentrated along a curve. However, the lack of an internal vortical structure within a superfluid vortex has led to several complications in adapting the results concerning helicity conservation to superfluids. In particular, the notion of twist for a superfluid vortex is not well defined. We will illustrate how twist can be formulated and defined for a superfluid vortex in a physically intuitive way. After mathematically formulating twist for a superfluid vortex, we will present a number of illustrative examples of vortex configurations calculated numerically. This will include helical vortices, breather excitations on vortex filaments, and knotted vortices. The latter is motivated by recent experiments concerning the creation of knotted vortices in the laboratory.

Background

A microscopic model for a superfluid exists in the form of the Gross-Pitaevskii equation given by

$$i\hbar\frac{\partial\psi}{\partial t} = \frac{-\hbar^2}{2m}\nabla^2\psi + g|\psi|^2\psi, \tag{1}$$

where ψ represents the wavefunction of the condensate, m is the mass of the atomic species, and g is an interatomic interaction coefficient. By introducing the Madelung transformation given by $\mathbf{v} = (\hbar/m)\boldsymbol{\nabla}\phi$ and $\rho = m|\psi|^2$ where ϕ is the phase of the wavefunction such that $\psi = \sqrt{\rho/m}\exp(i\phi)$, the Gross-Pitaevskii equation can be recast in hydrodynamic form. The original equation for the complex wavefunction is then transformed into a system of two equations for the density ρ and the phase ϕ which correspond to a continuity equation for a compressible fluid and an unsteady Bernoulli equation given by

$$\frac{\partial\rho}{\partial t} + \boldsymbol{\nabla}\cdot(\rho\mathbf{v}) = 0, \tag{2}$$

$$\left(\frac{\hbar}{m}\right)\frac{\partial\phi}{\partial t} + \frac{1}{2}|\mathbf{v}|^2 = \frac{-g\rho}{m} + \frac{\hbar^2}{2m}\frac{\nabla^2\rho^{1/2}}{\rho^{1/2}}. \tag{3}$$

Given that the flow is derived from the gradient of the phase, which plays the role of a velocity potential in this context, the flow is irrotational. However, solutions with singular distributions of vorticity are permitted by allowing the phase to become a non-single valued function. In 2D, the vorticity corresponds to that of a point vortex whereas in 3D it corresponds to that of a vortex filament. Since the velocity is divergent in the vicinity of a vortex filament, the density of the superfluid vanishes at the centre of the vortex to ensure the momentum remains finite. The variation of the density from the background value, denoted by ρ_∞, towards zero occurs on a characteristic length scale that is set by the healing length of the system given by $l_h = \hbar/\sqrt{2g\rho_\infty}$. Therefore, for superfluids, the internal structure of the vortex is determined by the variation of the density profile. In contrast, there is no internal structure associated with the vorticity field. For these reasons, quantized vortices correspond to topological defects of the superfluid.

The quantum pressure term corresponding to the last term in Eq. (3) is negligible on distances exceeding the healing length scale. Moreover, if the intervortex separation and the radius of curvature of the vortex filaments far exceed the healing length, the motion of the defects to leading order can be described by that of an incompressible fluid. This allows a reduced level of description where one can track only the positions of the topological defects given by Biot-Savart law. Denoting the positions of the points along the i'th vortex filament by $\mathbf{r}_i$, we obtain

$$\mathbf{v}(\mathbf{x},t) = \sum_i \frac{\kappa_i}{4\pi} \oint_{\mathcal{C}_i} \frac{(\mathbf{r}_i - \mathbf{x}) \times \mathrm{d}\mathbf{r}_i}{|\mathbf{x} - \mathbf{r}_i|^3}, \tag{4}$$

where the sum is taken over all the vortex filaments and κ_i is the circulation associated with the i'th vortex.

The above considerations have important consequences on the evaluation of Helicity for superfluid vortices. In 1969 Moffatt [1] showed that, in addition to mass, momentum and energy conservation, an ideal inviscid fluid in 3D has another invariant known as helicity that is given by $\mathcal{H} = \int_V \boldsymbol{\omega} \cdot \mathbf{v} \mathrm{d}^3\mathbf{x}$ where $\mathbf{v}$ is the velocity field and $\boldsymbol{\omega} = \nabla \times \mathbf{v}$. This invariant quantifies the degree of knottedness of vortex lines within the fluid. Although an inviscid fluid is considered to be an idealisation of a real classical fluid in which viscosity is neglected, superfluids provide an excellent paradigm of an ideal inviscid fluid. It is now well understood that Helicity conservation is established by a balance between three different contributions, the linking number Lk, the Writhe $\mathcal{W}r$, and the total twist Tw such that [2]

$$\mathcal{H} = \kappa^2(Lk + \mathcal{W}r + Tw). \tag{5}$$

However, the lack of an internal vortical structure within a superfluid vortex has led to several complications in adapting the results concerning helicity conservation to superfluids. In particular, the notion of twist for a superfluid vortex is not well defined. We will illustrate how twist can be formulated and defined for a superfluid vortex in a physically intuitive and mathematical self-consistent way. After formulating twist for a superfluid vortex, we will present a number of illustrative examples of vortex configurations calculated numerically as illustrated in Fig. 1. This will include breather excitations [3], and knotted vortices that have now been created in the laboratory [4].

Fig. 1: Helical vortex shown on left and knotted trefoil vortex shown on right with Seifert surface.

Acknowledgements. The author would like to thank Risto Hänninen and Niklas Hietala for many valuable discussions. The author also acknowledges support for a Research Fellowship from the Leverhulme Trust under Grant R201540.

References

[1] Moffatt, H.K. (1969) The degree of knottedness of tangled vortex lines. *J. Fluid Mech.*, **35**, 117–129.

[2] Moffatt, H.K. & Ricca, R.L. (1992) Helicity and the Călugăreanu invariant, *Proc. R. Soc. Lond. A*, **439**, 411–429.

[3] Salman, H. (2013) Breathers on Quantized Superfluid Vortices *Phys. Rev. Lett.*, **111**, 165301.

[4] Kleckner, D. & Irvine, W.T.M. Creation and dynamics of knotted vortices, *Nature Physics*, **9** 253-258.

Notes

Helical vortices generated by flapping wings of bumblebees

Thomas Engels[1,2], Dmitry Kolomenskiy[3], Kai Schneider[1], Marie Farge[4], Fritz-Olaf Lehmann[5] and Jörn Sesterhenn[2]

[1] *M2P2-CNRS, Aix-Marseille Université, Marseille, France*
[2] *ISTA, Technische Universität Berlin, Berlin, Germany*
[3] *Biomechanical Engineering Laboratory, Chiba University, Chiba, Japan*
[4] *LMD-CNRS, Ecole Normale Supérieure, Paris, France*
[5] *Department of Animal Physiology, Universität Rostock, Rostock, Germany*

Summary

Insects fly even under heavy turbulent air flow conditions. To understand the impact of turbulent fluctuations on the aerodynamics of flapping wings, we model a bumblebee with fixed body and prescribed wing motion, flying in a numerical wind tunnel. The inflow condition of the tunnel varies from unperturbed laminar to strongly turbulent. Massively parallel simulations show that turbulence does not significantly alter the wing's leading edge vortex that is required for elevated lift production. Mean flight forces, moments and aerodynamic power expenditures are thus unaffected, suggesting little significance of turbulence on overall flight performance in insects. The increase in variance of the aerodynamic measures with increasing turbulence intensity, however, leads to flight instabilities in freely flying animals. Here we focus on analyzing the helicity of the generated vortices and study their contribution at different scales using wavelets.

Insect flight receives considerable attention from both engineers and biologists. This growing interest is fostered by the recent trend in miniaturization of unmanned air vehicles that naturally incites reconsidering flapping flight as a bio-inspired alternative to fixed-wing and rotary flight. For all small flyers it is challenging to fly outdoors in an unsteady environment, and it is essential to know how insects face that challenge.

Current research on the flow generated by flapping wings indicated the important role of the leading edge vortex. This vortex has a conical structure to due the three-dimensional motion of the wings. This flow configuration produces strong vorticity on the sharp leading edge and the outwards velocity (from the root to the tip of the wing) in the span-wise direction, see e.g. [4, 5]. Such flows are characterised by strong helicity, see fig. 1.

The aim of the present work is to analyze high resolution numerical simulation data of a bumblebee flying in turbulent flow, presented in [1]. We focus on the helicity of the generated vortices and use the orthogonal wavelet decomposition to analyze the scale dependence of helicity.

The bumblebee flaps its wings at Reynolds numbers of approximately 2000 at forward flight speed of 2.5 m/s. We developed a numerical wind tunnel and placed the animal in a $6R \times 4R \times 4R$ large, virtual rectangular box, where $R = 13.2$ mm is the wing length. The computational domain is discretized with 680 million grid points and the three-dimensional Navier-Stokes equations are solved by direct numerical simulation on a massively parallel computer. The volume penalization method is used to handle the no-slip boundary conditions on the time-varying geometry. The mean inflow velocity accounts for the equivalent forward flight speed of the tethered insect. For simplicity we modeled the wings as flat rigid plates with prescribed kinematics. To model atmospheric turbulence, we used homogeneous isotropic turbulence (HIT) as turbulent inflow. We varied the turbulence intensity by altering the energy content of the turbulent perturbations superimposed to the mean flow. The entire procedure allowed us to study insect flight from laminar to fully-developped turbulent flow conditions. Details on the numerical code, which is open source, can be found in [2].

A visualization of the flow fields of the bumblebee with laminar inflow is shown in fig. 1. The isosurfaces of the Q-criterion illustrate the vortical structures generated by the flapping wings. To get insight into the helicity of the vortices we colored the isosurfaces with the relative helicity,

$h(\boldsymbol{x}) = \frac{\boldsymbol{u}\cdot\boldsymbol{\omega}}{|\boldsymbol{u}|\,|\boldsymbol{\omega}|}$, where $\boldsymbol{u}$ is the velocity field and $\boldsymbol{\omega} = \nabla\times\boldsymbol{u}$ the vorticity field. Values of ± 1 correspond to alignement and anti-alignement of vorticity with velocity vectors, respectively. Integrating the

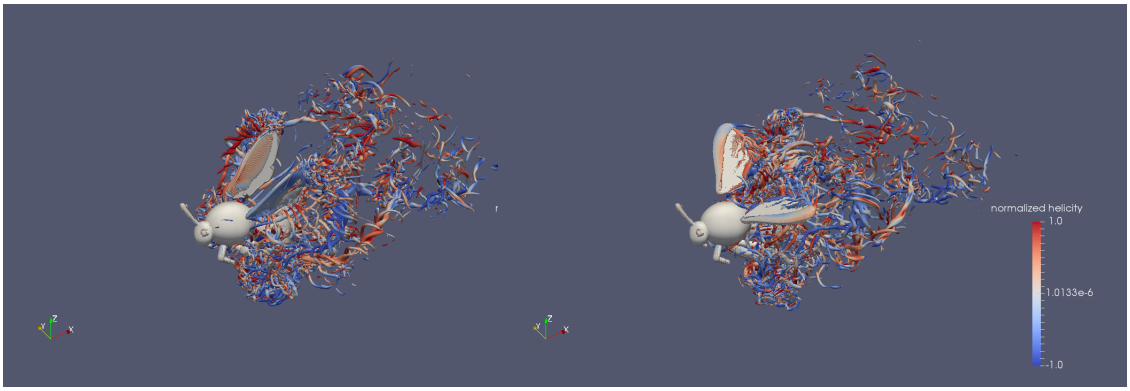

Fig. 1: Bumblebee in laminar inflow: Isosurfaces of Q-criterion colored with relative helicity h.

helicity over the half-space of the computational domain with respect to the vertical centerplane of the insect, one obtains the mean helicity generated by the left and the right wing. The time evolution of both contributions is shown in fig. 2 for laminar and turbulent inflow. We observe that the left and right wing contributions behave similarly with opposite sign and that in the turbulent case the amplitudes are much larger. Decomposing the velocity and vorticity fields into orthogonal

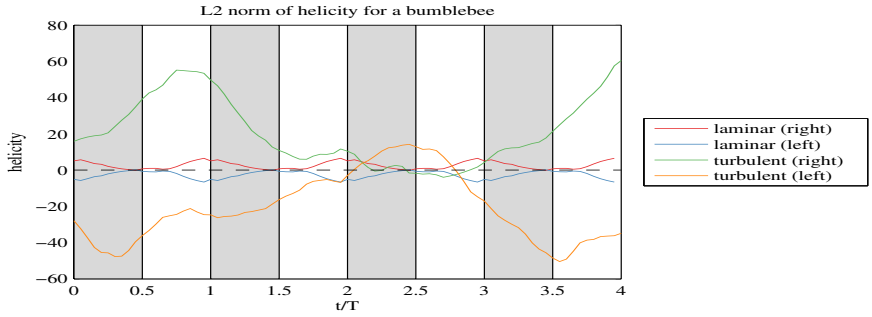

Fig. 2: Time evolution of the helicity H integrated over the left and right domain with respect to the vertical center plane of the bumblebee for laminar inflow and turbulent inflow.

wavelets the scale-dependent helicity can be introduced. For a review we refer to [3]. We note that it preserves Galilean invariance, though the kinetic helicity itself does not. In the talk we shall present analyses of the generated vortices using scale-dependent helicity to examine at which scales the alignment is most pronounced. The challenging question, how the turbulent inflow modifies the scale distribution, will thus be clarified.

References

[1] T. Engels, D. Kolomenskiy, K. Schneider, F.O. Lehmann and J. Sesterhenn. Bumblebee flight in heavy turbulence. *Phys. Rev. Lett.*, 12/2015, accepted.

[2] T. Engels, D. Kolomenskiy, K. Schneider and J. Sesterhenn. FluSI: A novel parallel simulation tool for flapping insect flight using a Fourier method with volume penalization. arXiv:1506.06513, 2015.

[3] M. Farge and K. Schneider. Wavelet transforms and their applications to MHD and plasma turbulence: a review. *J. Plasma Phys.*, **81**(6), 435810602, 2015, arXiv:1508:05650.

[4] D. Kolomenskiy, H.K. Moffatt, M. Farge and K. Schneider. Two- and three-dimensional numerical simulations of the clap-fling-sweep of hovering insects. *J. Fluids Struct.*, *27*, 784-791, 2011.

[5] D. Kolomenskiy, Y. Elimelech and K. Schneider. Leading-edge vortex shedding from rotating wings. *Fluid Dyn. Res.*, **46**, 031421, 2014.

Notes

Asymptotic Solutions for Linear and Nonlinear MHD Systems with a Rapid Jump near a Surface. Dynamics of the Surface of the Jump and Evolution of the Magnetic Field

A. Shafarevich[1], A. Allilueva[2]

[1] *Department of Mathematics and Mechanics, Moscow State University, Moscow, Russia*
[2] *Institute for Problems in Mechanics, Russian Academy of Sciences, Moscow, Russia*

Summary

We describe the asymptotic structure of the solution both for linear and nonlinear MHD system with a rapid jump near a 2D-surface. For the linear system we demonstrate the effect of the instantaneous growth of the solution. We also study the weak limit of the solution and the corresponding generalized problem. For the nonlinear system we describe the asymptotic division into different modes, the free boundary problem for the movement of the surface and the equation on the moving surface for the profile of the asymptotic solution. We also study the possibility of the instantaneous growth of the magnetic field. It appears that the growth is possible only in the case of the so-called degenerate Alfvén modes.

Equations of magnetohydrodynamics (MHD equations) describe the motion of the magnetic field in a conducting fluid. This nonlinear system of PDEs consists of the Navier Stokes equations for the velocity field of the fluid and the Maxwell equations for the magnetic field. Usually the viscosity and the resistance of the fluid are small enough and one can study the asymptotic solutions of the system with respect to the corresponding small parameter. This problem was studied in a lot of papers; note that in the linear approximation to the MHD equations the structure of the asymptotics is the subject of the famous dynamo theory (see, e.g., [1], [2], [3], [4], [5], [6], [7], [8], [9]). The main mathematical problem of the theory is whether there exists a velocity field such that the solution (i.e., the magnetic field) grows exponentially as time tends to infinity. Such a growth is one of the popular scenarios of the origin of earths, galaxies and stars magnetic fields from small initial perturbations. The origin of the growth is connected with the chaotic behavior of the trajectories of the velocity field of the fluid. Let us mention several well-known results of the theory.

- In the two-dimensional case, the so-called antidynamo theorem [2], [**?**], [9] states that there is no exponential growth of magnetic field as time tends to infinity.
- In [3], the growth was proved in the artificial example - the induction equation defined on a 3D Riemannian manifold with exponentially unstable geodesics.
- In [8], [5] the resolving operator for the Cauchy problem was studied as well as the behavior of localized solutions on the finite time interval. The explicit formulas show the temporal growth in the ABC flow.
- An alternative effect was studied in [10], [11] (in the linear approximation to the MHD equations also). Namely, we described the instantaneous growth of the magnetic field, induced by the jump of the velocity field of the fluid. In other words, we studied the asymptotics of the solution for the Cauchy problem for the linear induction equation with a rapidly varying velocity field. We assumed that this field has a rapid jump in a small vicinity of the fixed 2D surface. We proved that the solution grows rapidly with respect to the corresponding small parameter, and has a delta-type singularity near the surface of the jump.
- In the recent paper [12] we studied the formal asymptotics for the nonlinear MHD system describing the fields with the rapid jump near a surface. We obtained the free boundary

problem governing the movement of the surface as well as the equations on the moving surface governing the evolution of the magnetic and velocity fields. We proved that the instantaneous growth takes place for the so-called degenerate Alfvén modes only.

Here we present our results concerning the asymptotic solutions for both linear and nonlinear MHD equations. We describe the asymptotic structure of the solution with a rapid jump near the 2D-surface. For the linear system we demonstrate the effect of the instantaneous growth of the solution. We also study the weak limit of the solution and the corresponding generalized problem. For the nonlinear system we describe the asymptotic division into different modes, the free boundary problem for the movement of the surface and the equation on the moving surface for the profile of the asymptotic solution. We also study the possibility of the instantaneous growth of the magnetic field. It appears that the growth is possible only in the case of the so-called degenerate Alfv?en modes; the latter appear if the main term of the magnetic field is tangent to the surface of the jump.

References

[1] V.I. Arnold, B.A. Khesin, Topological methods in hydrodynamics// Springer, 1998.

[2] V.I. Arnold, Several remarks about antidynamo theorem// Messenger MSU. ser. 1- 1982-5-50-57.

[3] V.I. Arnold, Yu. B. Zeldovich, A.A. Ruzmaikin, D.D. Sokolov, Magnetic field in steady flow with sprains in Riemann space// Journal of experimental and theoretical physics- 1981- 81, 26 - 2052-2058.

[4] Childrss S. Fast dynamo theory. Topological aspects of the dynamics of fluids and plasmas (Eds: H. K. Moffatt, G. M. Zaslavsky, M. Tabor and P. Comte).- Dordrecht: luwer Academic Publishers, 1992.- 111-147.

[5] S. Yu. Dobrokhotov, A. A. Ruzmaikin, V.M. Olive, A.I. Shafarevich. Magnetic field asymptotics in a well conducting fluid// Geophys. Astrophys. Fluid Dynamics, 1996, 82 (3-4), 255-280.

[6] H.K. Moffatt Magnetic fie1d generation in e1ectrically conducting fluid.- Cambridge: Cambridge University Press, 1978.

[7] Roberts G.O. and Soward A.M. Dynamo theory // Annua1 Review in Fluid Mechanics - 1992 - 24 - 459-512.

[8] M.M. Vishik, Magnetic field generation by the motion of a highly conducting fluid.// Geophys. Astrophys. Fluid Dynamics, 1989, 48, 151-167.

[9] Yu. B. Zeldovich, A.A. Ruzmaikin and D. Sokolov,// Magnetic fields in astrophysics. - Gordon Breach, 1983.

[10] A. I. Esina and A. I. Shafarevich, Delta-type Solutions for the system of induction equations with discontinuous velocity field.// Methods of Functional Analysis and Topology, 2014, v.20, N 1, 17 — 33.

[11] A. I. Allilueva and A. I. Shafarevich, Delta-type solutions for the non-Hermitian system of induction equations. International Journal of Theoretical Physics, v.15, issue 11, 2015, 3932 – 3944.

[12] A. I. Allilueva and A. I. Shafarevich, Asymptotic solutions of the MHD system, describing smoothened discontinuities.// To appear in Mathematical Notes, 2016.

Notes

Homotopy string links and the $[\kappa]$-invariant

F. Cohen[1], R. Komendarczyk[2], R. Koytcheff[3], C. Shonkwiler[4]

[1] *Department of Mathematics, University of Rochester, USA*
[2] *Department of Mathematics, Tulane University, USA*
[3] *Department of Mathematics, University of Massachussetts Amherst, USA*
[4] *Department of Mathematics, Colorado State University, USA*

Summary

Since helicity is an average asymptotic linking number, the search for higher helicities has long centered on trying to extend the scope of higher-order link invariants from links to vector fields. While perhaps not well-known to physicists, in the 1990s Koschorke conjectured a homotopy-theoretic interpretation of link homotopy which, if proved, would yield an abundance of numerical link invariants computed by iterated integrals. In this work we make progress towards proving Koshorke's conjecture by showing that the analogous statement for string links is true.

As Moffatt [16] first observed, the helicity of a vector field measures the extent to which its orbits wrap and coil around one another. Indeed, Arnold [1] proved that helicity is the average asymptotic linking number of the orbits of the field and, although this is not the path Woltjer [18] originally took, one could have arrived at the definition of the helicity integral by suitably generalizing the Gauss linking integral.

The linking number is the simplest possible linking invariant and, since helicity is an average asymptotic linking number, mathematicians have conjectured for many years that there should be "higher helicities" of vector fields which are average asymptotic versions of more sophisticated linking invariants. While this idea has had some success [2, 6], no completely general higher helicity has ever been defined. Part of the problem is that interpretations of higher linking invariants which yield Gauss-type integral formulas have been rather hard to come by.

Recently, we gave an interpretation [5, 4] of the triple linking number, which distinguishes the Borromean rings from the three-component unlink [14], as a Hopf invariant and gave an explicit Gauss-type integral formula for it, setting the stage for a (unfortunately, only partial) definition of a third-order helicity [9, 10]. The key idea was to interpret a parametrized three-component link in $\mathbb{R}^3$ as a map from the three-dimensional torus T^3 to the configuration space $\mathrm{Conf}(\mathbb{R}^3, 3)$ of 3 distinct points in $\mathbb{R}^3$, and to prove that the homotopy periods of this map record the link homotopy invariants (pairwise and triple linking numbers) of the link.

This phenomenon is a special case of a more general conjecture of Koschorke [11, 12] relating link homotopy invariants of parametrized links to homotopy invariants of associated maps. More precisely, Koschorke observed that each parametrized link induces a map $\kappa : T^n \to \mathrm{Conf}(\mathbb{R}^3, n)$, where T^n is the n-dimensional torus and $\mathrm{Conf}(\mathbb{R}^3, n)$ is the configuration space of n distinct points on $\mathbb{R}^3$, and that link homotopies[1] of the link induce homotopies of the map. Therefore, the homotopy class $[\kappa]$ of the map is a link homotopy invariant of the link, and Koschorke conjectured that it is actually a *complete* link homotopy invariant, meaning that links with different $[\kappa]$-invariants cannot be link homotopic. Koschorke's conjecture is true when restricted to Brunnian links [12, 3]

One of Koschorke's primary motivations was to define an invariant which extended Milnor's $\overline{\mu}$-invariants [14, 15] to higher-dimensional links, and indeed he and others (e.g., [13, 17]) have given very precise descriptions of the higher-dimensional situation.

Despite its rather abstract appearance, the $[\kappa]$-invariant gives a natural way of defining numerical link-homotopy invariants: the $[\kappa]$-invariant of a link is a homotopy class of maps, so the homotopy periods of the map [8] are link-homotopy invariants of the link. Since link-homotopy invariants are

[1] A link homotopy is a deformation during which each component of the link may cross itself but distinct components must remain disjoint.

otherwise relatively hard to come by and since homotopy periods can naturally be computed as integrals, this is an important potential source for numerical link-homotopy invariants which may be extended to higher helicities.

In this work we define an analog $\check{\kappa}$ of κ for homotopy string links (see Fig. 1) and show that $[\check{\kappa}]$ is a complete invariant of homotopy string links. This provides the platform for a potential proof of Koschorke's conjecture: the next step is to show that that the "closure" map $[\check{\kappa}] \mapsto [\kappa]$ is compatible with Habegger and Lin's [7] classification of link homotopy classes of links based on a Markov-type theorem for closures of homotopy string links.

The key practical advantage of working with string links is that they form a group, and the essential technical step is to show that the map $\check{\kappa}$ is a homomorphism.

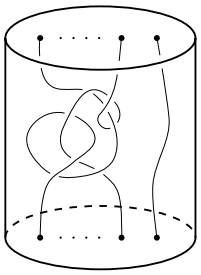

Fig. 1: An n-component string link.

References

[1] V. Arnold. The asymptotic Hopf invariant and its applications. *Selecta Math. Soviet.*, 5(4):327–345, 1986.

[2] M. Berger. Third-order link integrals. *J. Phys. A*, 23:2787–2793, 1990.

[3] F. R. Cohen, R. Komendarczyk, and C. Shonkwiler. Homotopy Brunnian links and the κ-invariant. *Proc. Amer. Math. Soc.*, 143(3):1347–1362, 2015.

[4] D. DeTurck, H. Gluck, R. Komendarczyk, P. Melvin, H. Nuchi, C. Shonkwiler, and D. S. Vela-Vick. Generalized Gauss maps and integrals for three-component links: toward higher helicities for magnetic fields and fluid flows, part II. *Algebr. Geom. Topol.*, 13(5):2897–2923, 2013.

[5] D. DeTurck, H. Gluck, R. Komendarczyk, P. Melvin, C. Shonkwiler, and D. S. Vela-Vick. Generalized Gauss maps and integrals for three-component links: toward higher helicities for magnetic fields and fluid flows. *J. Math. Phys.*, 54(1):013515, 48, 2013.

[6] M. Freedman and Z. He. Divergence-free fields: energy and asymptotic crossing number. *Ann. of Math. (2)*, 134(1):189–229, 1991

[7] N. Habegger and X.-S. Lin. The classification of links up to link-homotopy. *J. Amer. Math. Soc.*, 3(2):389–419, 1990.

[8] R. Hain. Iterated integrals and homotopy periods. *Mem. Amer. Math. Soc.*, 47(291), 1984.

[9] R. Komendarczyk. The third order helicity of magnetic fields via link maps. *Comm. Math. Phys.*, 292:431–456, 2009.

[10] R. Komendarczyk. The third order helicity of magnetic fields via link maps. II. *J. Math. Phys.*, 51:122702, 2010.

[11] U. Koschorke. Link homotopy. *Proc. Nat. Acad. Sci. U.S.A.*, 88(1):268–270, 1991.

[12] U. Koschorke. A generalization of Milnor's μ-invariants to higher-dimensional link maps. *Topology*, 36(2):301–324, 1997.

[13] U. Koschorke. Link homotopy in $S^n \times \mathbb{R}^{m-n}$ and higher order μ-invariants. *J. Knot Theory Ramifications*, 13(7):917–938, 2004.

[14] J. Milnor. Link groups. *Ann. of Math. (2)*, 59:177–195, 1954.

[15] J. Milnor. Isotopy of links. In R. Fox, editor, *Algebraic Geometry and Topology*, pages 280–306. Princeton University Press, 1957.

[16] H. K. Moffatt. The degree of knottedness of tangled vortex lines *J. Fluid Mech.*, 35:117–129, 1969.

[17] B. A. Munson. Derivatives of the identity and generalizations of Milnor's invariants. *J. Topol.*, 4(2):383–405, 2011.

[18] L. Woltjer. A theorem on force-free magnetic fields. *Proc. Nat. Acad. Sci. U.S.A.*, 44:489–491, 1958.

Notes

Self-generating magnetic knots in Plasma

C. B. Smiet[1], S. Candelaresi[2], A. Thompson [3], J. Swearngin[3], J. W. Dalhuisen[1],d and D. Bouwmeester[1,3]

[1] *Huygens-Kamerlingh Onnes Laboratory, Leiden Unversity, Netherlands*
[2] *Division of Mathematics, University of Dundee, United Kingdom*
[3] *Department of Physics, University of California Santa Barbara, United States*

Summary

Plasma configurations with magnetic helicity self-organize into knotted magnetic sturctures characterized by magnetic field lines lying on nested toroidal surfaces. The regularity of this structure allows us to construct an analytical approximation of the field using the Hopf map. Detailed Inspection of the high-β self-organized structure occuring in our full-MHD simulations reveals dynamics similar to magnetic confinement devices: magnetic islands on rational surfaces, a balance of pressure and Lorentz forces, and a toroidal depression in the pressure, with a minimum on the magnetic axis of the configuration.

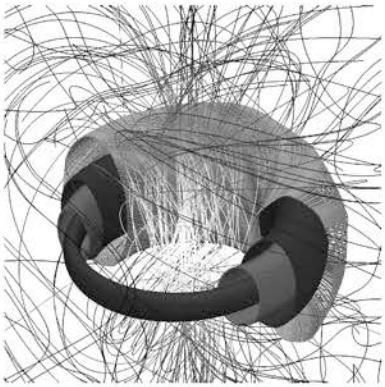

Fig. 1: Magnetic surfaces in a self-organized magnetic structure.

Magnetic helicity, defined as

$$H_{\mathrm{m}} = \int \mathbf{A} \cdot \mathbf{B} \mathrm{d}^3 x \tag{1}$$

is an invariant in an ideal plasma that quantifies the amount of linking of magnetic field lines [2]. In a resistive plasma helicity is only approximately conserved, i.e. the decay of helicity is generally on a much slower timescale than reconfiguration through fluid motion. This allows the fluid to reconfigure a helical magnetic field to a geometry that minimizes magnetic energy, whilst reconnection slowly changes the topology.

We perform full-MHD simulations starting with initial conditions that are unequivocally helical: rings of magnetic flux that are all linked with each other and/or twisted. These fields all pass through a turbulent phase, and reconfigure into organized structures that consist of field lines lying on nested toroidal surfaces. These structures have low dissipation and are quasi-stable. The magnetic forces are balanced by the pressure gradient caused by a toroidal depression in pressure. The nested magnetic organization bears resemblance to the mathematical structure of the Hopf map, a celebrated result in the field of topology. The Hopf map $h : S^3 \to S^2$ is a funtion between spheres such that the fibers of the map (preimages of points on S^2) are all circles lying on nested toroidal surfaces. We show that generalizations of this map [3, 4] can be used to generate an analytical expression that approximates this field.

The different magnetic surfaces in this structure are characterized by a nearly constant rotational transform. The rotational transform of a magnetic surface is a measure introduced in the context of

magnetic confinement fusion and is the (asymptotic) ratio of poloidal to toroidal winding number of a field line on that magnetic surfaces. In the self-organzied magnetic structure the rotational transform varies less than 15% from surface to surface in a continuous way. At the surfaces where the value of this rotational transform crosses rational values, only a single (m, n) torus knotted field line remains (with n/m the rational value of the rotational transform on that surface), and nearby field lines form magnetic surfaces around that knotted curve.

Acknowledgements. We wish to thank the FOM DIFFer institute for kind collaboration, in particular Marco de Baar, Hugo de Blank, Hans Goedbloed, Hennie van der Meiden and Egbert Westerhof. This work is funded by NWO VICI 680-47-604 and NSF Award PHY-1206118. CBS is supported by the NWO Graduate Programme. SC acknowledges financial support from the UK STFC (grant number STK/K000993/1). We acknowledge support from the Casimir Research program Leiden-Delft and from NWO through a Spinoza award.

References

[1] Smiet, C. B., et al. (2015) Self-organizing knotted magnetic structures in plasma. *Phys. Rev. Lett.* 2015 **115.9**, 095001.

[2] Moffatt, H.K. (1969) The degree of knottedness of tangled vortex lines. *J. Fluid Mech.* 1969 **35**, 117–129.

[3] Arrayás, Manuel, and José L. Trueba. (2011) Electromagnetic torus knots. *arXiv preprint* 2011 arXiv:1106.1122.

[4] Sagdeev, Z. (1986) Theory of Strong Turbulence and Topological Solitons. In *Nonlinear phenomena in plasma physics and hydrodynamics Vol. 1* Mir Publishers, Moscow, **1986**.

Notes

Magnetic helicity and higher helicity invariants as constrains for dynamo action

D. Sokoloff[1], E. Illarionov[2]

[1] *Department of Physics, Moscow State University, Russia*
[2] *Department of Mechanics and Mathematics, Moscow State University, Russia*

Summary

We discuss important role of magnetic helicity conservation as nonlinear constrain of dynamo in celestial bodies and possible role of higher helicity invariants as nonlinear constrains for dynamo.

1 Magnetic helicity transport, dynamo suppression and observations

Magnetic helicity becomes famous in the MHD community after the fundamental paper [1]. Now magnetic helicity conservation is considered as a more important nonlinear limiter for dynamo action in comparison with the energy conservation (see for review [2]). This concept was developed in the course of discussion of catastrophic α-quenching that indeed constrains large-scale magnetic field growth in some dynamo models, e.g. authors of [3] stress that magnetic helicity being a pseudoscalar quantity is a more natural limiter for pseudoscalar α-effect rather than magnetic energy which is a scalar quantity. Large-scale dynamo action in a body amplifies knotted large-scale magnetic field. Because of the helicity conservation this knottedness has to be compensated by knottedness of small-scale field which suppresses α.

It looks plausible that the large-scale magnetic field in celestial bodies even being constrained by magnetic helicity conservation can reach energy equipartition with kinetic energy of turbulence due to the spatial transport of magnetic helicity density (e.g. [3] for galactic and [4] for solar dynamos).

Contemporary observational facilities provide some methods for observational identification of magnetic helicity at least in solar active regions. The idea suggested by N. Seehafer [5] presumes local homogeneity and isotropy of small-scale solar magnetic fields in order to extract current and magnetic helicity from surface vector magnetograms of solar active regions. Long-term solar activity monitoring undertaken at Huairou Solar Station nearby Beiging allows to obtain time-latitude distribution (butterfly diagram) of current helicity and conclude about distribution of magnetic helicity which occurs to be more or less compatible with expectations of solar dynamo theory [6]. A substantial anisotropy of small-scale magnetic fields in solar active regions revealed by detailed analysis of Huairou data constrains however observational efforts in this direction.

2 Higher helicity invariants: many other constrains for dynamo?

An important message from topology is that apart from the simplest Gauss invariant for a system of closed lines there are higher topological invariants which give a more detailed description of magnetic field line knottedness. Corresponding generalizations of higher invariants for magnetic field and knottedness of magnetic tubes provide a sequence of conservation laws some of which deal with pseudoscalar quantities and in principle could contribute to the α-effect suppression as well as magnetic helicity. Such a perspective to get various constraints for dynamo action looks not very exciting for application of dynamo theory to particular celestial bodies.

We argue however that in practice situation with higher helicity invariants is less dramatic and possible constraints for dynamo action are not so severe than that one from the Gauss invariant. The point is that as far as it is known there are no densities associated with higher topological

invariants. Correspondingly, we can not follow conservation of such invariant with a help of its density balance and have to consider its conservation in the whole system. It looks plausible that because of the symmetry arguments the mean value of the mirror-asymmetric higher invariants in the whole body vanishes and nothing have to be compensated by small-scale field knottedness.

One more point is that the open magnetic flux which is clearly revealed in solar observations makes conservation of higher invariants even more delicate. One have to distinguish magnetic field knottedness of the whole space including very remote regions and that one of the solar magnetic field in the strict sense. The first one can vanish while the second one can remain non-vanishing in the course of solar cycle. Something like that happens presumably with the invariant $\int \mathbf{H}\, d^3x$ taken over the whole space. This invariant can be considered as a topological one as well as helicity invariants and is proportional to the magnetic dipole moment of the whole system [7]. On the other hand, dipole magnetic moment of the Sun does not vanish in strict sense and changes its sign each 11-year cycle (see for details [8]). Note that the integral presented dipole magnetic moment converges very slow (in sense of principal value only) and magnetic field of solar wind which decays even slowly as dipole field makes the problem even more complicated.

Acknowledgements. The research presented is supported by RFBR project 15-02-01407. Fruitful discussions with M. Georgoulis are acknowledged.

References

[1] Moffatt, H.K. (1969) The degree of knottedness of tangled vortex lines. *J. Fluid Mech.* 1969 **35**, 117–129.

[2] Brandenburg, A. & Subramanian, K. (2005) Astrophysical magnetic fields and nonlinear dynamo theory. *Phys. Rep.*2005 **417**, 1–209. Springer-Verlag, Berlin.

[3] Kleeorin, N., Moss, D., Rogachevskii, I. & Sokoloff, D. (2009) Helicity balance and steady-state strength of the dynamo generated galactic magnetic field. *Astron. & Astrophys.* 2000, **361**, L5-L8.

[4] Pipin, V.V., Sokoloff, D.D., Zhang, H. & Kuzanyan, K. M. (2013) Helicity conservation in nonlinear mean-field solar dynamo. *Astrophys. J.* 2013, **768**, id 46.

[5] Seehafer, N. (1990) Electric current helicity in the solar atmosphere. *Solar Phys.* 1990, **125**, 219–232.

[6] Zhang, H., Sakurai, T., Pevtsov, A., Gao, Y., Xu, H., Sokoloff, D.D. & Kuzanyan, K. (2010) A new dynamo pattern revealed by solar helical magnetic fields. *Month. Not. Roy. Astron. Soc.* 2010, **402**, L30-L33.

[7] Arnold, V.I., Zeldovich, Ya.B., Ruzmaikin, A.A. & Sokoloff, D.D. (1982) Steady-state magnetic field in a periodic flow. *Sov. Phys. Dokl.* 1982, **27**, 814-816.

[8] Moss, D., Kitchatinov, L.L. & Sokoloff, D. (2013) Reversals of the solar dipole. *Astron. & Astrophys.*2013, **550**, id. L9.

Notes

Spin-down in a rapidly rotating cylinder container with mixed rigid and stress free boundary conditions

A. Soward[1], L. Oruba[2], E. Dormy[2]

[1] *School of Mathematics and Statistics, Newcastle University, Newcastle upon Tyne, NE1 7RU. UK*
[2] *MAG (ENS/IPGP), LRA, Département de Physique, Ecole Normale Supérieure, 24, rue Lhomond, F-75231 Paris Cedex 05, France*

Summary

Greenspan and Howard (J. Fluid Mech., 1963) studied the linear spin-down of a rapidly rotating viscous fluid at small Ekman number E inside a container with rigid boundaries, following an instantaneous small change in container angular velocity. Outside the Ekman layers, thickness $O(E^{1/2})$, the mainstream is in almost rigid rotation (geostrophic) but spins down rapidly due to Ekman suction. Additionally, there are thickening quasi-geostrophic and very weak ageostrophic $E^{1/3}$ shear layers adjacent to the cylindrical side-wall. Motivated by applications to isolated atmospheric structures (e.g., tropical cyclones, tornadoes) without side and top boundaries, we study numerically and asymptotically a variant with stress-free side-wall and top boundaries, which leads to unexpected consequences. The mainstream no longer rotates rigidly, while the ageostrophic $E^{1/3}$ shear layer, far from being passive, determines a spin-down rate dependent on $\ln E$. It is linked to an $E^{1/2} \times E^{1/2}$ corner region, where the rigid base and the stress-free side-wall meet; a singularity that limits asymptotic progress.

Notes

Helical bottleneck effect in 3D homogeneous isotropic turbulence

R. Stepanov[1,3], E. Golbraikh[2], P. Frick[1], S. Shestakov[1]

[1] *Institute of Continuous Media Mechanics, Perm, Russia*
[2] *Physics Department, Physics Department, Beer-Sheva, Israel*
[3] *Department of Applied Mathematics and Mechanics,Perm National Research Polytechnic University, Russia*

Summary

It is generally believed that helicity can play a significant role in turbulent systems, e.g., supporting the generation of large-scale magnetic fields, but its impact on the spectral properties of turbulent flows is practically negligible. We elaborate the phenomenology of isotropic turbulence for a flow with a high relative helicity over a wide range of scales. Various scenarios of turbulent cascades are discussed. We obtain helicity effect which can be interpreted as a quenching of the spectral energy transfer. The effect is demonstrate by high Reynolds number numerical simulations based on a shell model of helical turbulence. The energy in our model is injected at a certain large scale only, whereas the source of helicity is distributed over all scales. In particular, we found that, depending on the parameters of the injection helicity, a "helical bottleneck effect" can appear in the energy spectrum of isotropic turbulence.

1 Motivation

Many years ago, K. Moffatt delivered a verdict on the influence of helicity on spectral properties of turbulent flows [4]:

> *no matter how strong the level of helicity injection may be at wave-numbers of order k_0, the relative level of helicity as measured by the dimensionless ratio $H(k)/2kE(k)$ must grow progressively weaker with increasing k; and when k/k_0 is sufficiently large it may be conjectured (Brissaud et al., 1973) that the helicity has negligible dynamical effect, and is itself convected and diffused in much the same way as a dynamically passive scalar contaminant (Batchelor, 1959).*

Thus the mean helicity can play a significant role in turbulent systems, e.g., supporting the generation of large-scale magnetic fields [2], but its impact on the spectral properties of turbulent flows is practically negligible.

We revise the view that helicity is injected into the flow together with energy at the same scale. Theoretically, one can assume that turbulence is excited by a source of energy at the largest scale and an independent source of pure helicity, acting at a certain scale or over all scales in the inertial interval. Then, the helicity spectral flux is not constant anymore and the helicity spectral density can reach significantly higher values and influence the energy cascade. Real physical situations usually are far from ideal, but can be similar to some extent e.g. in rotating convective flows [3].

2 Phenomenology

First, we adopt the basic statement of Kolmogorov's approach, which claims that in the inertial range at any scale n the energy flux is equal to the dissipation rate, $\Pi_n^E = \varepsilon$. We consider a geometric sequence of scales and corresponding wave numbers $l_n^{-1} \sim k_n \sim \lambda^n$. The energy flux is related to the velocity pulsations v_n at this scale as

$$\Pi_n^E \approx v_n^3 k_n. \tag{1}$$

Second, we follow the decomposition of velocity pulsations in two helical modes [6], $v_n = v_n^+ + v_n^-$, with corresponding energies $E_n^\pm \sim (v_n^\pm)^2$. Then the energy and helicity at the scale n are

$$E_n = E_n^+ + E_n^-, \quad H_n = H_n^+ + H_n^- = k_n(E_n^+ - E_n^-). \tag{2}$$

The energy flux at scale n is decomposed into four terms: $k_n(v_n^+)^3$, $k_n(v_n^-)^3$, $k_n(v_n^+)^2 v_n^-$ and $k_n(v_n^-)^2 v_n^+$. For the direct cascades of the energy and helicity the contribution of terms $k_n(v_n^\pm)^2 v_n^\mp$ is dominant [6].

The relative helicity $H_n^r = H_n/(k_n E_n)$ allows us to link the intensity of two helical modes $v_n^- = v_n^+ \sqrt{(1-H_n^r)/(1+H_n^r)} = \xi_n v_n^+$. Then the energy flux provided by local interactions can be estimated as

$$\Pi_n^E \approx k_n(v_n^+)^3 + k_n(v_n^-)^3 = k_n(v_n^+)^3(\xi_n + \xi_n^2). \tag{3}$$

Replacing (1) by (3) we finally obtain $E_n^+ \sim \left(\varepsilon/(k_n(\xi_n + \xi_n^2))\right)^{2/3}$. One can express $E_n^- = \xi_n^2 E_n^+$ from (2) and obtain the total energy

$$E_n = E_n^+ + E_n^- \sim (\varepsilon\zeta_n/k_n)^{2/3}, \tag{4}$$

where the dimensionless variable ζ_n

$$\zeta_n = (1+\xi_n^2)^{3/2}/(\xi_n + \xi_n^2) \tag{5}$$

depends on $H_r(k)$ and defines "the degree of helical blocking" of the spectral energy flux at a given scale. $|H_r(k)|$ characterizes the dominance of some helical modes over others with the opposite sign, i.e. it is the helical part of the energy. Then a new parameter $\delta(k) = 1 - |H_r(k)|$ corresponds to the non-helical part of the energy, which is free of helicity. For the highly helical case $H_n^r \to \pm 1$, formula (5) has as asymptote $\zeta_n \approx \delta_n^{-1/2}$. The corresponding spectral energy density

$$E(k) \approx \varepsilon^{2/3} k^{-5/3} \delta(k)^{-1/3} \tag{6}$$

is independent of the sign of the injected helicity. Usually for the single-scale forcing of helicity, $H_n^r \propto k^{-1}$ and the parameter δ_n does not differ from unity. One can expect a significant change in the turbulent spectra for highly helical turbulence only. We verify the realizability of the energy spectrum (4) with helical correction (5) by numerical simulation using the helical shell model of turbulence [5].

We interpret our results as a quenching effect on the spectral energy transfer in scales with high relative helicity. The energy should be accumulated and redistributed so that the efficiency of nonlinear interactions will be enough to provide the constant energy flux, which is predetermined by the energy injection rate. A similar consequence is observed as a result of the bottleneck phenomenon [1] in the non-helical turbulent cascade when non-local interactions drop out of the spectral energy transfer at the end of the inertial range. We exploit this analogy to name our effect the *helical* bottleneck effect, having in mind the helical mechanism of cascade blocking.

Acknowledgements. Financial support from RFBR grants (14-01-96010 and 14-01-96011) is kindly acknowledged.

References

[1] G. Falkovich, *Bottleneck phenomenon in developed turbulence*, Phys. Fluid, 6 (1994), pp. 1411–1414.

[2] F. Krause and K.-H. Radler, *Magnetohydrodynamics and Dynamo Theory*, Oxford, 1980.

[3] R. Marino, P. D. Mininni, D. Rosenberg, and A. Pouquet, *Emergence of helicity in rotating stratified turbulence*, Phys. Rev. E, 87 (2013), p. 033016.

[4] H. K. Moffatt, *Magnetic Field Generation in Electrically Conducting Fluids*, Cambridge, 1978.

[5] R. Stepanov, E. Golbraikh, P. Frick, and A. Shestakov, *Hindered Energy Cascade in Highly Helical Isotropic Turbulence*, Physical Review Letters, 115 (2015), p. 234501.

[6] F. Waleffe, *The nature of triad interactions in homogeneous turbulence*, 4 (1992), pp. 350–363.

Notes

Conservation of writhe helicity under anti-parallel reconnection

De Witt Sumners

Department of Mathematics, Florida State University, USA

Summary

The helicity of a flux tube can be calculated in terms of writhe and twist contributions. We prove that the writhe is conserved under anti-parallel reconnection. This is joint work with Christian Laing and Renzo Ricca [1].

Reconnection is a fundamental event in many areas of science, from the interaction of vortices in classical and quantum fluids, and magnetic flux tubes in magnetohydrodynamics and plasma physics, to recombination in polymer physics and DNA biology. By using fundamental results in topological fluid mechanics, the helicity of a flux tube can be calculated in terms of writhe and twist contributions. We prove that the writhe is conserved under anti-parallel reconnection. Hence, for a pair of interacting flux tubes of equal flux, if the twist of the reconnected tube is the sum of the original twists of the interacting tubes, then helicity is conserved during reconnection. Thus, any deviation from helicity conservation is entirely due to the intrinsic twist inserted or deleted locally at the reconnection site. This result has important implications for helicity and energy considerations in various physical contexts.

We will discuss the mathematical similarities between reconnection events in biology and physics, and the relationship between iterated reconnection and curve topology. In particular, the minimal reconnection cascade from $(2, 2k+1)$ torus knots to $(2, 2k)$ torus links to the unlink of two unknotted circles observed in DNA site-specific recombination is also observed in fluid vortex reconnections.

Acknowledgements. Financial support from a Simons Foundation Collaboration Grant for Mathematicians is kindly acknowledged.

References

[1] Laing C.E., Ricca R.L. & Sumners D.W. (2015) Conservation of writhe helicity under anti-parallel reconnection. *Nature Scientific Reports* **5** 9224.

Notes

Chiral anomalies, helicity and information geometry

P. Surówka[1]

[1] *Center for the Fundamental Laws of Nature, Harvard University, Cambridge, MA 02138, USA*

Summary

Fluid helicity is an important observable that captures topological properties of hydrodynamics. It naturally emerges in the context of parity-breaking fluids with knotted vortex lines. If the fluid constituents exhibit quantum anomalies the topological nature of fluid helicity can be elucidated using microscopic physics. In this case the helicity is given by a polynomial function of temperature and chiral chemical potential and completely fixed by the anomalies. We explain this relation and address the question of instabilities of such fluids using methods of information geometry. We introduce the metric on a parameter space and show that a non-zero vorticity leads to a curvature on the statistical manifold. We calculate the curvature invariant and analyze its divergences, which contain the information about phase transitions of the system. The transition points are universal and expressed in terms of ratios of anomaly coefficients.

Hydrodynamics is an effective field theory which can be used to describe many different physical systems. One of the recent applications of the theory of relativistic hydrodynamics is the study of the evolution chiral fluids. The relativistic hydrodynamic equations have been proposed many years ago [1]; such equations describe the dynamics of an interacting relativistic theory at large distance and time scales. The hydrodynamic variables are the local velocity $u^\mu(x)$ (satisfying $u^2 = -1$), the local temperature $T(x)$ and chemical potential(s) $\mu^a(x)$, where the index a numerates the conserved charges. The hydrodynamic equations govern the time evolution of these variables; they have the form of the conservation laws $\partial_\mu T^{\mu\nu} = 0$, $\partial_\mu j^{a\mu} = 0$, supplemented by the constitutive equations which express $T^{\mu\nu}$ and $j^{a\mu}$ in terms of u^μ, T, and μ^a. These equations are the relativistic generalization of the Navier-Stokes equations.

One feature of relativistic quantum field theory that does not have direct counterpart in non-relativistic physics is the presence of triangle anomalies [2, 3]. For currents associated with global symmetries, the anomalies do not destroy current conservations, but are reflected in the three-point functions of the currents. When the theory is put in external background gauge fields coupled to the currents, some of the currents will no longer be conserved.

In the simplest case when there is one U(1) current with a $\mathrm{U}(1)^3$ anomaly. We consider only global currents that are not coupled to dynamical gauge fields, and assume the associated symmetries are not spontaneously broken. The constitutive equation for the conserved current j^μ must contain an additional term proportional to the vorticity.

$$j^\mu = nu^\mu - \sigma T(g^{\mu\nu} + u^\mu u^\nu)\partial_\nu\left(\frac{\mu}{T}\right) + \xi\omega^\mu, \tag{01}$$

$$\omega^\mu = \frac{1}{2}\epsilon^{\mu\nu\lambda\rho}u_\nu\partial_\lambda u_\rho, \tag{02}$$

where n is the charge density, σ is the conductivity, and ξ is the new kinetic coefficient.

Even in a parity-invariant theory, the vorticity-induced current $\xi\omega^\mu$ is allowed by symmetries if, e.g., j^μ is a chiral current. This term contains only one spatial derivative, and its effect is as important as those of viscosity or diffusion. Before very recently, this term has been completely overlooked. In fact, if one follows the standard textbook derivation, the new term seems to be disallowed by the existence of an entropy current with manifestly positive divergence, required by the second law of thermodynamics.

In this presentation we will show that this new term is not only allowed, but is required by anomalies. Moreover, the parity-odd kinetic coefficient ξ is completely determined by the anomaly coefficient C, defined through the divergence of the gauge-invariant current, $\partial_\mu j^\mu = -\frac{1}{8}C\epsilon^{\mu\nu\alpha\beta}F_{\mu\nu}F_{\alpha\beta}$,

and the equation of state,

$$\xi = C\left(\mu^2 - \frac{2}{3}\frac{\mu^3 n}{\epsilon + P}\right), \tag{03}$$

where ϵ and P are the energy density and pressure. The key ingredient required to derive such transport is the second law of thermodynamics. The entropy current has to be modified to cancel the unwanted terms containing the Levi-Civita symbol which can in principle violate the second law. Therefore the effect is non-dissipative - it does not contribute to the entropy production. As a result it is convenient to formulate it in terms of partition functions [5, 6]. Such a formulation sheds new light on the quantum origin of the transport and allows for generalizations e.g. include gravitational anomalies [7]. The topological nature of anomalies manifests itself through the anomaly polynomials $\mathcal{P}_{anom}(F, R)$. They are functions of gauge field strength and curvature, which represent a compact way to describe anomalies. It was argued in [5, 6] that the anomaly induced transport can be described by a closely related polynomial object $\mathfrak{F}^{\omega}_{anom}(\mu, T)$, provided we do the the following substitution

$$\mathfrak{F}^{\omega}_{anom} = \mathcal{P}_{anom}\left(F \mapsto \mu\ ,\ p_1(R) \mapsto -\beta^{-2},\ p_{k>1}(R) \mapsto 0\right), \tag{04}$$

where $p_1(R)$ is the first Pontryagin class of space-time curvature. Subsequently the polynomial object $\mathfrak{F}^{\omega}_{anom}$ was connected to the helicity of the thermal state [8].

Partition functions are primary objects in studying field theories and statistical systems. Unfortunately the number of models, for which partition functions are known exactly is very limited and in order to get a nonperturbative answer one usually invokes underlying integrability or supersymmetry of the model. However, most models do not have such a symmetry and the partition function is known only perturbatively in a limited range of the parameter space. Anomalous hydrodynamics is an exception in this respect. The powerful constraints coming from the connection of QFT symmetry breaking and the laws of thermodynamics make the transport nondissipative and fixed purely in terms of field theory data. As a result the partition function of the theory in the hydrodynamic regime can be constructed analytically. This gives as a closed form expression for the Gibbs probability distribution for the anomalous state. The statistical distributions can be viewed as geometrical manifolds, which has a non-zero curvature and possibly nontrivial phase structure if the system is interacting. This represents a new quantitative tool for the study of fluctuation phenomena, known as information geometry [9].

References

[1] C. Eckart, Phys. Rev. **58**, 919 (1940).

[2] S. L. Adler, Phys. Rev. **177**, 2426 (1969).

[3] J. S. Bell and R. Jackiw, Nuovo Cim. A **60**, 47 (1969).

[4] D. T. Son and P. Surowka, Phys. Rev. Lett. **103** (2009) 191601

[5] R. Loganayagam and P. Surowka, JHEP **1204** (2012) 097

[6] K. Jensen, R. Loganayagam and A. Yarom, JHEP **1302** (2013) 088 [arXiv:1207.5824 [hep-th]].

[7] K. Landsteiner, E. Megias and F. Pena-Benitez, Phys. Rev. Lett. **107** (2011) 021601

[8] R. Loganayagam, JHEP **1311** (2013) 205 [arXiv:1211.3850 [hep-th]].

[9] P. Surowka, arXiv:1507.00985 [hep-th].

Notes

Helicity and Dynamo Waves at High Magnetic Reynolds Number

S.M. Tobias[1], F. Cattaneo[2]

[1] *Department of Applied Mathematics, University of Leeds, U.K.*
[2] *Department of Astronomy and Astrophysics, University of Chicago, U.S.A*

Summary

We consider dynamo action in the astrophysically interesting limit of high Rm. We show that at large Rm the role of shear is to suppress the small-scale kinematic dynamo. When the small-scale flow is helical this suppression is enough for large-scale dynamo action to occur in the form of propagating dynamo waves as predicted by Parker [1] and discussed extensively by Moffatt [2].

1 Helicity, Dynamo Waves and The Suppression Principle

We consider the generation of magnetic activity — dynamo waves — in the astrophysical limit of very large magnetic Reynolds number. We consider kinematic dynamo action for a system consisting of helical flow and large-scale shear. We demonstrate that large-scale dynamo waves persist at high Rm if the helical flow is characterised by a narrow band of spatial scales and the shear is large enough. However for a wide band of scales the dynamo becomes small-scale with a further increase of Rm, with dynamo waves re-emerging only if the shear is then increased. We show that at high Rm the key effect of the shear is to suppress small-scale dynamo action, allowing large-scale dynamo action to be observed. We argue strongly that dynamo calculations at high Rm can only be assessed if the ratio $\chi = (Rm - Rm_c)/Rm_c$ is quoted, where Rm_c is the Rm for which dynamo action first sets in. We argue that this supports a general "suppression principle" — large-scale dynamo action can only be observed if there is a mechanism, such as shear or nonlinearity, that suppresses the small-scale fluctuations. We further argue that the key quantity that determines whether large-scale kinematic (and indeed dynamic) dynamo action is ever observed is not the mean electromotive force (though of course this must be non-zero — as it will be for helical flows) but the fluctuations about that mean. In the presence of a suppressing mechanism the standard deviation of the emf is reduced significantly, allowing large-scale dynamo action re-establish itself [3, 4, 5].

References

[1] Parker, E.N. (1955) *Hydromagnetic Dynamo Models.* Astrophysical Journal **122**, p. 293

[2] Moffatt, H.K. (1978) *Magnetic Field Generation in Electrically Conducting Fluids.* Cambridge University Press, Cambridge. *J. Fluid Mech.* 1969 **35**, 117–129.

[3] Tobias, S.M. & Cattaneo, F. (2013) *Shear Driven Dynamo Waves at High Magnetic Reynolds Number.* Nature **497**, p. 463

[4] Cattaneo, F. & Tobias, S.M. (2014) *On Large-Scale Dynamo Action at High Magnetic Reynolds Number.* Astrophysical Journal **789**, p. 70

[5] Tobias, S.M. & Cattaneo, F. (2015) *The electromotive force in multi-scale Flows at high magnetic Reynolds number.* Journal of Plasma Physics, **81**, 395810601

Notes

Periodic orbits of analytic Euler fields

F. Torres de Lizaur

ICMAT, Spain

Summary

On any compact analytic 3-manifold without boundary which is not a torus bundle over the circle, any analytic vector field with no zeros and which is solution to the stationary Euler equations has a periodic orbit. This result can be traced back to the works of A. Rechtman [2] and K. Cieliebak and E. Volkov [1]. In this talk we will present an alternative proof of this fact, using ideas from contact and differential topology.

The existence of closed orbits is one of the most natural qualitative questions on the behaviour of a dynamical system. We want to address it in the context of stationary Euler flows.

A stationary Euler flow on a three dimensional Riemannian manifold (M, g) is described by a velocity field $u(x)$ which satisfies the stationary Euler equations

$$i_\omega i_u \mu = dB\,, \qquad di_u \mu = 0$$

where μ is the volume form on (M, g), $B(x)$ is the so-called Bernoulli function and $\omega := curl\ u$ is the vorticity field.

In this talk we are to present a proof of the following:

Theorem Let (M, g, μ) be a three dimensional compact, analytic, Riemannian 3-manifold without boundary (where the volume form μ is not necessarily the one given by the metric g). Let u be a nowhere vanishing C^ω vector field verifying the stationary Euler equations

$$i_\omega i_u \mu = dB\,, \qquad di_u \mu = 0$$

Then, if M is not a torus bundle over $\mathbb{S}^1$, u has a closed orbit.

If, instead of being analytic, the field is just C^∞, the question remains completely open: the stratified structure of critical sets of analytic functions is key to the proof.

References

[1] K. Cieliebak and E. Volkov, A note on the stationary Euler equations of hydrodynamics. Ergodic Theory and Dynamical Systems (2015).

[2] A. Rechtman, Existence of periodic orbits for geodesible vector fields on closed 3-manifolds. Ergodic Theory and Dynamical Systems 30(6) (2010) 1817-1841.

Notes

Numerical simulation of quantum turbulence in superfluid helium -Inhomogeneous quantum turbulence-

M. Tsubota[1], S. Yui[1]

[1] *Department of Physics, Osaka City University, Japan*

Summary

We review the recent numerical studies of quantum turbulence in superfluid helium. The numerical simulation based on the vortex filament model was pioneered by Schwarz, and has revealed lots of physics in thermal counterflow of superfluid helium. Almost all previous numerical works supposed that the system was homogeneous. However, the recent visualization experiments found that the normal fluid flow was inhomogeneous strongly affected by the geometry. Motivated by the experiments, we performed the simulation in a square channel under the inhomogeneous normal fluid flow to study inhomogeneous vortex tangle. Then we found the logarithmic velocity profile of a superfluid flow.

1 Introduction

Quantum turbulence (QT) in thermal counterflow of superfluid ^{4}He has been studied more than half century. Any rotational motion of superfluid is sustained by quantized vortices, which have the quantum circulation $\kappa = h/m_4$, where h is Planck's constant and m_4 is a mass of a ^{4}He atom. Since the core of a quantized vortex is extremely thin, namely the order of atomic scale, a vortex filament model works well in this system. A random tangle of quantized vortices is a typical example of QT. A characteristic of QT is that vortices are definite and well-defined as elements of turbulence, which differs from eddies in classical traditional turbulence.

The numerical simulation of the vortex filament model in superfluid ^{4}He was developed by Schwarz [1], revealing that counterflow turbulence was a self-sustained vortex state caused by the competition between the excitation due to the external flow and the dissipation by the mutual friction. However, most numerical works used the Localized-Induction Approximation (LIA) neglecting the interaction between the vortices, and needed some artificial mixing procedure in order to sustain a homogeneous vortex tangle under the periodic boundary condition. Adachi *et al.* performed the simulation not using the LIA but by the full Biot-Savart integral, succeeding in obtaining statistically steady states without any artificial procedures [2].

These previous studies assumed that the system was uniform, because there were no information on how the system was affected by the geometry. By using a laser-induced fluorescence technique, Marakov *et al.* observed an inhomogeneous velocity profile of a normal fluid component in a square channel [3]. Motivated by the experiment, the scientists have started to get interested in inhomogeneous QT in a channel. Baggaley *et al.* numerically studied the inhomogeneous vortex tangle between two parallel plates under the prescribed Hagen-Poiseuille flow [4].

2 Inhomogeneous quantum turbulence in thermal counterflow

We study numerically inhomogeneous vortex tangle in a square channel [5] supposing that the normal fluid flow is prescribed to be Hagen-Poiseuille flow or tail-flattend flow [3]. The vortex tangle shows a characteristic space-time oscillation. Vortices are denser near the channel walls (shown in Figure 1), suggesting turbulent boundary layer of superfluid.

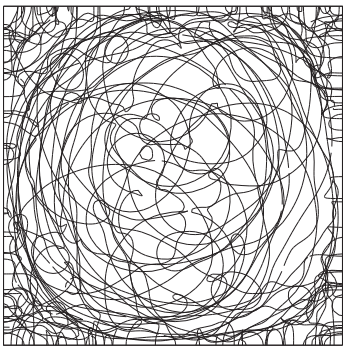

Fig. 1: Typical inhomogeneous vortex tangle viewed along the flow direction in a square channel.

3 Logarithmic velocity profile

Turbulent boundary layer reminds us of the log-law, namely the logarithmic velocity profile. We study the vortex dynamics under pure normal Poiseuille flow between two parallel plates [6]. When we calculate superfluid velocity field due to the inhomogeneous vortex tangle, it shows the logarithmic velocity profile as shown in Figure 2. This is the first numerical confirmation of the log-law in QT.

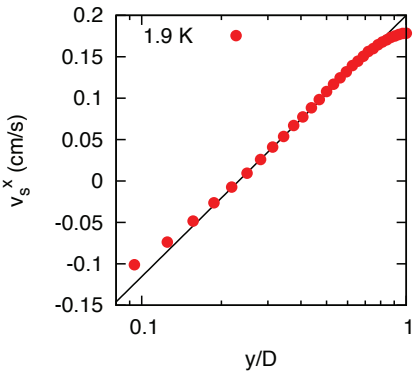

Fig. 2: Logarithmic velocity profile of quantum turbulence in thermal couterflow.

References

[1] Schwarz, K.W. (1988) Three-dimensional vortex dynamics in superfluid ^{4}He: Homogeneous superfluid turbulence. *Phys. Rev. B.* 1988 **38**, 2398–2417.

[2] Adachi, H., Fujiyama, S. and Tsubota, M. (2010) Steady-state counterflow quantum turbulence: Simulation of vortex filaments using the full Biot-Savart law. *Phys. Rev. B.* 2010 **81**, 104511.

[3] Marakov, A., Gao, J., Guo, W., Van Sciver, S. W., Ihas, G. G., McKinsey, D. N. and Vinen, W. F. (2015) Visualization of the normal-fluid turbulence in counterflowing superfluid ^{4}He. *Phys. Rev. B.* 2015 **91**, 094503.

[4] Baggaley, A. W. and Laurie, J. (2014) Thermal Counterflow in a Periodic Channel with Solid Boundaries. *J. Low Temp. Phys.* 2014 **178**, 35-52.

[5] Yui, S. and Tsubota, M. (2015) Counterflow quantum turbulence of He-II in a square channel: Numerical analysis with nonuniform flows of the normal fluid. *Phys. Rev. B.* 2015 **91**, 184504.

[6] Yui, S., Fujimoto, K. and Tsubota, M. (2015) Logarithmic velocity profile of quantum turbulence of superfluid ^{4}He. *Phys. Rev. B.* 2015 **92**, 224513.

Notes

Hybrid convection in astrophysical discs

Francesco Volponi[1]

[1] *University of Information Science and Technology, Ohrid, R. Macedonia*

Summary

We examine the local convective stability of hydrodynamic discs with radial and vertical stratification in the presence of thermal diffusion (or relaxation). We find that in the regime of comparable radial and vertical Richardson numbers (i.e. $|Ri_x| \sim |Ri_z|$) and wavenumbers (i.e. $|k_x| \sim |k_z|$) the disc becomes unstable, even in the presence of radial and vertical stratifications with $Ri_x > 0$ and $Ri_z > 0$. The origin of this resides in an hybrid radial-vertical Richardson number. We will present an equilibrium profile with temperature depending on the radial and vertical coordinates and with $Ri_z > 0$ for which this destabilization mechanism occurs in the proximity of the midplane.

Astrophysical discs composed of ionized gases accrete toward a central object because subject to the magnetorotational instability (MRI), which induces transport of angular momentum outwardly. Extended zones of protoplanetary discs are, however, scarcely ionized. In these regions the MRI drive is absent and other instabilities of hydrodynamical nature must be active in order to explain the process of planet formation. Convection is a possible candidate.

Urpin (2003) investigated generally the local stability of a fully stratified and thermally diffusing disc in the presence of radial and vertical convection. Assuming exponential time dependence of the type e^{st} for the perturbations, the relevant axisymmetric dispersion relation ([1], [2]) in non-dimensional form reads

$$s^3 + k^2 Pe^{-1} s^2 + s\left[\frac{k_z^2}{k^2}[2(2-\tilde{q}) + Ri_x] - \frac{k_x k_z}{k^2}\Big(2A_z + \frac{L_{Sx}}{L_{Sz}}Ri_x + \frac{L_{Sz}}{L_{Sx}}Ri_z\Big) + \frac{Ri_z k_x^2}{k^2}\right] + Pe^{-1}[2k_z^2(2-\tilde{q}) - 2k_x k_z A_z] = 0, \qquad (1)$$

where Pe is the Peclet number, L_S represents the entropy length scale, $\tilde{q}$ and A_z are the radial and vertical velocity shear coefficients respectively. Ri is the Richardson number and k the wavenumber, x and z represent the radial and vertical coordinates respectively. From this equation we can obtain the condition for convective instability which reads

$$\left[\frac{k_z^2}{k^2}Ri_x - \frac{k_x k_z}{k^2}\Big(\frac{L_{Sx}}{L_{Sz}}Ri_x + \frac{L_{Sz}}{L_{Sx}}Ri_z\Big) + \frac{Ri_z k_x^2}{k^2}\right] < 0 \qquad (2)$$

Here we are particularly interested in studying equation (2) when radial and vertical stratifications are comparable (i.e. $|Ri_z| \sim |Ri_x|$) and for wavenumbers $|k_z| \sim |k_x|$. If k_x and k_z have the same sign equation (2) reads:

$$Ri_x\Big(1 - \frac{L_{Sx}}{L_{Sz}}\Big) + Ri_z\Big(1 - \frac{L_{Sz}}{L_{Sx}}\Big) < 0. \qquad (3)$$

When $Ri_x > 0$ and $Ri_z > 0$ the disc is unstable if $L_{Sx}/L_{Sz} > 0$. The critical term driving the disc to instability is the hybrid Richardson number

$$Ri_{xz} = \frac{L_{Sx}}{L_{Sz}}Ri_x + \frac{L_{Sz}}{L_{Sx}}Ri_z. \qquad (4)$$

This points at the fact that when discs are fully stratified, instability drives arise not only from purely radial and vertical gradients but as well from mixed radial-vertical ones.
At the presentation we will discuss some concrete examples of equilibrium profiles where this hybrid convective instability occurs with growth rates in some regions of the same order of the local orbital frequency.

References

[1] Urpin V. (2003) A comparison study of the vertical and magnetic shear instabilities in accretion discs. *Astronomy & Astrophysics* 2003 **404**, 397-403.

[2] Volponi, F. (2014) Non-axisymmetric vertical shear and convective instabilities as a mechanism of angular momentum transport. *Monthly Notices of the Royal Astronomical Society* 2014 **441** 813-820.

Notes

Optimal dynamical systems of Navier-Stokes equations based on generalized helical-wave bases and the fundamental elements of turbulence

C. J. Wu[1], N. F. Peng[1,2], H. Guan[3], Z. J. Wei[2]

[1] *State Key Laboratory of Structural Analysis for Industrial Equipment, School of Aeronautics and Astronautics, Dalian University of Technology, Dalian 116024, China*

[2] *State Key Laboratory for Turbulence and Complex Systems, Center for Applied Physics and Technology, College of Engineering, Peking University, Beijing 100871, China*

[3] *College of Meteorology and Oceanography, PLA University of Science and Technology, Nanjing 211101, China*

Summary

In this paper, we present the theory of constructing optimal generalized helical-wave coupling dynamical systems. Applying the helical-wave decomposition method to Navier-Stokes equations, we derive a pair of coupling dynamical systems. With the method of multi-scale global optimization based on coarse graining analysis, a set of global optimal generalized helical-wave bases is obtained. On the one hand, optimal generalized helical-wave bases retain the good properties of classical helical-wave bases; on the other hand, they are optimal for the dynamical systems of Navier-Stokes equations, and suitable for complex physical and geometric boundary conditions. Then we find that the optimal generalized helical-wave vortexes fitted by a finite number of optimal generalized helical-wave bases can be used as the fundamental elements of turbulence, and have important significance for studying physical properties of complex flows and turbulent vortex structures in a deeper level.

1 The fundamental element of turbulence and its properties

In the researches of turbulent physics, we believe that there exist the fundamental elements of turbulence (Wu & Zhao [1], 2000), which should have the following properties.

(1) In dynamical aspect, they must deeply reflect the typical dynamical properties of turbulence, such as the process of shear and expansion, fluctuation, and chaos.

(2) In physical space, they must be concentrated, and decay fast enough at the far field.

(3) At the time revolution aspect, they must have the property of slow changing, i.e., the evolution of fundamental elements is much slower than the fluctuations of flow field's evolution, so the nonlinear interaction among these fundamental elements' slow changing causes fast variations of turbulent flows.

In our previous researches, it has been proved that the vortex element is not a good candidate of the fundamental element of turbulence, while the helical-wave base based on the method of helical-wave decomposition [2, 3] (HWD) is a good one. However, classical helical-wave bases have three kinds of drawbacks [1]. In this way, we find a new kinds of fundamental elements of turbulence called optimal generalized helical-wave bases.

2 Optimal generalized helical-wave coupling dynamical systems of Navier-Stokes equations

As for the general three-dimensional incompressible viscous flow, non-dimensional Navier-Stokes equations [4], continuity equations, initial and boundary conditions after HWD are as follows.

$$\begin{cases} \dot{u}_i^+ + \dot{u}_i^- + u_j^+ u_{i,j}^+ + u_j^+ u_{i,j}^- + u_j^- u_{i,j}^+ + u_j^- u_{i,j}^- + p_{,i} - \dfrac{1}{Re}\left(u_{i,jj}^+ + u_{i,jj}^-\right) = 0 \\ u_{i,i}^+ = u_{i,i}^- = 0 \\ u_i^+\big|_{t=0} = u_{0i}^+,\ u_i^-\big|_{t=0} = u_{0i}^- \\ \left[\alpha\left(u_i^+ + u_i^-\right) + \beta\left(u_{i,j}^+ + u_{i,j}^-\right) n_j\right]_{\partial\Omega} = \alpha\left(u_{Bi}^+ + u_{Bi}^-\right) + \beta\left(u_{Bi,j}^+ + u_{Bi,j}^-\right) n_j \end{cases} \tag{1}$$

For low-dimensional model of Eq.(1), the problem can be limited in N-dimensional Hilbert space, so the function space $\mathcal{B}_N^{\mathrm{HWD}}$ spanned by generalized helical-wave bases $\xi_{\hat{k}i}^{\pm}$ is:

$$\begin{aligned} \mathcal{B}_N^{\mathrm{HWD}} = \Bigg\{ \left[\xi_{\hat{k}i}^{\pm}\right]_{\hat{k}=1}^{N} \Big| \ \xi_{\hat{k}i}^{\pm} \in \mathcal{H}^N(\Omega),\ \int_\Omega \xi_{\hat{k}i}^{\pm}\xi_{\hat{l}i}^{\pm}\,\mathrm{d}\Omega = \delta_{\hat{k}\hat{l}},\ \int_\Omega \xi_{\hat{k}i}^{+}\xi_{\hat{l}i}^{-}\,\mathrm{d}\Omega = 0, \\ \text{and } \xi_{\hat{k}i}^{\pm} \text{ is twice differentiable; } \hat{k} \neq l,\ \varepsilon_{ijk}\xi_{\hat{k}i}^{\pm}\xi_{lk,j}^{\pm} = 0 \Bigg\} \end{aligned} \tag{2}$$

And the low-dimensional approximate expressions of $u_i^{\pm}$ in $\mathcal{B}_N^{\mathrm{HWD}}$ are:

$$u_i^{\pm} \approx a_{\hat{k}}^{+}\xi_{\hat{k}i}^{\pm} \tag{3}$$

Where the truncated order is N, which is omitted.

Under the theoretical framework of constructing optimal dynamical systems based on weighted residual [5], the objective functional and the generalized objective functional without constraint conditions can be built. Then by the variational operation, we eventually obtain the optimal generalized helical-wave coupling dynamical systems of Navier-Stokes equations as follows.

(1) The ODEs of $a_{\hat{k}}^{\pm}$ (optimal generalized helical-wave coupling dynamical systems).

$$\begin{aligned} &\dot{a}_{\hat{k}}^{+} + B_{\hat{k}lm}^{+++}a_l^+a_m^+ + B_{\hat{k}lm}^{++-}a_l^+a_m^- + B_{\hat{k}lm}^{+-+}a_l^-a_m^+ \\ &+ B_{\hat{k}lm}^{+--}a_l^-a_m^- + \frac{1}{Re}\left(C_{\hat{k}l}^{++}a_l^+ + C_{\hat{k}l}^{+-}a_l^-\right) = 0 \end{aligned} \tag{4a}$$

$$\begin{aligned} &\dot{a}_{\hat{k}}^{-} + B_{\hat{k}lm}^{---}a_l^-a_m^- + B_{\hat{k}lm}^{--+}a_l^-a_m^+ + B_{\hat{k}lm}^{-+-}a_l^+a_m^- \\ &+ B_{\hat{k}lm}^{-++}a_l^+a_m^+ + \frac{1}{Re}\left(C_{\hat{k}l}^{--}a_l^- + C_{\hat{k}l}^{-+}a_l^+\right) = 0 \end{aligned} \tag{4b}$$

(2) The ODEs of $\lambda_{\hat{k}}^{\pm}$.

$$\begin{aligned} \dot{\lambda}_{\hat{k}}^{+} = &\left(B_{l\hat{k}m}^{+++} + B_{lm\hat{k}}^{+++}\right)\tilde{\lambda}_l^+a_m^+ + \left(B_{l\hat{k}m}^{++-} + B_{lm\hat{k}}^{+-+}\right)\tilde{\lambda}_l^+a_m^- + \\ &\left(B_{l\hat{k}m}^{-++} + B_{lm\hat{k}}^{-++}\right)\tilde{\lambda}_l^-a_m^+ + \left(B_{l\hat{k}m}^{-+-} + B_{lm\hat{k}}^{--+}\right)\tilde{\lambda}_l^-a_m^- + \\ &\frac{1}{Re}\left(C_{\hat{k}l}^{++}\tilde{\lambda}_i^+ + C_{\hat{k}l}^{+-}\tilde{\lambda}_l^-\right) \end{aligned} \tag{5a}$$

$$\begin{aligned} \dot{\lambda}_{\hat{k}}^{-} = &\left(B_{l\hat{k}m}^{---} + B_{lm\hat{k}}^{---}\right)\tilde{\lambda}_l^-a_m^- + \left(B_{l\hat{k}m}^{--+} + B_{lm\hat{k}}^{-+-}\right)\tilde{\lambda}_l^-a_m^+ + \\ &\left(B_{l\hat{k}m}^{+--} + B_{lm\hat{k}}^{+--}\right)\tilde{\lambda}_l^+a_m^- + \left(B_{l\hat{k}m}^{+-+} + B_{lm\hat{k}}^{++-}\right)\tilde{\lambda}_l^+a_m^+ + \\ &\frac{1}{Re}\left(C_{\hat{k}l}^{--}\tilde{\lambda}_i^+ + C_{\hat{k}l}^{-+}\tilde{\lambda}_l^+\right) \end{aligned} \tag{5b}$$

(3) The equations of the gradient of the generalized objective functional.

In the domain Ω:

$$
\begin{aligned}
&-\tilde{\lambda}_{\hat{k}}^{+}(0)\,u_{0i}^{+}+P_{\hat{k}lm}^{+++}\xi_{lj}^{+}\xi_{mi,j}^{+}+P_{ml\hat{k}}^{+++}\left(\xi_{mj}^{+}\xi_{lj,i}^{+}-\xi_{lj}^{+}\xi_{mi,j}^{+}\right)+P_{\hat{k}lm}^{++-}\xi_{lj}^{+}\xi_{mi,j}^{-}\\
&+P_{ml\hat{k}}^{-++}\left(\xi_{mj}^{-}\xi_{lj,i}^{+}-\xi_{lj}^{+}\xi_{mi,j}^{-}\right)+P_{\hat{k}lm}^{+-+}\xi_{lj}^{-}\xi_{mi,j}^{+}+P_{ml\hat{k}}^{+-+}\left(\xi_{mj}^{+}\xi_{lj,i}^{-}-\xi_{lj}^{-}\xi_{mi,j}^{+}\right)\\
&+P_{\hat{k}lm}^{+--}\xi_{lj}^{-}\xi_{mi,j}^{-}+P_{ml\hat{k}}^{--+}\left(\xi_{mj}^{-}\xi_{lj,i}^{-}-\xi_{lj}^{-}\xi_{mi,j}^{-}\right)-\frac{1}{Re}\left(S_{\hat{k}l}^{++}+S_{l\hat{k}}^{++}\right)\xi_{li,jj}^{+}\\
&-\frac{1}{Re}\left(S_{\hat{k}l}^{+-}+S_{l\hat{k}}^{-+}\right)\xi_{li,jj}^{-}+4\mu^{+}\left(E_{ll}^{++}-1\right)\xi_{\hat{k}i}^{+}+2\mu^{+}\left(E_{\hat{k}l}^{++}\xi_{li}^{+}\right)_{\hat{k}\neq l}\\
&+2\nu^{+}\left(\varepsilon_{ijk}F_{\hat{k}l}^{++}\xi_{\hat{k}k,j}^{+}\right)_{\hat{k}\neq l}=0
\end{aligned}
\tag{6a}
$$

$$
\begin{aligned}
&-\tilde{\lambda}_{\hat{k}}^{-}(0)\,u_{0i}^{-}+P_{\hat{k}lm}^{---}\xi_{lj}^{-}\xi_{mi,j}^{-}+P_{ml\hat{k}}^{---}\left(\xi_{mj}^{-}\xi_{lj,i}^{-}-\xi_{lj}^{-}\xi_{mi,j}^{-}\right)+P_{\hat{k}lm}^{--+}\xi_{lj}^{-}\xi_{mi,j}^{+}\\
&+P_{ml\hat{k}}^{+--}\left(\xi_{mj}^{+}\xi_{lj,i}^{-}-\xi_{lj}^{-}\xi_{mi,j}^{+}\right)+P_{\hat{k}lm}^{-+-}\xi_{lj}^{+}\xi_{mi,j}^{-}+P_{ml\hat{k}}^{-+-}\left(\xi_{mj}^{-}\xi_{lj,i}^{+}-\xi_{lj}^{+}\xi_{mi,j}^{-}\right)\\
&+P_{\hat{k}lm}^{-++}\xi_{lj}^{+}\xi_{mi,j}^{+}+P_{ml\hat{k}}^{++-}\left(\xi_{mj}^{+}\xi_{lj,i}^{+}-\xi_{lj}^{+}\xi_{mi,j}^{+}\right)-\frac{1}{Re}\left(S_{\hat{k}l}^{--}+S_{l\hat{k}}^{--}\right)\xi_{li,jj}^{-}\\
&-\frac{1}{Re}\left(S_{\hat{k}l}^{-+}+S_{l\hat{k}}^{+-}\right)\xi_{li,jj}^{+}+4\mu^{-}\left(E_{ll}^{--}-1\right)\xi_{\hat{k}i}^{-}+2\mu^{-}\left(E_{\hat{k}l}^{--}\xi_{li}^{-}\right)_{\hat{k}\neq l}\\
&+2\nu^{-}\left(\varepsilon_{ijk}F_{\hat{k}l}^{--}\xi_{\hat{k}k,j}^{-}\right)_{\hat{k}\neq l}=0
\end{aligned}
\tag{6b}
$$

In the boundary, for Dirichlet boundary conditions:

$$
\begin{aligned}
&S_{m\hat{k}}^{++}\xi_{li}^{+}\left(u_{Bj}^{+}+u_{Bj}^{-}\right)n_j+S_{m\hat{k}}^{-+}\xi_{li}^{-}\left(u_{Bj}^{+}+u_{Bj}^{-}\right)n_j\\
&+\frac{1}{Re}\left(S_{\hat{k}l}^{++}+S_{l\hat{k}}^{++}\right)\xi_{li,j}^{+}n_j+\frac{1}{Re}\left(S_{\hat{k}l}^{+-}+S_{l\hat{k}}^{-+}\right)\xi_{li,j}^{-}n_j=0
\end{aligned}
\tag{7a}
$$

$$
\begin{aligned}
&S_{m\hat{k}}^{--}\xi_{li}^{-}\left(u_{Bj}^{+}+u_{Bj}^{-}\right)n_j+S_{m\hat{k}}^{+-}\xi_{li}^{+}\left(u_{Bj}^{+}+u_{Bj}^{-}\right)n_j\\
&+\frac{1}{Re}\left(S_{\hat{k}l}^{--}+S_{l\hat{k}}^{--}\right)\xi_{li,j}^{-}n_j+\frac{1}{Re}\left(S_{\hat{k}l}^{-+}+S_{l\hat{k}}^{+-}\right)\xi_{li,j}^{+}n_j=0
\end{aligned}
\tag{7b}
$$

For Newman boundary conditions:

$$
\begin{aligned}
&P_{ml\hat{k}}^{+++}\xi_{mi}^{+}\xi_{lj}^{+}n_j+P_{ml\hat{k}}^{+-+}\xi_{mi}^{+}\xi_{lj}^{-}n_j+P_{ml\hat{k}}^{-++}\xi_{mi}^{-}\xi_{lj}^{+}n_j+P_{ml\hat{k}}^{--+}\xi_{mi}^{-}\xi_{lj}^{-}n_j\\
&+\frac{1}{Re}T_{\hat{k}}^{+}\left(u_{Bi,j}^{+}+u_{Bi,j}^{-}\right)n_j+\frac{1}{Re}\left(S_{\hat{k}l}^{++}\xi_{li,j}^{+}+S_{\hat{k}l}^{+-}\xi_{li,j}^{-}\right)n_j=0
\end{aligned}
\tag{8a}
$$

$$
\begin{aligned}
&P_{ml\hat{k}}^{---}\xi_{mi}^{-}\xi_{lj}^{-}n_j+P_{ml\hat{k}}^{-+-}\xi_{mi}^{-}\xi_{lj}^{+}n_j+P_{ml\hat{k}}^{+--}\xi_{mi}^{+}\xi_{lj}^{-}n_j+P_{ml\hat{k}}^{+++}\xi_{mi}^{+}\xi_{lj}^{+}n_j\\
&+\frac{1}{Re}T_{\hat{k}}^{-}\left(u_{Bi,j}^{+}+u_{Bi,j}^{-}\right)n_j+\frac{1}{Re}\left(S_{\hat{k}l}^{--}\xi_{li,j}^{-}+S_{\hat{k}l}^{-+}\xi_{li,j}^{+}\right)n_j=0
\end{aligned}
\tag{8b}
$$

For Robin boundary conditions:

$$
\begin{aligned}
&S_{m\hat{k}}^{++}\xi_{li}^{+}\left(u_{Bj}^{+}+u_{Bj}^{-}\right)n_j+S_{m\hat{k}}^{-+}\xi_{li}^{-}\left(u_{Bj}^{+}+u_{Bj}^{-}\right)n_j\\
&+\frac{1}{Re}T_{\hat{k}}^{+}\left(u_{Bi,j}^{+}+u_{Bi,j}^{-}\right)n_j+\frac{1}{Re}\left(S_{\hat{k}l}^{++}\xi_{li,j}^{+}+S_{\hat{k}l}^{+-}\xi_{li,j}^{-}\right)n_j=0
\end{aligned}
\tag{9a}
$$

$$
\begin{aligned}
&S_{m\hat{k}}^{--}\xi_{li}^{-}\left(u_{Bj}^{+}+u_{Bj}^{-}\right)n_j+S_{m\hat{k}}^{+-}\xi_{li}^{+}\left(u_{Bj}^{+}+u_{Bj}^{-}\right)n_j\\
&+\frac{1}{Re}T_{\hat{k}}^{-}\left(u_{Bi,j}^{+}+u_{Bi,j}^{-}\right)n_j+\frac{1}{Re}\left(S_{\hat{k}l}^{--}\xi_{li,j}^{-}+S_{\hat{k}l}^{-+}\xi_{li,j}^{+}\right)n_j=0
\end{aligned}
\tag{9b}
$$

Where,

$$\begin{cases} B^{\pm\pm\pm}_{\hat{k}lm} = \int_\Omega \xi^{\pm}_{\hat{k}i}\xi^{\pm}_{lj}\xi^{\pm}_{mi,j}\ \mathrm{d}\Omega \\ C^{\pm\pm}_{\hat{k}l} = \int_\Omega \xi^{\pm}_{\hat{k}i,j}\xi^{\pm}_{li,j}\ \mathrm{d}\Omega \\ E^{\pm\pm}_{\hat{k}l} = \int_\Omega \xi^{\pm}_{\hat{k}i}\xi^{\pm}_{li}\ \mathrm{d}\Omega \\ F^{\pm\pm}_{\hat{k}l} = \int_\Omega \varepsilon_{ijk}\xi^{\pm}_{\hat{k}i}\xi^{\pm}_{lk,j}\ \mathrm{d}\Omega \\ P^{\pm\pm\pm}_{\hat{k}lm} = \int_0^T \tilde{\lambda}^{\pm}_{\hat{k}} a^{\pm}_l a^{\pm}_m\ \mathrm{d}t \\ S^{\pm\pm}_{\hat{k}l} = \int_0^T \tilde{\lambda}^{\pm}_{\hat{k}} a^{\pm}_l\ \mathrm{d}t \\ T^{\pm}_{\hat{k}} = \int_0^T \tilde{\lambda}^{\pm}_{\hat{k}}\ \mathrm{d}t \end{cases} \tag{10}$$

With the multi-scale global optimization method [5], we can solve the above ODEs and obtain the optimal generalized helical-wave bases $\xi^{*+}_{\hat{k}i}$ and $\xi^{*-}_{\hat{k}i}$ directly from Navier-Stokes equations.

3 Optimal generalized helical-wave bases and their properties

For the numerical simulation example, we choose the backward facing step flow with Reynolds number $Re = 800$. Then we construct the coupling dynamical systems and obtain six pairs of optimal generalized helical-wave bases $\boldsymbol{\xi}^{*+}_{\hat{k}}$ and $\boldsymbol{\xi}^{*-}_{\hat{k}}$, $(\hat{k} = 1, 2, \cdots, 6)$, and the contour lines of the magnitudes of $\boldsymbol{\xi}^{*\pm}_1$ and $\boldsymbol{\xi}^{*\pm}_2$ in the streamwise middle section of the channel is shown in figure 1.

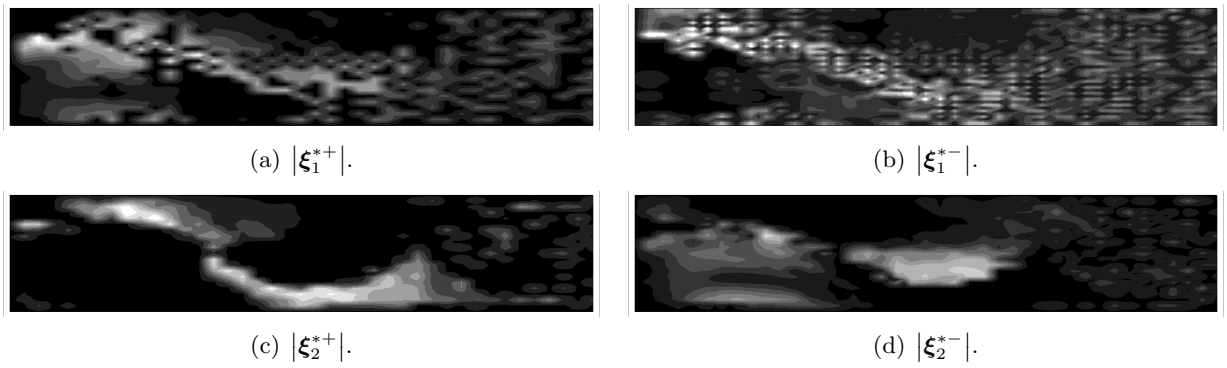

(a) $|\boldsymbol{\xi}^{*+}_1|$. (b) $|\boldsymbol{\xi}^{*-}_1|$.

(c) $|\boldsymbol{\xi}^{*+}_2|$. (d) $|\boldsymbol{\xi}^{*-}_2|$.

Fig. 1: The contour lines of the magnitudes of $\boldsymbol{\xi}^{*\pm}_1$ and $\boldsymbol{\xi}^{*\pm}_2$ in the streamwise middle section.

From these pictures, we can find the properties of optimal generalized helical-wave bases as follows.

(1) Optimal generalized helical-wave bases reflect the properties of smaller scale structures, especially compared with POD bases.

(2) They show the parity property and the coupling interaction between the positive one $\boldsymbol{\xi}^{*+}_{\hat{k}}$ and the negative one $\boldsymbol{\xi}^{*-}_{\hat{k}}$.

(3) They are more complex and broken in the spatial distribution, which contain the properties of Beltrami flow's chaotic particles.

(4) They do not distribute continuously in physical space, which is the most important difference with POD bases, and they are concentrated.

4 Optimal generalized helical-wave vortexes – the fundamental elements of turbulence

Then we use the six pairs of optimal generalized helical-wave bases $\boldsymbol{\xi}_{\hat{k}}^{*+}$ and $\boldsymbol{\xi}_{\hat{k}}^{*-}$ to fit the positive component and negative component of the vorticity fields and obtain $\boldsymbol{\omega}^{*+}$ and $\boldsymbol{\omega}^{*-}$ respectively satisfying left-handed and righted-handed parity symmetry properties, which we called the optimal helical-wave vortexes. The contour lines of the magnitudes of $\boldsymbol{\omega}^{*+}$, $\boldsymbol{\omega}^{*-}$ and the original vorticity field $\boldsymbol{\omega}$ at the same moment in the streamwise middle section is shown in figure 2.

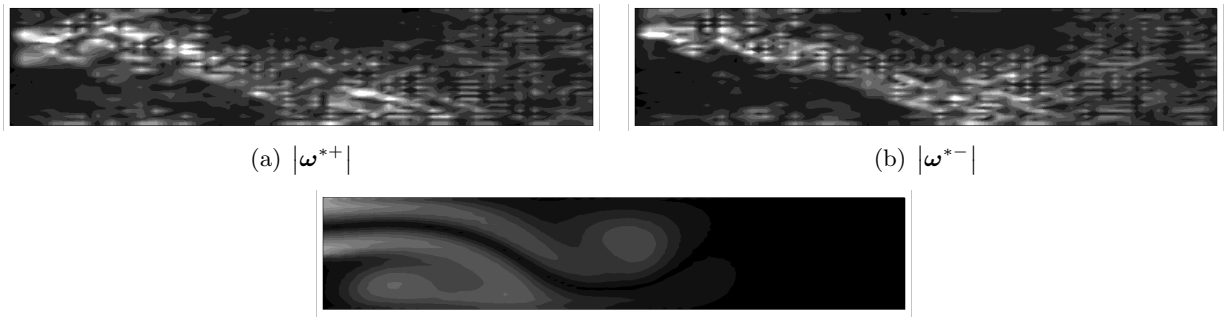

(a) $|\boldsymbol{\omega}^{*+}|$ (b) $|\boldsymbol{\omega}^{*-}|$

(c) $|\boldsymbol{\omega}|$

Fig. 2: The contour lines of the magnitudes of $\boldsymbol{\omega}^{*+}$, $\boldsymbol{\omega}^{*-}$ and $\boldsymbol{\omega}$ at the same moment in the streamwise middle section.

From figure 2, we can find that:

(1) $\boldsymbol{\omega}^{*+}$ and $\boldsymbol{\omega}^{*-}$ show small scale vortex structures of the vorticity field, and their interaction and superposition result in large vortex structures in $\boldsymbol{\omega}$.

(2) $\boldsymbol{\omega}^{*+}$ and $\boldsymbol{\omega}^{*-}$ are concentrated in physical space, and in some locations the vorticity magnitudes $|\boldsymbol{\omega}^{*+}|$ and $|\boldsymbol{\omega}^{*-}|$ are much bigger than $|\boldsymbol{\omega}|$, which reflects the high polarization effect from large scale vortexes to small scale ones.

Then when considering the evolution over time, we find that $\boldsymbol{\omega}^{*+}$ and $\boldsymbol{\omega}^{*-}$ change much more slowly than $\boldsymbol{\omega}$, so i.e. the interaction and superposition of $\boldsymbol{\omega}^{*+}$ and $\boldsymbol{\omega}^{*-}$ which change slowly result in the fast changing of $\boldsymbol{\omega}$. In this way, it is proved that optimal generalized helical-wave bases meet the three properties mentioned in section 1, so they can be used as the fundamental element of turbulence.

5 Conclusion

In this paper, we present the theory of constructing optimal generalized helical-wave coupling dynamical systems and obtain the optimal generalized helical-wave bases, which have many good properties. On the one hand, they retain the good properties of classical helical-wave bases; on the other hand, they are global optimal for dynamical systems of Navier-Stokes equations, and suitable for complex physical and geometric boundary conditions. Then we find that the optimal generalized helical-wave vortexes fitted by the optimal generalized helical-wave bases can be used as the fundamental elements of turbulence, and have important significance for studying physical properties of complex flows and turbulent vortex structures in a deeper level.

Acknowledgements. This work was supported by the National Natural Science Foundation of China grant No.11372068, the National Basic Research Program of China grant No.2014CB744104 and the National Natural Science Foundation of China grant No.11572350.

References

[1] Wu, C.J. & Zhao, H.L. (2000) Generalized HWD-POD method and coupling low-dimensional dynamical systems on turbulence. *Discrete Contin. Dyn. Syst.* 2000 **7 (Added Volumn)**, 371–379.

[2] Moses, H.E. (1971) Eigenfunctions of the curl operator, ratationally invarient Helmholtz theorem, and applications to electromagnetic theory and fluid mechanics. *SIAM J. Appl. Math.* 1971 **21**, 114–144.

[3] Lesieur, M. (1990) *The Physics of Fluid Turbulence*. Oxford University Press, Oxford.

[4] Fu, D.X. & Ma, Y.W. & Li, X.L. & Wang, Q. (2010) *Direct Numerical Simulations of Compressible Turbulence* (in Chinese). Science Press, Beijing.

[5] Peng, N. F. & Guan, H. & Wu, C. J. Research on the optimal dynamical systems of three-dimensional Navier-Stokes equations based on weighted residual. submitted to *Sci. China Ser. G-Phys. Mech. Astron.*

Notes

Variational Principles for non-Barotropic Magnetohydrodynamics and Local Topological Conservation Laws

A. Yahalom[1]

[1] *Department of Electrical & Electronic Engineering, Ariel University, Israel*

Summary

Variational principles for magnetohydrodynamics (MHD) were introduced by previous authors both in Lagrangian and Eulerian form. In this talk we introduce simpler Eulerian variational principles which is appropriate for some magnetic field topologies from which all the relevant equations of non-barotropic MHD can be derived. The variational principle is given in terms of five independent functions for non-stationary barotropic flows. This is less then the eight variables which appear in the standard equations of barotropic MHD which are the magnetic field $\vec{B}$ the velocity field $\vec{v}$, the entropy s and the density ρ. The functions which are needed in addition to the entropy and density are two co-moving surfaces χ and η (Euler potentials) and a multiple valued Bernoulli type function ν. We will show that the discontinuity of ν is a conserved quantity and contains information about the cross helicity per unit of magnetic flux.

1 Barotropic MHD

Variational principles for MHD were introduced by previous authors both in Lagrangian and Eulerian form. Sturrock [1] has discussed in his book a Lagrangian variational formalism for MHD. Vladimirov and Moffatt [2] in a series of papers have discussed an Eulerian variational principle for incompressible MHD. However, their variational principle contained three more functions in addition to the seven variables which appear in the standard equations of incompressible MHD which are the magnetic field $\vec{B}$ the velocity field $\vec{v}$ and the pressure P. Kats [3] has generalized Moffatt's work for compressible non barotropic flows but without reducing the number of functions and the computational load. Sakurai [4] has introduced a two function Eulerian variational principle for force-free MHD and used it as a basis of a numerical scheme, his method is discussed in a book by Sturrock [1]. Yahalom & Lynden-Bell [5] combined the Lagrangian of Sturrock [1] with the Lagrangian of Sakurai [4] to obtain an **Eulerian** Lagrangian principle for barotropic MHD which will depend on only six functions. The variational derivative of this Lagrangian produced all the equations needed to describe barotropic MHD without any additional constraints. The equations obtained resembled the equations of Frenkel, Levich & Stilman [6]. Yahalom [7] have shown that for the barotropic case four functions will suffice. Moreover, it was shown that the cuts of some of those functions [8] are topological local conserved quantities. It was also shown [5] that the cross helicity conservation law can be derived via the Noether theorem using a method similar to the method used to derive the conservation of helicity in non magnetic fluids [9].

2 Non-Barotropic MHD

Variational principles of non barotropic MHD can be found in the work of Bekenstein & Oron [10] in terms of 15 functions and V.A. Kats [3] in terms of 20 functions. Moreover, A. V. Kats in a remarkable paper [11] (section IV,E) has shown that there is a large symmetry group (gauge freedom) associated with the choice of those functions, this implies that the number of degrees of freedom can be reduced. Morrison [12] has suggested a Hamiltonian approach but this also depends on 8 canonical variables (see table 2 [12]). Here we will show that only five functions will suffice to describe non barotropic MHD in the case that we enforce a Sakurai [4] representation for the magnetic field. The functions which are needed in addition to the entropy and density are two co-moving surfaces χ and η (Euler potentials) and a multiple valued Bernoulli type function ν [13, 14].

We will show that the discontinuity of ν is a conserved quantity and contains information about the cross helicity per unit of magnetic flux. (See [8] for the analogous barotropic case)

We anticipate applications of this study both to linear and non-linear stability analysis of known non barotropic MHD configurations [15, 16, 17, 18] and for designing efficient numerical schemes for integrating the equations of fluid dynamics and MHD [19, 20, 21, 22]. Another possible application is connected to obtaining new analytic solutions in terms of the variational variables [23].

References

[1] P. A. Sturrock, *Plasma Physics* (Cambridge University Press, Cambridge, 1994)

[2] V. A. Vladimirov and H. K. Moffatt, J. Fluid. Mech. **283** 125-139 (1995)

[3] A. V. Kats, Los Alamos Archives physics-0212023 (2002), JETP Lett. 77, 657 (2003)

[4] T. Sakurai, Pub. Ast. Soc. Japan **31** 209 (1979)

[5] A. Yahalom and D. Lynden-Bell, "Simplified Variational Principles for Barotropic Magnetohydrodynamics," (Los-Alamos Archives physics/0603128) *Journal of Fluid Mechanics*, Vol. 607, 235-265, 2008.

[6] A. Frenkel, E. Levich and L. Stilman Phys. Lett. A **88**, p. 461 (1982)

[7] Yahalom A., "A Four Function Variational Principle for Barotropic Magnetohydrodynamics" EPL 89 (2010) 34005, doi: 10.1209/0295-5075/89/34005 [Los - Alamos Archives - arXiv: 0811.2309]

[8] Asher Yahalom "Aharonov - Bohm Effects in Magnetohydrodynamics" Physics Letters A. Volume 377, Issues 31-33, 30 October 2013, Pages 1898-1904.

[9] A. Yahalom, "Helicity Conservation via the Noether Theorem" J. Math. Phys. 36, 1324-1327 (1995). [Los-Alamos Archives solv-int/9407001]

[10] J. D. Bekenstein and A. Oron, Physical Review E Volume 62, Number 4, 5594-5602 (2000)

[11] A. V. Kats, Phys. Rev E 69, 046303 (2004)

[12] P.J. Morrison, Poisson Brackets for Fluids and Plasmas, AIP Conference proceedings, Vol. 88, Table 2.

[13] A. Yahalom "Simplified Variational Principles for Non-Barotropic Magnetohydrodynamics - Further Details" Proceedings of the Fourteenth Israeli-Russian Bi-National Workshop 2015 Optimization of the Composition, Structure and Properties of Metals, Oxides, Composites, Nano and Amorphous Materials, pages 23-34. 12-16 July, 2015, Ariel University, Israel.

[14] A. Yahalom "Simplified Variational Principles for non-Barotropic Magnetohydrodynamics". (arXiv: 1510.00637 [Plasma Physics])

[15] V. A. Vladimirov, H. K. Moffatt and K. I. Ilin, J. Fluid Mech. 329, 187 (1996); J. Plasma Phys. 57, 89 (1997); J. Fluid Mech. 390, 127 (1999)

[16] J. Katz, S. Inagaki, and A. Yahalom, "Energy Principles for Self-Gravitating Barotropic Flows: I. General Theory", Pub. Astro. Soc. Japan 45, 421-430 (1993).

[17] Yahalom A., Katz J. & Inagaki K. 1994, *Mon. Not. R. Astron. Soc.* **268** 506-516.

[18] Asher Yahalom, "Stability in the Weak Variational Principle of Barotropic Flows and Implications for Self-Gravitating Discs". Monthly Notices of the Royal Astronomical Society 418, 401-426 (2011).

[19] A. Yahalom, "Method and System for Numerical Simulation of Fluid Flow", US patent 6,516,292 (2003).

[20] A. Yahalom, & G. A. Pinhasi, "Simulating Fluid Dynamics using a Variational Principle", proceedings of the AIAA Conference, Reno, USA (2003).

[21] A. Yahalom, G. A. Pinhasi and M. Kopylenko, "A Numerical Model Based on Variational Principle for Airfoil and Wing Aerodynamics", proceedings of the AIAA Conference, Reno, USA (2005).

[22] D. Ophir, A. Yahalom, G.A. Pinhasi and M. Kopylenko "A Combined Variational and Multi-Grid Approach for Fluid Dynamics Simulation" Proceedings of the ICE - Engineering and Computational Mechanics, Volume 165, Issue 1, 01 March 2012, pages 3 -14 , ISSN: 1755-0777, E-ISSN: 1755-0785.

[23] A. Yahalom "Using fluid variational variables to obtain new analytic solutions of self-gravitating flows with nonzero helicity" Procedia IUTAM 7 (2013) 223 - 232.

Notes

The Global Distribution of Magnetic Helicity in the Sun's Corona

A. R. Yeates[1], G. Hornig[2]

[1] *Department of Mathematical Sciences, Durham University, UK*
[2] *Division of Mathematics, University of Dundee, UK*

Summary

Modern observations are revealing the Sun's large-scale magnetic field to have a complex, non-potential structure. Moreover, it is now widely believed that the loss of equilibrium of twisted magnetic flux ropes is responsible for many (if not all) coronal mass ejections. But predicting where these flux ropes will form, and in particular whether or when they might erupt, remains a challenge for model reconstructions of the coronal magnetic field. In this talk, I will introduce the "field line helicity" as an appropriate and practical diagnostic for identifying twisted structures in coronal models. Since field lines are magnetic sub-domains, this is a more meaningful measure than the density of magnetic helicity at individual points. On the other hand, it provides local information that the globally-integrated magnetic helicity cannot. I will illustrate the power of this diagnostic on my own numerical non-potential evolution model of the global corona.

1 Introduction

Numerous approaches have been used to characterize the twist in individual active regions in the corona, based on knowing only the lower boundary condition on the Sun's surface. For example, various techniques to extrapolate force-free magnetic fields (i.e., $\mathbf{B}$ such that $\nabla \times \mathbf{B} = \alpha \mathbf{B}$) allow estimates of their free magnetic energy and (relative) magnetic helicity [1]. For linear force-free fields (where α is a constant), one can quantify overall twist by the best-fit α value. For nonlinear force-free fields (where α varies between magnetic field lines), one can study the distribution of this local field-line twist [2]. Indeed, Yeates *et al.* [3] have also studied this distribution in global simulations of the solar corona (of the type illustrated here).

An alternative approach that avoids the need for magnetic extrapolation is to measure the flux of magnetic helicity into the corona through the Sun's surface, using available observations on that surface. However, the helicity flux density at any particular location is not well-defined [4], as helicity is a global invariant. This makes it difficult to subsequently infer the resulting distribution of twist within the corona without an accompanying magnetic field extrapolation.

The fact that total magnetic helicity is only a *global* invariant also prevents its use to analyse the detailed twist distribution in global simulations. To get around this, Berger & Ruzmaikin [5] divided the corona into two subdomains – the Northern and Southern hemispheres – and estimated the amount of helicity imparted into the solar wind by the Sun's differential rotation within each hemisphere. Here, we effectively divide the corona into many more subdomains, in order to study the detailed helicity distribution.

2 Field line helicity

To construct a meaningful measure of the helicity distribution, we subdivide the coronal volume not into arbitrary subdomains but into "magnetic" subdomains (whose boundaries within the corona are magnetic surfaces). In the limit, each magnetic field line f represents an individual subdomain [6]. The *field line helicity* $\mathcal{A} = \int_f \mathbf{A} \cdot \mathrm{d}\mathbf{l}$ is then defined for each field line. It is a global measure that depends not only on the twisting of this particular field line but also on how this field line winds around all others in the domain. This reflects the global nature of $\mathbf{A}$ as an integral of $\nabla \times \mathbf{A} = \mathbf{B}$. In the more restrictive case of a cylindrical domain, $\mathcal{A}$ has be shown to be a complete invariant,

capable of uniquely identifying whether two magnetic fields can be linked by an ideal evolution or not [7]. Here it remains a meaningful subdivision of the total helicity.

Two complications arise with the definition of $\mathcal{A}$. Firstly it fails for ergodic field lines, since they have infinite length. Fortunately, such field lines do not typically occur in coronal extrapolations. However, the second complication does occur: open field lines that leave the domain. In fact, (almost) all field lines do so. Just like total magnetic helicity, this renders $\mathcal{A}$ gauge dependent. To fix a meaningful definition, one could impose a gauge condition on the boundary akin to the relative helicity. Instead, here we use the so-called DeVore gauge [8], which is suited to identifying the helicity stored within different coronal arcade structures (Fig. 1).

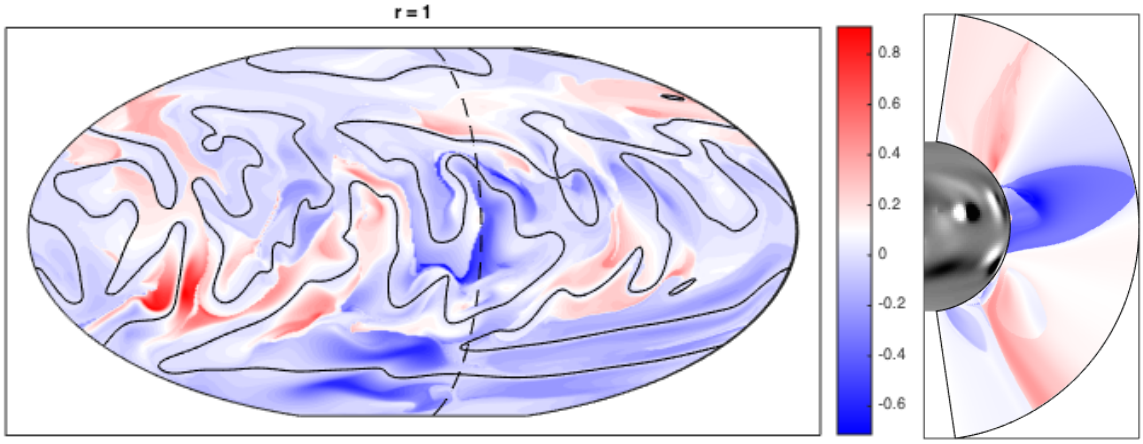

Fig. 1: Distribution of field line helicity $\mathcal{A}$ (colour shading) at one time during a global magneto-frictional simulation of the solar corona [9]. The left panel shows $\mathcal{A}$ on the solar surface and the right panel shows $\mathcal{A}$ in a meridional slice (longitude indicated by the dashed line). Grayscale shading in the right panel shows B_r on the solar surface, while the solid line in the left panel shows the polarity inversion line $B_r = 0$. The right panel reveals one particular arcade containing significant twist, whose footpoints are visible in the left panel.

Acknowledgements. This work was funded by STFC consortium grant ST/K001043/1 to the Universities of Dundee and Durham.

References

[1] Wiegelmann, T. & Sakurai, T. (2012), Solar Force-Free Magnetic Fields. *Living Rev. Solar Phys.* **9**, 5.

[2] Liu, R., et al. (2015), Structure, Stability, and Evolution of Magnetic Flux Ropes from the Perspective of Magnetic Twist. *arxiv:1512.02338v1.*

[3] Yeates, A.R., Mackay, D.H. & van Ballegooijen, A.A. (2008), Evolution and Distribution of Current Helicity in Full-Sun Simulations. *Astrophys. J.* **680**, L165–L168.

[4] Pariat, E., Démoulin, P. & Berger, M.A. (2005), Photospheric Flux Density of Magnetic Helicity. *Astron. Astrophys.* **439**, 1191–1203.

[5] Berger, M.A. & Ruzmaikin, A. (2000), Rate of Helicity Production by Solar Rotation. *J. Geophys. Res.* **105**, 10481–10490.

[6] Berger, M.A. (1988), An Energy Formula for Nonlinear Force-Free Magnetic Fields. *Astron. Astrophys.* **201**, 355–361.

[7] Yeates, A.R. & Hornig, G. (2014), A Complete Topological Invariant for Braided Magnetic Fields. *J. Phys. Conf. Ser.* **544**, 012002.

[8] Amari, T., Aly, J.-J., Canou, A. & Mikić, Z. (2013). Reconstruction of the Solar Coronal Magnetic Field in Spherical Geometry. *Astron. Astrophys.* **553**, A43.

[9] Yeates, A.R. (2014), Coronal Magnetic Field Evolution from 1996 to 2012: Continuous Non-Potential Simulations. *Solar Phys.* **289**, 631–648.

Notes

Flow induction and transport suppression due to helicity, with its implication to subgrid-scale modelling of turbulence

N. Yokoi[1]

[1] *Institute of Industrial Science, University of Tokyo, Japan*

Summary

Effect of helicity in inhomogeneous turbulence is investigated with special reference to spontaneous large-scale flow generation and transport suppression. With the aid of the multiple-scale perturbative renormalization analysis of non-mirrorsymmetric turbulence, a Reynolds stress expression is derived, which includes inhomogeneous turbulent helicity as the coupling coefficient for the mean absolute vorticity. This inhomogeneous helicity effect may counterbalance the enhanced transport due to turbulence such as eddy viscosity, leading to the possibility of transport suppression and flow generation. Examples of helicity effect are presented. Also a subgrid-scale (SGS) turbulence model with structural effects incorporated through helicity is proposed.

1 Closure analysis of helicity effect

Helicity is an inviscid topological invariant of hydrodynamics. Its turbulent local density (velocity–vorticity correlation) represents the breakage of mirrorsymmetry in turbulence. The Reynolds stress of inhomogeneous turbulence is theoretically calculated in a propagator renormalization method with a multiple-scale analysis. With the aid of derivative expansion:

$$\left\langle u'^{\alpha}u'^{\beta}\right\rangle = \left\langle {u'_{\rm B}}^{\alpha}{u'_{\rm B}}^{\beta}\right\rangle + \left\langle {u'_{\rm B}}^{\alpha}{u'_{01}}^{\beta}\right\rangle + \left\langle {u'_{01}}^{\alpha}{u'_{\rm B}}^{\beta}\right\rangle + \cdots + \left\langle {u'_{\rm B}}^{\alpha}{u'_{10}}^{\beta}\right\rangle + \left\langle {u'_{10}}^{\alpha}{u'_{\rm B}}^{\beta}\right\rangle + \cdots . \quad (1)$$

Homogeneity and isotropy with non-mirrorsymmetry are assumed for the lowest-order field $\mathbf{u}'_{\rm B}$:

$$\begin{aligned}&\langle {u'_{\rm B}}^{\alpha}(\mathbf{k},\mathbf{X};\tau,T){u'_{\rm B}}^{\beta}(\mathbf{k}',\mathbf{X};\tau',T)\rangle/\delta(\mathbf{k}+\mathbf{k}')\\ &\quad = D^{\alpha\beta}(\mathbf{k})Q_{\rm B}(k,\mathbf{X};\tau,\tau',T) + (ik^a/2k^2)\epsilon^{\alpha\beta a}H_{\rm B}(k,\mathbf{X};\tau',T).\end{aligned} \quad (2)$$

Effects of inhomogeneity and anisotropy systematically arise from the higher-order terms in Eq. (1). The traceless part (denoted by $[\ldots]_{\rm D}$) of the Reynolds stress is derived as[1]

$$\langle u'^{\alpha}u'^{\beta}\rangle_{\rm D} = -\nu_{\rm T}\mathcal{S}^{\alpha\beta} + [\Gamma^{\alpha}(\Omega^{\beta}+2\omega_{\rm F}^{\beta}) + \Gamma^{\beta}(\Omega^{\alpha}+2\omega_{\rm F}^{\alpha})]_{\rm D}, \quad (3)$$

where the transport coefficients are given as

$$\nu_{\rm T} = \frac{7}{15}\int {\rm d}\mathbf{k}\int_{-\infty}^{t} d\tau_1\; G(k;\tau,\tau_1)Q(k;\tau,\tau_1), \quad \mathbf{\Gamma} = \frac{1}{30}\int k^{-2}{\rm d}\mathbf{k}\int_{-\infty}^{t} d\tau_1\; G(k;\tau,\tau_1)\nabla H(k;\tau,\tau_1) \quad (4)$$

(G: Green's function of turbulence, Q: energy spectral function, H: helicity spectral functions). The first term in Eq. (3) is the effect of the turbulent intensity [1st of Eq. (4)] coupled with the mean velocity strain, usually known as the eddy viscosity, which enhances the effective momentum transport. The second term represents the effects of the helicity-gradient [2nd of Eq. (4)] coupled with the absolute vorticity, which may counterbalance the eddy-viscosity effect.

2 Transport suppression and flow induction by helicity

Transport suppression - swirling flow Using the analytical expression of the Reynolds stress [Eq. (3)], a turbulence model with the helicity effect is constructed. In addition to the turbulent energy and its dissipation rate, the turbulent helicity is considered as a measure of the transport suppression. This model is reduced to the usual eddy-viscosity model for vanishing turbulent helicity, and is a natural extension of the usual eddy-viscosity turbulence model. The model is applied to a turbulent swirling flow (Fig. 1). It is shown that flow properties such as the deceleration at the central axis, etc. are reproduced, which can not be obtained from the standard model.

Flow generation - vortex dynamo In addition to the transport suppression, this inhomogeneous helicity effect may play an essential role in vortex dynamo, global vorticity generation mechanisms in turbulence. With the aid of direct numerical simulations (DNSs) of a rotating turbulence with inhomogeneous helicity externally imposed, it is shown that a large-scale flow can be induced from inhomogeneous turbulent helicity (Fig. 2)[2]. Physical origin of such a global flow is also discussed.

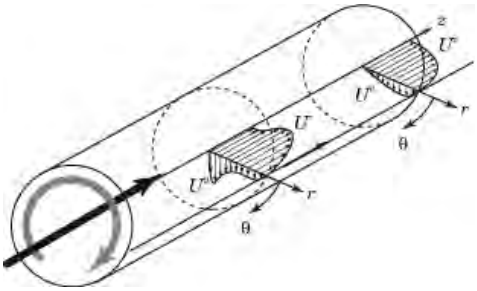

Fig. 1: Schematic turbulent swirling flow. Axial and circumferrential velocity profiles.

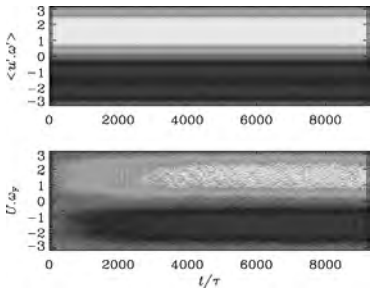

Fig. 2: Temporal evolutions of the turbulent helicity (upper) and mean axial velocity (lower).

3 SGS modelling with helicity

It has been pointed out that in order to improve large-eddy simulation (LES) performance, structural information of turbulence should be implemented into the SGS modelling. On the analogy of Eq. (3), we construct the SGS model, where effects of structure including streamwise vorticity are incorporated into the SGS stress through the SGS helicity as

$$[\overline{u^\alpha u^\beta} - \overline{u}^\alpha \overline{u}^\beta]_{\rm D} = -\nu_{\rm SGS}\overline{s}^{\alpha\beta} + [\gamma^\alpha \overline{\omega}_*^\beta + \gamma^\beta \overline{\omega}_*^\alpha]_{\rm D}, \tag{5}$$

where $\overline{f}$ denotes the filtered or grid-scale (GS) quantity of f ($\overline{s}$: GS velocity strain, $\overline{\omega}_*$: GS absolute vorticity). Several levels of the SGS model are proposed. The most straightforward one is to use Eq. (5) in the GS momentum equation with the transport equations of the SGS energy and helicity. At the simplest zero equation model, where no additional equations are solved other than the GS momentum equation as in the Smagorinsky model, we have to estimate the SGS helicity, as well as the SGS energy, in terms of the GS quantities. By assuming the local equilibrium between the production and dissipation of the SGS helicity, a candidate for the SGS helicity estimate is proposed. It is expected that the problem of constant adjustment (too much turbulent transport) associated with the usual Smagorinsky-type model is alleviated with this helicity SGS model.

Acknowledgements. Collaborations and discussions with A. Yoshizawa, A. Brandenburg are cordially acknowledged.

References

[1] Yokoi, N. & Yoshizawa, A. (1993) Statistical analysis of the effects of helicity in inhomogeneous turbulence. *Phys. Fluids* 1993 A**5**, 464–477.

[2] Yokoi, N. & Brandenburg, A. (2016) Large-scale flow generation by inhomogeneous helicity. *Phys. Rev. E* 2016, submitted.

Notes

Rattleback: a prototype of chiral dynamics

Z. Yoshida[1], T. Tokieda[2], P. J. Morrison[3]

[1] *Department of Advanced Energy, The University of Tokyo, Japan*
[2] *Department of Mathematics, Stanford University, USA*
[3] *Department of Physics and Institute for Fusion Studies, University of Texas at Austin, USA*

Summary

A rattleback is a rigid body whose ellipsoid of inertia is skewed with respect to the principal axes of the contact surface. The chirality of this toy, the breaking of mirror symmetry as manifested by rotational preference, gives us a hint to delineate the origin of chiral dynamics in various systems ranging from classical fluids/plasmas to quantum regimes. From the rattleback rigid-body equations of motion one can extract a prototypical rattleback system composed of three first order coupled differential equations [1], which, in the non-dissipative idealization, has two first integrals, energy and an intriguing function. It is the further study of this system that is the purpose of the present work; we devise a noncanonical three-dimensional Hamiltonian system. The underlying Lie algebra is of Bianchi Type VI, which appears for the first time in a physical example. Its Casimir, whose existence makes the system noncanonical, is the intriguing first integral. The chirality of the rattleback motion is caused by the geometric skewness of the leaf.

1 Model equations and Hamiltonian formalism

The equations of the prototypical rattleback system (called here PRS) are as follows:

$$\frac{\mathrm{d}}{\mathrm{d}t}\begin{pmatrix} P \\ R \\ S \end{pmatrix} = \begin{pmatrix} R \\ \lambda P \\ 0 \end{pmatrix} \times \begin{pmatrix} P \\ R \\ S \end{pmatrix} = \begin{pmatrix} \lambda PS \\ -RS \\ R^2 - \lambda P^2 \end{pmatrix}. \tag{1}$$

Compared with equation (5.5) of [1], we have adopted a more felicitous notation where P, R, S stand for the *pitching*, *rolling*, and *spinning* modes of the motion. The quantity λ is a positive parameter that encodes the *aspect ratio* of the rattleback.

Despite the fact that the phase space is odd-dimensional, it is possible, and useful, to cast the equations (1) in a Hamiltonian form; the system becomes noncanonical and the [2], In terms of the coordinates $\boldsymbol{X} = (P\ R\ S)^{\mathrm{T}} \in \Omega \subset \mathbf{R}^3$, define a Poisson matrix

$$J = \begin{pmatrix} 0 & 0 & \lambda P \\ 0 & 0 & -R \\ -\lambda P & R & 0 \end{pmatrix}, \tag{2}$$

and denote by $\langle\ ,\ \rangle_\Omega$ the standard inner product on the phase space Ω. If we take the *Hamiltonian*

$$H = \frac{1}{2}\langle \boldsymbol{X}, \boldsymbol{X}\rangle_\Omega = \frac{1}{2}\left(P^2 + R^2 + S^2\right), \tag{3}$$

then (1) is cast into the following Hamilton form:

$$\frac{\mathrm{d}}{\mathrm{d}t}\boldsymbol{X} = J\partial_{\boldsymbol{X}} H = \{\boldsymbol{X}, H\}_J, \tag{4}$$

where in the second equality the Poisson bracket $\{F, G\}_J = \langle \partial_{\boldsymbol{X}} F, J\partial_{\boldsymbol{X}} G\rangle_\Omega$ makes $C^\infty(\Omega)$ into a Poisson algebra, a Lie algebra realization on functions, since it is bilinear, antisymmetric, and can be shown to satisfy the Jacobi identity.

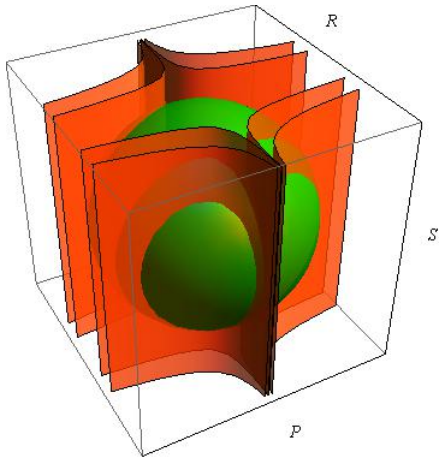

Fig. 1: Orbits are the intersections of an energy level $H = \frac{1}{2}(P^2 + R^2 + S^2) = \text{const.}$ (green sphere) and a Casimir surface $C = PR^\lambda = \text{const.}$ (red curved sheet); the leaves $C = 1, 0.1, -0.1, -1$ are shown. The aspect-ratio parameter is taken to be $\lambda = 4$.

The degeneracy of J yields a *Casimir invariant*

$$C = PR^\lambda, \tag{5}$$

characterized by the property $\{C, G\}_J = 0 \ \forall G \in C^\infty(\Omega)$. Since

$$\det(zI - J) = z(z^2 + \lambda^2 P^2 + R^2),$$

we have rank$J = 2$ except along the singular set $\lambda^2 P^2 + R^2 = 0$, i.e. $P = R = 0$, where rank$J$ drops to 0. In this paper we study the dynamics in the regime $\lambda^2 P^2 + R^2 > 0$; for example it suffices to take the phase space Ω to be an open set in $\mathbf{R}^3$ on which $|C| = |PR^\lambda|$ is bounded away from 0.

2 Skewed space and chirality

Thanks to the Hamiltonian structure, the system (1) is integrable. Examination of the intersection of the Hamiltonian with the Casimir reveals that every orbit is periodic (cf. Fig. 1).

The curious guiding idea of this paper is that we can formulate the dynamics as if a symmetric body were moving in an asymmetric space—recall the formalism of the previous section, where the Hamiltonian is symmetric but there is something asymmetric in the phase space of the Bianchi type $\text{VI}_{h\neq -1}$ Lie-Poisson algebra. The chirality, then, comes from the skewness of the Casimir leaves.

Philosophically, it is interesting to think of the interchangeability of a Hamiltonian and a Casimir as a duality between matter and space. A complex material system may be made simple by transferring complexity to the geometry of space; conversely, a skewed space may be made flat by skewing the matter or the energy. The list of Bianchi algebras provides us with plenty of transfer possibilities.

References

[1] Moffatt, H.K. & Tokieda, T. (2008) Celt reversals: a prototype of chiral dynamics. *Proc. Royal Soc. Edinburgh* **138A**, 361–368.

[2] Morrison, P.J. (1998) Hamiltonian description of the ideal fluid. *Rev. Mod. Phys.* **70**, 467–521.

Notes

Cascade process of linked quantum vortex loops

Simone Zuccher[1] and Renzo L. Ricca[2]

[1] *Department of Computer Science, University of Verona, Italy*
[2] *Department of Mathematics & Applications, University of Milano-Bicocca, Italy*

Summary

Here we present for the first time a detailed study of the cascade process of two linked quantum vortex loops under the Gross-Pitaevskii equation. After a series of successive reconnections the vortex system decays to three distinct loops. Kinetic helicity as well as various geometric and topological properties associated with helicity are examined throughout the reconnection events, providing a complete structural analysis of the whole process.

1 Quantum vortex evolution under the Gross-Pitaevskii equation

Quantum vortex dynamics is governed by the Gross-Pitaevskii equation (GPE)

$$\frac{\partial \psi}{\partial t} = \frac{\mathrm{i}}{2}\boldsymbol{\nabla}^2\psi + \frac{\mathrm{i}}{2}(1-|\psi|^2)\psi \ , \tag{1}$$

with background density $\rho_b = 1$. It is well-known that under the Madelung transformation $\psi = \sqrt{\rho}\exp(\mathrm{i}\theta)$ eq. (1) can be written in terms of a continuity equation and a momentum equation of an ideal fluid with density $\rho = |\psi|^2$ and velocity $\boldsymbol{u} = \boldsymbol{\nabla}\theta$. Defects in the wave function ψ are infinitesimally thin vortices of constant circulation $\Gamma = \oint \boldsymbol{u}\cdot \mathrm{d}\boldsymbol{s} = 2\pi$ and healing length $\xi = 1$. An important physical quantity is kinetic helicity, given by

$$H = \int \boldsymbol{u}\cdot\boldsymbol{\omega}\ \mathrm{d}^3\boldsymbol{x} \ , \tag{2}$$

that in ideal conditions is known to be conserved. In the case of two distinct vortex loops, helicity can be written in terms of Gauss' linking number Lk and Călugăreanu-White's self-linking number SL [1, 2]. Since for a 2-component link $Lk_{12} = Lk_{21}$ and vortex circulations are equal, we have

$$H = \Gamma^2\left(2Lk_{12} + SL_1 + SL_2\right) \ , \tag{3}$$

where $SL_i = Wr_i + T_i + N_i$ $(i = 1, 2)$ admits decomposition in terms of writhe Wr_i, total torsion T_i and intrinsic twist N_i of the i-th vortex centerline. Helicity can therefore be computed by two independent methods; one based on the velocity-vorticity distribution by using eq. (2), and the other by extracting geometric and topological information by using eq. (3). In recent numerical simulations [3] we implemented the computation of all these quantities to study the reconnection of two vortex loops. Details of the numerical code and of the procedure adopted for the extraction of the vortex centerline can be found there. In particular we showed that the intrinsic twist can be computed by identifying the reference ribbon defined on the vortex centerline with the phase associated with the wave function ψ, a prescription that provides reliable information for the computation of geometric and dynamical properties involved during reconnection events as well. That exercise served as a test benchmark for the present investigation.

2 Cascade process of two linked vortex loops

Here we present preliminary results on the evolution of two linked, vortex loops that, through interaction and successive reconnections, untie and generate a system of unlinked, unknotted loops.

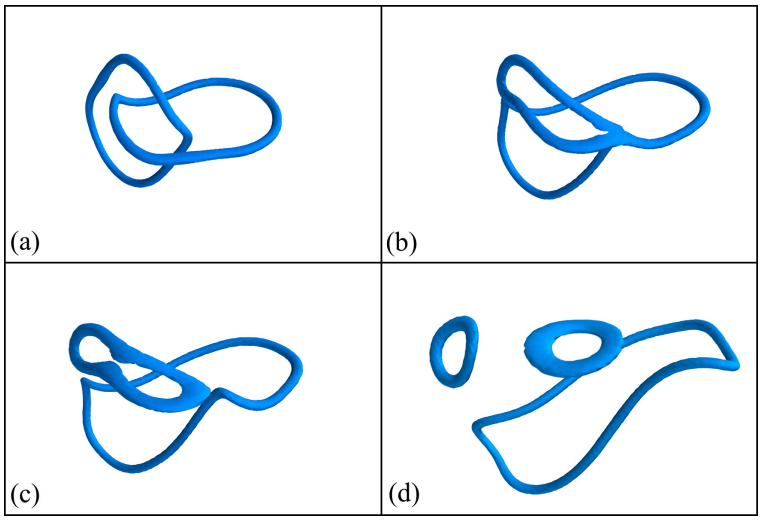

Fig. 1: Time evolution of two linked vortex loops under GPE. (a) The vortex system undergoes a first reconnection to form (b) a large, folded loop. (c) After a subsequent reconnection two secondary unlinked, vortex loops are produced, and after a third reconnection (d) the system decays to form three distinct loops. Tubes visualize constant density surfaces.

The whole process is shown in Figure 1. After a first reconnection the two loops untie to form a large folded loop (Figure 1b), that quickly reconnects to produce a secondary structure that after a third reconnection generates two smaller loops. This cascade process reveals interesting features and some details are similar to analogous experiments done by using a three-dimensional vortex-in-cell code in a nearly inviscid context [4].

A detailed analysis of the geometric, topological and dynamical properties associated with helicity is presented. Accurate computations of all the quantities across scales and during each reconnection event are discussed and compared with helicity computation based on eq. (2).

References

[1] Moffatt, H.K. (1969) The degree of knottedness of tangled vortex lines *J.Fluid Mech.* **35**, 117–129.

[2] Moffatt, H.K. & Ricca, R.L. (1992) Helicity and the Călugareănu invariant. *Proc. R. Soc. Lond. A* **439**, 411–429.

[3] Zuccher, S. & Ricca, R.L. (2015) Helicity conservation under quantum reconnection of vortex rings. *Phys. Rev. E* **92**, 061001–5.

[4] Aref, H. & Zawadzki, I. (1991) Linking of vortex rings. *Nature* **354**, 50–53.

Notes